Study of supercooling in latent heat thermal energy storage

Ibrahim Shamseddine

Université Libanaise
École Doctorale
Sciences et Technologies
Doyen

UNIVERSITÉ
Clermont
Auvergne

Doctoral thesis in Cotutelle

To obtain the degree of University Doctor issued by

The Lebanese University	**And**	**Clermont Auvergne University**
Ecole doctorale		École doctorale
Sciences et technologie		Science pour l'ingénieur de Clermont-Ferrand

Speciality: Materials

Presented and defended by

Ibrahim Shamseddine

on December 01, 2022

Study of supercooling in latent heat thermal energy storage

The jury members:

Mr. Laurent Zalewski, Professor, Artois University	Reviewer
Mr. Jean-Pierre Bedecarrats, Professor, Pau University	Reviewer
Mrs. Marie Duquesne, Professor, Lorraine University	Examiner
Mr. Fadi Hage Chehade, Professor, Lebanese University	Examiner
Mr. Pascal Biwole, Professor, Institut Pascal, UCA	Director
Mr. Farouk Fardoun, Professor, Lebanese University	Director
Mrs. Fabienne Pennec, Associate Professor, Institut Pascal, UCA	Supervisor

Université Libanaise
École Doctorale
Sciences et Technologies
Doyen

UNIVERSITÉ
Clermont
Auvergne

Thèse de doctorat en Cotutelle

Pour obtenir le grade de Docteur délivré par

L'Université Libanaise	**Et**	**Université Clermont Auvergne**
Ecole doctorale		École doctorale
Sciences et technologie		Science pour l'ingénieur de Clermont-Ferrand

Spécialité : Matériaux

Présentée et soutenue publiquement par

Ibrahim Shamseddine

Le 01 Décembre 2022

Etude de la surfusion dans le stockage d'énergie thermique par chaleur latente

Les membres du jury :

M. Laurent Zalewski, Professeur, Université d'Artois	Rapporteur
M. Jean-Pierre Bedecarrats, Professeur, Université de Pau	Rapporteur
Mme. Marie Duquesne, Professeur, Université de Lorraine	Examinatrice
M. Fadi Hage Chehade, Professeur, Université Libanaise	Examinateur
M. Pascal Biwole, Professeur, Institut Pascal, UCA	Directeur
M. Farouk Fardoun, Professeur, Université Libanaise	Directeur
Mme. Fabienne Pennec, Maître des conférences, Institut Pascal, UCA	Encadrante

Abstract

The limitations of traditional energy sources, as well as the increasing demand for energy, push scientists to lower the energy demand of engineering systems and to search for clean energy sources. Latent heat thermal energy storage systems are emerging as one solution for reducing energy demand. These systems use phase change materials to store and release heat when needed, taking advantage of the latent heat of the materials. They aid in lowering the energy demand by distributing the energy load throughout the day. However, these systems still have several issues, one of which is supercooling, which occurs when the PCM remains liquid rather than solidifying. This natural phenomenon prevents the release of latent heat. The present work first provides a review of the supercooling phenomenon, listing its benefits and drawbacks depending on the application. The challenges encountered during the modeling of supercooling and the solutions employed by various authors are also discussed. The review serves as the foundation for achieving the goal of this work, which is to build a numerical model that accounts for supercooling during cooling.

The proposed model uses an in-lab existing enthalpy-porosity model that accounts for natural convection during melting. The latter model is adjusted and modified to include supercooling, mainly by adding a heat source term that represents the latent heat release. The model is then validated through a series of experiments. The experiments are carried out in accordance with the factors identified in the review as having the greatest impact on supercooling. They include several PCM types, namely an organic PCM (octadecane), a eutectic PCM, and an inorganic PCM (sodium acetate trihydrate). They also use various PCM container geometry and cooling rates. The results demonstrate the effect of the container's volume, surface roughness and thermal insulation, PCM type, cooling rate, and mechanical shocks on the supercooling degree. The experiments also investigate the impact of natural convection on the melting and solidification processes. The obtained results may provide benchmark experimental data for numerical models of phase change. Finally, the validated model is used to investigate the effect of supercooling in thermal engineering systems. The first application is a hot water tank, in which the PCM is charged with thermal energy during off-peak hours and discharges when the water temperature drops. The second application is a PCM-integrated free heating system in a residential building. It is discovered that the presence of supercooling has a significant effect on the system's performance, which is represented by the transient temperature of the water and the air, respectively for each application. The final temperature reached is lower when supercooling is present.

Keywords: Thermal energy storage; Phase change material; Supercooling; Experiment; Numerical model

Résumé

Les limites connues des sources d'énergie traditionnelles, ainsi que la demande croissante en énergie, poussent les scientifiques à réduire la demande énergétique des systèmes techniques et à rechercher des sources d'énergie propres. Les systèmes de stockage de chaleur latente apparaissent comme une solution pour réduire cette demande énergétique. Ces systèmes utilisent des matériaux à changement de phase (MCP) pour stocker et libérer la chaleur en cas de besoin, en tirant parti de la chaleur latente des matériaux. Ils contribuent à réduire la demande d'énergie en répartissant la charge énergétique tout au long de la journée. Cependant, ces systèmes présentent encore un certain nombre de problèmes, comme la surfusion, qui se produit lorsque le MCP reste liquide plutôt que de se solidifier. Ce phénomène naturel empêche le dégagement de chaleur latente lors du changement de phase. Ce travail de thèse présente d'abord un état des lieux du phénomène de surfusion, en listant ses avantages et ses inconvénients selon l'application. Les défis rencontrés lors de la modélisation de la surfusion et les solutions employées par divers auteurs sont également discutés. Cette revue de littérature scientifique sert de base pour atteindre l'objectif du travail, qui est de construire un modèle numérique tenant compte de la surfusion pendant le refroidissement du MCP.

Le modèle proposé utilise un modèle d'enthalpie-porosité développé au laboratoire qui tient compte de la convection naturelle pendant la fusion. Ce dernier modèle est ajusté et modifié pour inclure la surfusion, principalement en ajoutant un terme de source de chaleur qui représente le dégagement de chaleur latente. Le modèle est ensuite validé par une série d'expériences. Ces dernières sont réalisées en fonction des facteurs identifiés dans l'état de l'art comme ayant le plus grand impact sur la surfusion. Elles incluent plusieurs types de MCP, à savoir un MCP organique (octadécane), un MCP eutectique et un MCP inorganique (acétate de sodium trihydraté). Les expériences utilisent également diverses géométries de réservoirs et différentes vitesses de refroidissement du MCP. Les résultats démontrent l'effet du volume du récipient, de sa rugosité de surface, de l'isolation thermique, du type de MCP employé, de la vitesse de refroidissement et des chocs mécaniques sur le degré de surfusion. Les expériences étudient également l'impact de la convection naturelle sur les processus de fusion et de solidification. Les résultats obtenus peuvent fournir des données expérimentales de référence pour les modèles numériques de changement de phase. Enfin, le modèle validé est utilisé pour étudier l'effet de la surfusion dans les systèmes de génie thermique. La première application est un ballon d'eau chaude, dans lequel le MCP est chargé en énergie thermique pendant les heures creuses et se décharge lorsque la température de l'eau baisse. La deuxième application est un système de chauffage à MCP intégré dans un bâtiment résidentiel. On découvre que la présence de surfusion a un effet significatif sur les performances des systèmes, qui est représenté par les réponses transitoires de la température de l'eau et de l'air, respectivement pour chaque application. La température finale atteinte est plus faible lorsque la surfusion est présente.

Mots clés : Stockage d'énergie thermique ; matériau à changement de phase ; surfusion ; Expérience ; Modèle numérique

Acknowledgments

My first thanks go to my project directors, Prof. Pascal Biwole, Prof. Farouk Fardoun, and Dr. Fabienne Pennec. First and foremost, thank you for providing me with the opportunity to complete this thesis on such an interesting topic and in such a pleasant work environment. Thank you for believing in me throughout this process and teaching me so much on both intellectual and professional levels. I would like to emphasize your human qualities and your unbreakable supervision, which have contributed to the success of this project.

I would like to thank the members of the jury for taking the time to read my work. Especially the reviewers, Laurent Zalewski, Jean-Pierre Bedecarrats, and Marie Duquesne, who had the difficult task of carefully reading the lengthy manuscript and providing constructive feedback. I also want to thank the other members of the jury, Pascal Biwole, Farouk Fardoun, and Fabienne Pennec, for their insightful comments, advice, and direct or indirect contributions to my thesis work.

My deepest thanks go to Clermont Auvergne University, Ecole doctorale Science Pour Ingenieur, and Institute Pascal and to the Lebanese University, Ecole doctorale de Sciences et Technologie.

I also express my sincere thanks to “Le Département de l’Allier” for their financial support for this work. It is greatly appreciated.

Thank you to everyone at the Institute Pascal and IUT Clermont Auvergne at Montlucon who helped me with my research. I would like to thank Myriam and Stephane for our scientific discussions and your assistance with the test’s instrumentation and data collection throughout this thesis. I would also like to thank Prof. Frédéric Raynaud for helping me with the Labview code used during the experimental part.

I would like to thank my doctoral colleagues for their help, support, and unforgettable memories with them.

One final thought goes to my family, who has always supported me and has always been there for me, in good and bad times. They gave me everything possible to enable me to reach higher education levels. I only hope that they know how their love, support, and patience encouraged me to fulfill my and their dream...

Table of Contents

Table of Contents

Table of Contents

List of Figures

List of Figures

List of Figures

List of Figures

List of Figures

List of Tables

General Introduction

Context of the thesis

One of the foundations of human activities is energy. With the rising demand for energy and limited resources, achieving energy efficiency and developing new clean energy sources has become critical. One of the strategies employed is using phase change materials (PCM) based thermal energy storage systems. PCM can be utilized to improve the operation of thermal energy storage systems by lowering energy loads and moving peak demand hours. Consecutive solidification and melting of the materials adds or removes a considerable amount of energy to the systems, represented by the material's latent heat. PCM has been used in a wide range of applications such as renewable energy [1], building energy savings [2], heat pumps [3], electronic temperature management [4], food and biomaterial preservation [5], and the automotive industry [6] (conventional and electric).

These materials, however, continue to face a variety of hurdles posed by their thermophysical characteristics and thermal behavior, such as the low thermal conductivity of most organic and eutectic PCM, the PCM degradation due to consecutive heating and cooling cycles, phase segregation, chemical stability, and their hysteresis upon melting and solidification and supercooling. In this study, we are interested in supercooling, a natural phenomenon in which the material remains liquid at temperatures lower than the solidification temperature. This broad description allows this phenomenon to manifest in a variety of everyday applications. The behavior of a material in a supercooled state is determined by a variety of factors, including the material's properties and the surrounding applied conditions. The arbitrary presence of supercooling is a disadvantage, but if thoroughly investigated, it can be avoided in applications such as latent heat thermal energy storage systems where the prevention of latent heat release reduces the system’s performance, or promoted in applications such as the preservation process of food, drugs, and organs for transplantation where it may be wanted.

Several studies have been done on the behavior of a material in a supercooled state and the influencing factors on the degree of supercooling. These factors can be divided into three categories as follows:

- The thermophysical properties of the material: thermal conductivity, heat capacity, density, purity of material, type (organic, inorganic, eutectic), and thermal history.
- The container: insulation, thermal conductivity, thickness, surface roughness, shape, and volume.
- The applied conditions: cooling rate, mechanical and electric shocks.

Thesis question and methodology

The direct impact of supercooling on the performance and efficiency of a system requires a good representation in the numerical models. Several computational fluid dynamics codes exist to represent the melting and solidification of a PCM in the presence of natural convection. Such an in-lab, experimentally validated code can be found at the *Institut Pascal*. So far, most numerical models of supercooling are one-dimensional, with very few attempts reporting 2D and 3D modeling. Therefore, the goals of the present thesis are twofold:

- Design and validate experimentally a multidimensional CFD model of PCM melting and solidification that includes natural convection and supercooling. The model should reproduce the kinetics, flow, and temperature fields of the PCM, according to the above-mentioned parameters that affect its behavior.
- Investigate the impact of supercooling on latent heat thermal energy storage systems.

To achieve these goals, several steps have to be followed. Firstly, it is necessary to clearly understand the supercooling phenomenon, especially the significant factors that directly affect the degree of supercooling. Including only the important factors in the numerical model may reduce its complexity by finding a simple and accurate manner to represent them. Some of the main challenges encountered during modeling are summarized as follows:

- The degree of supercooling depends on the before mentioned affecting factors.
- The increase in temperature due to latent heat release. When solidification is initiated, latent heat is released and the temperature of the PCM increases.
- The reduction of latent heat during solidification, since a part of the latent heat is used to increase the temperature of the PCM

Secondly, the numerical model must be validated using experimental results. There are numerous experimental results in the literature; however, they lack detailed information on the used PCMs and container characteristics or exact data on the boundary and initial conditions. As a result, an in-house experimental setup is needed. By holding all other parameters constant, the effect of each factor on supercooling may be studied individually.

After the model has been validated, it can be used to study the performance of a system in real-world applications. The presence of supercooling in a latent heat thermal energy storage system is numerically investigated in two applications. The first one is a hot water tank, which encloses a PCM. The water is heated during the day with solar panels and heated at night with the PCM. The second application is a residential building ventilation system with a PCM in the pipework. The PCM is heated by ambient hot air during the day and releases this heat to the cold air passing through the pipes at night. The effect of supercooling is investigated by comparing the temperature curves of water or air in the two systems with and without supercooling.

Plan of the manuscript

The thesis work is presented in four chapters in the manuscript, which are as follows:

Chapter 1: State of art on the supercooling phenomenon.

The first section introduces the supercooling phenomenon and the applications in which it may occur. It describes the impact of its presence on the behavior of the PCM and the system that contains the PCM. The second section discusses the major factors influencing this phenomenon. A series of experiments conducted by several authors examine the impact of each factor. The next section summarizes the difficulties encountered while modeling supercooling. The dependence of supercooling on several factors complicates the determination of the supercooling degree, crystallization phase, and solidification process. The solutions used by various authors to overcome these challenges are discussed. Fourth, a set of recent models that incorporate supercooling during the cooling process are presented. Finally, this review emphasizes the work that needs to be done and positions the work of this thesis. It identifies the critical points to be investigated as well as the key parameters to be considered during the modeling and experimental processes.

Chapter 2: A CFD model of solid-liquid phase change with natural convection and supercooling.

The numerical model is detailed in this chapter. First, the modeling challenges discussed in the first chapter are redefined, and a solution for each is found. Second, these solutions are added to an existing

model that has already been validated for natural convection during heating. Finally, the physical model is presented, and the numerical scheme used is described in detail. This chapter reports the first attempt to incorporate natural convection and supercooling phenomena into a model using this method.

Chapter 3: Experimental benchmark on solid-liquid phase change in the presence of supercooling and natural convection.

Following the construction of the numerical model, accurate experimental results with precise initial and boundary conditions, physical model dimensions, and material properties are required. As a result, a benchmark experiment is constructed using three different PCMs with different melting temperatures and thermophysical properties. The first PCM chosen is octadecane, an organic PCM with a melting temperature $T_m = 28^{\circ}C$; the second is a eutectic PCM with a melting temperature $T_m = 21.5^{\circ}C$; and the third is sodium acetate trihydrate (SAT), an inorganic salt hydrate with a melting temperature $T_m = 58^{\circ}C$. According to Chapter 1, the major factors that influence the degree of supercooling are the cooling rate, PCM volume, container surface roughness, PCM purity, and mechanical shocks. The effect of the aforementioned factors on the degree of supercooling is investigated using two different PCM containers. The first is small scale in a test tube, and the second is large scale in a cuboid-shaped container.

Chapter 4: Validation of the numerical model and applications.

This chapter is split into two parts. The physical model is represented in the first section by assigning the used boundary and initial conditions, and the values of the materials' properties. The numerical results obtained are compared and validated against the experimental results obtained in Chapter 3. The model's limitations and required improvements are then identified. The second part studies and numerically examines two applications of thermal energy storage systems using phase change materials in the presence and absence of supercooling. The first is a hot water storage tank, while the second is a residential heating ventilation system. This numerical study then investigates the effect of the presence of supercooling.

The manuscript ends with a "General Conclusions and Perspectives" section that summarizes the main findings and proposes a few perspectives for the work.

This research work was funded by the *Conseil départemental de l'Allier*. It is an international joint research project of the University Clermont Auvergne (UCA), France, and the Lebanese University (LU), Lebanon, under the supervision of Professor Pascal Henry Biwole (UCA), Professor Farouk Fardoun (LU), and Associate Professor Fabienne Pennec (UCA).

Chapter 1: State of art on the supercooling phenomenon

Presentation of the chapter

With the growing public awareness of the environmental vulnerability of our planet and the recent issue, in many countries, of stricter regulations in terms of carbon emissions and energy consumption, it has seemed to us important to establish a state of the art regarding the supercooling phenomenon in phase change materials (PCM). Depending on the application, supercooling can be either an advantage or a disadvantage. PCM can be used in thermal storage systems to enhance their performance by decreasing the demand on energy supply and shifting the peak hour demand. This is done by the alternating solidification and melting processes that serve in the release and absorption of latent heat. Supercooling negatively affects the performance of such system by delaying or preventing solidification. On the other hand, supercooling can be beneficial in the sectors of preservation and survival of plants. This chapter first presents a comprehensive review of the daily applications where this phenomenon can appear. Then, a detailed analysis of the effect of different factors on the degree of supercooling is done. It was found that there is still a lack of information regarding the correlation between the different factors. Afterward, a detailed explanation of the challenges encountering researchers when modeling supercooling is done, followed by a set of models showing the different methods to overcome the challenges. A final discussion on needed future works is provided. The chapter ends by stating the positioning of the present work relative to the state of the art.

Nomenclature

a_0, a_1, a_2	Constants	T	Temperature, K
Bi	Biot number, -	Δt	Time step, s
CR	Cooling rate, $°\,C/min$	T_a	Average value of nucleation and solidification temperatures, K
C_p	Heat capacity, J/K	ΔT_{am}	Melting point depression, K
d	The molecular diameter, m	T_c	Coolant temperature, K
F_{cry}	Crystallization probability function, -	T_{di}	Density change temperature, K
Fo	Fourier number, -	T_E	Equilibrium melting point temperature, K
f_c	Crystallization factor, -	t_{end}	Duration of simulation, s
f	Nucleation barrier reduction factor, -	T_f	Freezing temperature, K
f_{super}	Phase supercooling indicator, -	ΔT_h	Degree of overheating, K
H	Latent heat, J/kg	T_Iw	Capsule's internal wall temperature, K
h	Planck's constant, -	T_i	Initial temperature, K
Δh	$\frac{latentheat \times molecularweight}{Avogadro'snumber}$	T_m	Melting temperature, K
I	Homogeneous nucleation rate	T_n	Nucleation temperature, K
I_n	Nucleation factor	T_s	Solidification temperature,K
k	Boltzmann constant, -	ΔT_s	Degree of supercooling, K
K_1	Arbitrary constant, -	t_s	Duration of supercooling, K
K_2	Fitting parameter, K^{-2}	u	Internal energy, J
K_3	Calibration parameter, -		

L	Length, m	$v(T)$	Solidification rate, m/s
L_{adj}	Number of solid crystals in the adjacent segments, -	W	Normal surface velocity of the freezing front, m/s
L_f	Molar heat of fusion, J/mol	Δx	Size of the cell, m
N	Number of atoms of a system, -	X_i	The impurity fraction, -
n	Total number of measurements, -	β	State quantity, -
$P(T)$	Nucleation probability function, -	λ	Thermal conductivity, $W/(m.K)$
Q	Heat source, kW	ρ	Density, $kg/m3$
R	Molar gas constant, $J/(mol.K)$	α	$(water/PCM)$ convection coefficient, -
R	Surface roughness, μm	$\emptyset$	Solidification ratio, -
q	Activation energy, kJ/mol	γ	Surface tension, $N.m^{-1}$
SF	Solidified fraction, -	ΔG_n	Free energy variation, J
σ	Surface tension, N/m	α	Angle of notch, rad

1.1 Introduction

For a given phase change material, the melting temperature, T_m, is the theoretical temperature at which the material changes its phase from solid to liquid and vice versa. For a pure PCM, phase change is considered isothermal. In reality, for most PCM used in engineering applications, phase change occurs in a range of temperature around the melting temperature, as shown in Figure 1.1.

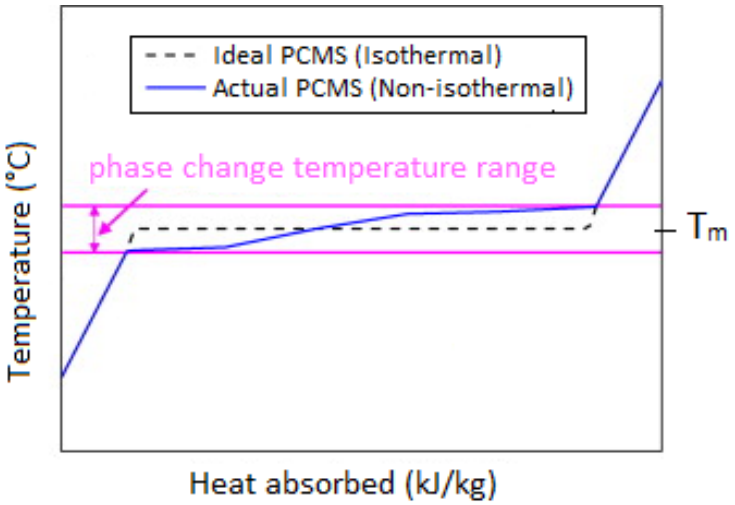

Figure 1.1 Temperature variation and phase change as a function of absorbed heat. The pink horizontal lines represent the actual phase change range. The blue line curve represents the actual temperature curve, whereas the black dotted curve represents the theoretical melting temperature [7]

A material remaining in liquid state at a temperature below its melting temperature is referred to a phenomenon known as supercooling, subcooling or undercooling. During supercooling, the material is in metastable state and plenty of factors can trigger solidification. Indeed, the initiation of solidification requires a solid particle referred to as a nucleus, which may be too small and even not present at the liquid state. This nucleus is formed and grows by the solidification of the liquid on the solid surface. In this case, the liquid releases its heat to reach minimum energy. The heat release and solid formation depend

on the radius *r* of the nucleus. The released heat is the function of the volume (proportional to r^3) while the solid formation depends on the surface area of the nucleus (proportional to r^2). An energetic barrier is formed for small values of *r*, which means that the gained surface energy is larger than the heat released by solidification [8]. Liquids enter the supercooled state when energy release from the nucleus necessary to form the solid-liquid interface is not sufficient [9]. In this case, solidification is prevented and the liquid enters into the supercooling state. Solidification initiates when the radius of the nucleus is sufficiently large. The initiation of solidification results in the release of the latent heat, which causes a temperature rise within the material. If the energy contained in the liquid is sufficient, the temperature of the liquid will increase to its melting temperature as shown in Figure 1.2. The degree of supercooling is the difference between the theoretical melting temperature and the lowest temperature reached by the liquid phase, called the nucleation temperature hereafter denoted as T_n.

Depending on the given application, supercooling can be either useful or destructive. However, treating this phenomenon requires a good knowledge of its behavior under different conditions. If supercooling is desired, a set of actions can be taken to increase the degree of supercooling and insure no solidification in the operating range below the melting temperature. For example, in applications of preservation, it is suitable avoid solidification while maintaining low temperatures. In this case, supercooling allows decreasing the quantity of energy needed to reach such temperatures, which is represented by the latent heat of solidification. However, if supercooling is not desired like in latent heat thermal energy storage systems, some parameters should be modified in a way to eliminate or decrease as much as possible the degree of supercooling. The importance of this phenomenon is reflected by the increasing number of articles, conferences and patents containing supercooling in their titles and abstracts, throughout the last decades. Based on Google scholar data, Figure 1.3 illustrates this trend.

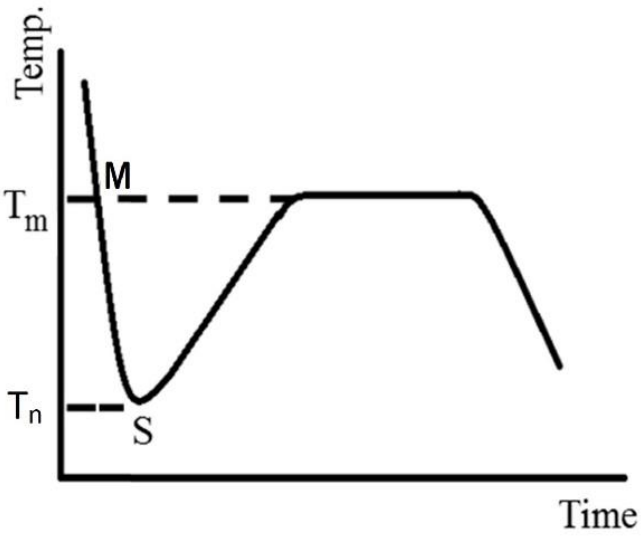

Figure 1.2 Plot of liquid undergoing supercooling upon cooling [10]

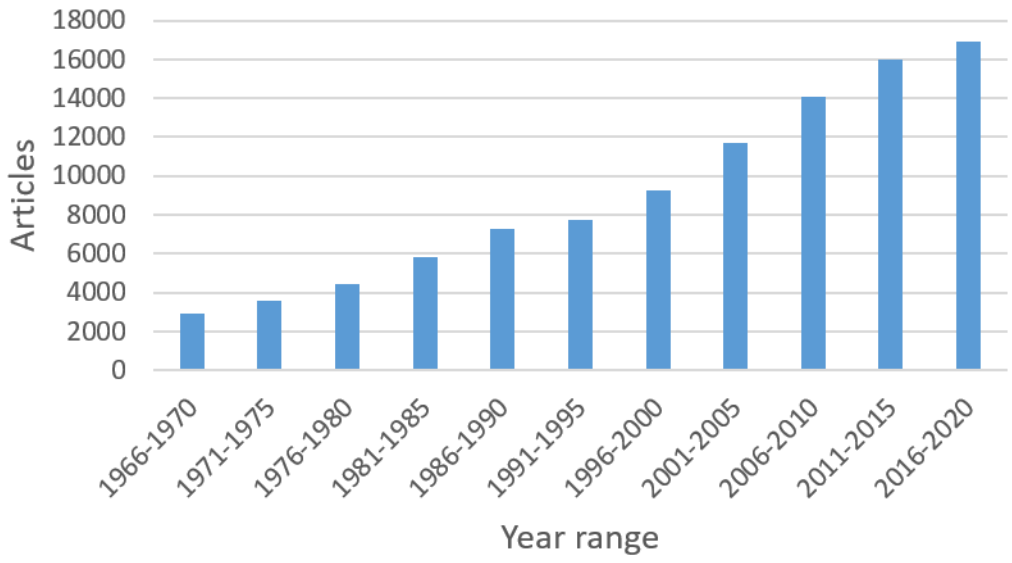

Figure 1.3 The increasing number of articles containing supercooling

Moreover, Figure 1.4 shows a statistical study done on a sample of 130 papers published in the year 2020 including the supercooling phenomenon. Those papers can be either a review paper, presenting a new numerical model, showing the current difficulty to address supercooling by numerical methods.

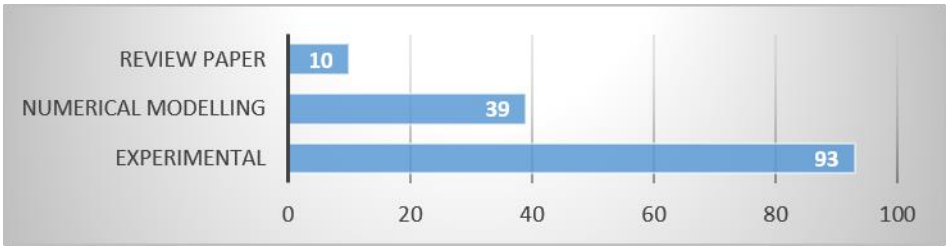

Figure 1.4 Investigation of type of publications of the year 2020 from a sample of 130 articles

Existing reviews focus on one specific application such as food preservation [5], [11], [12], TES systems [13] or on very specific materials [14]–[16]. Such reviews only consider methods to reduce supercooling [17]–[20] or to increase supercooling, depending on the application, without presenting both aspects. In the same way, most existing review focus either on experimental methods or on numerical modeling methods to deal with supercooling, with almost no paper discussing both. Only two recent reviews [21], [22] discussed both aspects but limited the study to man-engineered PCMs only, without considering supercooling in nature and preservation processes. Therefore, there is still a need for a foundational comprehensive review on all aspects of supercooling, cataloging and discussing its main occurrences in nature and human processes, the experimental methods to increases or decrease its occurrence depending on the application, and the existing numerical models. The present chapter aims at filling this gap.

First, an overall introduction to supercooling is conducted through its occurrence in nature or daily applications such as food preservation and thermal energy storage systems. The importance of considering this phenomenon in experimental and research works is explained by presenting its direct effects on the applications' performance and efficiency. In the second part, the chapter details the most

important factors having an effect on the degree of supercooling. According to the application, if these factors are well treated, the degree of supercooling can be increased, decreased or even eliminated at low cost using simple techniques. When trying to include supercooling in the numerical models, a set of challenges arises due to the metastable state of the material. The third section presents these challenges, along with the adapted solutions. The most recent models for supercooling, their methodology, the used mathematical equations and the taken assumptions are discussed. Then, the numerical results obtained by several researchers are compared and the gaps in the models are presented. At last, clear guidelines are provided for the optimal experimental design or numerical modeling of applications in the presence of supercooling and the required future works are discussed.

1.2 Supercooling in nature and human applications

Supercooling is a natural phenomenon that depends on the surrounding circumstances, the liquid's properties and its response to different applied conditions. This variety of factors of supercooling presence causes this phenomenon to appear in various applications such as in plants, living creatures, food preservation and thermal storage systems using phase change materials.

1.2.1 Animals, plants and specimen organs

In nature and especially in freezing climate zones, the living creatures have three main options: they can either migrate to a warmer land, die freezing or survive by supercooling. Supercooling exists among plants and animals living in a very cold freezing climate in order to prevent these living creatures from dying due to the solidification of their body water content, body cells and blood. Some examples of animals are: Nematodes, insects that were found alive at a temperature of -80°C in Antarctica; Vallonia perspectiva, a small land snail [23]; Hippodamia convergens, a lady bird beetle; the larvae of goldenrod fly that were found alive at a temperature of -9°C and Chrysemys picta, a north american turtle that faces ice and freeze [24]. In addition, arctic fishes were found alive at a temperature of -1~-3°C [25].

Similarly, plants tissues can be damaged due to freezing of the water content inside the plant, especially the xylem tissues that are responsible of water and nutrients transport to several parts of a plant such as leaves [26]. The experiment carried by Hacker *et al.* [27] on a cushion of *Saxifraga caesia* at bud stage and *Saxifraga moschata* during anthesis shows that the solidification of supercooled inflorescences occurs when reaching the minimum temperature and that 77% of *caesia* buds and 44% of *moschata* flowers solidified, causing lethal damage. However, the unfrozen inflorescences survived. Depending on the time spent in supercooling state and the temperature reached, Figure 1.5 shows in gray circles and black diamonds the number of solidification cases for caesia and moschata respectively.

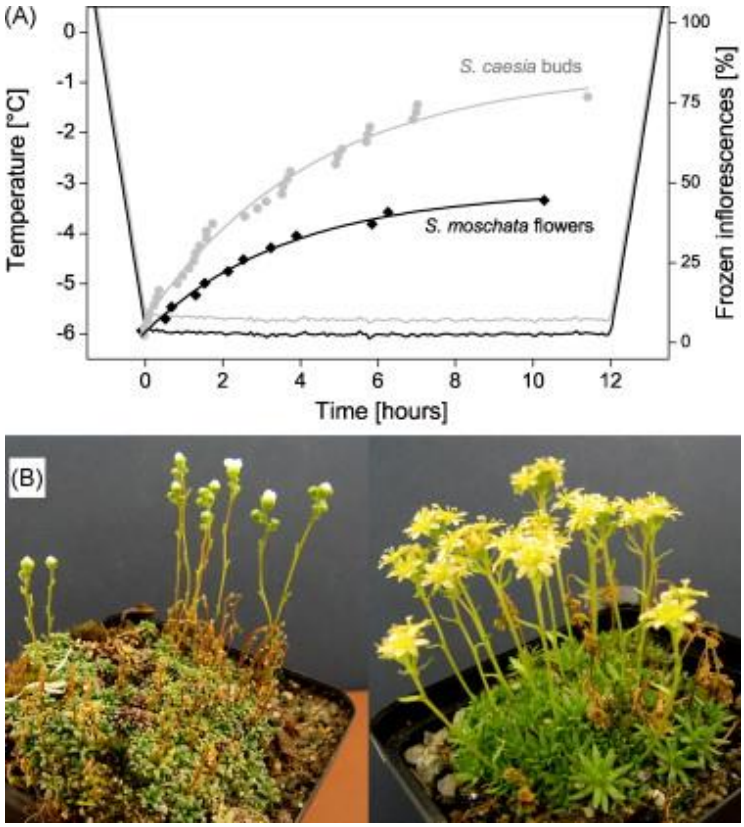

Figure 1.5 (A) Plot showing the percentage of frozen S. caesia and S. moschata with respect to temperature and time, (B) Captured photo of the experiment showing the impact of supercooling [27]

The preservation of mammalian body parts specimens is essential. It aims to have available cells, organs or tissues maintained at certain standards. In the presence of oxygen, the body is able to create energy by the degradation of aminoacids, carbohydrates, proteins and fats by aerobic metabolism process. According to Sicular *et al.* [28], for every 10°C of temperature decrease, the metabolism activity decreases by a factor of 1.5-2. Regarding the body temperature, preserving the organs at 4°C decreases the metabolism to 1/10, whereas the preservation at -4°C decreases it to 1/17. Monzen *et al.* [29] performed an experimental study on the preservation of rats' heart, liver and kidney in supercooled state, that is attained by an energized chamber using electric pressure. Preserving in supercooling state shows promising results, whereas cell and tissue damages are detected in the organs preserved at ordinary 4°C conditions. Moreover, the use of an electric field to attain supercooling state did not leave any trace or evidence of damage even when increased to 1000V. It is important to attain stable supercooling state to ensure that no solidification will take place which leads to organs damage. There are several techniques used to reach the stable state, one of which is adding antifreeze agents. However, the agents used in the experiment of Rubinsky *et al.* [30] left traces in the organs that caused inevitable damages. This technique of preservation is essential because it extends the storage life of the specimens, especially from human donners.

1.2.2 Food preservation

Supercooling is considered very helpful in food preservation when knowing that a material undergoing supercooling does not release its latent heat because it remains in liquid state. Therefore, preserving food, at a given temperature, in supercooled state rather than solid state, will require less energy. In addition

to economical savings, other benefits can be found. The growth of bacteria decreases with decreasing temperature, so preserving food in supercooled state keeps it fresh for a longer period with a high quality since the formation of ice ruins the food structure and properties. This technique leads to a decrease in food waste and an increase in the lifetime of fresh food at a lower cost [5]. The studies are still new, but they are promising in such fields as agricultural products [31], meat [32], [33] and fish [34], [35].

You *et al.* [36] conducted an experimental study on beefsteak, where the beef's internal temperature was held at a temperature of -4°C for 14 consecutive days using pulsed electric field and oscillating magnetic field. Figure 1.6 shows the obtained samples after 14 days for samples preserved by refrigeration (4°C), slow freezing (-10°C), fast freezing (-20°C) and fresh samples. By comparing these samples, no significant color change is observed between fresh (Figure 1.6a), rapid freeze (Figure 1.6e) and supercooled (Figure 1.6c) beef. Preserving by refrigeration (Figure 1.6b) shows an obvious change in color. The drawback of slow freezing (Figure 1.6d) is destroying the meat cells by the slow formation of ice. The slow formation of ice causes the ice to be formed as clusters that leads to drip loss, tenderization causing protein denaturation. Using rapid freezing can decrease the lipid oxidation and cell damage. Lipid oxidation causes a deterioration in the quality concerning the color, taste and nutritional value. However, low heat transfer rates in large sized food prevents using rapid freezing, which sets the technique of using supercooling in the scope of interest. Therefore, the quality of the beef represented by color, lipid oxidation, drip loss and texture can be attained similar to fresh meat by supercooling with less risk.

Studies done on fish meat show that the meat preserved at a supercooling state has a firm structure [37], [38], fresher, since at a refrigeration temperature, meat can be preserved for a few days only and loses its firmness after that. Using standard refrigeration preserving conditions, the preservation of chicken is less than one month. However, a chicken preserved at supercooling state can endure preservation for months, which gives an extended margin for the merchant to distribute his products. Similarly, the supercooled garlic at -6°C shows a higher quality, as shown in Figure 1.7, where the color and structure of the cloves of garlic are better than those frozen at -30°C [39]. Similarly, Figure 1.8 shows the effect of temperature and preservation technique on the garlic and shallot, where a severe structure damage is clear in the freezing case [40].

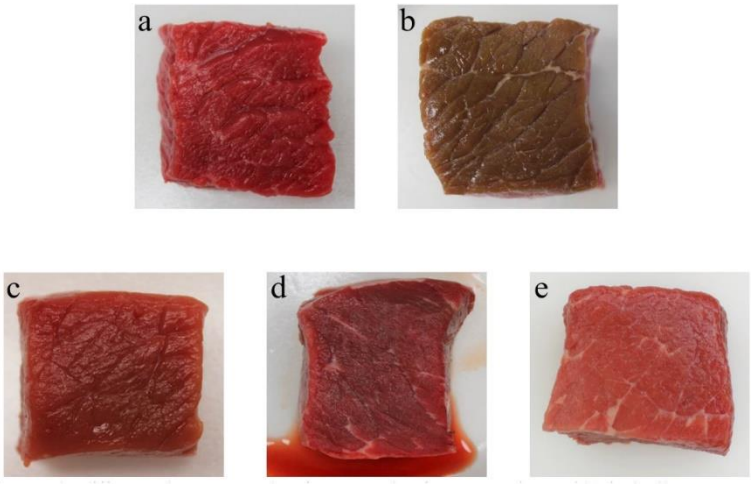

Figure 1.6 Images of a) fresh beefsteak compared to beefsteak samples preserved for 14 days by b) refrigeration, c) supercooling, d) slow freezing and e) rapid freezing [36]

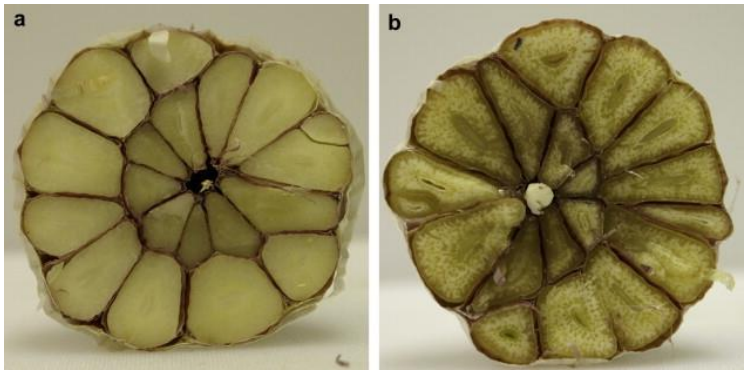

Figure 1.7 Garlic preserved unpeeled for one week a) supercooled at -6°C and b) frozen at -30°C [39]

Figure 1.8 Snapshots of a) garlic and b) shallot after being preserved unpeeled for a week at ambient temperature, chilled temperature 1.1°C, -6°C supercooled temperature and -30°C freezing temperature from left to right respectively [40]

James *et al.* [40], performed a series of experiments on vegetables and fruits. Table 1.1 summarizes the results, where the melting temperature is the temperature of phase change in case of no supercooling. From the below table, two things can be observed. The first is the dependence of the degree of supercooling on the type of sample, knowing that the supercooled material, water content, is the same. The degree of supercooling and standard deviation vary indeed from one to another. The second thing is the sensitivity of supercooling to any change. When performing an experiment on a given vegetable or fruit, efforts are done to take identical samples and apply similar external conditions. However, the degree of supercooling for some samples have a wide range and high standard deviation (sd).

As presented above, supercooling is beneficial for food preservation. A good knowledge of supercooling behavior helps applying the suitable techniques needed to obtain a narrow range of supercooling degree and low standard deviation with an optimal cost and better quality.

Table 1.1 Supercooling experimental results performed on vegetables and fruits [40]

Sample	Average melting temperature (°C) and standard deviation	Number of samples $\left(\frac{supercooled}{Total}\right)$	Degree of supercooling		
			Min	Max	Avg (sd)
Broccoli	-2.1 (0.3)	9/10	0.4	7.7	2.5 (2.3)
Carrot	-1.6 (0.6)	9/10	0.4	2.6	1.1 (0.7)
Cauliflower	-1.5 (0.3)	7/10	0.6	6.9	3.8 (2.6)
Garlic	-2.7 (0.3)	15/15	4.9	12	10.3 (1.6)
Leek	-1.9 (0.3)	9/10	0.6	2.3	1.6 (0.6)
Parsnip	-2.2 (0.2)	4/10	0.4	0.9	0.7 (0.2)
Shallot	-1.6 (0.2)	10/10	1.1	4.7	3.3 (1.3)

1.2.3 Thermal storage systems

Energy is the main demand for humans to fulfill their activities. The global energy demand is constantly increasing, with the increase in living standards and the growth of the economy and human population. The limited amount of traditional energy sources, such as coal and fuel, prompts the search for other clean, inexpensive and unabated energy sources. The renewable energies are often intermittent and therefore need to be stored. Phase change materials (PCM) have drawn attention due to their importance in applications of thermal energy storage. PCM are promising materials that store energy in a relatively small volume of material. PCM store thermal energy by changing phase and taking advantage of their high latent heat. PCM in wallboards or HVAC systems serves in increasing the thermal comfort in the building by shifting the hour of peak load demand, decreasing this peak, reducing the sharp variation of daily energy demand and enhancing the building's thermal and energy behavior. In addition to that, using transparent PCM can serve in providing natural day light that also interferes in energy saving and adding comfort to the building. PCM can also act as a temperature regulator and heat sinks by delaying the rise in temperature of various electronic systems such as photovoltaic panels [41], [42]. Figure 1.9 shows the behavior of a PCM during heating and cooling, where making use of the big amount of latent heat serves to make PCM supplementary and even alternative to traditional cooling systems.

For that reason, PCM are precisely chosen according to their melting temperature to obtain the maximum efficiency of the thermal energy storage system in which they are integrated. One of the challenges facing the success of solid-liquid PCM systems is the supercooling phenomenon. The PCM remains liquid rather than solidifying, which prevents the system from benefiting of the latent heat. For such systems, researchers pay great attention to supercooling because of the direct negative impact on the efficiency, which may cause a damage and a fail in serving their purpose. Jin *et al*. [7] performed an experiment to study the supercooling degree of sodium acetate trihydrate (SAT). Three different cases were studied. The first starts the cooling process when the SAT is in solid state. In this case, no latent heat

is released because there is no phase change and no supercooling. The second starts the cooling process when the SAT is in a partially melted state. In this case, the released latent heat and the degree of supercooling are relatively small. The third starts the cooling process when the SAT is in liquid state. Here, the liquid remains in supercooled state and latent heat is not released. The main challenging problem is that the degree of supercooling depends on several factors and differs from one fluid to another. There is no general methodology to obtain a specific degree of supercooling for each material. Therefore, experiments are conducted to study the effect of each factor separately. By the help of such experiments, a number of the used PCM have a well-known range of supercooling degree. In addition to the experiments, efforts are done to establish numerical models simulating the PCM behavior under supercooling. The following paragraphs discuss the details of supercooling in PCM.

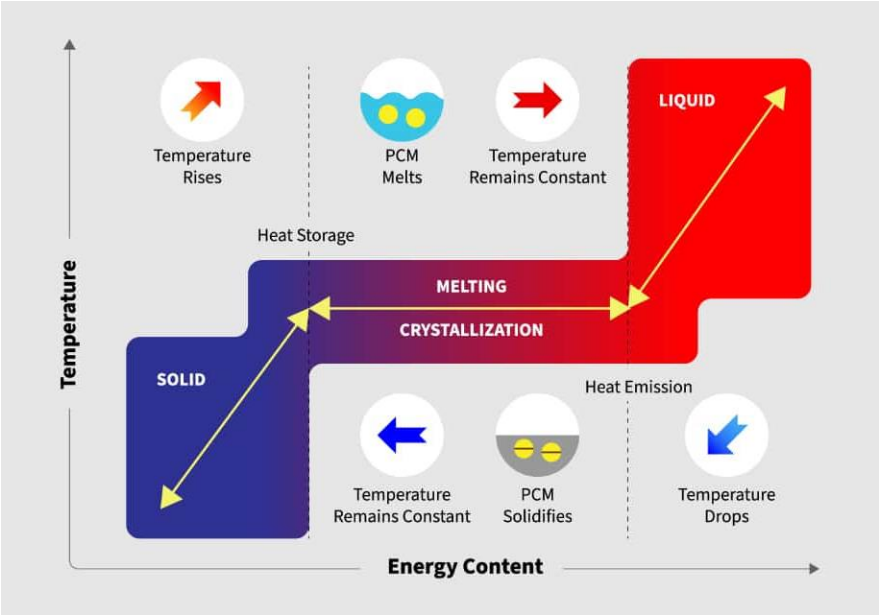

Figure 1.9 Schematic drawing representing a PCM during absorption and release of heat [43]

1.3 Effects of supercooling on PCM behavior

When choosing a PCM to include in a heating/cooling system, the main parameters taken into consideration are the melting temperature T_m and the latent heat H. The melting temperature has to be chosen close to the desired operating temperature or within the thermal comfort temperature range. Supercooling may be catastrophic to the PCM system efficiency. For example, in buildings, solidification mainly takes place naturally at night during a limited time. If the PCM undergoes supercooling instead of solidification, it will not be able to discharge the stored thermal energy. Therefore, the main goal of the presence of the PCM is not achieved during the day, leading to a system failure. Schranzhofer *et al.* [44] highlighted this problem by using a validated TRNSYS model, where they compared a brick wall layer with a PCM wall layer. The simulations highlight reduced temperature peaks with the use of PCM plaster since the latent heat plays an important role in shifting and decreasing the peak load. However, in the case of solidification prevention at night due to supercooling, the PCM remains liquid. In this case, the liquid PCM has a similar performance to that of the brick wall.

The following sections present a set of recent experimental and numerical results showing the effect of supercooling on the PCM behavior. The effect of supercooling degree on the temperature distribution, crystallization and quantity of released latent heat is outlined.

1.3.1 Different behaviors during cooling

Five typical cooling curves for water are presented in Figure 1.10, where T_i, T_{di}, T_f, T_n and T_c are the initial, density change, freezing, nucleation and coolant temperatures respectively. Five steps of PCM cooling process are displayed: (a): phase of release of sensible heat from liquid water and density changes until reaching freezing temperature; (b): metastable state of supercooled liquid; (c): process of dendritic ice formation and temperature increase; (d): release of latent heat and solid formation; (e): cooling of solid water where temperature decreases by sensible heat release [45].

1. In Figure 1.10-1, water freezes without any presence of supercooling. Upon cooling, the temperature of water decreases by releasing its sensible heat until reaching T_f, after which the latent heat is released and phase change takes place. After releasing all latent heat, the solid water starts to cool down by releasing sensible heat. Since no supercooling takes place, dendritic ice is absent and crystalline ice is formed.
2. In Figure 1.10-2, the above five steps (a) □ (e) take place, dendritic ice is formed during step (c) once T_n is reached. The temperature increases until it reaches T_f, and this is done by the release of the latent heat from the dendritic ice and its absorption by the supercooled liquid.
3. Figure 1.10-3 shows the case of water with low level of energy, which causes the freezing to take place immediately once T_f is reached.
4. Figure 1.10-4 shows a case similar to the case in Figure 1.10-3. However, the energy is low in a way that all the latent heat of the crystallized portion is released at a temperature lower than T_f and the latent heat is insufficient to raise the temperature to T_f.
5. In Figure 1.10-5, water stays in supercooled state and no phase change takes place. In this case, water stays in process (b) for an undetermined period. This can be due to a value of T_c higher than T_n and close to T_f ; or to a capsule material having low thermal conductivity, which fosters a higher degree of supercooling.

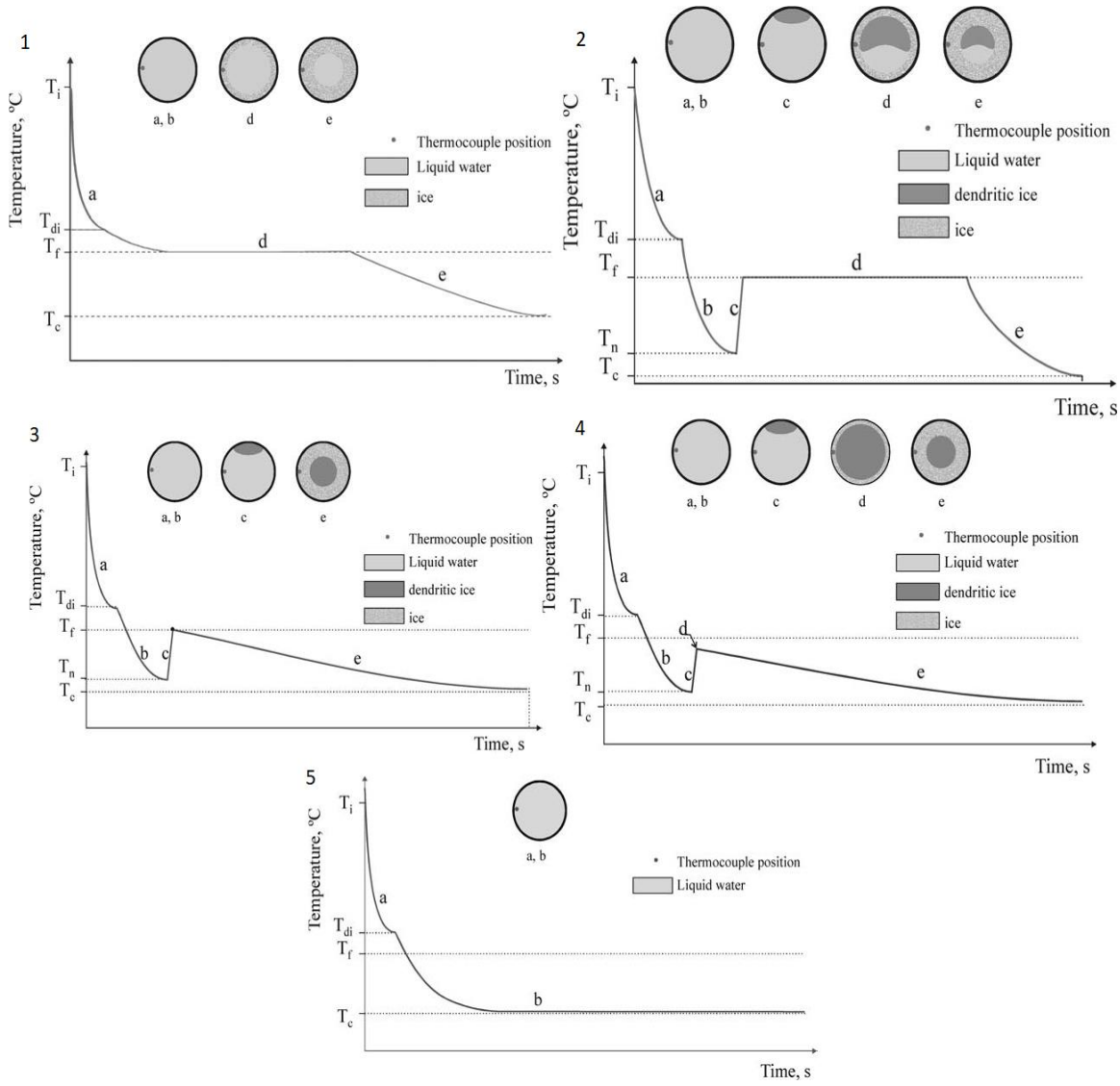

Figure 1.10 Process of 1) freezing with no supercooling, 2) instantaneous freezing with supercooling, 3) freezing with supercooling where all latent heat released to reach T_f, 4) freezing with hyper-cooling and 5) permanent supercooling with no process of freezing [45]

1.3.2 PCM performance

When choosing a PCM, its phase change temperature should be close to the comfort temperature or the desired functioning temperature of an apparatus, and the latent heat of fusion per unit volume should be high. The advantage of latent heat over sensible heat is the larger heat storage capacity with the same mass of material. However when solidification initiates in the presence of supercooling, the liquid PCM absorbs part of this latent heat to increase its temperature from the nucleation temperature up to the melting temperature T_m as shown in Figure 1.10. The higher the degree of supercooling, the lower the amount of latent heat that is released at the actual phase change temperature. When comparing with a case not suffering supercooling, this consumed portion is equal to $c_{p,l}\Delta T_s$, where $c_{p,l}$ is the liquid phase heat capacity and ΔT_s is the degree of supercooling. If ΔT_s increases, more energy is needed to rise the temperature to the melting temperature, which may cause a lack of useful energy needed during phase

change. When solidification initiates, the temperature of the supercooled liquid increases sharply at a constant enthalpy. According to the experiments held by Sandnes *et al.* [46], this increase can be easily highlighted from enthalpy plots. They measured enthalpy-temperature curves for disodium hydrogen phosphate dodecahydrate, sodium acetate trihydrate and STL-47 that are well-known supercooling salt hydrates and found that the nucleation temperature decreases as the supercooling degree ΔT_s increases. This decrease of nucleation temperature causes a delay in the onset of crystallization, which is shown in the studies done by Hu *et al.* [47]. The one-dimensional mathematical heat transfer model of a PCM is initially set at the same temperature before decreasing the temperature of the left side. For different degrees of supercooling, Figure 1.11a shows the temperature distribution of the domain at a given instant, and Figure 1.12 shows the temperature variation at a given node. The temperature at the same location decreases with the increase of supercooling degree, because the initially liquid PCM, experiencing supercooling, releases sensible heat upon cooling, resulting in a temperature drop, while the other releases its latent heat and maintains a constant temperature. Moreover, as shown in Figure 1.11b, the heat flux variation depends on the PCM state and temperature. A PCM undergoing phase change has approximately equal temperature through all the sample. As a result, the maximum value reached increases before phase transition with the increase of supercooling degree; while during the whole process of solidification, it decreases [47].

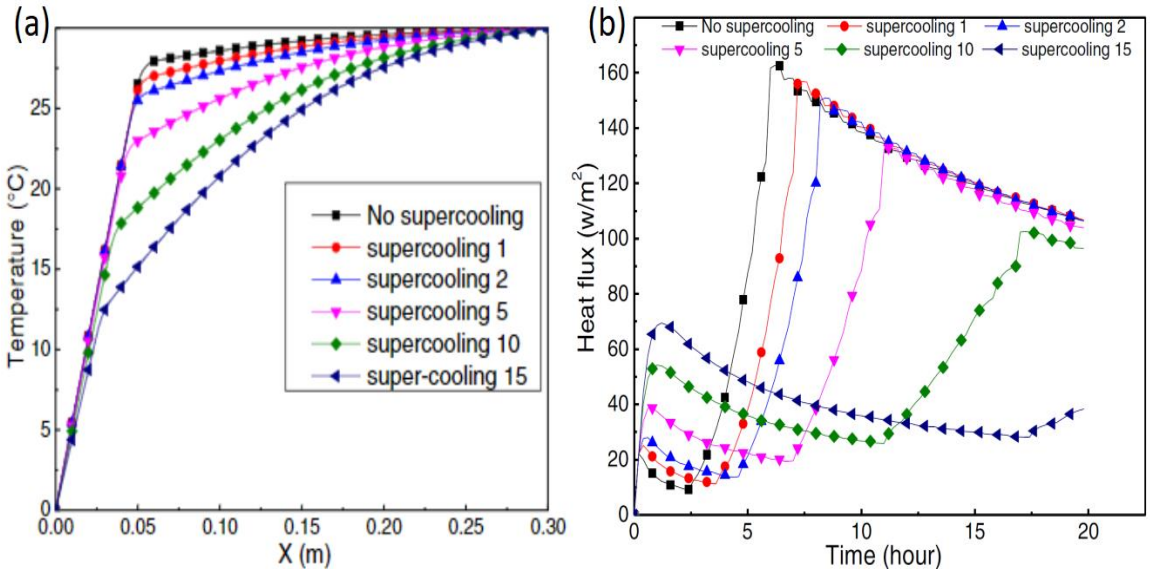

Figure 1.11 Plots showing the variation of the (a) temperature after 20 hours, (b) heat flux at a specific PCM node as a function of time under different degrees of supercooling [47]

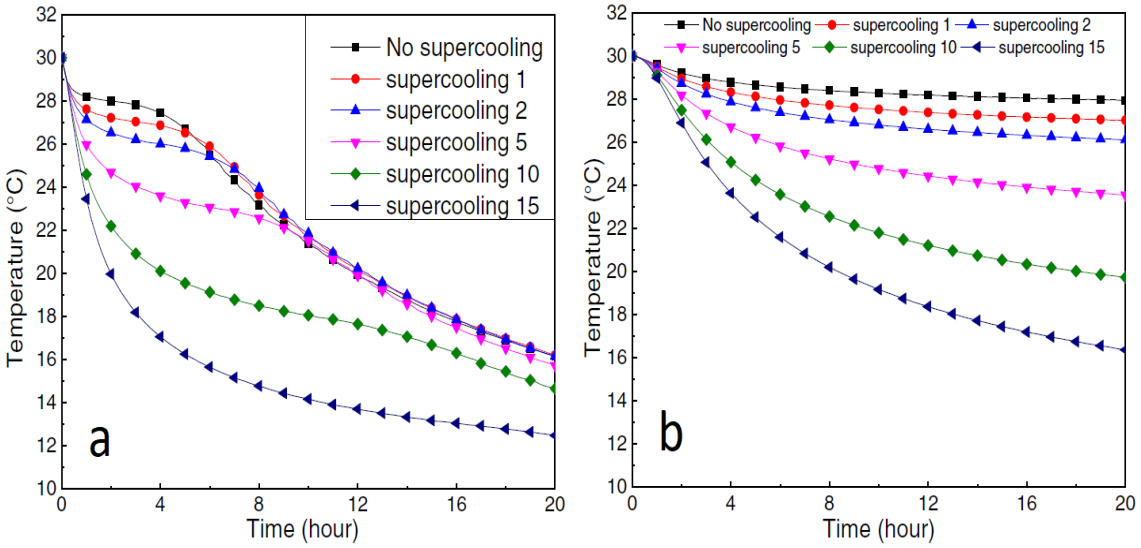

Figure 1.12 Temperature variation as a function of time for different degrees of supercooling at the same node having abscissa a) L/10, b) L/5, with t1=30°C, t2=0°C and a phase transition temperature range of 26–28°C [47]

Another effect of supercooling on the PCM is increasing the time required to discharge the stored heat. This phenomenon is due to the small temperature difference between the cold temperature applied at the heat exchange surface and the nucleation temperature T_n causing the PCM to approach the exchanger's temperature by sensible heat extraction. If $T_n$is lower than the exchanger temperature, the PCM fails to change phase, which means that the latent heat will not be extracted. The small temperature gradient just before reaching T_n causes a slow heat extraction. Using a numerical parametric study, Günther *et al.* [48] reproduce qualitatively the main effects of supercooling in the PCM. The PCM is connected on one side to a heat exchanger and on the other side to an insulating material. Another supercooling effect is represented by the phase change plateau's time span, which is the PCM buffering effect. By plotting the material average temperature versus time, the latent heat can be detected by a plateau of constant temperature. Increasing the degree of supercooling has several effects on the PCM behavior. First, the length of the plateau during which the release of latent heat takes place decreases meaning that less latent heat is released at T_m. In the case of severe degree of supercooling this plateau vanishes. Second, the temperature rise due to latent heat release becomes sharper, which causes problems in the performance of an application by releasing a sudden amount energy causing a sharp temperature variation. Moreover, this behavior causes numerical problems in simulation. Third, the instant of onset of solidification becomes late. Finally, the temperature of the PCM approaches the temperature of the node of heat exchanger, which decreases heat transfer rate between the PCM and the exchanger.

Even if the supercooling effect is inconspicuous, it does not mean its absence and it should be taken into account in numeral modeling since it may have a major impact on the heat transfer rate [49]. As shown above, the two main drawbacks of supercooling presence in heat storage systems are the shift in the phase change temperature, the reduction of the amount of useful latent heat energy and even its absence in some cases. Any loss in the latent heat is a loss of the useful heat and a decrease of the system's efficiency. The sudden and sharp increase of temperature due to latent heat release contradicts with the

PCM goal to reduce sharp energy demand variation. This phenomenon, if not taken into consideration, can cause severe effects on the PCM performance.

1.4 Factors affecting supercooling

Generally, the presence of chaotic and unexpected supercooling in an application is not recommended. Handling and controlling this phenomenon requires a good knowledge of the factors responsible for its presence. Precisely knowing the role of each factor and of the PCM behavior with their variations is essential to understand the basis of supercooling control. Controlling supercooling can be either increasing the degree of supercooling if its presence is desired, or decreasing it as much as possible if not. In this section, a number of important factors that have a direct responsibility in changing the degree of supercooling is presented.

1.4.1 Volume of the liquid

The dimensions of the PCM container have a direct influence on the degree of supercooling, where a decrease in the sample's volume generally increases the degree of supercooling. Figure 1.13 shows the results obtained by Adachi *et al.* [50] of the experiments done on 99% pure Erythritol. The results reveal that decreasing the PCM container's volume from 16cm^3 to 0.025cm^3 increases the degree of supercooling of erythritol from 48K to 88K. As the volume of the container decreases, the solidification initiation shifts toward the surface of the container. In this way, the influence of suspended impurities in the PCM on the solidification initiation decreases compared to the influence of the container's wall. Similarly, the supercooling in metals is influenced by volume change, where a change from mm^3 to µm^3 scale may increase the degree by a factor of 3 [51]. Dumas *et al.* [52] found an increase of the supercooling degree in benzene from 19.5K to 71.5K when the volume decreased from 1cm^3 to few cubic micrometers. The same influence is observed for organic bodies [52]. Lafargue *et al.* [53] found crystallizations at a temperature of -40.5°C and -14°C for a water container of a few cubic micrometers and 10mm^3 respectively.

Conversely, when the supercooling effect is required, the use of a single volume of high dimensions should be avoided, especially in applications that seek longer-term storage. Indeed, such a volume has many germination sites, which facilitates crystallization and risks releasing all of the stored energy as soon as crystallization initiates. It then becomes necessary to compartmentalize the storage. Chen S.L. and Chen C.L. [54] studied the probability of crystallization per sample. They found that with a larger size sample, the probability of crystallization increases. The best solutions in this area remain the encapsulation or emulsion processes, where the material is divided into microscopic portions serving in increasing the heat exchange surface and improving heat exchange. Each capsule then has a reduced number of impurities, which limits solidification and accentuates the degree of supercooling.

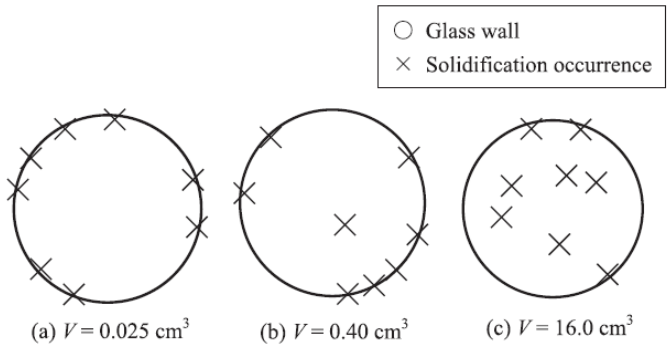

Figure 1.13 The position of solidification initiation for three different volumes having a measured degree of supercooling for the same PCM of a) 88°C, b) 58°C and c) 48°C [50]

When the mass of material is sufficiently low, a new phenomenon may appear, in particular during imposed thermal cycles. Due to the low number of impurities, crystallization is not possible until reaching a very low temperature corresponding to a very high degree of supercooling. However, the lower temperature of the sample also increases its viscosity, until it evolves into an amorphous solid. It is then necessary to wait until the material is heated again to allow the release of the stored energy. This phenomenon is called cold crystallization**.** Nakano *et al.* [53] finds that at a cooling rate of 1K/min of erythritol, the crystallization of 4.5g is possible at around 24°C while a mass of 3.5g remains supercooled till -50°C and doesn't crystallize until the temperature rises to -14°C approximately.

1.4.2 Rate of cooling

The rate of cooling directly affects the degree of supercooling on one hand, and the time spent in supercooling state on the other hand. Taylor *et al.* [55] conducted an experiment on commercial hydrated calcium chloride salts known as PC25 and PC29. As shown in Figure 1.14a, the degree of supercooling increases with the increase of the cooling rate. The cooling rate corresponds to the slope of the curves in Figure 1.14b before reaching the melting temperature and entering supercooling. So, as the bath temperature decreases, the cooling rate increases and the degree of supercooling increases too. Figure 1.14b confirms the observation of Figure 1.14a, where an increase in the degree of supercooling is observed for samples cooled with higher rates. It can be seen that the minimum temperature, reached before the initiation of solidification, decreases as the cooling rate increases. The figure also shows that the nucleation is delayed as the cooling rate decreases that is the PCM remains in supercooled state for a longer period. For example, the crystallization of samples cooled by 0°C and 20°C baths, corresponding to cooling rates of 166.3°C/min and 31°C/min respectively, is delayed for about 100s and 1400s respectively. In other words, this figure shows that decreasing the cooling rate decreases the degree of supercooling and delays nucleation initiation. This result is also observed in the experimental study done by Chen *et al.* [56] on water inside horizontal cylinders. Moreover, holding the PCM at a lower temperature increases the probability of solidification as shown in Figure 1.14b. This observation is also highlighted in the experiments of Dannemand *et al.* [57] on 10 samples sodium acetate trihydrate, where 73% of the containers remained supercooled at a degree of supercooling $\Delta T = 23K$, while only 42% remained in this metastable state at $\Delta T = 45K$.

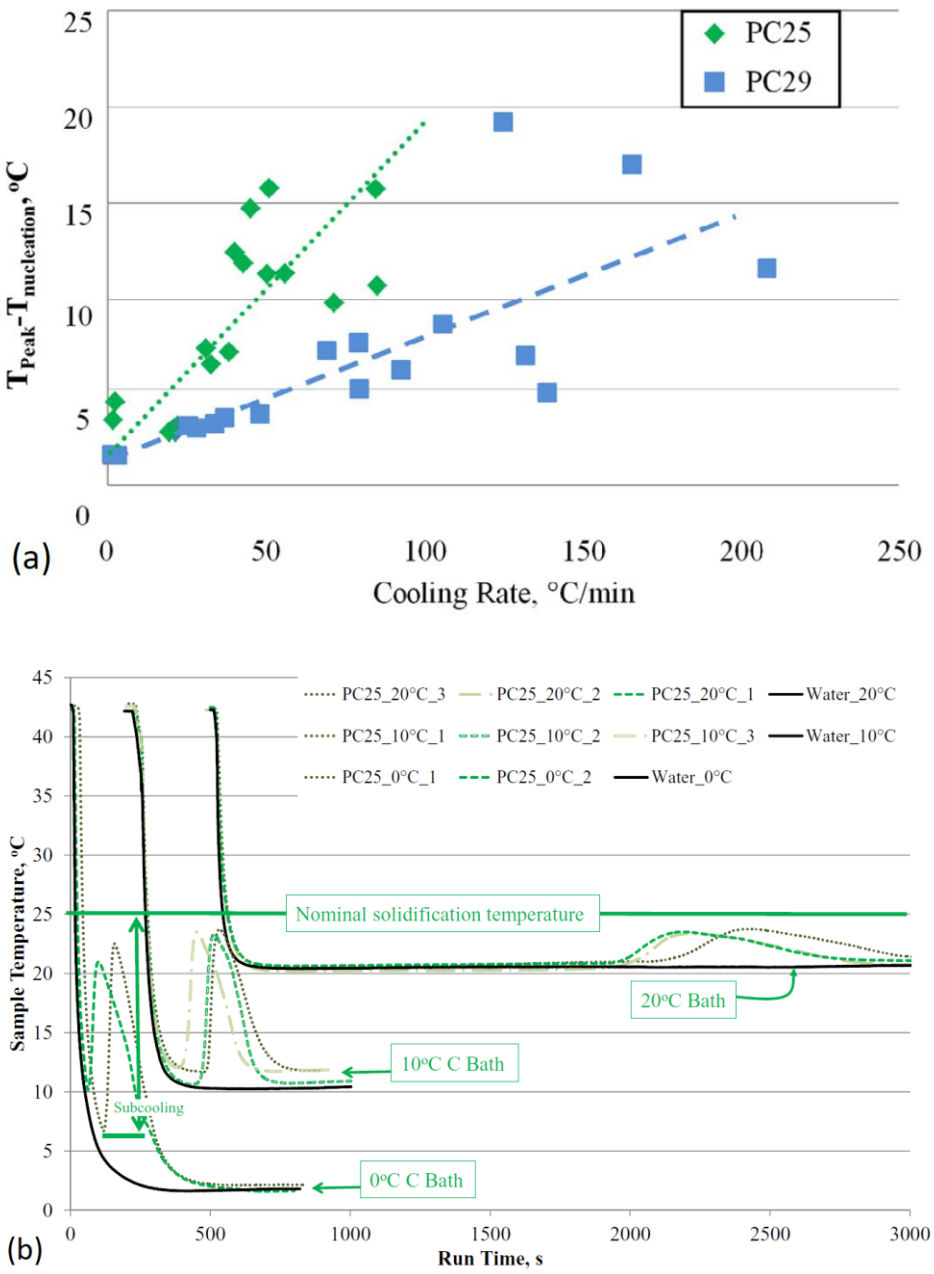

Figure 1.14 Plots showing (a) the variation of degree of supercooling as a function of cooling rate, (b) instantaneous temperature for PCM cooled in different bath temperatures [55]

The effect of coolant temperature and capsule's material on the probability of nucleation of encapsulated water is shown in Figure 1.15 [45]. The capsule material is represented by its thermal conductivity and roughness. By comparing the cases having similar surface roughness, the plot shows that the probability of nucleation decreases with decreasing cooling rate and with lower thermal conductivity materials. In other words, to reduce supercooling in an application having low cooling rate recommends using materials having high thermal conductivity. The cooling rate is also dependent on the surface of heat transfer. There are several passive and active techniques used to enhance the heat transfer rate [58]. An example of passive technique is adding fins to increase the heat transfer area. On the other hand,

adding a certain percentage of additives can also increase the thermal conductivity of a PCM as reported by Kant *et al.* [59]. Asgari *et al.* [60] studied the effect of fin structure and thickness on the heat transfer rate in addition to using nanoparticles. They showed that thin branch-shaped fins and nanoparticles with 0.04 volume fraction help in increasing contact surface area and thus the heat transfer rate.

From Figure 1.10, the cooling rate, CR, can be obtained by evaluating the temperature variation of capsule's internal wall T_{Iw}, from the beginning until the end of supercooling or by dividing the degree of supercooling, ΔT_S, by the duration of supercooling, t_s, [45]:

$$CR = \frac{\sum_{i=1}^{n} CR_i}{n} = \frac{\sum_{i=1}^{n} \frac{((T_{Iw})_i - (T_{Iw})_{i-1})}{t_s}}{n} \qquad CR = \frac{\Delta T_S}{t_s} \tag{1.1}$$

where i is the index of the measurement and n is the total number of measurements.

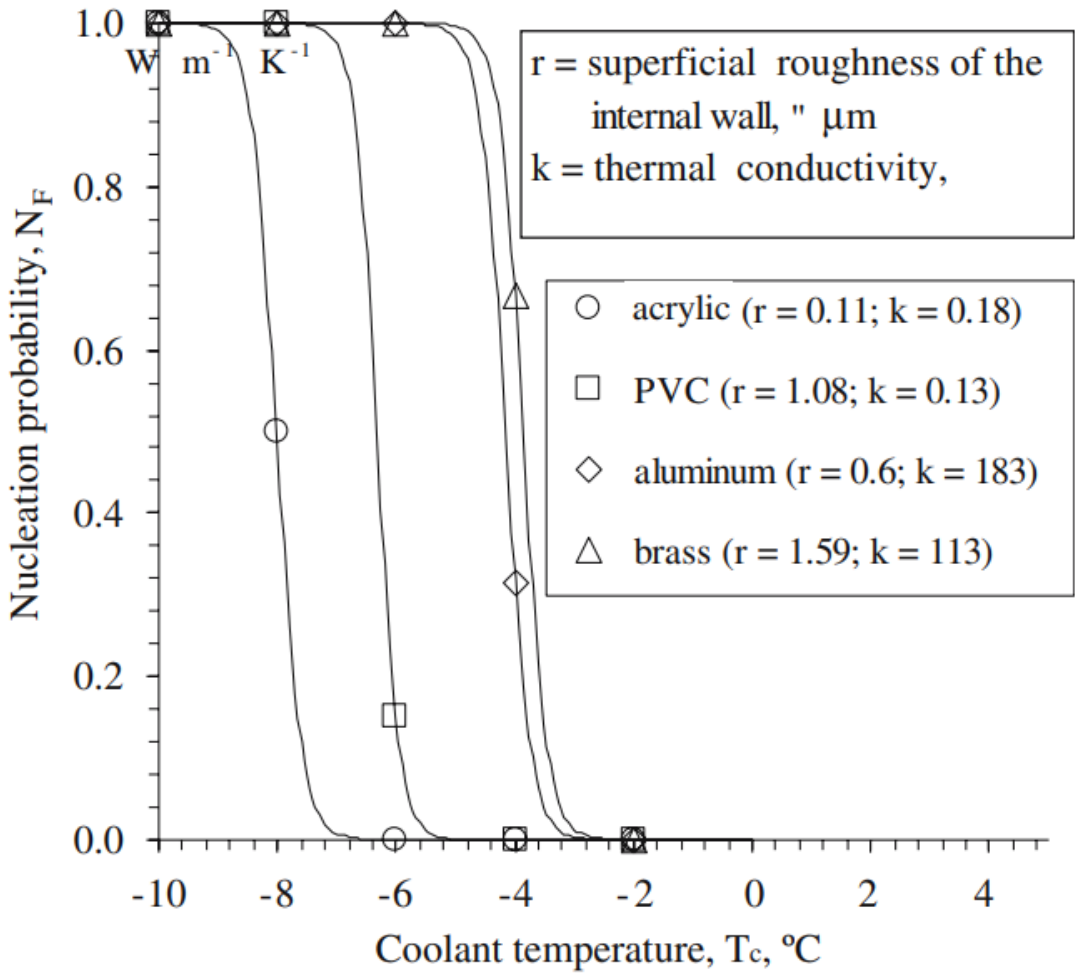

Figure 1.15 Variation of nucleation probability as a function of cooling temperature for materials with different thermal conductivities and various roughness of the internal wall [45]

Figure 1.16 shows the time spent in supercooled state for four different containers. Regardless the thermal conductivity and wall roughness of the container, Guzman *et al.* [45] obtained the same results as Taylor *et al.* [55] concerning the supercooling period: the time spent in supercooled state increases as the cooling rate decreases. As the rate of cooling increases, it becomes dominant over other factors, where the graph becomes confined.

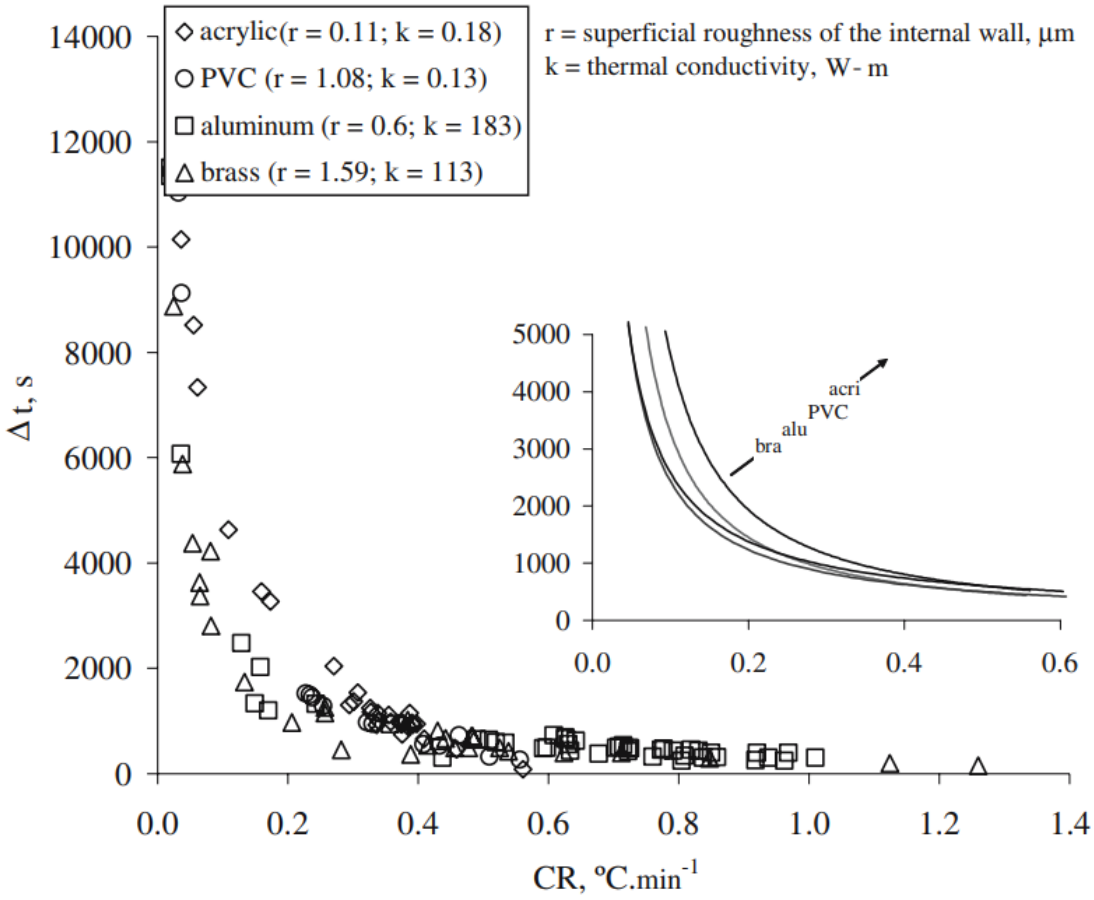

Figure 1.16 Time spent in supercooling state for different materials as a function of cooling rate. r is the container surface roughness and k is the thermal conductivity [45]

1.4.3 Thermal history of the PCM

The degree of supercooling is directly affected by the PCM history which has an impact on crystal growth, nucleation and their properties [61]. This dependence can be illustrated as a relationship between the degree of supercooling and the degree of over-heating (ΔT_h). The degree of superheating is given by $\Delta T_h = T_{PCM} - T_m$. This relationship has been studied for different (semi)metals (Sn, Bi, Ga) [53] and alloys [62]. Figure 1.17a shows this relation, where the degree of supercooling changes sharply beyond a certain value of degree of superheating. In a molten metal, the imbedded impurities may stay in solid clusters. Heating the melt above a critical temperature, will lead to the melting of these impurities and change their structure later. In addition to that, metals tend to change their physical properties depending on their thermal history and temperature variation. For example, Rudolph *et al.* [63] show that the degree of supercooling changes according to the time spent by the PCM at molten phase as shown in Figure 1.17b.

In addition to the before mentioned effect, Mei and Li [64] results show a significantly reduced melting temperature of Al encapsulated in Al_2O_3 after several cooling-heating cycles.

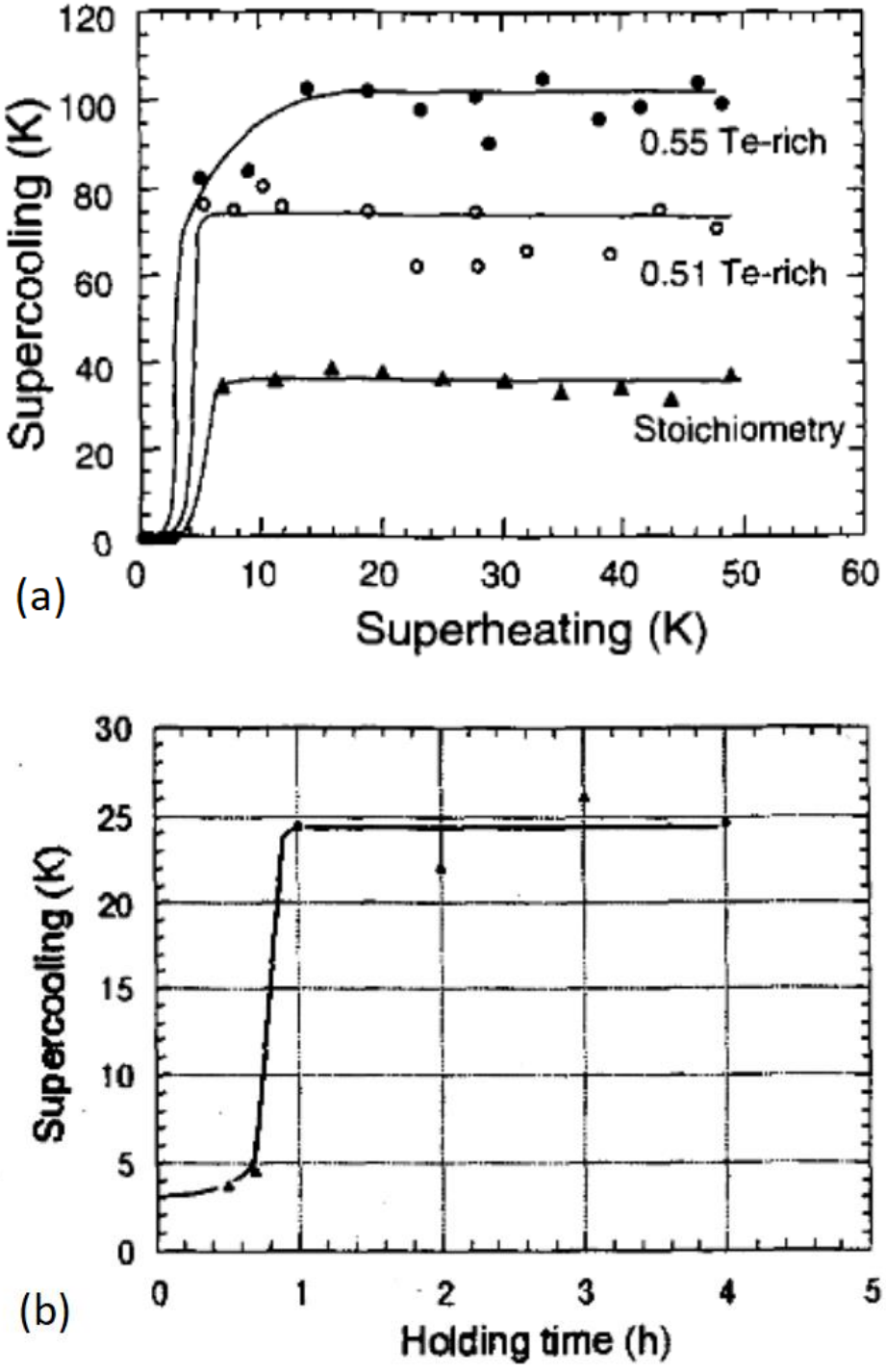

Figure 1.17 Variation of the degree of supercooling as a function of (a) degree of superheating of CdTe for stoichiometric, 1% and 5% excess mole fraction of Te, (b) holding time at 10°C superheated state of stoichiometric CdTe [63]

Fatty acids are known for their low degree of supercooling and large applications in different heat storage systems. Fatty acids have a threshold temperature above which if heated and held for a given time, the alkyl chain becomes more mobile and the molecular clusters break apart [65]. Upon cooling, the clusters do not reform quickly causing a barrier to nucleation that leads to supercooling. The obtained results by Noël *et al.* [65] are in agreement with those of Rudolph *et al.* [63] and show the significant difference in the degree of supercooling between samples heated above the threshold temperature and others that are not. Figure 1.18 shows the influence of holding dodecanoic acid at a temperature above its melting temperature. The figure shows that, as the difference between the holding temperature and the melting temperature increases, the degree of supercooling increases too. For a 125°C holding temperature, a dramatic change in the degree of supercooling is observed, which approximately corresponds to the above mentioned threshold temperature. Similarly, the probability of crystallization of emulsions varies with the number of cooling-heating cycles [66], [67].

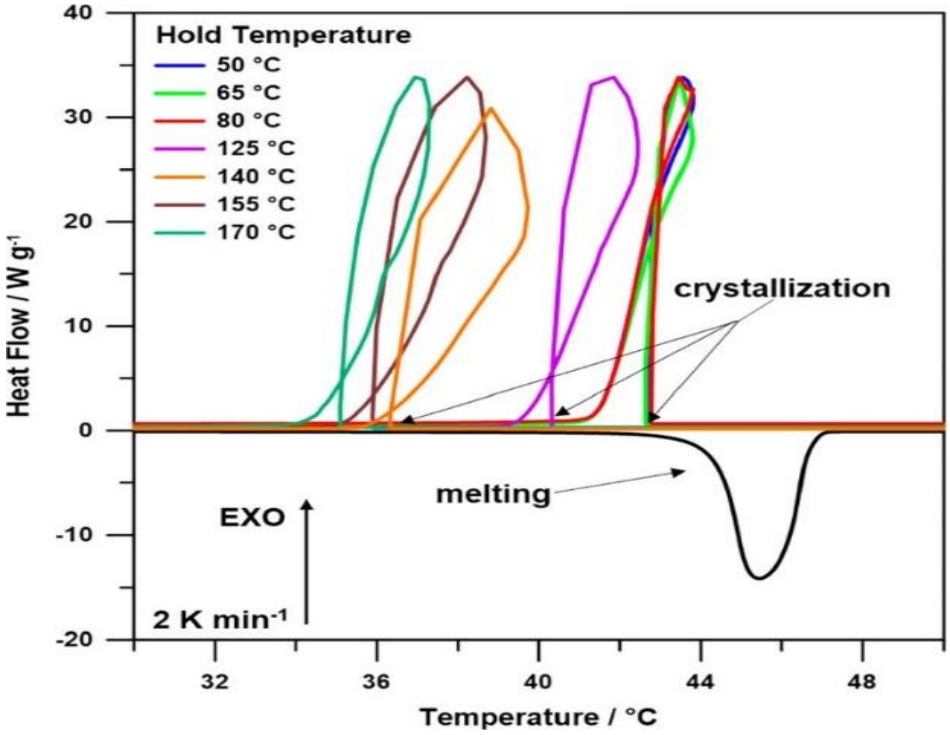

Figure 1.18 Thermal cycling of dodecanoic acid [65]

For the case of salt hydrates, Wada *et al.* [68]–[70] performed studies on sodium acetate trihydrate (SAT), by investigating its thermal stability after several cooling-heating cycles. SAT has a melting temperature of 58°C and is used in solar heating systems. SAT can undergo stable supercooling if extra heat is needed. The problem comes from the phase separation during supercooling and the probability of solidification of the supercooled SAT. Indeed, melting phase separation can affect the solubility, volume and density, which in turn may cause a change in the thermal conductivity, heat transfer rate and the amount of latent heat available for the next cycle. Some solutions consist of adding excessive water, thickening agents or mixing. However, although adding water or thickening agents is helpful, attention should be given to the functioning range of the system and the change in the properties of the SAT solution, such as melting temperature, density and thermal conductivity. After each thermal cycle, part of SAT solidifies and precipitates, which also eventually leads to a change in the properties. In [68]–[70], the

probability of solidification decreased to zero upon heating above 80°C, due to the melting of the entire precipitated solid. Similar results are obtained by Fashandi and Leung [71], where heating the encapsulated SAT in nanocapsules above 70°C causes a significant increase of the supercooling degree as shown in Figure 1.19. In addition, the use of sodium dodecyl (SDS) as a thickening agent decreases the degree of supercooling to almost zero as shown in Figure 1.20. Furthermore, the particle size of the SAT powder used to prepare the solution also has an effect on the degree of supercooling as shown in Figure 1.21. The increase of the particle size interferes in increasing the degree of supercooling. This may be explained by a change in the solution homogeneity and by a phenomenon called sifting due to the phase segregation of the solution. Thus, heating history can play a role in changing the initial properties of the used PCM by changing size and structure of additives, thickening agents or impurities.

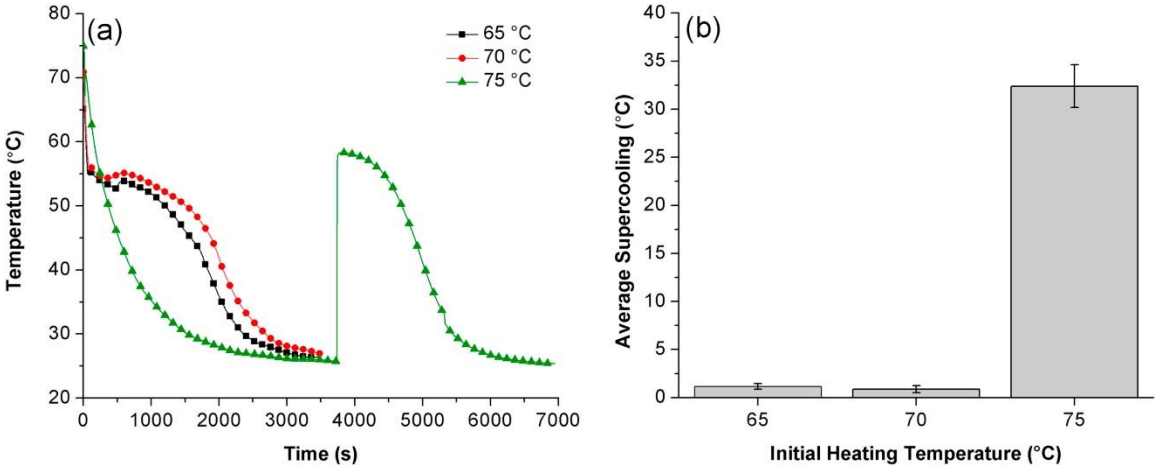

Figure 1.19 Effect of preheating a) on the temperature variation as a function of time during cooling and b) on the degree of supercooling [71]

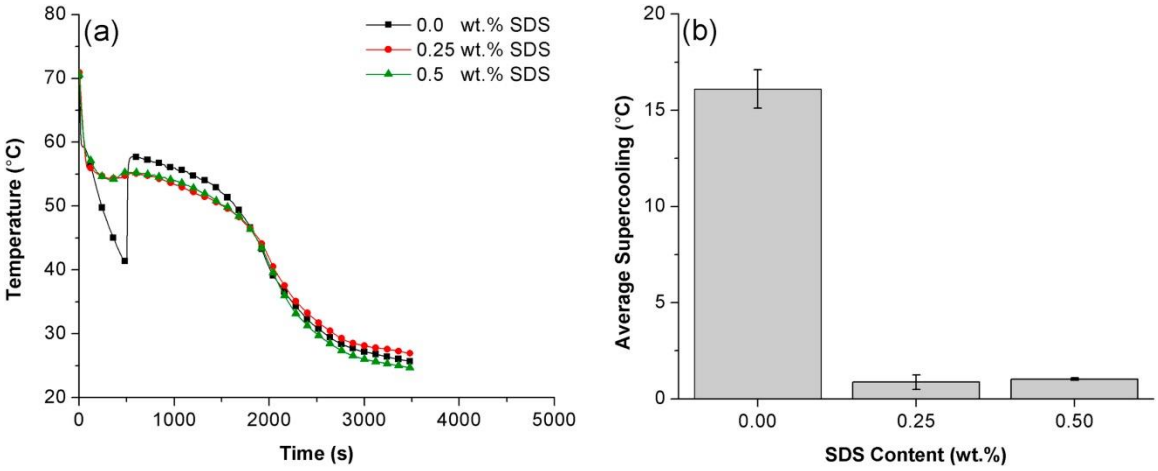

Figure 1.20 Effect of percentage of thickening agent a) on the temperature variation as a function of time during cooling and b) on the degree of supercooling [71]

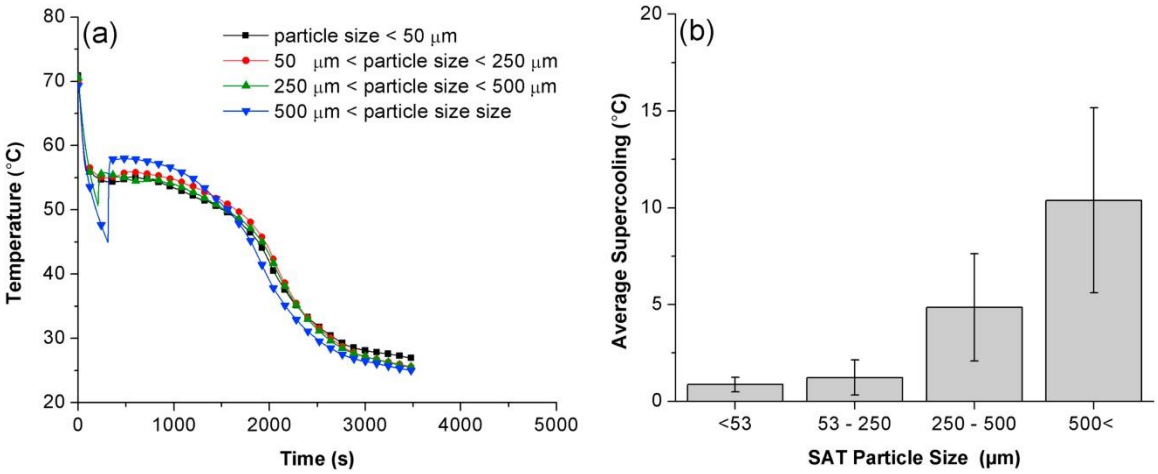

Figure 1.21 Effect of particle size a) on the temperature variation as a function of time during cooling and b) on the degree of supercooling [71]

The threshold temperature may also vary with respect to the history of the PCM. Johansen [72] also supposes that this is due to a decrease in the number of potential germination sites or to phase separation due density difference. In Wada's study mentioned above [68]–[70], a zero probability of nucleation is achieved by heating up to 80°C a sample kept 30 minutes at 20°C, while a sample left for 96 hours at 20°C requires heating up to 93°C. However, beyond this time, this threshold temperature remains constant. On the other hand, cooling the solid to -20°C for 96 hours requires a reheat to 83°C.

1.4.4 Roughness of contact surface

The degree of supercooling is directly affected by the surface roughness of the container that embraces the PCM. Rough surfaces are a factor in lowering and even eliminating supercooling [73] because the surfaces trigger the initiation of solidification. This direct impact can be observed using several techniques. The first technique is introducing the PCM in a very smooth container and scratching one of its sides. The second technique is performing the same experiment on a number of identical samples contained in containers of different roughness. The degree of supercooling is lower in the case of more rough surfaces. Below are couple of experiments performed on different PCM.

According to Faucheux *et al.* [74], the degree of supercooling of aqueous solution of ethanol decreases when changing the surface roughness of aluminum tubes from 0.63µm to 13.3µm. The used container has rough walls while the bottom has a smooth glassy poly (methyl methacrylate), PMMA. In all the experiments, the crystallization initiated from the container's rough surface rather than the smooth bottom. In this study, a correlation between the degree of supercooling and the surface roughness is demonstrated by the aid of the free energy variation equation and the conditions to permit nucleation and then phase change. This correlation is given by equation (1.2) [74]:

$$\Delta T_S = \sqrt{\frac{8\pi\gamma^3 T_m^2}{3H^2\Delta G_n}\left(1 - cos\frac{\alpha}{2}\right)} = aRa^b \qquad (1.2)$$

where γ is the surface tension, ΔG_n is the free energy variation and α is the angle of notch where crystallization takes place. H is the latent heat and Ra is the surface roughness. a and b are constant coefficients, obtained from experimental results by least square optimization [74]:

$$\Delta T_S = 7.15 Ra^{-0.196} \quad (1.3)$$

Similar results are reached by Sakurai *et al.* [75] for silver electrode embedded with SAT crystals and immersed in a supercooled SAT. In this experiment, low values of roughness of Ag anode leads to stability of the supercooled solution of SAT, while a higher surface roughness leads to a larger number of repeated cycles of electrical nucleation allowing the controlled release of latent heat.

Akio *et al.* [76] studied supercooling in water. In the first experiment, one side of the smooth container is scratched and as a result, crystallization is first formed on this rough scratched surface. In the second study, water contained in rough surfaces containers experience a lower degree of supercooling.

1.4.5 Additives

Nucleation is a spontaneous process that requires energy to solidify the liquid phase on its surface. The free energy volume, that is proportional to the heat released by crystallization, and surface energy are two components in competition forming a barrier between the liquid and crystallization. There are two types of nucleation: homogeneous and heterogeneous. In the homogeneous nucleation, the impurities have no impact on the nucleation process, which happens suddenly by generating crystal nuclei. On the other hand, the presence of any impurity or contact surface with the liquid play a role in triggering the nucleation process. This latter phenomenon is called heterogeneous nucleation.

The surface of nucleation is not limited to the surface of the container. Impurities embedded in the solution are also surfaces for nucleation. In this case, the role of nucleating agent additives becomes more obvious in increasing the nucleation probability, where additives increase the area of nucleating surfaces with the PCM. Chen *et al.* [56] confirmed the before mentioned researches by experiments done on water. Their results show that additives with higher surface roughness had a greater effect in decreasing degree of supercooling.

As mentioned in subsection 1.4.4, the contact surfaces with the PCM motivate crystallization. Any impurity present in the PCM reduces the required free energy surface and can be a surface for crystallization onset. From this concept, additives are chosen with a melting point higher than that of the PCM to ensure that they are solid during the phase change interval. Fashandi and Leung [71] studied the supercooling of SAT. In their study, a bio-derived nucleating agent called Chitin nanowhisker is added to the SAT contained in nanocapsules. The addition of nucleating agent affects significantly the degree of supercooling as shown in Figure 1.22a. The sample with no nucleating agent suffers from a severe degree of supercooling and does not solidify. However, the addition of the additive triggers solidification. First, the degree of supercooling decreases as percentage of additive increases to a given value after which it starts to increase again. The estimated value, at which the supercooling degree reaches the minimum value, is 1% as shown in Figure 1.22b. This is most probably due to the gathering of the additive particles, which leads to a decrease in the density of nucleation sites.

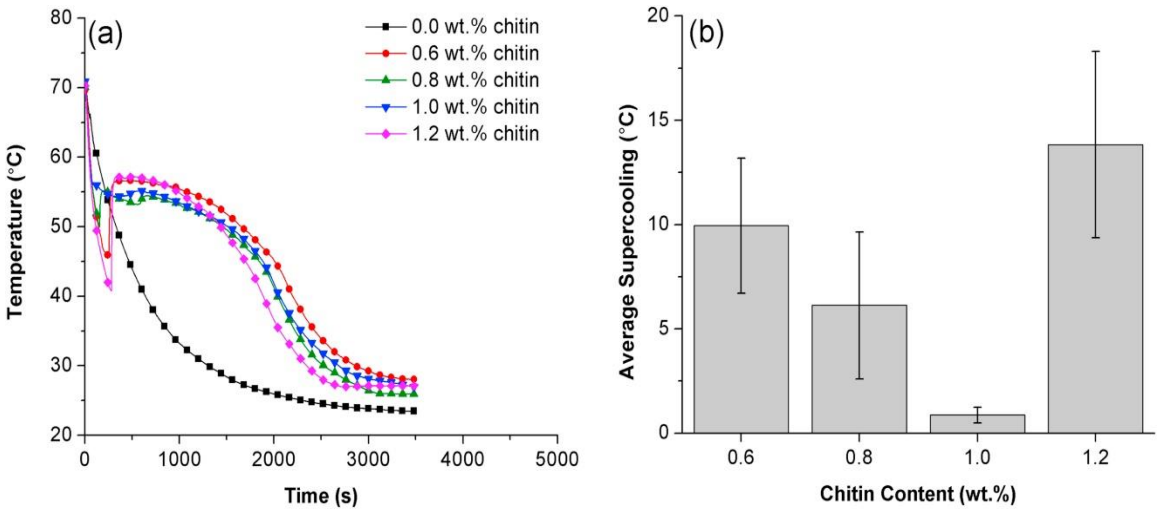

Figure 1.22 Effect of the percentage of nucleating agent a) on the temperature variation as a function of time during cooling and b) on the degree of supercooling [71]

Shamberger *et al.* [77] added $Cu_3(OH)_5(NO_3)\cdot 2(H_2O)$ as an additive to decrease the degree of supercooling of $LiNO_3\cdot 3H_2O$. The addition of additive decreased the degree of supercooling by up to 66%. On the other hand, it increased the stability of $LiNO_3\cdot 3H_2O$ for more than 900 phase change cycles and increased the aging at elevated temperature for extended periods of time (t > 250 days). Chen *et al.* [54] studied, for different cooling rates, the effect of nucleation agents by using several types of additives such as lead iodide, mud powder, silver iodide and river sand. A significantly lower degree of supercooling is noted for water with additives in comparison with pure water. Silver iodide shows an attractive performance while sand is the most recommended for its cheap price. Crystal mesh size variation of the additives must be 15% less than that of PCM to be crystallized [69,70]. This result has been the scope of work of many studies. Lane *et al.* [80], for example, studied the nucleating agents of several materials that distinguish them into isostructural materials or not. These studies report the difficulty to define the type and amount of the nucleating agent to be added to a specific PCM. Crystallization is not dependent only on these agents, and studying under all circumstances is time consuming. The most used variable is the nucleating agent-PCM mass fraction. Beaupere *et al.* [18] presented the results of several PCM nucleating agents' effectiveness in Figure 1.23. Similar to other conclusions, the best percentage to use is about 1%. This result is the average obtained by several researchers as shown in Table 1.2.

Table 1.2 Set of experiments showing the effect of different additives on the degree of supercooling (ΔT_s) and on the latent heat of fusion (H) for different PCM

Author (year)	PCM	Additives		Results
Hu *et al.* [81] (2011)	Sodium acetate trihydrate	Nothing added		$T_m = 58\ °C$ $\Delta T_s = 17\ °C$ $H = 238.54\ kJ/kg$
		AlN nanoparticles	3 wt%	$\Delta T_s = 2.4\ °C$
		CMC*	4 wt%	

		AlN nanoparticles	4 wt%	$\Delta T_s = 1\ °C$
		CMC	4 wt%	
		AlN nanoparticles	5 wt%	$T_m = 52.5\ °C$ $\Delta T_s = 0\ °C$ $H = 227.54\ kJ/kg$
		CMC	4 wt%	
Li *et al.* [82] (2016)	$CH_3COONa{\cdot}3H_2O$	Nothing added		$T_m = 58\ °C$ $\Delta T_s = 28.3\ °C$
	$CH_3COONa{\cdot}3H_2O$–2%KCl			$T_m = 54\ °C$ $\Delta T_s = 9.2\ °C$
	$CH_3COONa{\cdot}3H_2O$–4%KCl			$T_m = 53\ °C$ $\Delta T_s = 3.5\ °C$
	$CH_3COONa{\cdot}3H_2O$–6%KCl			$T_m = 52\ °C$ $\Delta T_s = 3.1\ °C$
	$CH_3COONa{\cdot}3H_2O$–8%KCl			$T_m = 50\ °C$ $\Delta T_s = 7.1\ °C$
	$CH_3COONa{\cdot}3H_2O$–10%KCl			$T_m = 50\ °C$ $\Delta T_s = 9\ °C$
	$CH_3COONa{\cdot}3H_2O$–8%KCl	Nucleating agent: Al_2O_3 nanoparticles and 4 wt% CMC	0.5%	$\Delta T_s = 3..5\ °C$
			1%	$\Delta T_s = 0.1\ °C$
			2%	$\Delta T_s = 2.3\ °C$
			2.5%	$\Delta T_s = 4.6\ °C$
			3%	$\Delta T_s = 5.3\ °C$
Pilar *et al.* [83] (2012)	MgCl2·6H2O	Nothing added		$\Delta T_s = 36.8\ °C$ $H = 168.9\ kJ/kg$
		$SrCO_3$	0.5 wt%	$\Delta T_s = 14.2\ °C$ $H = 159.7\ kJ/kg$
			1 wt%	$\Delta T_s = 6.4\ °C$

				$H = 157.7\ kJ/kg$
			2 wt%	$\Delta T_s = 1.8\ °C$ $H = 112.3\ kJ/kg$
			3 wt%	$\Delta T_s = 1.2\ °C$ $H = 100\ kJ/kg$
		$Sr(OH)_2$	0.5 wt%	$\Delta T_s = 4.3\ °C$ $H = 149.4\ kJ/kg$
			1 wt%	$\Delta T_s = 5.2\ °C$ $H = 150.9\ kJ/kg$
			2 wt%	$\Delta T_s = 0.1\ °C$ $H = 111.4\ kJ/kg$
			3 wt%	$\Delta T_s = 0\ °C$ $H = 94.4\ kJ/kg$
		$Mg(OH)_2$	0.5 wt%	$\Delta T_s = 18.9\ °C$ $H = 160.1\ kJ/kg$
			1 wt%	$\Delta T_s = 18.9\ °C$ $H = 143.6\ kJ/kg$
			2 wt%	$\Delta T_s = 14.8\ °C$ $H = 102.4\ kJ/kg$
			3 wt%	$\Delta T_s = 16\ °C$ $H = 108.2\ kJ/kg$
Ushak *et al.* [84] (2016)	bischofite	Nothing added		$\Delta T_s = 36$ °C $H = 115.5\ kJ/kg$
		CaO	0.5 wt%	$\Delta T_s = 16.3\ °C$ $H = 95.3\ kJ/kg$
			1 wt%	$\Delta T_s = 19.9\ °C$ $H = 57\ kJ/kg$
			1.5 wt%	$\Delta T_s = 21.4\ °C$ $H = 50.8\ kJ/kg$

			2 wt%	$\Delta T_s = 20.4\ °C$ $H = 46.6\ kJ/kg$
			3 wt%	$\Delta T_s = 11\ °C$ $H = 28.5\ kJ/kg$
		$Sr(OH)_2$	0.5 wt%	$\Delta T_s = 18.2\ °C$ $H = 104.4\ kJ/kg$
			1 wt%	$\Delta T_s = 2.9\ °C$ $H = 36.6\ kJ/kg$
			1.5 wt%	$\Delta T_s = 20.4\ °C$ $H = 73.1\ kJ/kg$
			2 wt%	$\Delta T_s = 18.7\ °C$ $H = 78.6\ kJ/kg$
			3 wt%	$\Delta T_s = 0\ °C$ $H = 71.1 kJ/kg$
		$SrCO_3$	0.5 wt%	$\Delta T_s = 23.7\ °C$ $H = 118.8\ kJ/kg$
			1 wt%	$\Delta T_s = 22.4\ °C$ $H = 106.8\ kJ/kg$
			1.5 wt%	$\Delta T_s = 15.7\ °C$ $H = 92.3\ kJ/kg$
			2 wt%	$\Delta T_s = 5.51\ °C$ $H = 94.5\ kJ/kg$
			3 wt%	$\Delta T_s = 1.7\ °C$ $H = 89.3\ kJ/kg$
		$LiOH.H_2O$	0.5 wt%	$\Delta T_s = 24.2\ °C$ $H = 99.7\ kJ/kg$
			1 wt%	$\Delta T_s = 18\ °C$ $H = 84.9\ kJ/kg$
			1.5 wt%	$\Delta T_s = 21.9\ °C$

				$H = 82.7\ kJ/kg$
			2 wt%	$\Delta T_s = 23.6\ °C$ $H = 85.6\ kJ/kg$
			3 wt%	$\Delta T_s = 18.3\ °C$ $H = 63.5\ kJ/kg$
		Li_2CO_3	0.5 wt%	$\Delta T_s = 27.8\ °C$ $H = 85.9\ kJ/kg$
			1 wt%	$\Delta T_s = 18.8\ °C$ $H = 76.3\ kJ/kg$
			1.5 wt%	$\Delta T_s = 22\ °C$ $H = 76.3\ kJ/kg$
			2 wt%	$\Delta T_s = 19.1\ °C$ $H = 64.1\ kJ/kg$
			3 wt%	$\Delta T_s = 25.6\ °C$ $H = 59.9\ kJ/kg$
Sutjahja *et al.* [85] (2016)	$CaCl_2.6H_2O$	Nothing added		$\Delta T_s = 1.8\ °C$ $Induction\ time^* = 178\ min$
		$SrCl_2.6H_2O$ (1 wt%)		$\Delta T_s = 0.3\ °C$ $Induction\ time = 19\ min$
		$BaCO_3$ (0.5 wt%)		$\Delta T_s = 0.95\ °C$ $Induction\ time = 50\ min$
		K_2CO_3 (0.5 wt%)		$\Delta T_s = 0.92\ °C$ $Induction\ time = 107\ min$

* CMC: Thickener: Carboxyl methyl cellulose

* Induction time is the time required for temperature to rise from nucleation temperature to melting temperature due to latent heat release and initiation of solidification

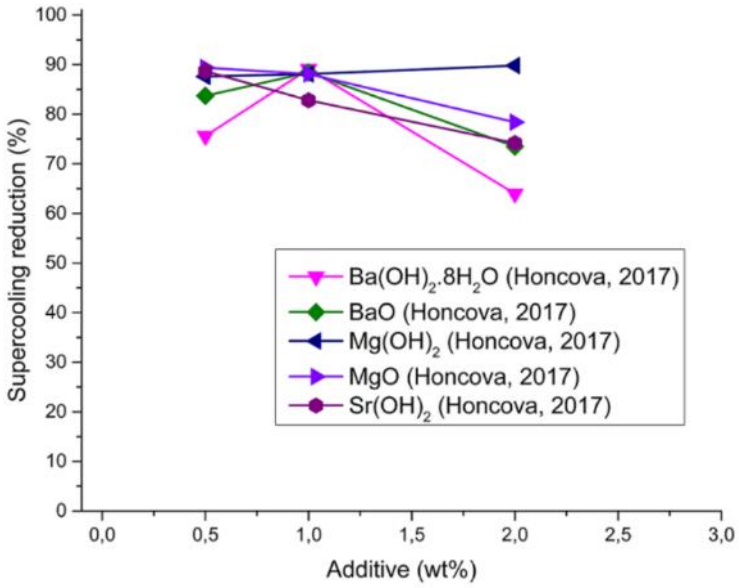

Figure 1.23 Percentage of supercooling reduction as a function of several additives percentage [18]

In a PCM application, using the appropriate concentrations of nucleating agents is an effective method used to reduce or even eliminate supercooling along with triggering crystallization in a shorter period. In the study of Liu *et al.* [86] on a nanofluid, the degree is reduced by 69.1% and nucleation time is shortened by 90.7%.

The above subsections present the main factors that contribute to change the behavior of a supercooling prone PCM. These factors are considered of great importance because they appear in almost all applications, experiments and even create problems in modeling the PCM behavior with supercooling. Table 1.3 summarizes these factors by presenting the results of a number of experiments performed on different types of PCM. It is worth noting that there are plenty other factors that interfere in influencing supercooling such as stirring, magnetic field, electric field, mechanical vibrations or shocks. These factors are not mentioned in this chapter, but more details can be found in [19].

Table 1.3 Summary of major experimental results on supercooling over the past 50 years

Author (Year)	Body/material	Method/measuring technique	Results
Packard *et al.* [24] (2001)	Turtles	Statistical analysis: Factorial analysis of variance (ANOVA)	Lower ambient temperatures improve the capacity for supercooling of acclimated turtles, the ingestion of particle of soil (as nucleating agents) may reduce the degree of supercooling.
Scholander *et al.* [25] (1971)	Fish	Thermometer	- Supercooling serves in the survival of the fish. - Ice formation can be triggered by contact with a freezing surface.
Hacker *et al.* [27]	Plants	Infrared thermography	- Ice formation is triggered by reaching minimum temperature and is affected by the duration of supercooling state. - Only the plants in supercooled state survived, where plants use hydrophobic barrier to prevent nucleation in its sensitive parts.
Wisniewski *et al.* [31] (2008)			
Fakuma *et al.* [35] (2012)	Fish meat	- Statistical analysis: one-way ANOVA - Measuring and analysis tools	- Fish meat achieves supercooling state by slow cooling due to insufficient kinetic energy necessary for the formation of ice nuclei.
Ando *et al.* [37] (2007)			
You *et al.* [36] (2020)	Beefsteak		- Beef steak achieves supercooling by pulsed electric field (PEF) and oscillating magnetic field (OMF).
Jeremiah *et al.* [33] (2001)	Muscle steak	- Low-temperature incubators - Temperature data loggers	- Stability of supercooling varies according to the material to be conserved. - Instability of supercooled state: any shock can trigger solidification.

Duun *et al.* [38] (2008)	Fillet salmon	- pH meter - Reflectance spectrophotometry	- Storing at refrigeration and freezing temperatures shows very rapid muscle deterioration, which causes softening. - Storing in supercooled state shows similar color, odor, drip loss and shear as fresh food. - Storing in supercooled state provides better quality (hardness) and increases storage life by limiting bacterial growth. - Drip loss is recorded during supercooling but it is not considered as a disadvantage. - Recommendations to use supercooling in preservation
James *et al.* [39] (2009) [17] (2011)	Garlic vegetables Sea food		
Yehya [43] (2015)	Paraffin based, organic 99% pure octadecane	Thermocouples, probes and meters	- Supercooling causes a vertical discontinuity in the temperature curve. - Increasing the cooling rates causes a higher degree of supercooling, however PCM stays in supercooled state for a shorter time. - Increasing the thermal conductivity increases the probability of nucleation. - Quantity of energy, needed to increase liquid's temperature to melting temperature, increases with the increase of supercooling degree.
Guzman et. al [45] (2005)	water		
Sandnes *et al.* [46] (2006)	Salt hydrates - Disodium hydrogen phosphate - Dodecahydrate sodium acetate trihydrate -STL-47		
Adachi *et al.* [50] (2014)	Organic 99% pure Erythritol	Differential scanning calorimetry (DSC) used to calculate latent heat and melting temperature	Time spent in supercooled state decreases as: - cooling rate increases - volume of container increases As the volume of the container decreases, solidification initiates from surface of container rather than impurities embedded in liquid.
Chen *et al.* a)[56] (1998)	Pure degasified water a) horizontal cylinders	Flow meters and thermocouples	

b)[87] (1998)	b) cylindrical capsules		Probability of nucleation increases as: - cooling rate increases - the volume container increases - the roughness of contact of surfaces increases Degree of supercooling decreases with: - decreasing the cooling rate - increasing the surface roughness - decreasing the particle size - adding thickening agents - adding additives, maximum reduction is obtained by adding 1% of additives Degree of supercooling increases dramatically by heating above a critical value - Stable supercooling is achieved when coolant temperature is higher than nucleation temperature - Crystallization starts from rough rather than smooth surface
Taylor *et al.* [55] (2016)	Calcium chloride hexahydrate-based salts PC25 and PC29	-T history method -Distilled water as a reference sample -Temperature measured by NTC thermistors	
Akio *et al.* [76] (1990)	Pure water	Thermocouples	
Fashandi and Leung [71]	Inorganic salt hydrate Sodium acetate trihydrate		
Faucheux *et al.* [74] (2006)	Organic Ethanol/water mixture	K-type thermocouples	- Concentration of the mixture has no significant effect on the degree of supercooling compared to roughness factor. - Power relation between the degree of supercooling and roughness is obtained.
Nakano *et al.* [53] (2015)	Organic- sugar alcohol 97% pure meso-Erythritol	Differential scanning calorimetry (DSC)	PCM in and around 2D mesoporous silica shows that as the pore diameter decreased: - amount of latent heat decreased - nucleation temperature increased

			Influence of thermal history on the behavior of PCM upon cooling and heating Heterogeneity of the solution induces surfaces for crystallization initiation.
Rudolph *et al.* [63] (1996)	Metals CdTe and PbTe	Direct temperature measure	The thermal history represented by the degree and time held at superheating affects: - the quality of the crystals - the crystal growth - degree of supercooling
Yin *et al.* [62] (2004)	Cast nickel-based super alloy M963	-X-ray diffraction measurement -ISM-6301F scanning electron microscope (SEM)	
Yang *et al.* [88] (2014)	Metal Pure Sn	DSC Dielectric measurements	Supercooling degree increases as the cooling rate increases until reaching a critical value of cooling rate after which the supercooling degree starts to decrease strongly depending on the volume of capsule and purity of PCM.
Mei and Li [64] (2016)	Metal Pure Al		Low cooling rate does not affect the supercooling degree.
Noël *et al.* [65] (2018)	Fatty acids - Octanoic acid - Dodecanoic acid - Tridecanoic acid - Hexadecanoic acid		Dependence of degree of supercooling on the degree of superheating, presence of a threshold temperature above which if heated, PCM undergoes significant degree of supercooling.

Zhou *et al.* [89] (2000)	Alloy metal Pure $Bi_{95}Sb_5$	Temperature measurement by thermocouple	Four factors affecting supercooling degree are investigated and listed from more to less important: - cooling rate - degree of superheating - number of cycles - soaking time
Johansen *et al.* [72] (2014)	Inorganic salt hydrate Sodium acetate trihydrate-water mixture	Heat conductivity measurement by Isomet heat transfer analyzer	- Graphite enhances the thermal conductivity of the mixture but does not affect the degree of supercooling. - Use of gelation agent to overcome the problem of phase separation over long periods of cycles. - The used gelation agent (carboxyl methylcellulose CMC) is affected by high temperatures causing its degradation and change in color.
Sakurai *et al.* [75] (2018)	Inorganic salt hydrate Sodium acetate trihydrate-water mixture	X-ray photoelectron spectroscopy- XPS Scanning electron microscopy- SEM	- Increasing the voltage applied to the Ag anodes immersed in the solution, decreases the time spent in supercooling state. - After 30000 cycles estimated by 10 years, the response to applied voltage becomes faster. - Roughness of the Ag surfaces affects the behavior of solution upon cooling. For a given interval of roughness, the behavior upon cooling is stable for repeated cycles.
Liu *et al.* [86] (2015)	Organic Water-based graphene oxide	Thermostatic water bath and thermocouple	Supercooling degree decreases when adding graphene oxide nano sheets. Structure of the sheet affects the onset of crystallization.

As presented above, it is clear that each factor has a direct impact on the degree of supercooling and this dependency is detailed as a function of each factor separately. However, some correlations exist between them and some factors have a higher impact. As an example, Figure 1.15 and Figure 1.16 show that as the thermal conductivity of a material increases, the impact of surface roughness on the probability of nucleation and time spent in supercooled state decreases. Moreover, some factors can affect PCM properties. For example, adding additives can change the thermal conductivity of the solution along with the ratio of the PCM volume compared to total volume, which in turn decreases the latent heat of the solution. When using a PCM, a set of procedures can be taken to control supercooling. These procedures should not prevent the PCM from performing its role. For example, in a thermal energy storage system, the procedures should not change the thermal conductivity, quantity of latent heat or melting temperature to a value outside the acceptable range, whereas in a preservation process, they should not cause a damage for preserved materials. It is essential to follow a combination of several techniques, where tradeoffs are done to obtain the optimal performance in terms of energy saving on one side and economical cost on the other side.

1.5 Challenges in modeling

Modeling is essential in almost all applications, where a well-modelled system gives fast and more accurate results than experiments. The advantage of modeling is the ability to track, at any time and any position of the model, the change of desired parameters and to apply desired conditions without facing the problem of devices' accuracy and effect of their presence on the system. This particularly suits an application with supercooling occurrence. However, modeling requires an accurate presentation of the system by means of mathematical equations. As previously mentioned, there are plenty of factors affecting supercooling. The correlation of these factors adds complexity and challenges to model this phenomenon, where any change of any factor can dramatically change the performance of the system. A set of theoretical equations exists and has been validated for pure elements, which is not the case for all PCMs used in thermal storage systems. For example, any impurity or surface roughness can play the role of surface for crystallization onset. Moreover, considering all the factors requires time and high computational cost. The following subsections present a set of common challenges that encounter when modeling supercooling and the methods developed by different authors to overcome these challenges.

1.5.1 Degree of supercooling and nucleation

The determination of crystallization initiation is still an open challenge. As shown above, the behavior of PCM changes for different supercooling degrees, where the crystallization onset depends on several factors and is sensitive to different circumstances. Different techniques are adapted to include the nucleation temperature in the models and simulations. The most used method is to preset the temperature of crystallization. The PCM stays liquid upon cooling until reaching the preset temperature. However, choosing that temperature is also challenging, so the used value is obtained from an experimental result or from the literature. Besides, using accurate values is challenging, because they are affected by several parameters, especially for impure PCMs. Some researches use a mathematical relation between the supercooling degree and the impurity fraction in the solution. To overcome this problem, Yehya [43] performed experimental studies on octadecane as PCM to obtain the real enthalpy curve and supercooling degree. In

buildings, octadecane contained in a Plexiglas enclosure is considered as an innovative technique, where the translucency of the PCM provides natural day light. The presence of soluble impurities lowers the melting temperature, widens the melting range and changes the heat flux curve as shown in Figure 1.24. This phenomenon is referred to as the "melting point depression" and this depression can be calculated according to the following relation [90]:

$$\Delta T_{am} = T_a - T_m = \frac{RT_a^2 X_i}{L_f} \tag{1.4}$$

where T_a and T_m are the melting temperatures for pure and impure PCM respectively and X_i is the impurity fraction. R is the molar gas constant and L_f is the molar heat of fusion.

The obtained values of melting temperature due to depression and degree of supercooling are implemented into a numerical model. When using the preset temperature method, experiments and simulations are done repeatedly to obtain accurate average solutions.

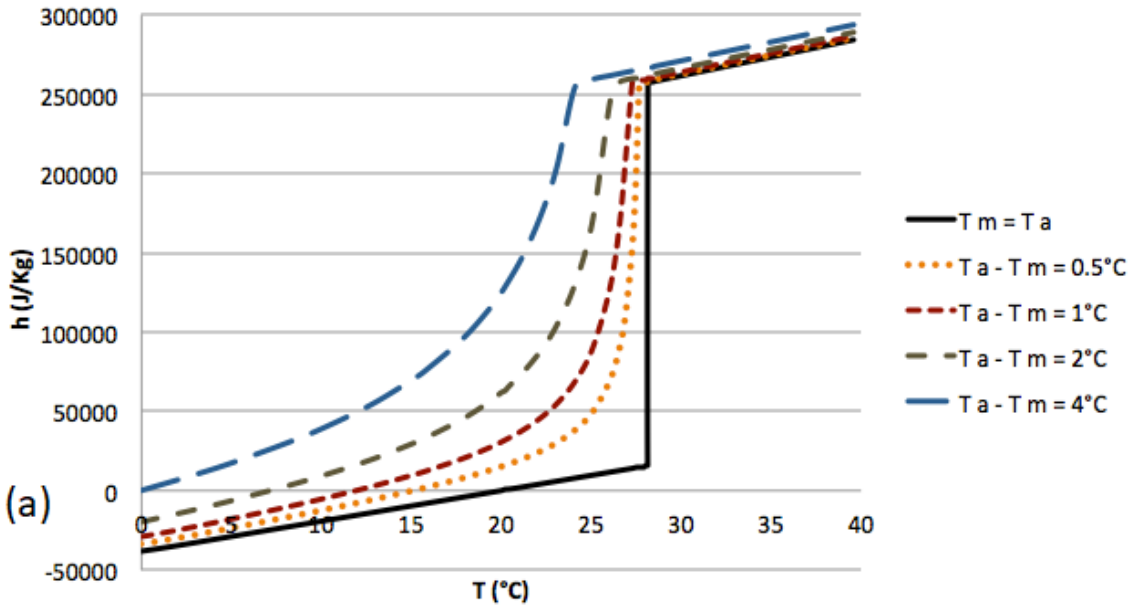

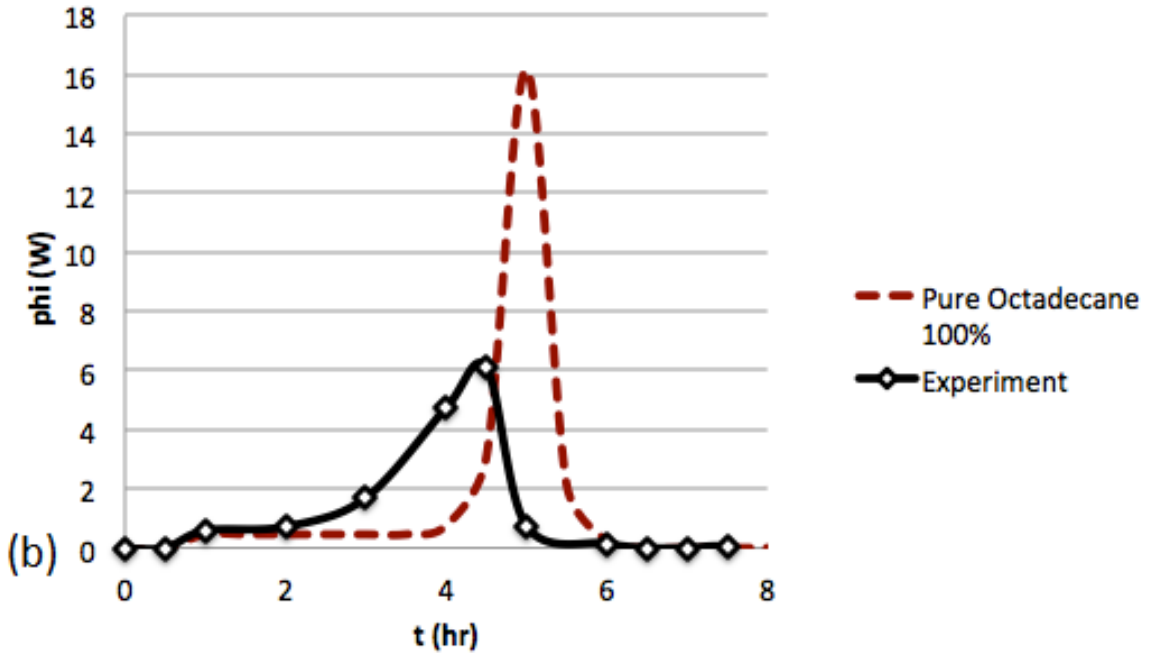

Figure 1.24 Effect of soluble impurities in octadecane on (a) the enthalpy-temperature curve variation for different depression values and (b) the heat flux variation as a function of time [43]

Another suitable method consists of representing the nucleation temperature by means of a probability function. Because of the stochastic nature of nucleation, Waser *et al.* [49] proposed a crystallization probability function F_{cry} dependent on time, location and temperature given by:

$$F_{cry}(t_s, I_n) = 1 - e^{-t_s . I_n} \qquad where \begin{cases} I_{nuc}(\Delta T_s, f) = K_1 . e^{-f . \frac{K_2}{\Delta T_s^2}} \\ f(L_{adj}) = 1 - \frac{L_{adj}}{K_3} \end{cases} \tag{1.5}$$

The supercooling time t_s and the nucleation factor I_n are the variables of this probability function. I_n depends on the degree of supercooling ΔT_s and the reduction factor of nucleation barrier f. K_1 is an arbitrary constant and K_2 is a fitting parameter that affects the critical degree of supercooling for which probability of crystallization increases. Solidification may take place due to contact between a supercooled liquid with a solidified PCM; f represents this phenomenon where L_{adj} corresponds to the number of solid crystals in the adjacent segments and calibrated by K_3. The values of these constants are obtained from the experimental study. Figure 1.25a shows that the probability function is mainly affected by the degree of supercooling where the probability of solidification increases as the degree of supercooling increases. This is because as the liquid become colder, its ability to trigger solidification increases. This result is in total agreement with the classic nucleation theory [91]. As L_{adj} decreases the number of solid particles in the adjacent node decreases too, meaning that the ability to solidify due to contact of liquid with solid also decreases. This is shown in Figure 1.25b, where the decrease of L_{adj} is represented by the increase of f causing the degree of supercooling increases too.

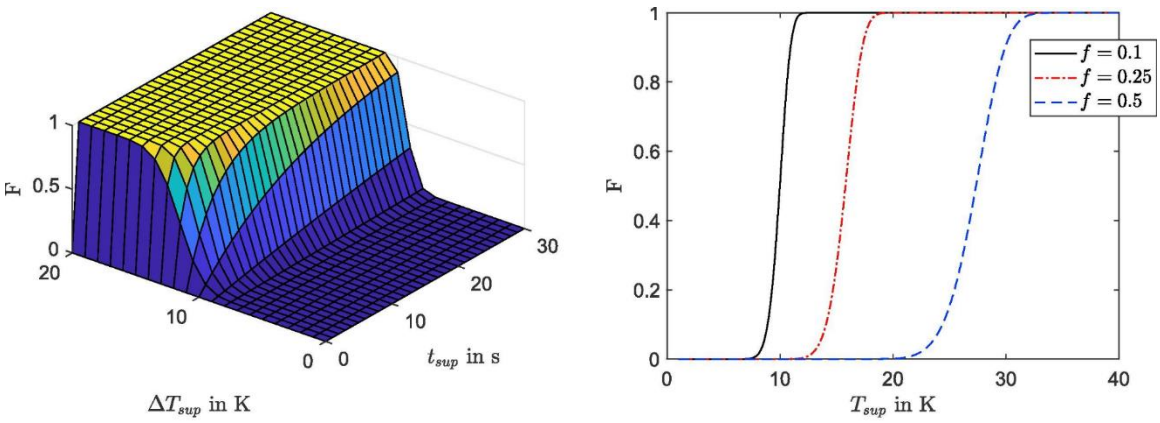

Figure 1.25 Variation of the probability function against a) supercooling time (t_{sup}) and degree (ΔT_{sup}) for $f = 0.1$; b) degree of supercooling for different values of f at $t_{sup} = 0.1s$ [49]

Yehya *et al.* [43] proposed another probability function to predict nucleation at a given temperature T:

$$P(T) = 1 - \left[\frac{1}{1 + e^{-\Delta T_S \cdot (T - T_a)}}\right] \tag{1.6}$$

where $T_a = (T_s + T_n)/2$, T_s et T_n are the temperatures of solidification and nucleation respectively. Figure 1.26 shows the difference between nucleation and solidification temperature where solidification takes place in the region between them. This probability function can change from one PCM to another according to the different parameters and conditions, so experiments and analytical studies are done to modify and calibrate it.

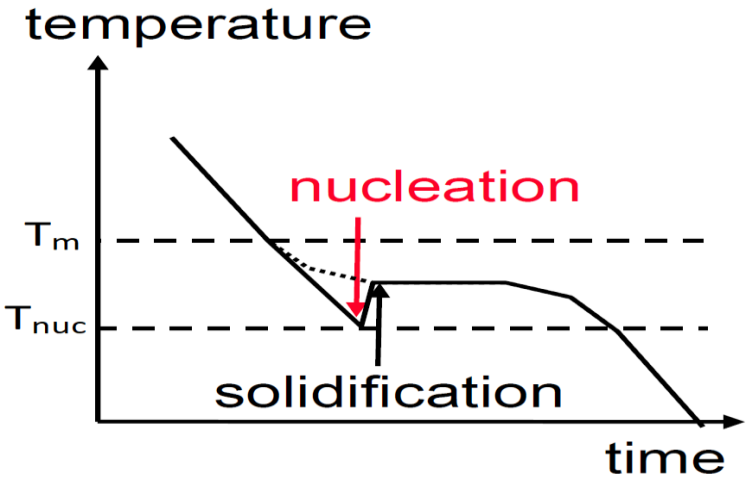

Figure 1.26 Solidification process [43]

1.5.2 Rate of solidification

Usually crystallization has a very high rate that may cause system instability in solidification modeling. The model requires fine grid with small time steps, which increases the simulation effort, time and complexity. To model the solidification phase efficiently, an equation relating the

rate of solidification to the degree of supercooling is required. A logical assumption is that the rate of solidification increases with the increase of degree of supercooling, because the sample is colder. However, as shown by the solid line in Figure 1.27, accounting for a typical form of the relation between the solidification speed and the degree of supercooling, this assumption is true until a limit. Indeed, beyond this limit, the molecules of PCM lack thermal energy and become more sluggish causing a decrease in the rate of solidification.

According to the classical nucleation theory [92], the homogeneous nucleation rate I can be written as:

$$I = \frac{NkT}{h} exp\left[\left(\frac{-16\pi}{3}\right)\left(\frac{\sigma_{LC}^3}{H^2}\right)\left(\frac{T_m^3}{\Delta T_s^2}\right)\left(\frac{1}{kT}\right)\right] \tag{1.7}$$

where N is the number of atoms of a system, k and h are Boltzmann and Planck's constant respectively, σ is the surface tension of the interface between the nucleus and its surrounding, H is the latent heat and T_m is the equilibrium melting temperature.

Font *et al.* [93] used the approximated results of solidification rate obtained by Ashby *et al.* [94]:

$$v(T) = \frac{d\Delta h}{6hT_m}(\Delta T_s) exp\left(\frac{-q}{kT}\right) \tag{1.8}$$

where d is the molecular diameter, $\Delta h = (latentheat \times molecularweight)/(Avogadro's\ number)$, and q is the activation energy.

The dashed line in Figure 1.27 is obtained from the linearization of equation (1.8).

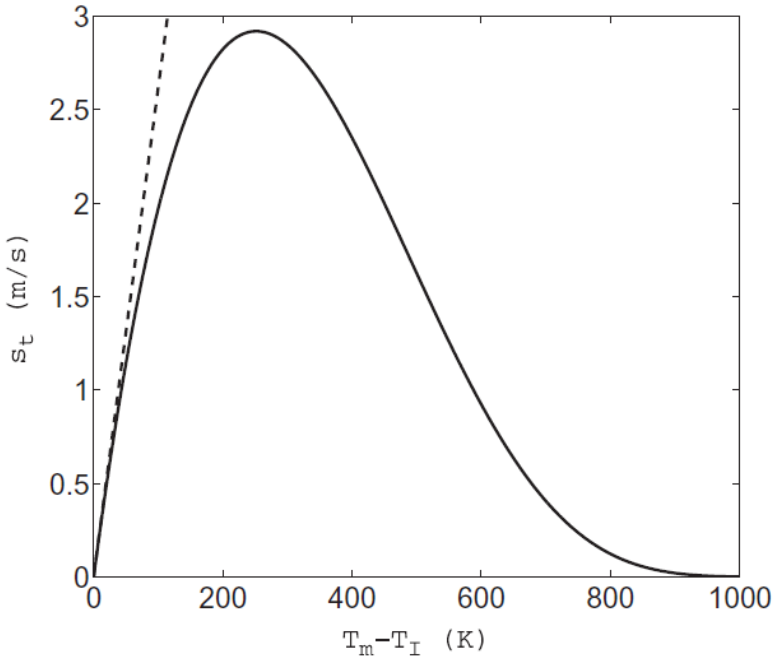

Figure 1.27 Variation of solidification speed of copper as a function of supercooling degree (T_I is the phase change temperature) [93]

In the numerical models, the rate of solidification is taken into account by different methods. Font [93] and Alexiades [95] use a one dimensional Stefan problem where the model consists initially of supercooled PCM. Both relate the rate of spread to the temperature gradient. The first supposes the solid/liquid interface temperature is equal to the nominal phase change temperature while the latter chooses the interface temperature as an unknown to be solved and uses an exponential function or an approximation to this function. Le Bot *et al.* [96] performed an experiment to obtain the required data of indium solidification and rate of spread. The obtained data from the experiment and an analytical model are used in their numerical model that starts solidification by the implementation of a small solid fraction. According to Günther *et al.* [48], solidification can start for two reasons: the PCM reaches the preset temperature or by direct contact of solid PCM node with its neighbor supercooled node. In their model, the rate of spread is thus controlled by isolating each node during its solidification, meaning that a node cannot trigger solidification in the neighboring node until it is totally solid. According to them, the rate of spread $v(T)$ is also temperature dependent and is given as [48]:

$$v(T) = v_0.(a_0 + a_1 T + a_2 T^2) \tag{1.9}$$

where $a_0, a_1\ and\ a_2$ are constants, determined by using a quadratic fit to measured data.

Uzan *et al.* [97] introduces a solidification ratio $\emptyset$ that is initially zero for total liquid node and is given as:

$$\emptyset^{n+1} = \emptyset^n + v.\Delta t/\Delta x \tag{1.10}$$

where n is the number of time steps and v is the speed of solidification.

The speed of solidification is given as [97]:

$$v = \frac{d}{6\mathrm{h}} exp\left(\frac{-q}{\mathrm{k}T}\right)\frac{L(T_m - T)}{T_m} \tag{1.11}$$

where d is the molecular diameter and q is the activation energy.

Moreover, Uzan *et al.* [97] improved Günther's isolation method, by defining a solid-liquid ratio $\emptyset$. Once a certain node reaches $\emptyset_{max}$, it can trigger solidification in the adjacent node before completing its solidification.

Davin *et al.* [98] use a relative factor β which is the inverse of crystallization factor f_c given by:

$$f_c = a_0 + a_1 \Delta T_s + a_2 \Delta T_s^2 \tag{1.12}$$

Note that ΔT_s can have different values according to the mode of solidification (i.e. reaching preset temperature or by solid-liquid contact). As previously mentioned, the proportionality relation between crystallization rate and f_c factor is sensitive to several parameters. During parameterization, if the enthalpy-temperature curve is available, f_c is estimated by curve fitting. However, if the rate of crystallization v_c is known, the same law for f_c is used such that calibration for the factor is needed by actual rate computing and checking. A very high value of f_c means a rapid solidification that requires a very fine grid since the time step of the solidification (time needed for a node to complete its solidification process) should be greater than that of the

simulation to overcome divergence and simulation errors. The beginning of solidification may also be chaotic as shown in Figure 1.28. On the other hand, a very low value of f_c can cause energy balance errors and in some cases solidification appear in two different locations. It is therefore recommended to assign a lower limiting value for f_c, to avoid a reach of crystallization temperature by a node different from the current one.

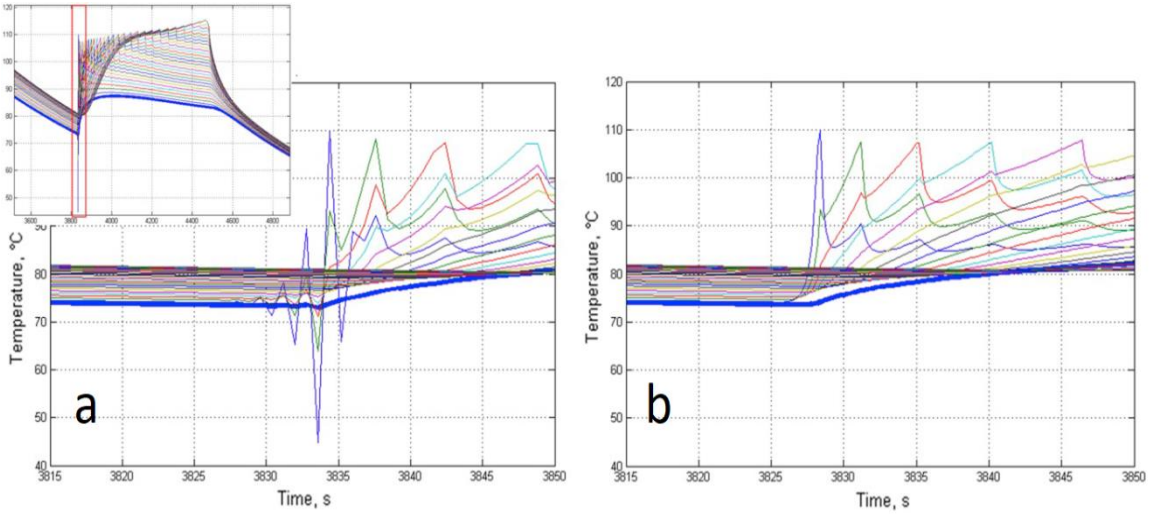

Figure 1.28 a) Chaotic behavior of temperature curve at the beginning of solidification of supercooled PCM and b) the enhancement due to fc limitation [98]

1.5.3 Thermal behavior

Another challenge in the modeling of the cooling process of a supercooled PCM is the simulation of the suitable thermal behavior of PCM. As shown in section 1.4.2, the behavior of PCM upon cooling is not the same in all cases. Once solidification initiates, the PCM enters the kinetic solidification phase, which is the phase where the latent heat is released to increase the PCM temperature. In this phase, several factors interfere in the kinetics of temperature increase. Figure 1.29 shows the different possible types of temperature increase [13]. The cases characterized in Figure 1.29a and Figure 1.29b are the same, where poor nucleation leads the PCM to attain supercooling. However, for higher values of thermal diffusivity, the temperature rises sharply (Figure 1.29b) to reach the melting temperature. In Figure 1.29c, the PCM attains supercooled state due the low crystal growth rate. This case shows the "kinetic controlled process", where the critical factor is the poor crystallization kinetics rather than the heat transfer rate. On the onset of PCM nucleation, the temperature stabilizes at a temperature lower than melting temperature rather than increasing to the melting point. This phenomenon is due to the balance between latent heat and heat removal. In Figure 1.29d, nucleation starts normally at the melting temperature, but the liquid undergoes supercooling during its solidification. The possible explanation for this case is the high rate of heat removal. The liquid in Figure 1.29e undergoes supercooling but is not seen in the temperature-time plot. This is due to the slow decrease of the temperature and the late reach to the melting temperature point and to a liquid with poor thermal diffusivity. Another explanation may be a difference between the position of the sensor and the solidification zone.

Davin *et al.* [98] developed a model based on the apparent specific heat capacity model by using a new formulation to represent the crystallization kinetics. The results show that by setting different coefficients for the crystallization factor law, it is possible to recover several typical thermal behavior of Figure 1.29. The results are discussed later in section 1.6 (Figure 1.37).

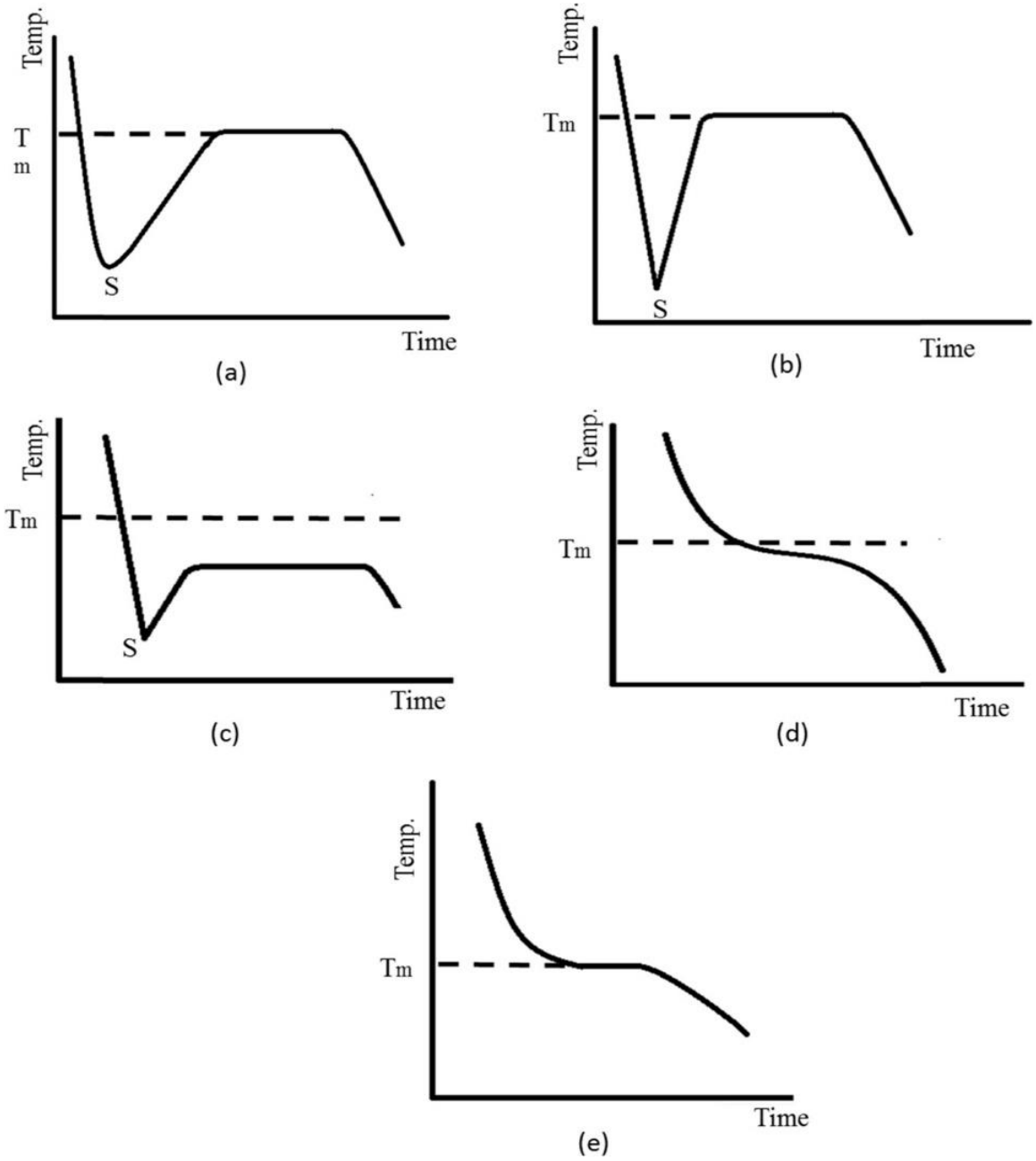

Figure 1.29 Plots showing different thermal behavior of PCM suffering supercooling [10]

As shown in the above subsections, the important parameters that represent supercooling are the degree of supercooling and rate of crystallization spread. It is challenging to represent these two parameters in a general equation to use in any application. These two parameters are also dependent on other factors previously mentioned which increases this challenge. Efforts are done

to define some correlations; however, these equations still need calibration and validation by experimental results to become valid for a specific PCM under certain well-defined conditions.

1.6 Existing models

As shown in the previous sections, different methods are adopted to model the parameters of the solidification process that are the degree of supercooling and the rate of spread. Some assumptions are often taken into consideration to simplify the model; such as neglecting the volume change due to thermal expansion, the natural convection and radiation heat exchange, etc. In order to model supercooling, researchers modify the different methods used in modeling phase change problem. Each method has its own advantages and disadvantages when modeling a phase change process as shown in Table 1.4. The below sections present different models, the method used, the taken assumptions and the technique followed in each model to deal with the additional difficulty of supercooling modeling.

Table 1.4 Advantages and disadvantages of different methods used in modeling phase change problems

Method	Criteria	Advantages	Disadvantages	Authors using this method
Enthalpy method	The enthalpy function includes both sensible and latent heat	1- Fast 2- Can handle sharp and gradual phase changes	Temperature oscillation at typical points of a grid	[99][100]–[109]
Heat capacity method	The heat capacity function includes both sensible and latent heat	1- Variable are only dependent on temperature 2- Easily programmable	1- Accurate results require fine grids and small time steps. 2- Requires a gradual phase change (phase change range) rather than sharp change 3- Latent heat is underestimated.	[100], [101], [110]–[123]
Temperature transformation method	The values of heat capacity and a source term are equivalent to both sensible and latent heat	1- can handle sharp and gradual phase changes 2- Can be used for large time steps and coarse grids	This method is not commonly used	[124]–[128]
Heat source method	The value of a source term is	1- Latent and sensible heats are	1- An optimal value for relaxation factor	[129]–[133]

	equivalent to latent heat	represented by different variables 2- Can handle sharp and gradual phase changes	is required to apply an under-relaxation. 2- Low computational efficiency 3- Difficulty in modeling supercooling	

1.6.1 One-dimensional models

Modeling is a method used to obtain the needed results to follow accurately the behavior of the tested material in a reliable period. Using a one-dimensional model reduces the complexity, where the heat equation is a function of time and one-direction. Moreover, the model is divided into several phases defined by state variables and functions. These variables and functions are introduced in the heat equation to represent the different phases and the values of different parameters. After dividing the model to a number of phases, some parameters do not affect the results a lot, so if neglected, this reduces the complexity and simulation time.

Frémond *et al.* [134] in 2001 developed a macroscopic predictive theory of supercooling to model the evolution of a supercooled body from its liquid state to its solid state. The domain is separated into two portions, solid and liquid, by the help of a state quantity β representing the volumetric fraction of liquid material. In this model, for simplicity, the latent heat is equal to 1 and solid-liquid portions are separated by a surface of discontinuity having a temperature related speed [135]. This leads to a problem having free boundary. Introducing the viscosity term in β leads to an irreversible model that is represented by differential equations obtained after deriving the energy equations as an affine function of local temperature u. The differential equations obtained in the continuous differentiable domain are [134]:

$$\frac{\partial \beta}{\partial t} + W(u)|\nabla \beta| = 0 \tag{1.13}$$

$$\frac{\partial u}{\partial t} + \frac{\partial \beta}{\partial t} - \Delta u = 0 \tag{1.14}$$

where W is the normal surface velocity of the freezing front. In these equations, when assigning the values for β, the free boundary appears explicitly. In the irreversible model, the end of the supercooling of liquid involves microscopic movements. During phase change, macroscopic effects occur due to these microscopic movements, which causes a slight change in density and volume. Since β is the state of the PCM, its change with time $(\partial \beta / \partial t)$ represents the microscopic velocities. Similarly, six differential equations are formed [135] and proved that there exists at least one solution.

Günther *et al.* [48] proposed in 2007 a linear and one-dimensional model based on the enthalpy method. Their model is connected to a heat exchanger on the left side and to an insulating material on the other side. The total volume of the container is equally divided into volume elements.

This model considers conduction as the only heat transfer mechanism and neglects the variations of volume resulting from phase change. The explicit finite volume method is used. The duration of the simulation is preset, and the used time step has a fixed value and is obtained from the CFL criterion [136]. In an enthalpy method, the enthalpy function is injective. To include supercooling in the enthalpy-temperature relation, two enthalpy curves for stable and metastable states are used and when the crystallization temperature is reached, switch is done between both curves. The drawback of this method is the discontinuity of the enthalpy due to phase change that may cause simulation errors and misrepresents the real case of phase change. In the ideal case, the PCM has a fixed melting and nucleation temperatures whereas the more realistic case is having a temperature interval to accomplish the two processes. For an ideal case, the heat capacity is considered constant; however, this is not accurate, so experimental values of $h(t)$ are implemented in the model.

Another challenge is to control the rate of crystallization. As mentioned before, the used PCM has a known degree of supercooling that is obtained by performing similar scenario experiments. Solidification can start when the PCM reaches the preset nucleation temperature or due to solid-liquid interaction. The used rate of spread is given as a function of temperature according to equation (1.9). In some cases, to decrease the computational effort and to use a finer mesh, the rate of solidification is decreased using the isolation method. This method restricts the ability of solidification by solid-liquid interaction, where a node cannot trigger solidification in the neighboring node until it completely finishes its solidification process [48].

$$v(T) = v_0.(a_0 + a_1 T + a_2 T^2) \tag{1.9}$$

Hu *et al.* [47] developed in 2017 a model that is solved by using the finite differences method. Using the equivalent specific heat capacity method, the heat capacity is considered constant during phase change along with isothermal system as shown in Figure 1.30. The model uses implicit scheme to discretize the control equations and boundary conditions.

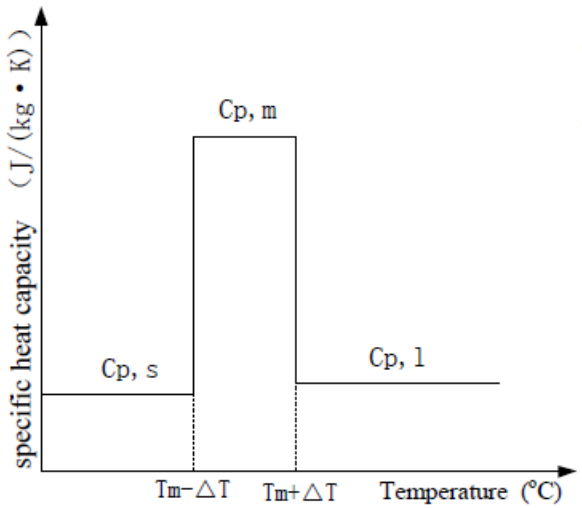

Figure 1.30 Equivalent rectangular specific heat capacity [47]

Bony [137] started from the existing type 60 in TRNSYS, dedicated to stratified fluid tanks based on sensible energy storage, and made an extension. The physical model consists of a water

heat exchanger tank filled with PCM modules of different shapes (cylinders, plates, spheres), which allows a bidimensional calculation model. The tank is vertical and constituted of multiple segments or nodes. An assumption of constant node temperature is taken. He uses the enthalpy method to calculate the heat transfer. The numerical equations are solved using the explicit method and to avoid calculation divergence, some conditions are applied on the nodes and the time step as follows [137]

For a surface node $$Fo(2 + Bi) \leq 1/2 \quad (1.15)$$

For a node inside material $$Fo \leq 1/4 \quad (1.16)$$

with: $Fo = \lambda.\Delta t/(\rho.C_p.\Delta x^2)$ and $Bi = \alpha.\Delta x/\lambda$

where Fo and Bi are Fourier and Biot numbers respectively, α is the convection coefficient between the water tank storage and the PCM container, λ is the thermal conductivity.

The maximum time step that can be used is [137]:

For a surface node $$\Delta t \leq \frac{\rho.C_p.x^2}{2\lambda\left[2 + \left(\frac{\alpha x}{\lambda}\right)\right]} \quad (1.17)$$

For a node inside material $$\Delta t \leq (\rho.C_p.x^2)/4\lambda \quad (1.18)$$

Hysteresis and supercooling phenomena are taken into account in the model as shown in Figure 1.31 by introducing a specific indicator for each of them. Due to the vertical shape of the container, the lower part of the cylinder is colder than the top. As a result, the lower part undergoes higher degree of supercooling and is the first to reach the preset crystallization temperature. Once solidification starts, it propagates to the above nodes with an instantaneous rate of spread (Figure 1.32). The thermal conductivity of PCM takes two different values for liquid and solid phases and is calculated by linear interpolation during the phase change. Concerning the convection coefficient between water and PCM, it is calculated according to the PCM container shape and the type of fluid flow.

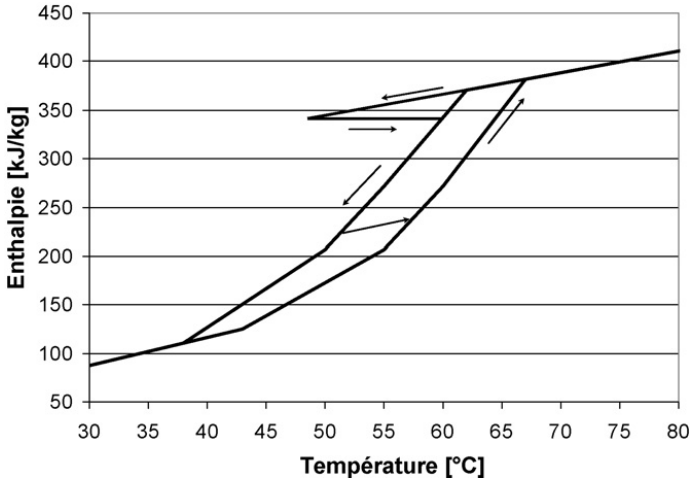

Figure 1.31 : New enthalpy functions to represent hysteresis and supercooling [137]

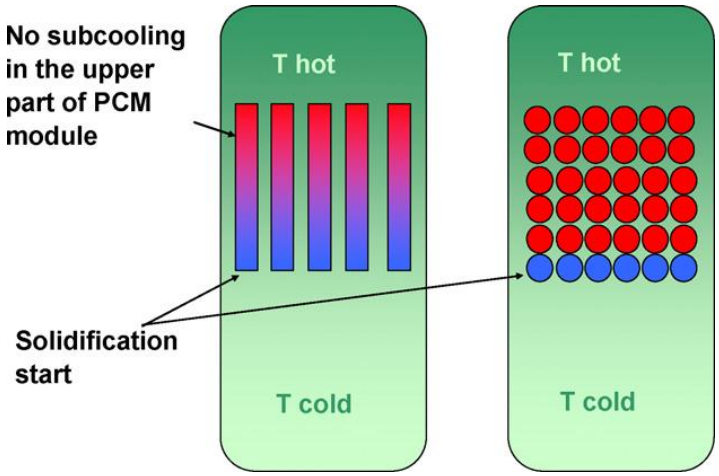

Figure 1.32 Solidification propagation according to the PCM module shape [137]

In 2020, Davin *et al.* [98] used, like Hu *et al.* [24], the apparent specific heat capacity method. The particularity of their method is related to the introduction of a negative Cp to accurately take into account supercooling. Their model is based on the lumped system or nodal method to discretize the heat equation as shown in Figure 1.33, with the main governing equation described in equation (1.19) [98]:

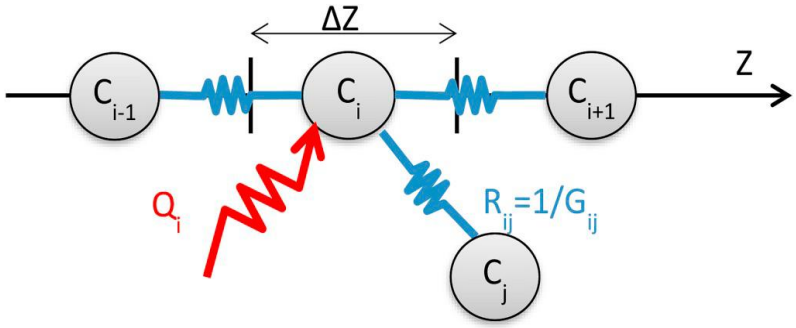

Figure 1.33 Lumped system network used for heat equation discretization [98]

$$\sum_j \lambda_{ij}(T_i - T_j) + Q_i = C_i \frac{dT_i}{dt} \qquad \forall i \in [1, N] \tag{1.19}$$

where λ is the thermal conductance, Q represents the heat sources and the boundary conditions, C is the heat capacitance that can insure phase change and i, j are the node indices.

Using an explicit scheme, the temperature is calculated for each time step. Similar to the before mentioned models using enthalpy method, the crystallization initiates either by reaching the present nucleation temperature T_n or by the liquid-solid interface. To reduce numerical errors and better represent the heat transfer, the Gaussian approximation is used to account for the specific capacity $C_p(T)$. Figure 1.34c shows two formulations for heat capacity change during the cooling phase at the crystallization temperature T_C. The first, blue arrow, considers the easy simple formulation while the second, green arrow, is more complex but represents the crystallization process. f_{super} is a phase supercooling indicator that allows to differentiate the specific capacity regarding the phase history. During fusion (Figure 1.34a), the Gaussian law is

used and $f_{super} = 0$. During cooling (Figure 1.34b), the PCM stays liquid until crystallization starts and f_{super} is set to 1. When crystallization starts (Figure 1.34c), f_{super} is incremented to 2. Finally, f_{super} returns to 0 as soon as crystallization ends and the solid begins to cool down (Figure 1.34d).

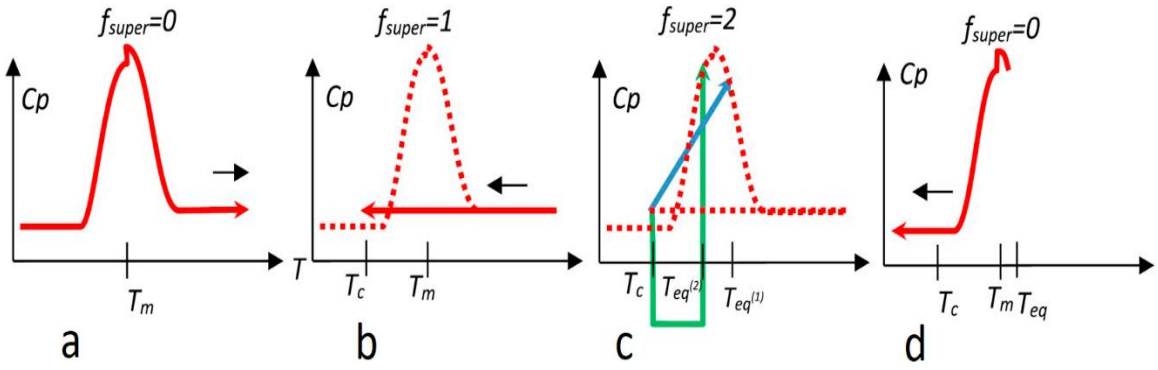

Figure 1.34 The different steps followed to represent supercooling: a) heating b) cooling until crystallization starts c) two formulations of crystallization and temperature rise represented by blue and green lines d) cooling of the solid PCM [98]

In formulation 1, the temperature directly increases from T_C to $T_{eq}^{(1)}$ by considering a very high rate of crystallization. The heat capacity for formulation 1 can then be written as [98]:

$$C_p(T) = \begin{cases} C_p^{gauss}(T) & if\ f_{super} = 0 \\ C_p^l & if\ f_{super} = 1 \\ C_p^{gauss}(T) & if\ f_{super} = 2 \end{cases} \quad (1.20)$$

where C_p^{gauss} is the Gaussian approximation, C_p^l et $C_p^s$are the heat capacity in liquid and solid phases respectively. Moreover, in case $f_{super} = 2$, $T = T_{eq}^1$ and $f_{super}(t + \Delta t) = 0$.

According to [48], [97], [138], C_p^{gauss}can be written as:

$$C_p^{gauss} = C_p^0 + \frac{H}{\Delta T\sqrt{\pi}} exp\left[\frac{-(T - T_m)^2}{\Delta T^2}\right] \quad (1.21)$$

where ΔT is the Gaussian standard deviation of Cp and H is the latent heat.

In Figure 1.35, A_0 corresponds to the enthalpy stored during heating process as shown in Figure 1.34a; A_1 corresponds to the enthalpy released during the cooling process in liquid or metastable state as shown in Figure 1.34b, and A_2 corresponds to enthalpy released during the cooling process from the equivalent phase change temperature T_{eq}^1 as shown in Figure 1.34d. The model has the same initial and final temperature. Thus, the enthalpy of heating is equal to that of cooling and the following equality relation is obtained [98]:

$$A_0 = A_1 + A_2 A_0' = A_1' \quad (1.22)$$

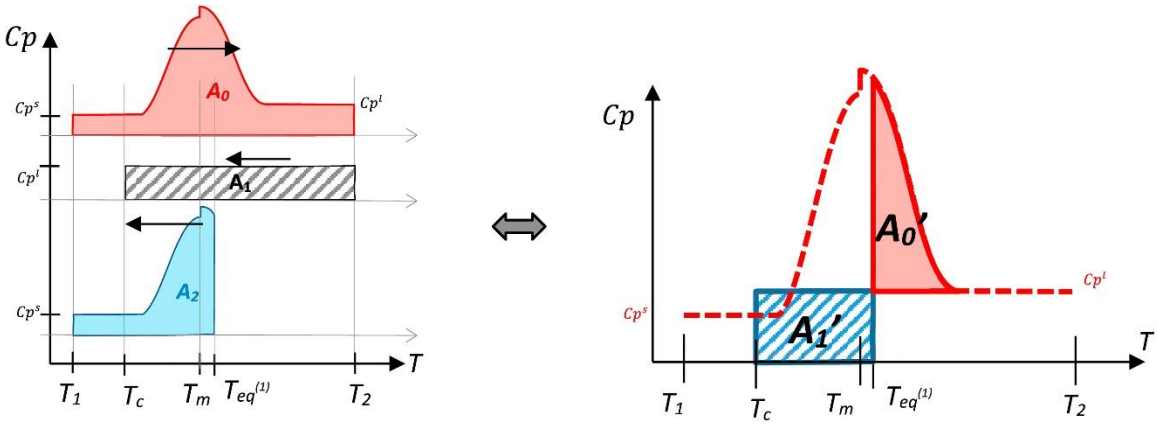

Figure 1.35 Blocks representing the equivalent enthalpy of the processes (heating/cooling) of formulation 1 [98]

By solving the equality of enthalpy blocks, performing change of variable, introducing error function and supposing ΔT is very small, $T_{eq}^{(1)}$ can be finally deduced as [98]:

$$T_{eq}^{(1)} = T_m + \Delta T.erf^{-1}\left[1 - \frac{2C_p^l(T_m - T_c)}{H}\right] \quad (1.23)$$

Formulation 2, shown in green in Figure 1.34c, is more complicated to model but more realistic. It is intuitive with a negative heat capacity chosen during phase change (i.e.: $f_{super} = 2$); the expression of the heat capacity for $f_{super} = 2$ in equation (1.20) becomes [98]:

$$C_p(T) = -\beta C_p^l(T); \quad if\ T \geq T_{eq}^2,\ f_{super}(t + \Delta t) = 0 \quad (1.24)$$

Figure 1.36 represents the enthalpy blocks of all stages mentioned before and equality of heating and cooling enthalpies is applied to determine T_{eq}^2.

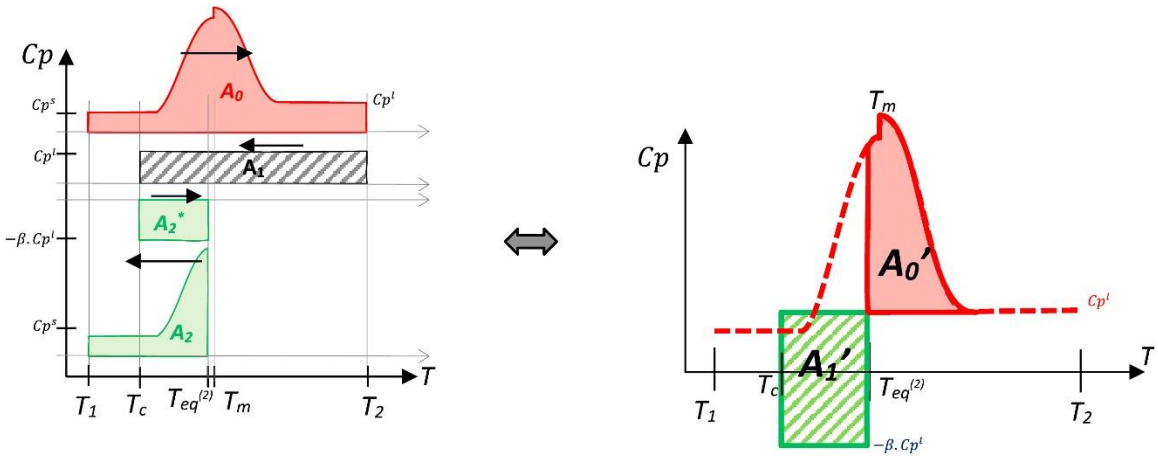

Figure 1.36 Blocks representing the equivalent enthalpy of the heating and cooling processes for formulation 2 [98]

Similar assumptions of formulation 1 are taken to obtain the expression of T_{eq}^2 [98]:

$$T_{eq}^2 = T_m + \Delta T.\, erf^{-1}\left[1 - \frac{2C_p^l(1+\beta)(T_m - T_c)}{H}\right] \quad (1.25)$$

Note that erf^{-1} accepts input value that belongs to the interval [-1,1]. In other words, if T_{eq}^2 is outside the melting range, then $C_p^l(1+\beta)(T_m - T_c) > H$ and an error occurs. In this case, the expression of T_{eq}^2 is replaced by equation (1.26) [98]:

$$T_{eq}^2 = \frac{H + T_m.\left(C_p^s - C_p^l\right) + T_c.C_p^l.(1+\beta)}{C_p^l.\beta + C_p^s} \quad (1.26)$$

The factor β is found to be the inverse of the crystallization factor f_c and is defined in equation (1.12), where the rate of crystallization is discussed in details. The value of β indicates the speed that a supercooled liquid reaches the phase change. If β is set to zero, then equations (1.23) and (1.25) become identical meaning that phase change takes place immediately.

The model has Neumann boundary conditions for elements in contact with the air including the natural convection coefficient. Heat transfer takes place in one direction so that the solid liquid/interphase is always planar. The heating source, insulation, capsules and other parts used in the experiment were included in the model.

To test this model, the simulated results are compared to experimental results. The study was done on erythritol, which presents a high degree of supercooling ($Tm = 118°C, Tn = 78°C$) and a relatively low crystallization rate. Erythritol is heated from 50°C to 150°C by a plate and cooling is done by ambient air through the same plate. During the cooling phase, several polynomial laws for the crystallization factor fc have been tested as shown in Figure 1.37. The actual crystallization rate is the calculated ratio of the distance between two nodes divided by the time between the two nodes crystallizations. These results show that it is possible to model different thermal behavior of supercooling for the PCM material.

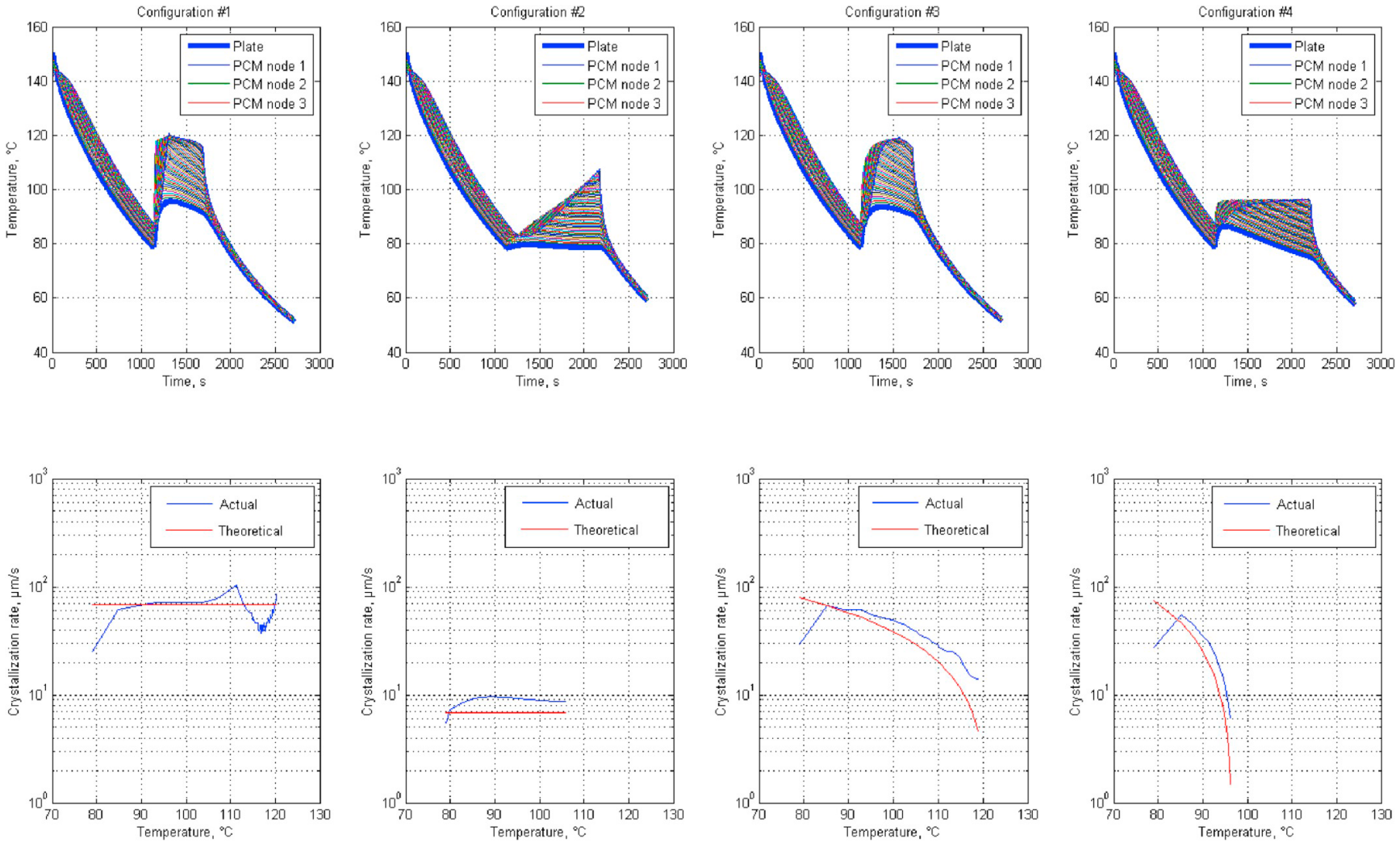

Figure 1.37 Simulation results showing the influence of the crystallization rate factor $fc(T)$ on the temperature and the crystallization rate [98]

1.6.2 Multi-dimensional models

In a multi-dimensional model, an extra dimension is added to the one-dimensional model. In this case, reproducing a more realistic image of the simulated case is better, where the effect of convection in the PCM can be detected by the deviation of the solid/liquid interface. This accuracy and these results cost more computational time and add complexity to the model

The model developed by Uzan *et al.* [97] in 2017 is based on the enthalpy formulation and resolved by using finite volumes. The two-dimensional model is able to simulate the solidification of a supercooled liquid using explicit numerical scheme. Upon cooling the cylindrical model from the bottom, the liquid's temperature decreases and the PCM is in supercooled stage until solidification starts either by reaching the preset temperature or by the solid-liquid interaction. After solidification, the temperature of the solid continues in decreasing. Similar to Günther [48], Figure 1.38 shows the phase change process that takes place during an interval of temperature to overcome the sharp variation of enthalpy that may cause simulation errors. The difficulty of using the enthalpy method is the undefined enthalpy values for supercooled liquid. Experimental results of gallium and analytical solutions are compared with the results of the model.

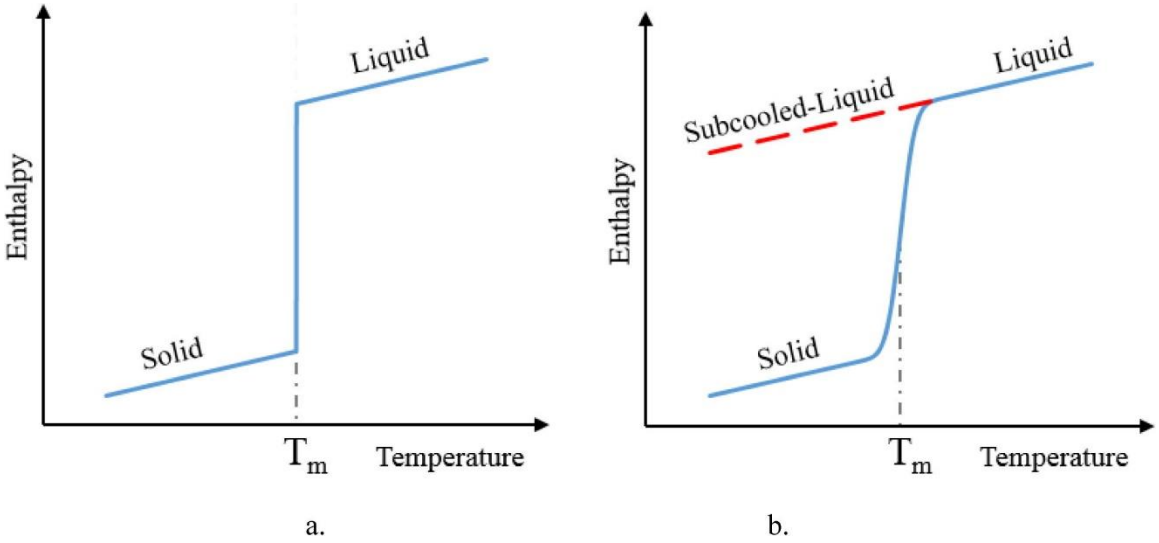

Figure 1.38 Enthalpy energy relation: a) used by enthalpy method; b) used by Günther and Uzan [97]

The heat capacity is in the form of a Gaussian function and a parameter "p" is used, as in the model of Günther *et al.* [48], to determine the state of the PCM. This indicator p is assigned for each node. A ratio for solid/liquid fraction Ø and the speed of solidification v are calculated according to equation (1.10) and equation (1.11) respectively [97].

$$\emptyset^{n+1} = \emptyset^{n} + \frac{\Delta t}{\Delta x} v \tag{1.10}$$

$$v = \frac{d}{6h_P} exp\left(\frac{-q}{k_B T}\right) \frac{L(T_m - T)}{T_m} \tag{1.11}$$

The temperature is calculated at each time step according to the following equation (1.27) [97]:

$$T = \frac{\emptyset}{\emptyset_{max}} T(Solid) + \left(1 - \frac{\emptyset}{\emptyset_{max}}\right) T(Liquid) \quad (1.27)$$

where $\emptyset$ is the solid-liquid fraction, and $\emptyset_{max}$ must be previously defined using the energy conservation equation. $T(Solid)$ and $T(Liquid)$ are obtained by using the enthalpy relations in stable solid and liquid phases as described in equations (1.28) and (1.29) respectively. If $\emptyset < \emptyset_{max}$ part (a) of equation (1.29) is used, else part (b) [97].

$$h(T) = C_p(T - T_m) + \frac{L}{2} erf\left(\frac{T - T_m}{\delta T}\right) \quad (1.28)$$

$$h(T) = \begin{cases} C_p(T - T_m) - 0.5L \ \ (a) \ \ solid \\ C_p(T - T_m) + 0.5L \ \ (b) \ \ liquid \end{cases} \quad (1.29)$$

Moreover, a solidified fraction SF defines the ratio of solid mass over total mass. Reaching its maximum means the end of the kinetic solidification, which is the increase of the liquid temperature to its melting point. As shown in equation (1.30), SF_{max} is a function of the degree of supercooling and material properties [97]:

$$SF_{max} = \frac{1}{1 + \frac{L - C_{ps}(T_m - T_n)}{C_{pl}(T_m - T_n)}} \quad (1.30)$$

where C_{ps} and C_{pl} are the solid and liquid heat capacities respectively.

Günther's model isolates each node until it finishes solidification. However, in this model, once the node reaches the $\emptyset_{max}$, it triggers solidification in the adjacent node.

For simplicity, the model neglects volume and density changes. First, the model considers heat transfer in radial direction only (1D problem) and after 1D validation, heat transfer along z direction is included to obtain a 2D model (Figure 1.39). Similar procedure for differential equation discretization is followed. For both 1D and 2D models, the cylinder's wall has constant

temperature and zero heat flux at the centerline. For 2D model, the base of cylinder has constant temperature while the top is insulated.

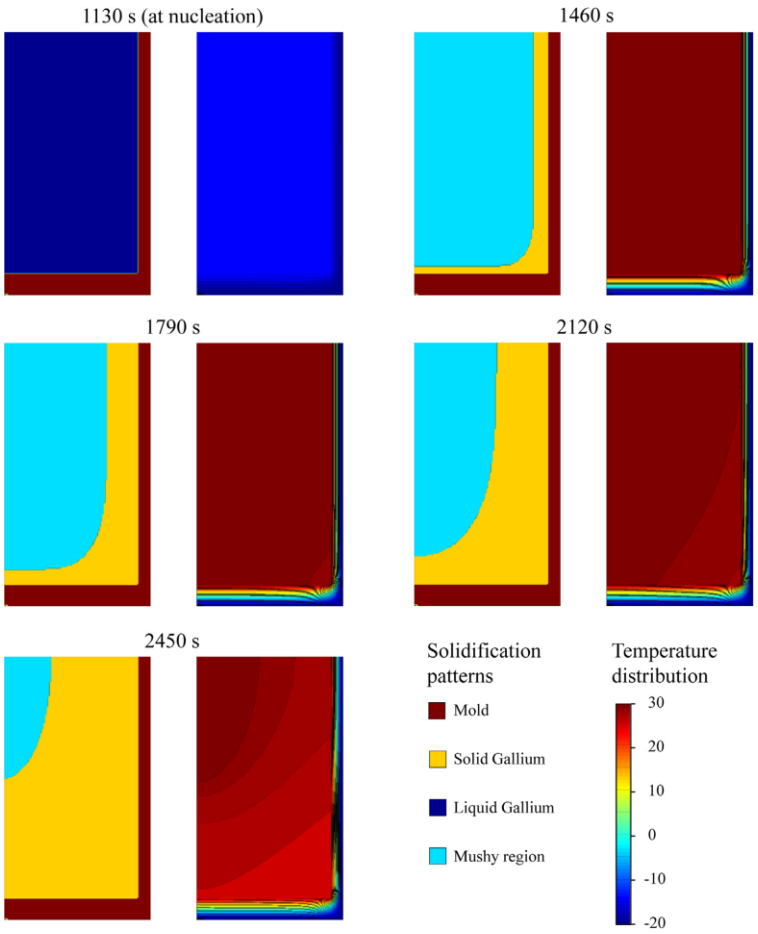

Figure 1.39 2D model simulated results from the start of cooling: solidification maps on the left and temperature fields on the right [97]

Waser *et al.* [49] proposed a 3D model consisting of a fin tube heat exchanger shown in Figure 1.40. To reduce the computational cost, the following assumptions are taken into account: convection heat transfer in PCM is neglected, as well as thermal losses to the ambient from the PCM. The material properties are constant, and the only considered heat transfer is from the PCM to the heat transfer fluid (HTF). The 3D model is reduced to 1/8 with symmetrical boundary conditions and a convective boundary condition is applied at the inner tube surface. Concerning the HTF, its model is one-dimensional with n segments and discretized using an upwind scheme to calculate the temperature in each segment. The energy equation of the PCM is discretized using finite volume method; the time discretization scheme used is implicit of first order and the spatial discretization scheme is second order. Using the enthalpy method, the latent heat is included in the enthalpy term of the energy equation. A temperature dependent state indicator β is used to indicate whether the PCM is in solid, liquid state or in the mushy zone. The mushy zone is a zone where phase transition takes place, and its role is to prevent the sudden phase change that causes simulation instabilities. The indicator β is written as [49]:

$$\beta = \begin{cases} 0 & if\ \ T < T_s \\ \frac{T-T_s}{T_l-T_s} & if\ \ T_s < T < T_l \\ 1 & if\ \ T > T_l \end{cases} \tag{1.31}$$

where T_s is the maximum temperature of the PCM when it is totally solid, T_l is the minimum temperature reached by the liquid PCM and T is the instantaneous temperature of the PCM. The indicator β can also be used to determine the enthalpy and the amount of the latent heat released.

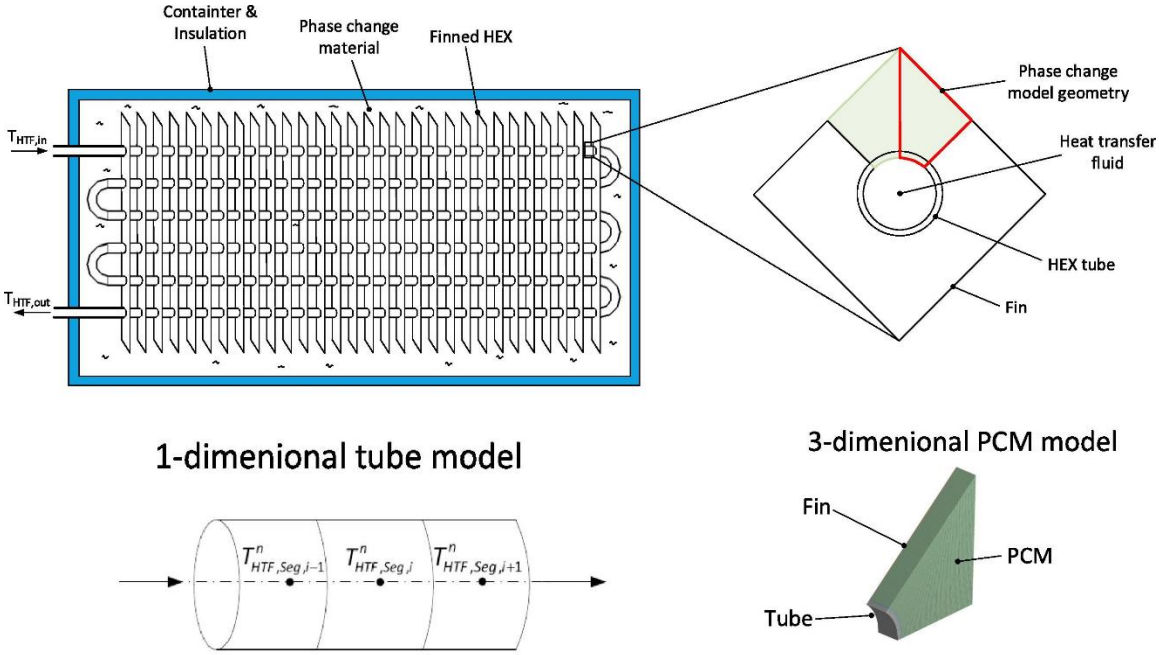

Figure 1.40 Illustration of the 3D model done by Waser et al. [49]

The temperature of the inflow is constant and PCM temperature is initially 68°C (10°C higher than melting temperature) and decreases to 15°C. As mentioned before, equation (1.5) shows the used crystallization probability function, which is calibrated by an experimental study [49].

$$F_{cry}(t_s, I_n) = 1 - e^{-t_s \cdot I_n} \qquad where \begin{cases} I_{nuc}(T_s, f) = K_1 . e^{-f.\frac{K_2}{\Delta T_s^2}} \\ f(L_{adj}) = 1 - \frac{L_{adj}}{K_3} \end{cases} \tag{1.5}$$

Figure 1.41 gives $K_2 = 7250K^{-2}$ and $K_3 = 0.7$ for the minimal deviation of 140W. Both models are linked to each other by the heat flow rates from PCM to HTF. The heat flow rates are generated by the 3D model and collected in two datasets. The former contains data as the phase change occurs and the latter contains data when PCM remains liquid. The heat flow rates are then used as source term in the 1D tube model.

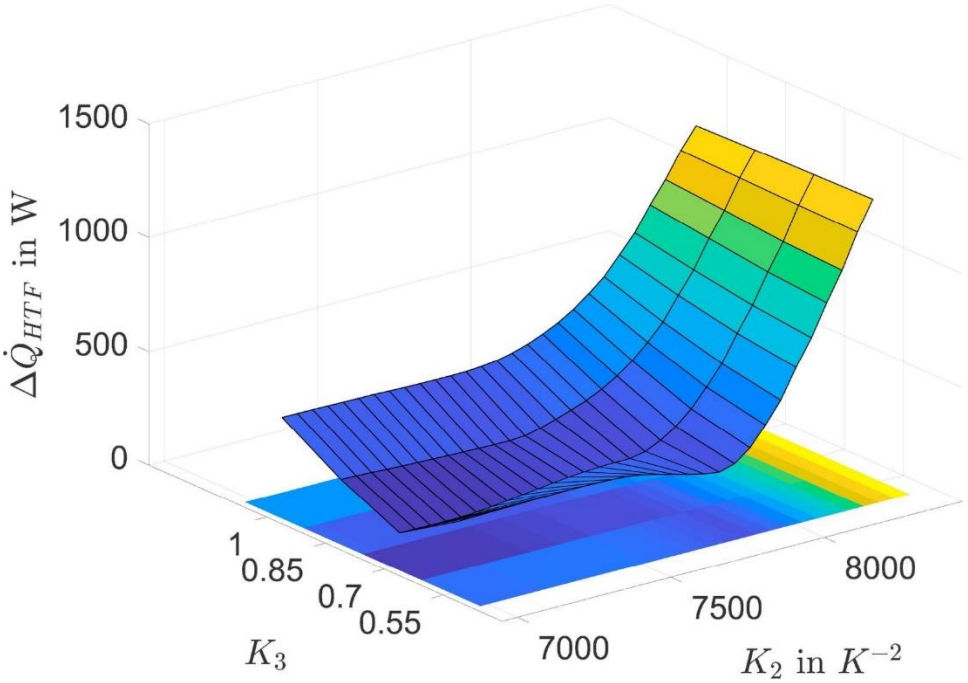

Figure 1.41 Averaged deviation between experimental and numerical results obtained for different values of K2 and K3 [49]

As shown above, the researchers tend to use different methods to include supercooling in numerical simulations. Simplifying the model is an important issue used to decrease the time and complexity of the simulation. Table 1.5 summarizes the above-discussed models showing the dimension, methods and assumptions taken.

Table 1.5 Summary of the most recent methods used for the numerical modeling of supercooling

Author (year)	Dimension	Method used	Assumptions	Results
Hu *et al.* [47] (2017)	1D	- Finite difference method - Heat capacity method - Implicit scheme to discretize the control equations and boundary conditions	Isothermal phase transition process	- Supercooling delays the onset of solidification. - As the degree of supercooling increases, the maximum value of heat flux reached before phase change increases. - The overall value of heat flux decreases as the degree of supercooling increases.
Frémond *et al.* [134] (2001)	1D	- Assigning a state quantity β representing the liquid volume fraction - Reversible and irreversible models, where the latter is obtained by adding the viscosity term in the partial differential equation of the moving front - Free velocity of freezing surface function of temperature	- The model consisted of two zones, liquid and solid, separated by a surface of discontinuity. - During phase change, the medium is at rest. - Latent heat value set to 1 kJ/kg.	Presence of a unique solution for the obtained differential equations for both cases

Bony *et al.* [137] (2007)	1D	- Enthalpy method to calculate heat transfer - Explicit method to solve numerical equations - Applying conditions on the nodes and the time step using Fourier and Biot numbers	Constant rate of crystallization	- Assuming constant rate of crystallization leads to inaccurate results - Temperature oscillations are observed during phase change that need to be reduced without dramatically increasing the calculation time.
Günther *et al.* [48] (2007)	1D	- Finite volume method - The values of enthalpy are implemented as a function of time to overcome the reality that enthalpy function is no longer injective. - Solidification is triggered either by reaching a preset temperature or by the solid front. - Rate of spread is a function of time. - A node could trigger solidification in the neighboring node when it finishes completely its phase change to solid.	- Conduction is the only heat transfer mechanisms - Constant volume during phase change - Melting and crystallization take place in a range and not at an exact value.	Using two curves of enthalpy to include supercooling causes a discontinuity of the enthalpy due to phase change. It causes simulation errors and misrepresents the real case of phase change
Davin *et al.* [98] (2020)	1D	- Lumped system or nodal method to discretize the heat equation - Time-explicit scheme to calculate the temperature at each time step - Enthalpy method based on heat capacity as a function of temperature	- Rate of solidification is a function of a crystallization factor which is a function of temperature. - One direction heat transfer - The crystallization factor is bounded in an interval	- Using different values for heat capacity, especially the negative values, may cause robustness problems - The crystallization rate factor and the time step are the major parameters

		- Modification of the heat capacity in the phase change range to include the latent heat to the equations (using negative heat capacity) - Solidification is triggered by either reaching a preset temperature or by the solid front. - Gaussian approximations for the heat capacity	for computational reasons concerning divergence and errors.	that influence stability of the system - The onset of heat release is a critical point - Decreasing the crystallization rate and using smaller time step improve the stability of algorithm - Using low values for crystallization rate factor can cause energy balance errors.
Uzan *et al.* [97] (2017)	2D	- Finite volumes method to resolve the enthalpy formulation - Solidification is triggered by either reaching a preset temperature or by the solid front. - Explicit numerical scheme to solve the solidification process - A node can trigger solidification in the neighboring node after reaching a preset value of percentage of solidification.	- Phase change takes place in a range and not at an exact value to overcome sharp variation of enthalpy. - No volume and density changes	- The model shows acceptable results compared to experimental data - Ability of the model to predict temperature behavior at different positions and to demonstrate the effect of boundaries - Ability to be a basis of complex multidimensional modeling
Waser *et al.* [49]	3D	- The model consists of PCM and	- No convection heat transfer	The proposed crystallization probability

(2008)		- Upwind scheme to discretized the inner heat transfer tube - Finite volume method to discretize the energy equation of the PCM - Implicit first order to discretize the time scheme - Second order spatial discretization scheme - Enthalpy method - Used a phase indicator as a function of temperature - Used an experimentally calibrated crystallization probability function	- No thermal loss with the surrounding ambient air - Constant material properties - No heat transfers between the segments of the model - The model was reduced by symmetry by a factor of 8 - The inner heat transfer tube is 1D	function must be calibrated using suitable experimental data.

1.7 Discussion

Obtaining an optimal performance with minimal supercooling degree is the main goal when using PCM in thermal storage systems. Each factor affecting supercooling was separately discussed and it was shown that the effect of some factors do not necessarily follow a monotonic tend such as the percentage of additives on the degree of supercooling. The effect of additives decreases after a mean value. The main challenge is to determine the combination between several factors like surface roughness, cooling rate, thermal conductivity, percentage of additives and thermal history that can lead to a PCM with optimal performance. For example, in Figure 1.15, the use of an aluminum capsule having surface roughness $r = 0.6$ and thermal conductivity $k = 183 W/m.K$ gives approximately similar nucleation probability curve as a brass having higher $r = 1.59$ and lower $k = 113 W/m.K$. Similarly, the decrease of container's volume, for example by the use of micro-encapsulation, leads to an increase in supercooling degree, but also to an increase of the heat transfer area in a thermal storage system.

The dependency of the supercooling phenomenon on many factors complicates its modeling. As shown above, most authors tend to perform experimental measurements to obtain the required parameters like supercooling degree and rate of spread. Nucleation theories are often used in the numerical models, but the implemented equations still need calibration using experimental data to fit the given case. It is better to increase the number of identical samples used to take the mean value and standard deviation, in order to overcome experimental inaccuracies, including changes in applied conditions and in materials properties. Implementing all known parameters/datasets in the simulations coupled to a statistical tool is still difficult, because of the models complexity and the simulation time that are restricted by the available computational power. Therefore, researchers take approximations, assumptions and neglect parameters to decrease this complexity.

So, it is recommended to use micro-capsulations to increase the heat transfer area and avoid sudden release of huge amount of latent heat. The whole knowledge of PCMs behavior should help in choosing a better PCM that can be a combination of several PCMs to obtain the desired melting temperature. For example, paraffins have high latent heat with a melting temperature near the indoor comfort temperature, which is needed in thermal energy storage in building walls; however, their thermal conductivity is low. Experimental results are important to validate the obtained results, but until now, they are being used to obtain several values to implement in equations and conditions in the model. This strategy restricts the field of work of the model to the applications having same conditions as the experiments. As a future work, it is important to be able to predict the degree of supercooling, which requires building the system of dependency between all parameters. Furthermore, the optimal performance of a PCM in terms of energy may not be the desired one in terms of investment. The chosen parameters should also include cost, energy saving and payback period studies. The ability of modeling a PCM regardless the changing parameters will provide an ability to choose the optimal conditions to be applied in a system from the energy, exergy, economic and environmental viewpoints.

Based on the above, the following guidelines should be followed for the optimal experimental design of an application:

1. Classification of the application: in this step, one should determine whether supercooling is desired (preservation process, animals and plants survival) or not desired (thermal storage systems). Supercooling chaotic behavior can dramatically change the system efficiency.

2. Determination of the parameters that can be modified and have a direct effect on the supercooling degree. For example, modifying the structure, roughness and size of the container of PCM is more easily achieved in thermal energy storage systems than in the processes of preservation. However, in preservation processes, controlling the cooling rate is easier than in thermal energy storage systems integrated in the walls of a building or a greenhouse, which depends on the exterior atmosphere.
3. Study of the correlation between the parameters to be changed. Some parameters have higher impact than others do; for example, the thermal conductivity and surface roughness of the container (see Figure 1.15).
4. Tradeoff between system performance and cost. The chosen techniques to increase or decrease supercooling should serve in increasing the system's efficiency with the lowest possible cost. Figure 1.42 summarized the most important decisions to take according to the application and whether supercooling is favored or not.

Regarding the numerical modeling of supercooling, the following guidelines might be followed:

1. Build a physical model with a simple geometry and dimension structure, to reduce computational time and cost.
2. Choose the appropriate modeling method: each method has its advantages and disadvantages. Table 5 summarizes the major characteristics of each model.
3. Make simplifying assumptions to reduce computational time and avoid divergence. Some parameters have negligible effect on heat transfer and PCM behavior while their implementation requires a high computational effort. For example, during solidification, conduction heat transfer is dominant over natural convection. Several assumptions have also been taken by different authors to initiate crystallization (preset temperature, probability equation, state functions)

Build the equations representing the temperature rise during latent heat release. Most authors tend to obtain it from experimental results. The manner of crystals spread differs for different temperatures and degrees of supercooling. This modeling challenge adds up to the modeling requirements for crystallization initiation (onset and position). A set of relations have been developed, but they are still limited to specific PCM, container properties and initial values.

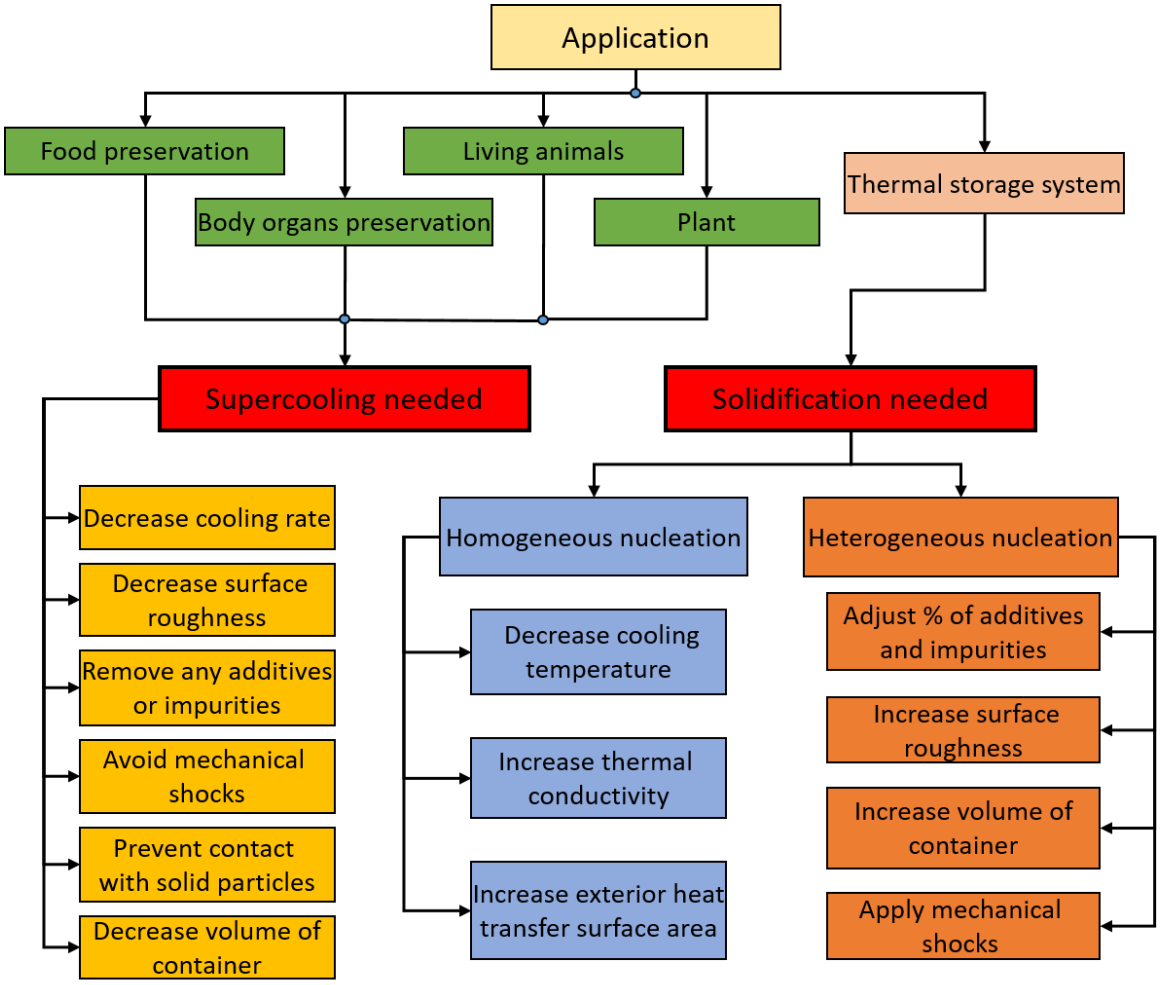

Figure 1.42 Flow chart showing different solutions to trigger or prevent solidification depending on the application

1.8 Conclusion

The present chapter is a comprehensive review of the supercooling phenomenon. The review of its principal occurrences in nature and human applications shows that it is usually beneficial for animal and plants survival and for the preservation of food and organs, while it is detrimental to the performance of most thermal energy storage systems. The investigation of the factors affecting the onset and degree of supercooling leads to the following conclusions:

- The occurrence and degree of supercooling increase with a decrease in the percentage of PCM impurities. Decreasing the cooling rate decreases the degree of supercooling but increases the time spent in supercooled state. Overheating the PCM over repeated cycles and the absence of mechanical shocks on the system also foster supercooling.
- Conversely, the onset and degree of supercooling are reduced by increasing the mixture's thermal conductivity, the container's surface roughness and volume, or by reducing the PCM mixture melting temperature. Adding suitable nucleating agents to the PCM is one of the most used methods to reduce the supercooling degree.

By reviewing the existing numerical models for the simulation of supercooling, it was found that:

- The main challenges are the instable, non-deterministic nature of supercooling and the lack of knowledge on the exact correlations between the various factors affecting its onset.
- Therefore, most models rely on experimental data to provide important parameters such as the degree of supercooling or the rate of crystallization spread. Preset nucleation temperatures, probability equations and state functions are the most used methods to initiate crystallization. However, this strategy limits the validity of the numerical models to very specific experimental cases.

Future experimental and numerical work should include:

- The research of general correlations relating the most important factors affecting supercooling, towards the better prediction of the degree of supercooling and of the onset of crystallization. The correlations should also take into consideration the degradation of the material that takes place due to repeated thermal cycles.
- The investigation of changes in material thermophysical properties as a function of the supercooling degree. This is especially important for high supercooling degrees where the traditional assumptions (density, thermal conductivity, rate of spread, etc.) are no longer applicable.
- The investigation of the PCM temperature increase due to latent heat release. This point is still not well established due to several factors such as degree of supercooling, the change in material's properties and the high rate of spread. Once the behavior is known, the numerical simulation of the system behavior may become more accurate.
- In a holistic approach, the evaluation of the energy and economic impact of supercooling on each application.

1.9 Positioning of the work

The primary goal of this work is to represent supercooling in a numerical model accurately and simply. It is found from the above literature that several critical points must be investigated to build this model.

- The degree of supercooling: It is one of the primary issues that arise in a supercooling problem. The authors of all attempts found in the literature rely on experimental results to assign a nucleation temperature or a nucleation probability formula. As a result, in our work, the model will be given the nucleation temperature. The nucleation process can be initiated by either reaching the predetermined temperature or triggered by the solid/liquid interface.
- The increase in PCM temperature is caused by the release of latent heat when supercooling is interrupted. The value of latent heat during solidification is affected by supercooling. A way to properly define this value should be researched.
- Supercooling degree sensitivity: The degree of supercooling varies as a function of several factors, including externally applied conditions as well as material properties. To validate the model, precise experimental results should be available, which is not the case in the literature. As a result, a benchmark is needed to provide different results using different PCM and by varying various parameters found in the literature to be influential.

The literature lacks quantitative evaluation of the effect of supercooling in real-life latent heat thermal energy storage systems. Such an investigation should be done.

Chapter 2: A CFD model of solid-liquid phase change with natural convection and supercooling

Presentation of the chapter

Considering the supercooling phenomenon in the numerical simulations gives a better prediction of the energy performance of a system. This work is the first attempt to include supercooling in a two-dimensional numerical model that accommodates natural convection during the melting process and supercooling during the cooling of the phase change material. The model represents supercooling using an internal domain heat source and a state function used to modify the thermophysical properties of the material. The goal is to simulate supercooling as simply and quickly as possible while also being as accurate as possible. Based on the literature reviewed in chapter 1, this is the first attempt to represent supercooling using this method.

Nomenclature

A	Function (-)	q	Conductive heat flux (W/m^2)
B	Melted fraction (-)	s, l	Subscripts solid and liquid respectively
C_1, C_2	Constants (-)	s	State function (-)
C_p	Thermal heat capacity (J/kg.K)	T_m	Melting temperature (°C)
D	Gaussian function (-)	$T_n,\ nt$	Nucleation temperature (°C)
$\vec{F}$	Volume force (N/m^3)	t_s	Time required for crystallization (s)
g	Gravity (m/s^2)	dT	Phase change temperature interval (°C)
k	Thermal conductivity (W/m.K)	$\vec{u}$	Velocity of liquid PCM (m/s)
L_F, LH	Latent heat of fusion (J/kg)	ΔH	Sensible enthalpy (J)
n	Normal vector, (-)	ρ	Density (kg/m^3)
Pe	Peclet Number, (-)	β	Thermal expansion coefficient (-)
Q	Heat source (W/m^3)	μ	Dynamic viscosity (Pa.s)
		Δx	Maximum length of mesh cells (m)

2.1 The modeling challenges

Incorporating supercooling into numerical simulations necessitates a number of precautions that increases the model's complexity. A mathematical bijective function from a set X to a set Y allocates exactly one element of Y to each element of X as shown in Figure 2.1a. If a value of X allocates two or more elements of Y, the system is no longer a bijective function as shown in Figure 2.1b. For a given typical phase change problem in the absence of supercooling, the PCM's thermophysical properties can be represented as a bijection of temperature. In the case of cooling in the presence of supercooling, the material examines four consecutive conditions defined as: cooling in liquid state (including supercooled liquid), temperature increase in liquid state caused by latent heat release, solidification in the temperature range of phase change, and cooling in solid state. For example, Figure 2.2 shows the density variation of a material undergoing supercooling as a function of temperature during the cooling process. The figure represents a material having a solid density greater than a liquid density, but the following discussion also applies to liquid densities greater than solid densities. From a liquid state, the material is cooled until it reaches the nucleation temperature T_n (orange), at which the temperature rises (blue) as solidification initiates and latent heat is released. When the material reaches the phase change

temperature, it undergoes solidification (green), and then it goes through a cooling phase of solid (yellow). For a given temperature T_1 where $T_n < T_1 < T_m - dT/2$, the material can be either in liquid state, solid state or in the phase of temperature rise because of initiation of solidification. Another example is for a temperature T that belongs to the phase change temperature range $[T_m - dT/2,\ T_m + dT/2]$. Here the material can be either liquid, in the phase of temperature rise or undergoing phase change. As a result, a PCM's thermophysical properties can no longer be represented solely as a bijective function of temperature.

Another difficulty is determining the temperature at which nucleation begins. Nucleation can be initiated by either reaching a predefined temperature T_n or triggered by the solid-liquid interface. The nucleation temperature varies from node to node, and it is critical because it determines the amount of energy required to raise the temperature to the melting temperature.

The required energy to raise the temperature is obtained from the material's latent heat. The third challenge is determining whether or not the latent heat is sufficient, as well as the temperature attained by the material.

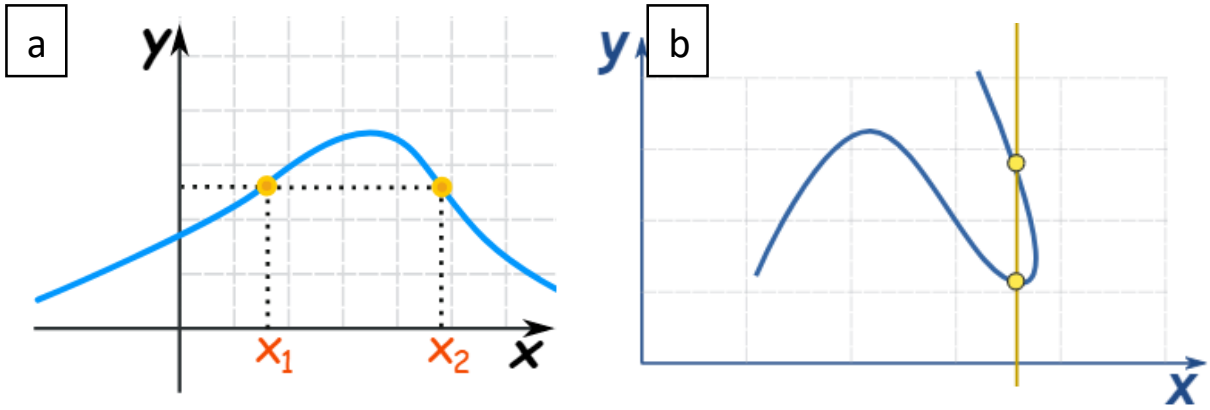

Figure 2.1 Difference between a) a bijective function and b) a non-function

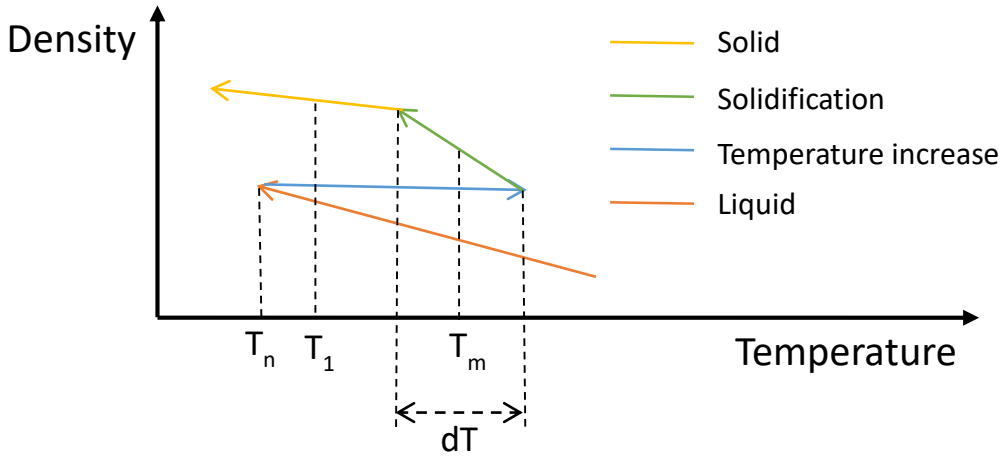

Figure 2.2 Density variation of a PCM undergoing supercooling

Furthermore, the temperature of the material in a supercooled state can rise. This rise can be attributed to the release of latent heat in the neighboring node or to heating the material with an external heat source applied at the boundary. The first assumption means that solidification will begin, which

necessitates the model raising the temperature to reach the phase change temperature and continue solidification. However, the second assumption is typical liquid heating, in which the temperature of the PCM rises without solidification.

Including supercooling in the numerical model necessitates consideration of all of the above-mentioned.

2.2 Mathematical model

2.2.1 Existing model without supercooling

The model built in this study is a modification of an already existing model of Biwole *et al.* [139], [140], which is a modification of Brent *et al.* [141] enthalpy-porosity model. The model assumes that phase change occurs over a temperature interval $[T_m - dT/2,\ T_m + dT/2]$ rather than a constant temperature. The melted fraction is calculated using the function $B(T)$ given by equation (2.1). $B(T)$ is 0 for temperatures less than $T_m - dT/2$ and 1 for temperatures greater than $T_m + dT/2$, and it varies linearly between these two values as shown in Figure 2.3. The density and thermal conductivity are modified depending on the temperature using the piecewise function $B(T)$ as shown in equations (2.2) and (2.3).

To include latent heat during phase change, the value of the specific heat capacity is modified in the interval $[T_m - dT/2, T_m + dT/2]$ by applying a Gaussian function denoted by $D(T)$ given by equation (2.4) and shown in Figure 2.4a. $D(T)$ is multiplied by the latent heat of the PCM and added to the thermal capacity as shown in equation (2.5) and Figure 2.4b.

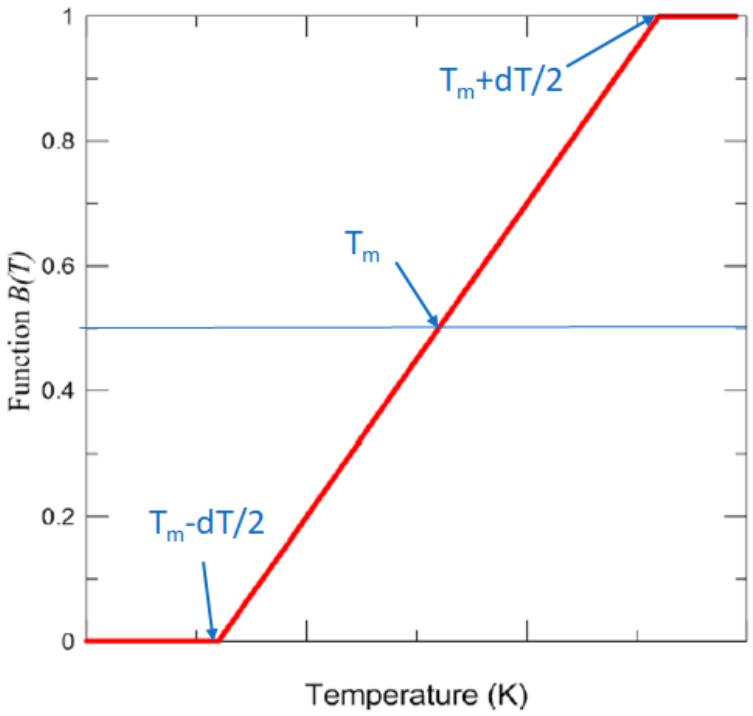

Figure 2.3 Variation of *B(T)* as a function of temperature

$$B(T) = \begin{cases} 0, & T \le Tm - dT/2 \\ \dfrac{T - Tm + dT/2}{dT}, & Tm - \dfrac{dT}{2} < T < Tm + \dfrac{dT}{2} \\ 1, & T \ge Tm + \dfrac{dT}{2} \end{cases} \quad (2.1)$$

$$k(T) = k_s + (k_l - k_s)B(T) \quad (2.2)$$

$$\rho(T) = \rho_s + (\rho_l - \rho_s)B(T) \quad (2.3)$$

$$D(T) = e^{\frac{(T-Tm)^2}{dT^2/4}} \Big/ \sqrt{\pi dT^2/4} \quad (2.4)$$

$$C_P(T) = C_{P_s} + \left(C_{P_l} - C_{P_s}\right) B(T) + L_F D(T) \quad (2.5)$$

The material is motionless in the solid phase. To represent the solid phase, the viscosity of the PCM is increased using a function $A(T)$ shown in Figure 2.5 and denotes as:

$$A(T) = \frac{C_1(1 - B(T))^2}{B(T)^3 + C_2} \quad (2.6)$$

where C_1 and C_2 are constants. C_1 has a very high value that depends on the material, as explained in [139], while C_2 has a very small value and prevents dividing by zero when the PCM is in the solid state. In the solid state $B(T) = 0$ and $A(T) = C_1/C_2$ which corresponds to a very large value, while in the liquid state $B(T) = 1$ and $A(T) = 0$. The viscosity function is then written as:

$$\mu(T) = \mu_l(1 + A(T)) \quad (2.7)$$

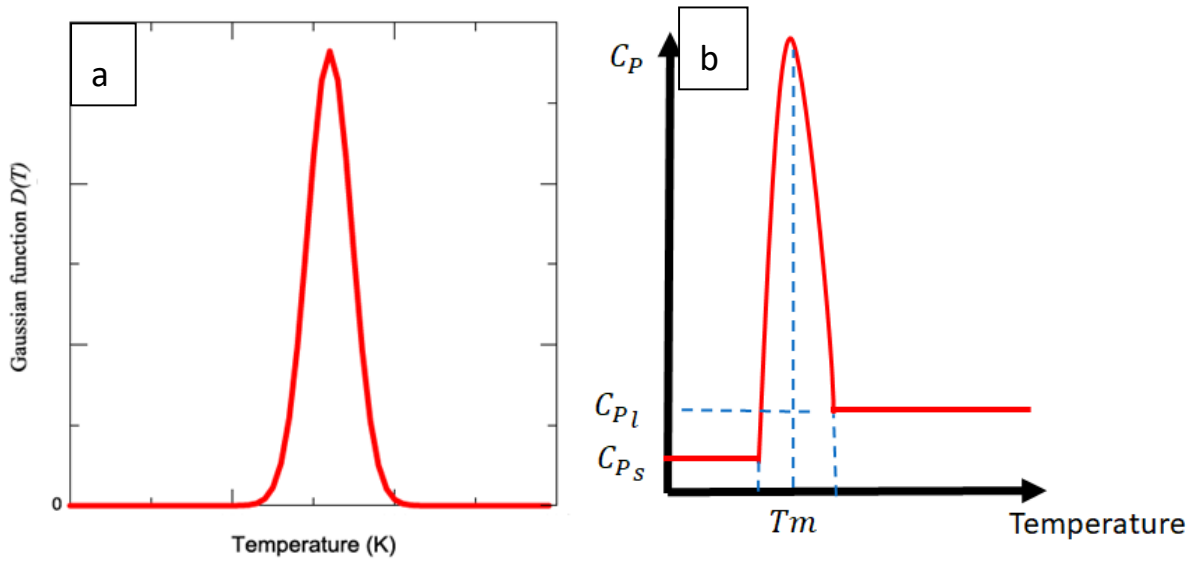

Figure 2.4 Variation of a) D(T) and b) the thermal conductivity as a function of temperature

In the momentum conservation equation, a volume force $\overrightarrow{F_a}$ is also added to dominate over all other forces in the solid phase. When this force overcomes all other forces, the velocity of the PCM ($\vec{u}$) converges to zero, corresponding to the solid state.

$$\overrightarrow{F_a} = -A(T).\vec{u} \tag{2.8}$$

The natural convection is included using a volume force given by:

$$\overrightarrow{F_b} = -\rho_l \beta (T - T_m))\vec{g} \tag{2.9}$$

where β is the coefficient of thermal expansion

The model has already been validated for natural convection during melting in [139], [140]. In those papers, the melting of RT25 and Lauric acid in rectangular enclosures was simulated and compared to an in-lab experiment, and to the experimental work of Shokouhmand and Kamkari [142]. Figure 2.6 shows the comparison of the melting front positions for octadecane, between the present model and other models presented in numerical benchmark of Bertand *et al.* [143] for Prandtl and Rayleigh numbers of value 50 and 10^8, respectively.

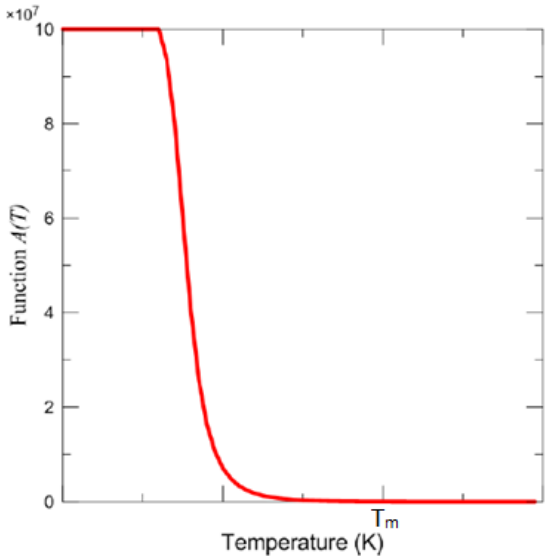

Figure 2.5 Variation of A(T) as a function of temperature

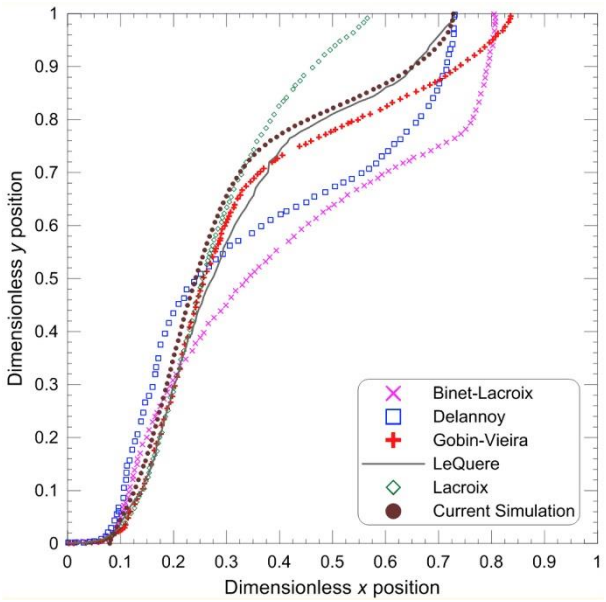

Figure 2.6 Position of the melting front obtained by the current model and the numerical benchmark [143]

2.2.2 Modifications and additions to accommodate supercooling

In the present study, the model is modified to include supercooling upon cooling. To address the issue that the thermophysical properties that can no longer be represented as a bijective function of temperature, a new piecewise state function $s(s,T)$ is developed to precisely represent the state of the material. This function varies according to the material's state and temperature as follows:

$$s(s,T) = \begin{cases} 1, & \text{Heating process} \\ 2, & \text{Liquid and supercooled states} \\ 3, & \text{Temperature rise} \\ 4, & \text{Solidification process and cooling of solid} \end{cases} \quad (2.10)$$

The nucleation temperature T_n is the temperature at which solidification initiates. In other words, it is the lowest temperature a PCM reaches in the liquid state. The nucleation temperature differs from one node of the computational grid to another. For this reason, it is calculated separately for each node and denoted by nt. The following strategy is used to model supercooling:

- First, the PCM in the liquid state stays liquid until solidification is triggered either by the solidification of the adjacent node or if a node reaches a preset nucleation temperature T_n.
- Second, when solidification initiates, the PCM uses a portion of the latent heat to increase its temperature to the upper temperature limit of melting range $T_m + dT/2$. The required energy can be calculated as $C_{P_l}(T_m - nt)$, as detailed in [144]. Therefore, the model increases its temperature by a domain heat source $Q(W/m^3)$ given by:

$$Q = \rho_l C_{P_l}(T_m - nt)/t_s \tag{2.11}$$

where t_s is the time required to raise the temperature from nt to $(T_m + dT/2)$ and is defined based on experimental observations.

- Third, when the temperature of the PCM reaches $(T_m + dT/2)$, the PCM continues solidification in a typical manner in an interval dT. Thereafter, the value of the latent heat is reduced by $C_{P_l}(T_m - nt)$, which is the consumed energy required to increase the temperature from nt to T_m.

However, if the latent heat is insufficient, that is, $C_{P_l}(T_m - nt) > L_F$, the node's temperature rises to a value lower than the melting temperature. Knowing that all the latent heat will be released, equation (2.12) can be written and the attained temperature T reads as in equation (2.13):

$$L_F = C_{P_l}(T - nt) \tag{2.12}$$

$$T = \frac{L_F}{C_{pl}} + nt \tag{2.13}$$

If the latent heat is insufficient, the temperature rises to the previously stated value and the PCM changes its phase directly to the solid phase.

In the equations, $s(s,T)$ will be written as "s" for simplicity. This function divides the heating and cooling cycle to four stages as shown in Figure 2.7. After defining the meaning of each value of s function in equation 2.14 and the possible cases, the state function can be written as follows:

$$s(s,T) = \begin{cases} 1, & s = 4 \; and \; T_{app} > T_m \\ 2, & s = 1 \; and \; T > T_m \; and \; T_{app} < T_m \\ 3, & s = 2 \; and \; T_{app} < T_m \; and \; (T = T_n \; or \; \dfrac{\partial T}{\partial t} > 0) \\ 4, & s = 3 \; and \; Q \le L_F \; and \; T \ge T_m + dT/2 \\ & \text{or} \\ & s = 3 \; and \; Q > L_F \; and \; T \ge L_F/C_{pl} + nt \end{cases} \tag{2.14}$$

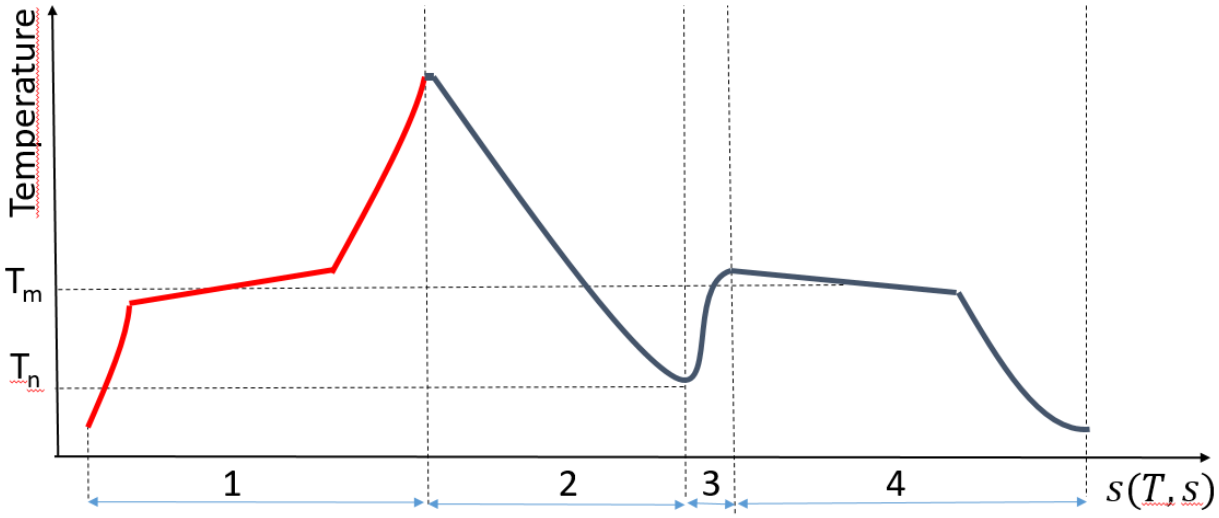

Figure 2.7 The value of the state function $s(s,T)$ as a function of the state of the PCM

The nucleation temperature and the heat source can now be defined as:

$$nt(s,T) = \begin{cases} T_m, & s = 1 \\ \min(T_m, T), & s = 2 \\ nt, & s \geq 3 \end{cases} \tag{2.15}$$

$$Q(s,T) = \begin{cases} \rho_l C_{P_l}(T_m - nt)/t_s, & s = 3 \\ 0, & else \end{cases} \tag{2.16}$$

The modified latent heat L_H depends on the state of the material and is defined as follows:

$$L_H(s,T) = \begin{cases} L_F, & s \leq 3 \\ 0, & s = 4 \; and \; \rho_l C_{P_l}(T_m - nt) > L_F \\ L_F - C_{P_l}(T_m - nt), & else \end{cases} \tag{2.17}$$

In supercooled state and during the temperature rise, the material is in liquid state, so the thermophysical properties of the PCM are conserved equal to the liquid properties. The modified density, thermal conductivity, heat capacity, and viscosity are represented by equations (2.18), (2.19), (2.20) and (2.21), respectively.

$$\rho(s,T) = \begin{cases} \rho_s + (\rho_l - \rho_s)B(T), & s = 1\ or\ s = 4 \\ \rho_l, & s = 2\ or\ s = 3 \end{cases} \quad (2.18)$$

$$k(s,T) = \begin{cases} k_s + (k_l - k_s)B(T), & s = 1\ or\ s = 4 \\ k_l, & s = 2\ or\ s = 3 \end{cases} \quad (2.19)$$

$$C_p(s,T) = \begin{cases} C_{ps} + \left(C_{pl} - C_{ps}\right)B(T) + LH * D(T), & s = 1\ or\ s = 4 \\ C_{pl}, & s = 2\ or\ s = 3 \end{cases} \quad (2.20)$$

$$\mu(s,T) = \begin{cases} \mu_l(1 + A(T), & s = 1\ or\ s = 4 \\ \mu_l, & s = 2\ or\ s = 3 \end{cases} \quad (2.21)$$

2.3 Numerical modeling

2.3.1 Physical model

The model is a 2D representation of a test tube partially filled with PCM and immersed in a water bath. The tube is 1.5 mm thick, 13 mm in internal diameter and 7.5 mm in height. Figure 2.8 shows the materials of each component in the model and the boundary conditions. Regarding the boundary conditions, the upper boundary condition is open, whereas the remaining boundaries have Dirichlet conditions with a fixed applied temperature denoted by T_{app}, which represents the temperature of a water bath. The Dirichlet (or first-type) boundary condition is one kind of boundary conditions used in the study of differential equations in mathematics [145]. It specifies the values that a solution must take along the domain's edge when applied to an ordinary or partial differential equation. When a Dirichlet condition is given, there is no need to solve for the dependent variable because it is predetermined. As a result, the problem can be solved without using equations for these degrees of freedom. The open boundary condition allows fluid flow through the boundary. It applies a zero conductive flux condition for an outgoing fluid flow across the boundary according to equation (2.22):

$$-n.q = 0, \qquad n.u \geq 0 \quad (2.22)$$

where n and q are the normal vector pointing out of the domain and conductive heat flux respectively.

It automatically takes into consideration the heat flux caused by the flow rate through a Danckwerts condition on the enthalpy for an incoming flow of velocity field u across the boundary given by the equation (2.23):

$$-n.q = \rho \Delta H u.n, \qquad n.u < 0 \quad (2.23)$$

where ΔH is the sensible enthalpy

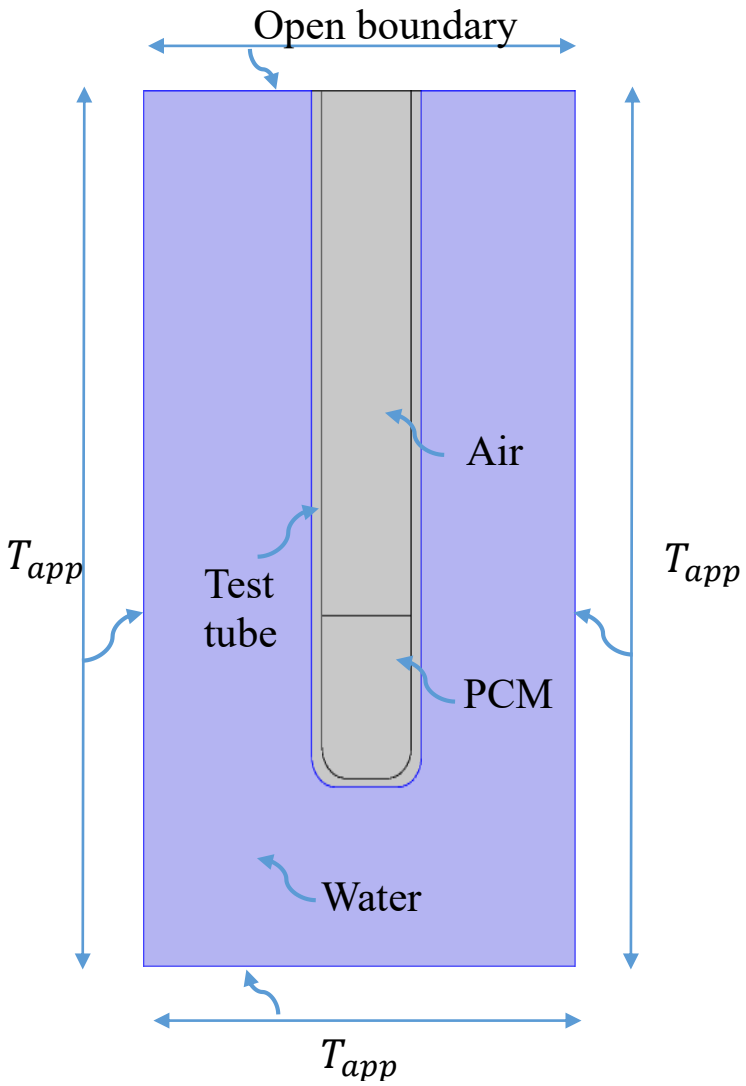

Figure 2.8 Geometry, materials and boundary conditions used in the numerical model

As an alternative, the temperature of an entering flow can be limited by the open border condition. For example, in an experiment with an open boundary to standard room temperature, the temperature border condition can be set to the ambient temperature. Both possibilities are predicated on knowledge of the upstream temperature at the virtual domain's outer boundary, however the first one should be chosen in order to take into consideration the feedback from the model's heat sources and temperature limits on the inlet temperature profile.

The PCM, tube, and air above the PCM have the same initial temperature while the initial temperature of water is T_{app}. If the initial temperature of PCM is higher than the phase change temperature, it is assumed to be in the liquid state; otherwise, it is assumed to be in the solid state.

2.3.2 Numerical scheme

The finite-element approach is frequently utilized for the thermal numerical simulation of heat treatment, casting, or welding operations. Due to the effects of latent heat, simulating phase changes necessitates simulation of extremely nonlinear problems. The numerical challenge of finite-element analysis of heat transfer systems incorporating phase changes has received a lot of attention lately [146]. The fixed-grid technique relies on the temperature profile to determine the position of the interface. Consequently, the interface can have a continuous, smooth front or not. The three different fixed grid approaches, which can be divided into three groups, are described in depth by Voller *et al.* [147]:

- The fictitious heat flow methods
- The effective heat capacity technique
- The total enthalpy methods

The above described mathematical model is implemented in a mesh built using linear free triangular elements (Figure 2.9). The mesh size is defined by ensuring a mass mesh Peclet number lower than two as shown in equation (2.24), to help numerical converge. The simulations first run with an extra-fine mapped mesh of 9818 elements (Figure 2.9a). The second batch of simulations is run with an extremely refined mesh composed of 21262 (Figure 2.9b).

$$Pe = \frac{u\Delta x}{\mu/\rho} < 2 \tag{2.24}$$

where Δx is the maximum length of mesh cells.

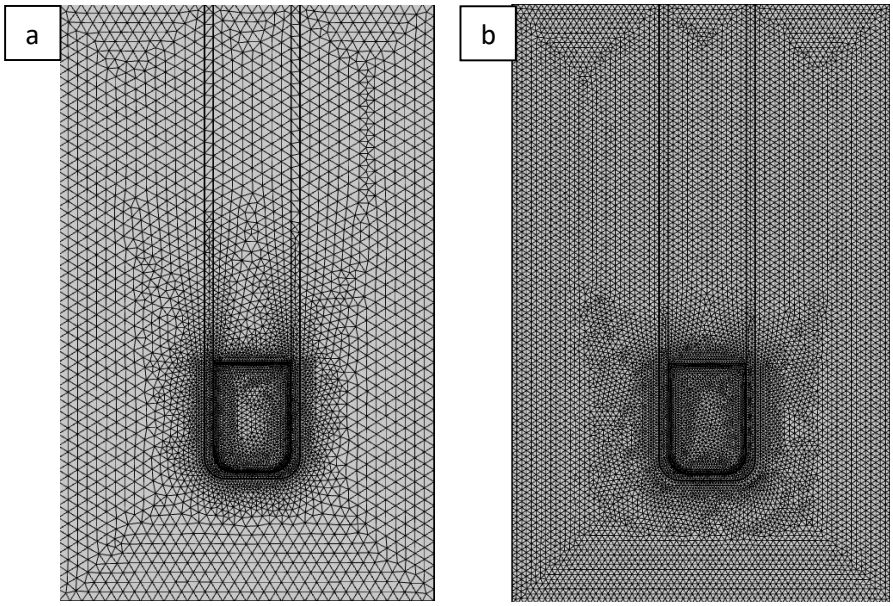

Figure 2.9 Meshes used in the COMSOL Multiphysics numerical model: a) extra fine and b) extremely fine

2.4 Chapter conclusion

Including the supercooling phenomenon in numerical simulations necessitated the addition of a piecewise state function that defined the material's state. The function is used to modify and control the

thermophysical properties of the PCM. The model represents supercooling and its effects on the PCM's behavior using a simple technique. The PCM is forced to remain at liquid state at a temperature below its melting point until it reaches a preset temperature or until a neighboring node triggers solidification. The core novelty of the model is the representation of the temperature rise by a domain heat source whose value depends on the nucleation temperature. The reached temperature and rest amount of latent heat to continue solidification are also calculated as functions of the nucleation temperature.

To validate this model, a series of experiments with various PCMs having different thermophysical properties is carried out in the following section of this manuscript. Validating the model and understanding its limitations later allow to use it in real applications of thermal energy storage systems, where the effect of supercooling is investigated.

Chapter 3: Experimental benchmark on solid-liquid phase change in the presence of supercooling and natural convection

Presentation of the chapter

Phase change materials (PCM) are used in thermal energy storage systems to enhance their performance. Supercooling and natural convection can occur respectively during the cooling and heating cycles of the material's solid-liquid phase change and modify the systems' efficiency. This study experimentally investigates the supercooling and convection behavior in three PCMs, namely pure octadecane (organic), a eutectic PCM, and sodium acetate trihydrate (inorganic). The aim is to provide benchmark data for numerical simulation models and to explore the effect of different factors on the degree of supercooling and on natural convection. Results show that the type of PCM, the temperature of the cooling fluid, mechanical shocks, the geometry of the PCM's container and its surface roughness have a direct effect on the degree of supercooling. The supercooled PCM shows a high sensibility to any changes in the applied conditions. The thermal insulation of the unheated PCM boundaries has a major effect on the solidification and melting dynamics and topology, particularly regarding the solid-liquid interface. The cross-sectional temperature profiles, the inclination of the solid-liquid interface, and the melting rate show that regardless of the PCM, natural convection plays a significant role during the heating process but not during the cooling process.

Nomenclature

ρ	Density (kg/m^3)	s, l	Subscripts solid and liquid respectively
k	Thermal conductivity (W/m.K)	$\emptyset$	Diameter (mm)
C_p	Thermal heat capacity (J/kg.K)	T_{max}	Maximum temperature (°C)
T_m	Melting temperature (°C)	L_F	Latent heat of fusion (J/kg)

3.1 Introduction

Phase change materials (PCM) employed in latent heat thermal energy storage systems (LHTESS) are divided into three categories, organic, inorganic, and eutectic. Organic materials are classified as paraffin (straight chain n-alkanes) and non-paraffin (glycol, alcohol, and fatty acid); inorganic materials are classified as salt hydrates, inorganic compounds, and metallic; and eutectics are mixtures of two phase change materials with different melting temperatures [148], [149]. Each category has its own characteristics that might have beneficial or adverse effect when used in LTES systems [150]. Table 3.1 summarizes the desired properties when selecting a PCM for integration in a LHTESS. The PCM used in a thermal energy storage system is critical to the system's efficiency and performance [151]. Supercooling refers to a material remaining in liquid state at a temperature lower than its melting temperature. Supercooling is undesirable in most LHTESS. According to the recent literature [59], a supercooled liquid is instable, and solidification can occur due to a variety of factors. Inorganic materials, for example, are subjected to more supercooling and phase separation than organic compounds. Natural convection in a PCM container refers to the transport of melted material due to buoyancy forces arising when the density of melting PCM parts decreases. Natural convection has a direct impact on the melting process by increasing the melting rate.

Several researchers have recently proposed numerical models of supercooling in PCMs [49], [152], [153]. Unfortunately, there is still a scarcity of experimental data that can be used to validate such models. This is especially true for supercooling. Waser *et al.* [49] modeled the solidification of PCM in a fin-tube heat exchanger, including supercooling, and sodium acetate trihydrate (SAT) was used in the experimental

model validation process. Huang *et al.* [152] numerically modeled the crystal growth of a supercooled PCM during phase change. SAT was also used to experimentally investigate the effect of supercooling on output heat. Zhao *et al.* [153] developed a numerical model of fin tube latent heat storage and validated it using experimental data from inorganic salt hydrates. Validation of the numerical models necessitates not only precise results, but also precise input parameters including the container geometry, the used materials, the initial and boundary conditions applied, and the various measurement tools and control systems. As a result, the authors prefer to conduct their own experiments to ensure precise results and well-known experimental conditions.

The goal of this research is to provide benchmark experimental data of PCM thermal behavior in the presence of supercooling and natural convection. The obtained results can be used in the computational fluid dynamics community to validate numerical models. The chapter first describes the experimental methodology, which includes a detailed description of the experimental setups, the thermophysical properties of the chosen materials and the temperature control and monitoring system. The study investigates three PCMs: octadecane, an organic PCM of phase change temperature 28 °C, sodium acetate trihydrate (SAT), an inorganic PCM of phase change temperature 58 °C, and a eutectic PCM of phase change temperature 21.3 °C. Then, experimental results are provided in the form of temperature variation as a function of time at several locations in the PCM container. Each PCM is tested on two containers of different geometry, with varying cooling and heating rates. For each experiment, the initial and boundary conditions are detailed. Last, a discussion section examines the main findings.

Table 3.1 Phase change material selection criterion based on the properties [154]

Thermodynamic properties	Melting temperature ranging in operating range of LHTESS	High thermal conductivity High latent heat	High thermal stability High specific heat
Environmental aspects	Reduction of global warming	Non-toxic to the environment	Sustainable product
Chemical properties	Non flammable High chemical stability	Non toxic No supercooling	Low volume expansion Non corrosive
Economical aspects	Low price	Availability	Low operating cost

3.2 Methodology

3.2.1 Phase change materials

A number of variables, including metabolic rate, clothes insulation, air relative humidity and velocity, affect the comfort temperature in a room. According to ASHRAE standard 55 [155] on thermal comfort,the indoor comfort temperature range for a person during summer and winter is, respectively, [22.8 °C, 26.1 °C] and [20 °C, 23.9 °C]. The phase change temperature of organic n-alkanes varies from 18 °C to 36 °C, making them suitable candidates for use in applications to maintain comfortable indoor temperatures. They also exhibit steady chemical activity under repeated phase changes [156]. The first selected PCM is

therefore octadecane $C_{18}H_{38}$. The manufacturer, FisherScientific, reports a 99+% purity. Table 3.2 lists the thermophysical properties of solid and liquid octadecane.

Table 3.2 Thermophysical properties of octadecane

Reference	Property	Solid	Liquid
Yehya *et al.* [157]	Cp (J/kg.K)	1910	2230
Yehya *et al.* [157]	k (W/m.K)	0.356	0.149
Supplier	ρ (kg/m^3)	777	777
Supplier	T_m = 28-30 °C	-	-
Supplier	L_F = 237 kJ/kg	-	-

The second PCM is a eutectic fatty acid previously used by Souayfane *et al.* [158] and supplied by Cristopia Energy Systems. Its thermophysical properties are listed in Table 3.3:

Table 3.3 Thermophysical properties of eutectic fatty acid PCM [158]

Property	Solid	Liquid
k (W/m.K)	0.182	0.182
Cp (J/kg.K)	1670	2090
ρ (kg/m^3)	960	884
T_m = 21.3 °C	-	-
L_F = 152 kJ/kg	-	-

The third chosen PCM is pure sodium acetate trihydrate (SAT). The manufacturer, FisherScientific, reports a 99+% purity. SAT possesses a number of characteristics that make it suitable for use in thermal energy storage systems. According to Wang *et al.* [159] SAT exhibits high latent heat, low thermal expansion, is chemically stable, non-toxic, low cost and easily accessible. However, the material has some drawbacks for LHTESS applications which are low thermal conductivity, high supercooling degree, phase segregation and corrosion with some metals [160]. Table 3.4 summarizes the thermophysical properties of SAT [159].

Table 3.4 Thermophysical properties of SAT

Reference	Property	Solid	Liquid
Wang *et al.* [159]	Cp (J/kg.K)	2900	3100
Wang *et al.* [159]	k (W/m.K)	0.600	0.385
Wang *et al.* [159]	ρ (kg/m^3)	1450	1280
Supplier	T_m = 58-60 °C	-	-
Supplier	L_F = 264 kJ/kg	-	-

3.2.2 Small-scale and large-scale experimental setups

A first setup, hereafter referred to as the small-scale experiment, consist of a test tube that is fixed to a stand and placed vertically inside a temperature-controlled chamber. The tube is 100 mm high, 1.5 mm thick, and has an outer diameter 16 mm. The temperature variation with time is collected using two T-type class 1 thermocouples of precision ± 0.5 °C and 1 mm junction diameter. As seen in Figure 3.1a, the first thermocouple measures the temperature of the PCM close to the boundary, while the other measures the temperature of the water in the chamber. The aim of the small scale experiment is to ensure limited amount of tested PCM, which reduces the risk of nucleation sites within the material, and smooth surface contact between the PCM and the glass container.

A second, large-scale experiment, is done in a polycarbonate container of dimensions 208 mm x 100 mm x 150 mm (width x depth x height). The container's wall is 10 mm thick, transparent and of thermal conductivity 0.20 W.m^{-1}.K^{-1}. As shown in Figure 3.1b, the container is divided into three chambers that are separated by two 3 mm thick aluminum plates with dimensions of 100 mm x 150 mm (depth x height). The PCM is located in the middle chamber, which is 80 mm x 100 mm x 150 mm (width x depth x height). The PCM chamber's temperature is controlled by the two adjacent chambers that act as thermostatic baths. The adjacent chambers are filled with water at regulated temperature, thus imposing Dirichlet boundary conditions to the PCM domain. In order to reduce heat loss to the outside and ensure the PCM receives heat predominantly from the thermostatic baths, 40 mm thick polyurethane foam with a thermal conductivity of 0.025 W/m.K insulates the polycarbonate plates in contact with the PCM from the exterior. The large-scale experiment provides the opportunity to view the effect of natural convection on the melting front, and the effect of PCM's volume on the supercooling degree.

These experiments allow for the use of a variety of cooling temperatures, to investigate their effect on the supercooling phenomenon. The container effect is represented by the structure's volume, and surface roughness.

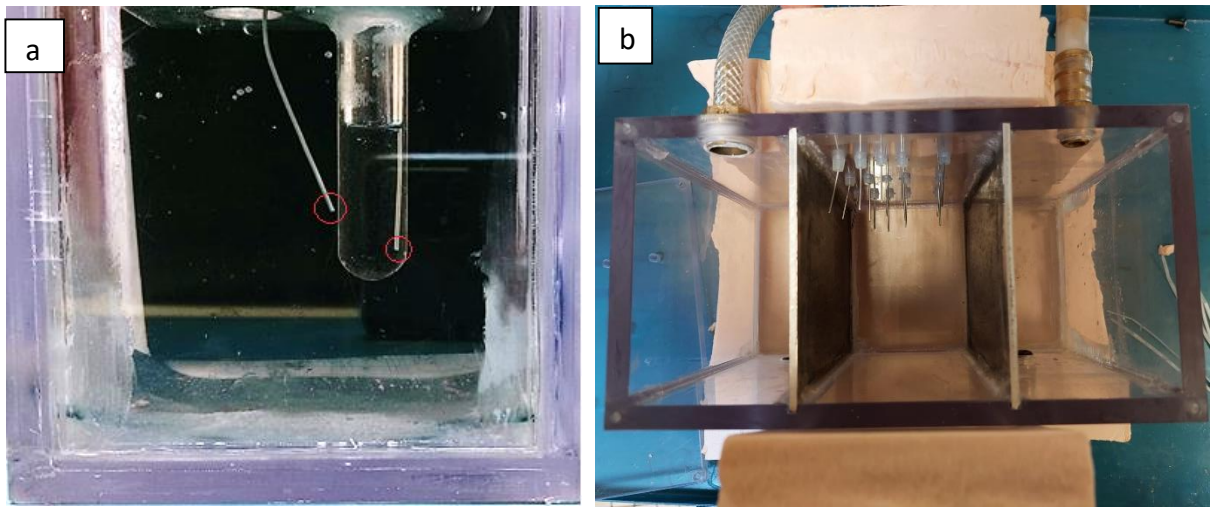

Figure 3.1 (a) Thermocouples position in the small-scale experiment and (b) top view of the large-scale experiment

3.2.3 Temperature control and monitoring system

The water temperature in the two adjacent chambers is controlled by a LabTech H50-500 water chiller and a Fisher Scientific Heating Circulator Polystat 5A+24. The temperature and flow rate controls are listed in Table 3.5. The water flows from the top to the bottom of each chamber, to maintain a consistent water temperature near the aluminum plate. Figure 3.2 shows one of the adjacent chambers.

To measure the temperature of the PCM at various locations, fifteen class 1 T-type thermocouples of precision ± 0.5 °C are inserted into the container's back plate. The thermocouples have a diameter $\emptyset = 1\ \mathrm{mm}$, an AISI 321 stainless steel coating, are hot weld insulated, and can withstand temperatures as high as 400 °C. As shown in Figure 3.3, the thermocouples are evenly spaced in the vertical direction and focused on one side in the horizontal direction. The thermocouples are inserted in the PCM at 2.5 cm from the back plate. The objective is to raise the thermocouple density close to the plate where solidification begins. To avoid leakage, the thermocouples are fixed using silicon caps. The presence of thermocouples enables the examination of temperature variations in both the vertical and horizontal directions.

Table 3.5 Characteristics of water chiller and heating circulator

	Temperature range ($°C$)	**Temperature stability ($°C$)**	**Temperature controller**	**Flow rate (L/min)**
Water chiller	$-5 \rightarrow 35$	± 0.3	PID	Up to 3
Heating circulator	$20 \rightarrow 100$	± 0.05	PID	Up to 10

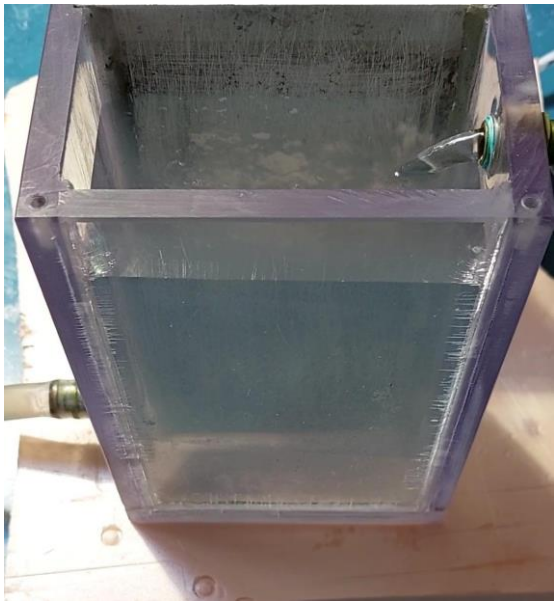

Figure 3.2 Water flow to control the temperature at the PCM boundaries

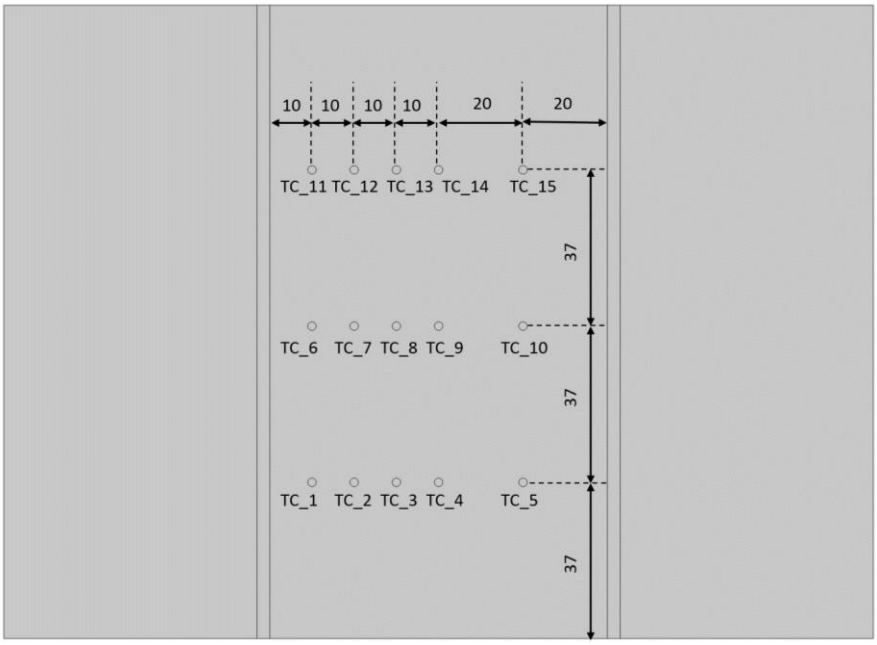

Figure 3.3 Positions (mm) and number of thermocouples used to measure the PCM temperature

Additionally, to monitor the temperature of the water near the aluminum plate, one T-type class 1 thermocouple of 3mm diameter is installed in each of the two neighboring chambers.

The thermocouples are connected to an NI cDAQ-9174 data acquisition device, enabling LabVIEW software to gather and save the measured data. Figure 3.4 shows the front view of the large-scale experiment. The figure shows the position of PCM, water, insulation and thermocouples that measure water temperature.

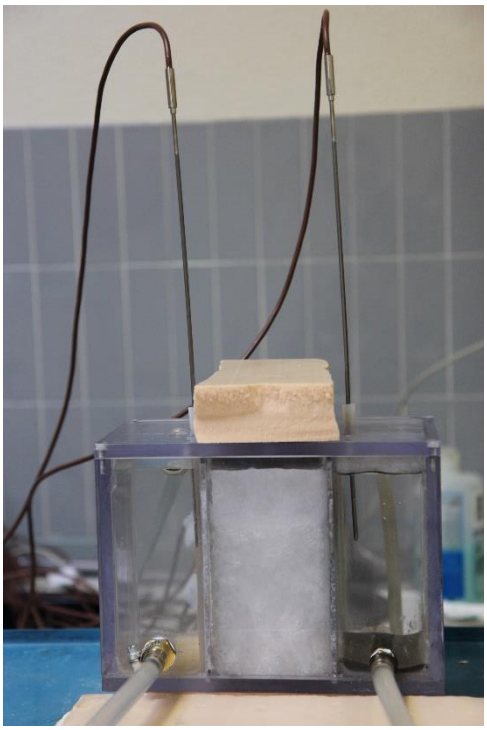

Figure 3.4 Front view of the large-scale experiment

3.3 Results

3.3.1 Small-scale experiment

3.3.1.1 Octadecane

A 35 °C bath is used to heat the test tube containing 1.8 g of octadecane. After melting, the tube is placed in a cooling water bath with a preset temperature. The study is done on how coolant temperature affects the occurrence of supercooling. The evolution of the PCM and water temperatures are recorded. Results show that when the coolant temperature is lower than 25 °C, supercooling does not occur. It occurs when the coolant temperature rises to 25.5 °C, which is closer to the phase transition temperature, with a recorded nucleation temperature of 26.34 °C as seen in Figure 3.5. Within the supercooled state, the nucleation temperature is defined as the temperature at which the local PCM temperature begins to rise as a result of latent heat release. In the case of the small-scale experiment with octadecane, the initiation of solidification is accompanied by the increase of the local PCM temperature to a temperature of 27.3 °C, where solidification takes place.

Figure 3.6 shows an additional series of tests that make use of a reduced temperature difference between the cooling bath and the PCM. The cooling bath's temperature progressively drops, affecting the PCM's temperature. The water temperature is adjusted several times, to reduce to cooling rate and impose a progressive temperature drop. The adjustment is reflected in the fluctuations of water temperature visible in Figure 3.6a. As shown in the Figure, fluctuations in the coolant temperature lead to fluctuations of the PCM’s temperature. In this case, the PCM's temperature gradually drops as well, entering a stable supercooled state from second 970 to second 1235. In the absence of nucleation initiation conditions, the PCM remains in a stable supercooled state. Once the PCM temperature hits 26.15 °C, solidification begins, showing that the nucleation temperature varies as a function of cooling rate. As

noticed by several researchers [45], [55], [57], [58] reduced cooling rates allow for lower nucleation temperatures. Figure 3.6b examines the effect of a water bath temperature close to the previously recorded nucleating temperature. Therefore, the bath's temperature is decreased from 26.5 °C to 26.3 °C. Similar to Figure 3.6a, PCM's temperature drops gradually until it reaches 26.3 °C, at which point solidification begins.

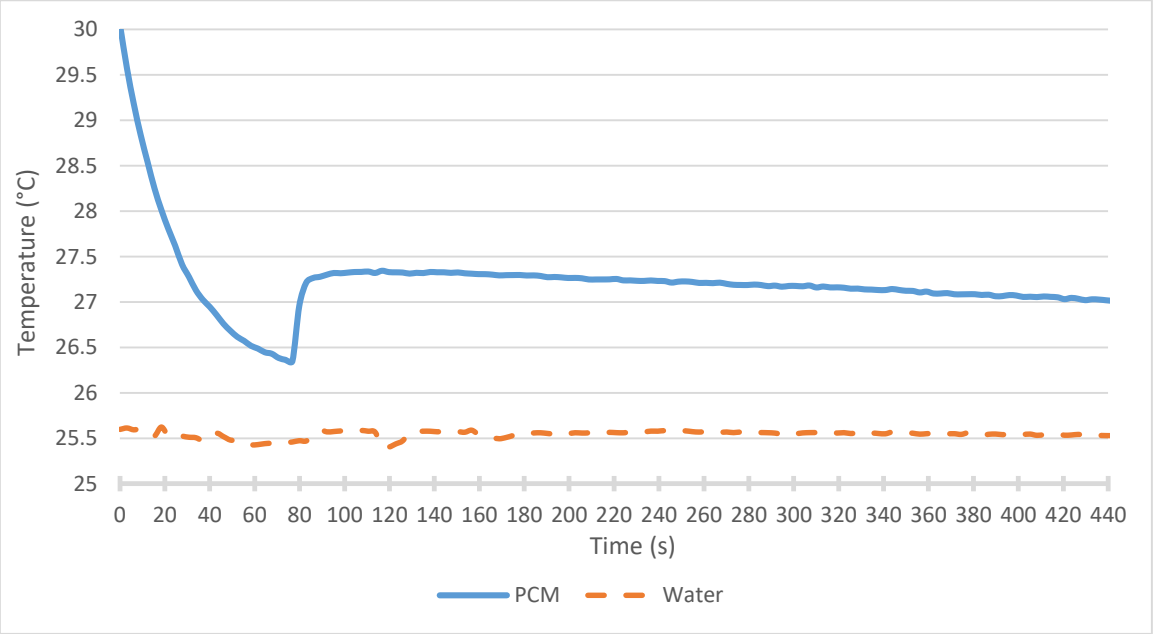

Figure 3.5 Cooling of octadecane using cold water (25 °C) and presence of supercooling

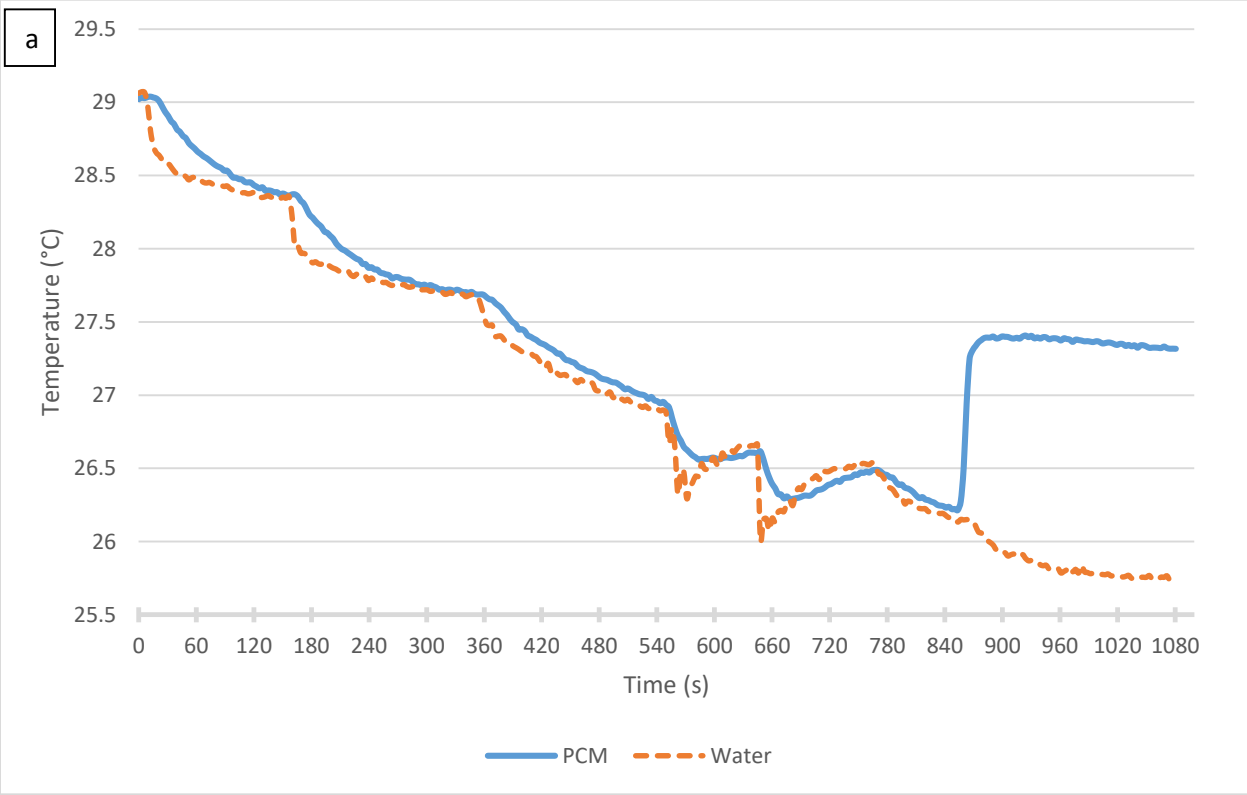

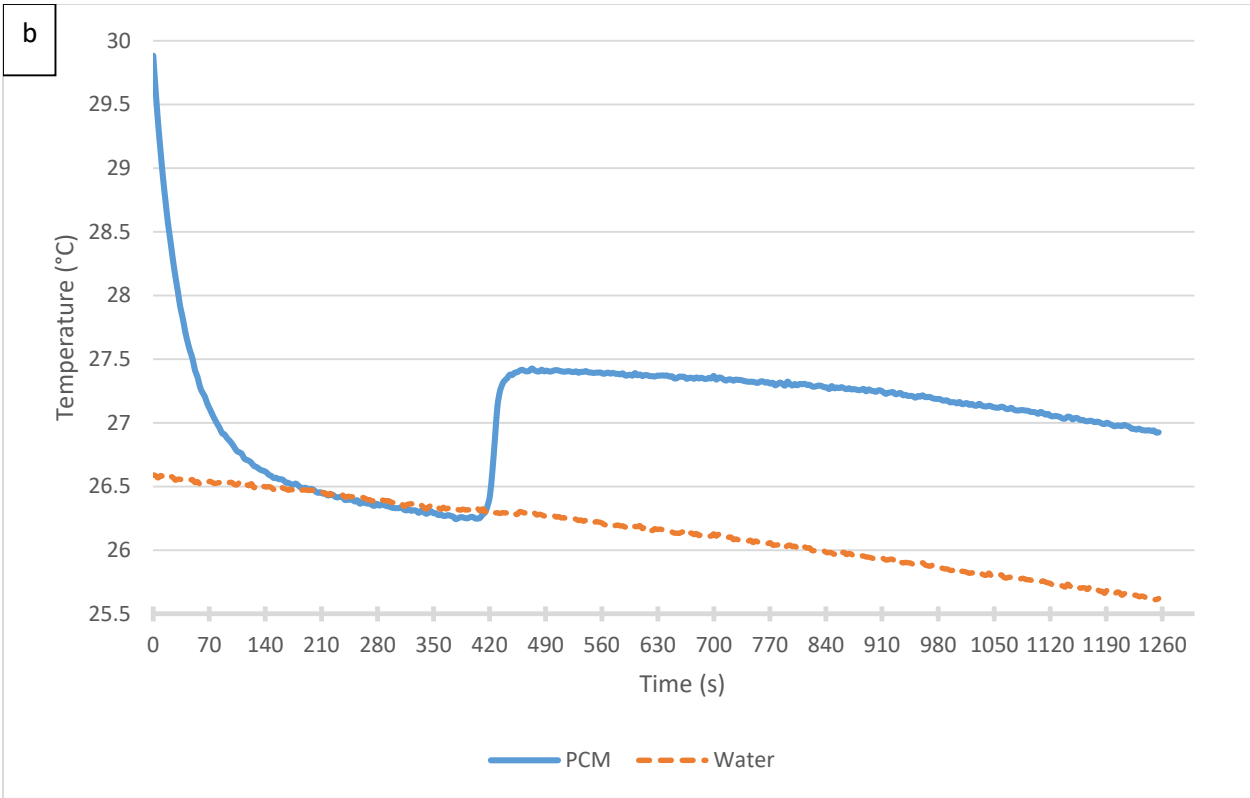

Figure 3.6 Octadecane entering in stable supercooling with a) gradually decreasing and b) relatively high cooling bath temperature

3.3.1.2 Eutectic PCM

The test tube containing 3.2 g of eutectic PCM is heated until the material melts. The same mass is used in a series of trials with various cooling temperatures. Table 3.6 details for each trial the cooling temperature used and the obtained nucleation temperature, supercooling degree, time spent in supercooled state, solidification temperature and elapsed time from the nucleation to the solidification temperature. The solidification temperature is the achieved temperature following the release of latent heat caused by solidification initiation. However, the supercooling degree is the difference between the nucleation temperature and the material's melting temperature. It is found from the performed trials that the melting temperature is actually 21.5 °C. The time spent in the supercooled state is the interval between the instant when the temperature of the liquid PCM falls below the melting temperature and the instant solidification is initiated.

The first two trials are done using the same coolant temperature. The results are close. However, even though the experiment is done using the same mass of the material, the same container, the same position of thermocouples, the same DAQ system and the same cooling temperature, the behavior of PCM for both tests is slightly different as shown in Figure 3.7. In the first trial, the nucleation starts earlier and the temperature reaches a higher value when latent heat is released. It also displays a one-degree difference in nucleation temperature and supercooling degree when compared to the second trial. This finding underlines the instable nature of supercooling. However, the different behavior might also be due to the precision of the thermocouples, which is $\pm$ 0.5 ℃.

Table 3.6 Cooling of eutectic PCM using different coolant temperatures

	Coolant temperature (°C)	Nucleation temperature (°C)	Supercooling degree (°C)	Time spent in supercooled state (s)	Solidification temperature (°C)	Time required during temperature increase (s)
Trial #1	18.1 °C	20.4 °C	1.1 °C	62 s	21.5 °C	158 s
Trial #2	18.1 °C	20.3 °C	1.2 °C	63 s	21.4 °C	154 s
Trial #3	13.2 °C	20 °C	1.5 °C	54 s	20.94 °C	154 s
Trial #4	8.5 °C	19.9 °C	1.6 °C	43 s	20.7 °C	98 s
Trial #5	3.6 °C	19.6 °C	1.9 °C	40 s	20.4 °C	89 s
Trial #6	Gradually decreasing (Figure 9)	19.8 °C	1.7 °C	64 s	21.5 °C	188 s
Trial #7	20.75 °C	20.87 °C	0.63 °C	Stable supercooling	21.4	74 s

In trials #3 to #5, the coolant temperature is decreased to 13.2 °C, 8.6 °C, and 3.6 °C, respectively. Although the PCM enters in supercooled state in each trial, its behavior varies depending on the cooling temperature. First, as the cooling temperature decreases, the PCM reaches the nucleation temperature faster. For this reason, the PCM spends less time in supercooled state. However, as the cooling temperature decreases, the degree of supercooling increases. In other words, the nucleation temperature is lower. These results are consistent with the findings published in several other experimental studies and literature reviews [55], [57], [58], [144]. Additionally, the PCM is unable to attain its phase transition temperature as the cooling temperature drops. As observed during the experiment, the PCM next to the test tube's wall begins to solidify before the PCM located near the thermocouple. The latent heat of the eutectic PCM is theoretically sufficient to increase the local temperature to the melting temperature, but this is not the case as shown in Figure 3.8. The PCM is not able to rise its local temperature to the melting temperature due to the slow temperature rise and the heat loss to the surrounding PCM parts.

The coolant temperature and PCM have the same initial temperature in trial #6, and the coolant temperature gradually decreases to a minimum temperature of 17.3 °C, as shown in Figure 3.9. In this case, the PCM is supercooled by 1.6 °C, yielding a value similar to those obtained when using very low cooling temperatures (trials #4 and #5). However, before reaching the nucleation temperature and initiating solidification, the PCM stays for a longer time in supercooled state. It should be noted that the variation in water temperature is caused by changing the temperature of the supplied water. It is not due to the latent heat release in the PCM.

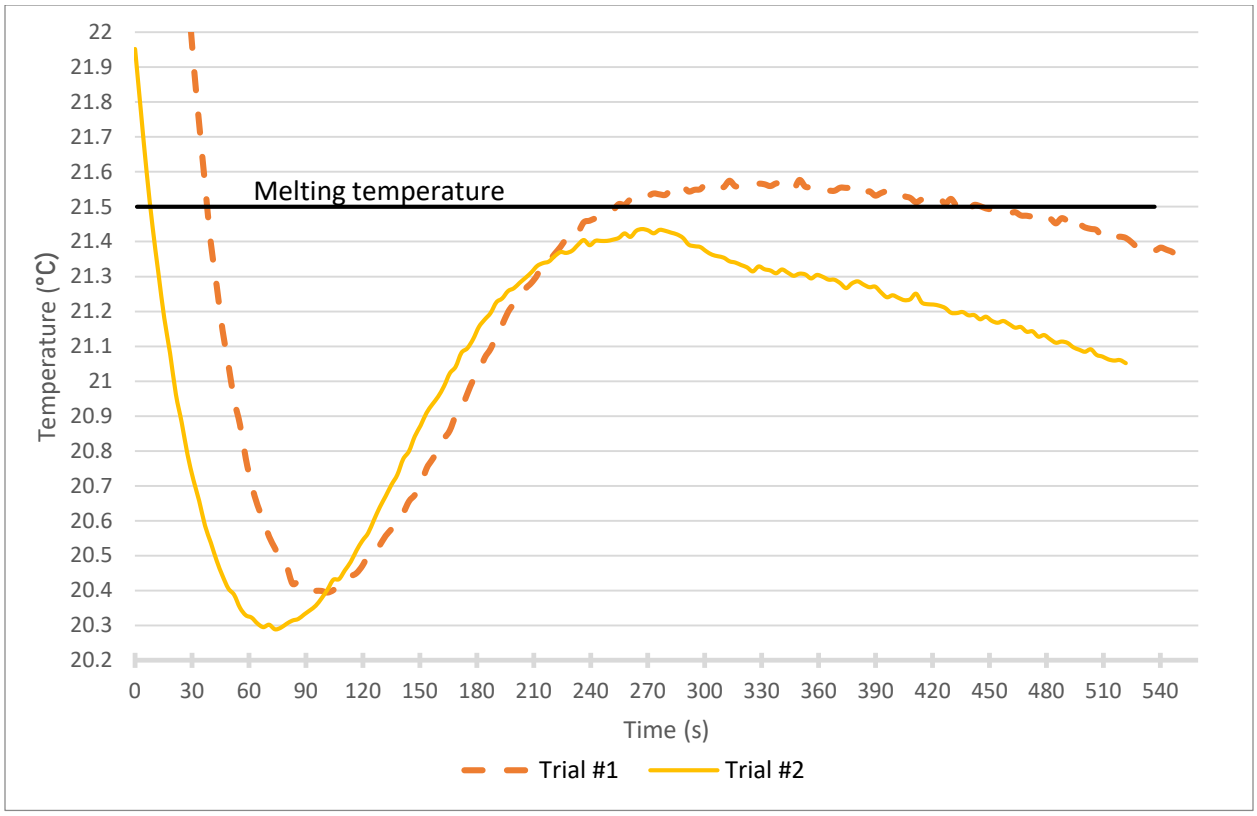

Figure 3.7 Cooling of the eutectic PCM using the same average coolant temperature (18.1 °C)

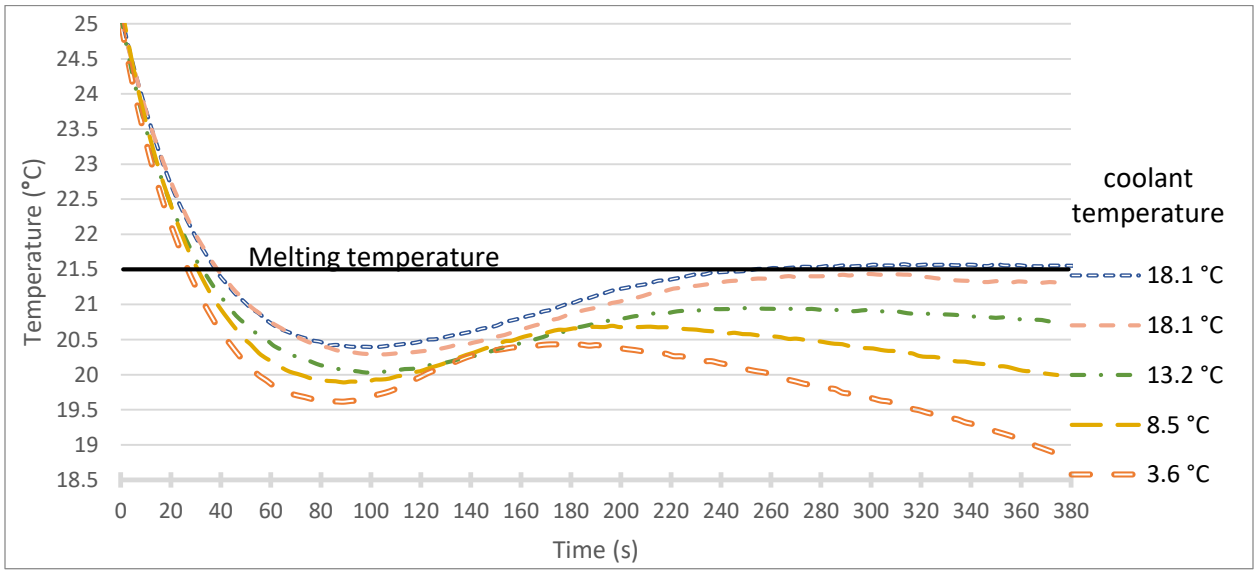

Figure 3.8 Eutectic PCM transient temperature under different coolant temperatures

Figure 3.10 shows stable supercooling with a coolant average temperature of 20.75 °C. The PCM stays in supercooled state for 807 seconds before a mechanical shock is applied, resulting in the start of solidification. The lowest temperature recorded in supercooled state is 20.87 °C resulting in 0.63 °C of supercooling. The temperature increases to 21.4 °C where solidification takes place. Another experiment is carried out and then repeated. In the first and second experiments, the average coolant temperature is

19.87 °C and 19.91 °C, respectively. Figure 3.11 represents the temperature variation of PCM and water in each experiment. It shows that despite the fact that the average temperature is nearly identical, PCM in supercooled state is sensitive to any small thermal amplitude. A slight difference in the coolant temperature causes a difference in the supercooling degree and PCM behavior during temperature increase and solidification.

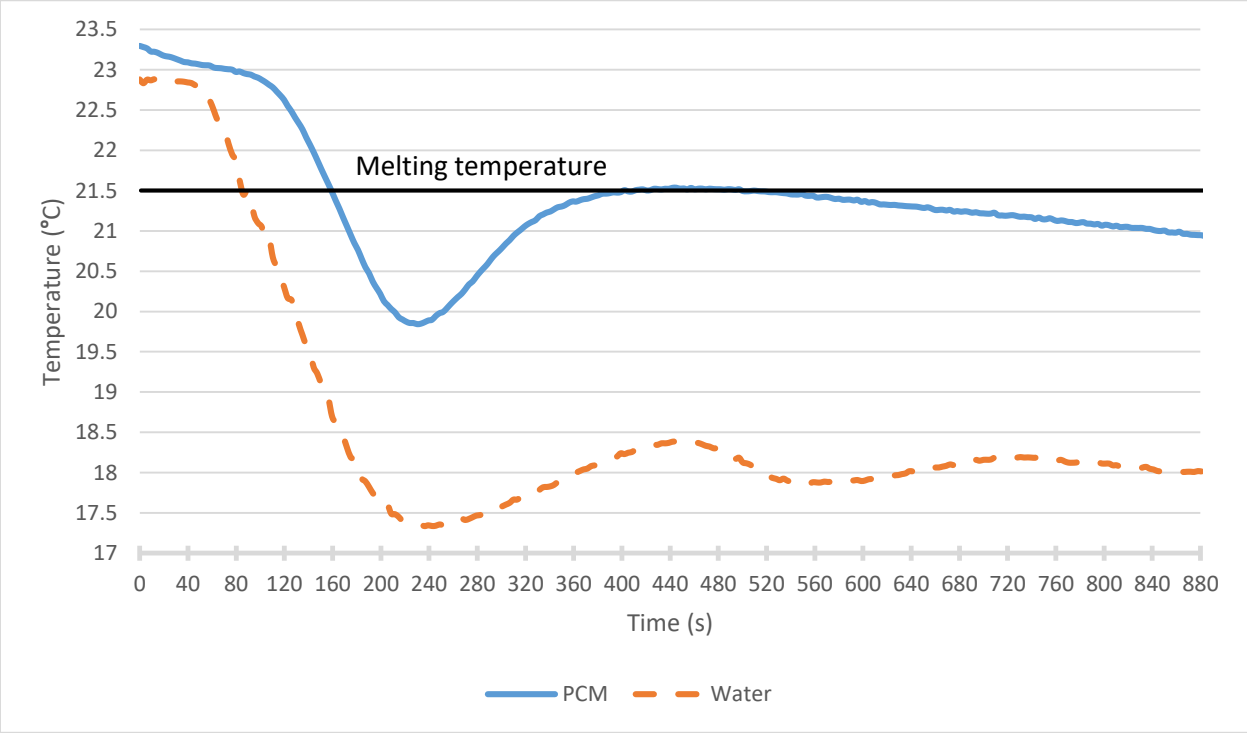

Figure 3.9 Cooling of eutectic PCM using gradually decreasing coolant temperature

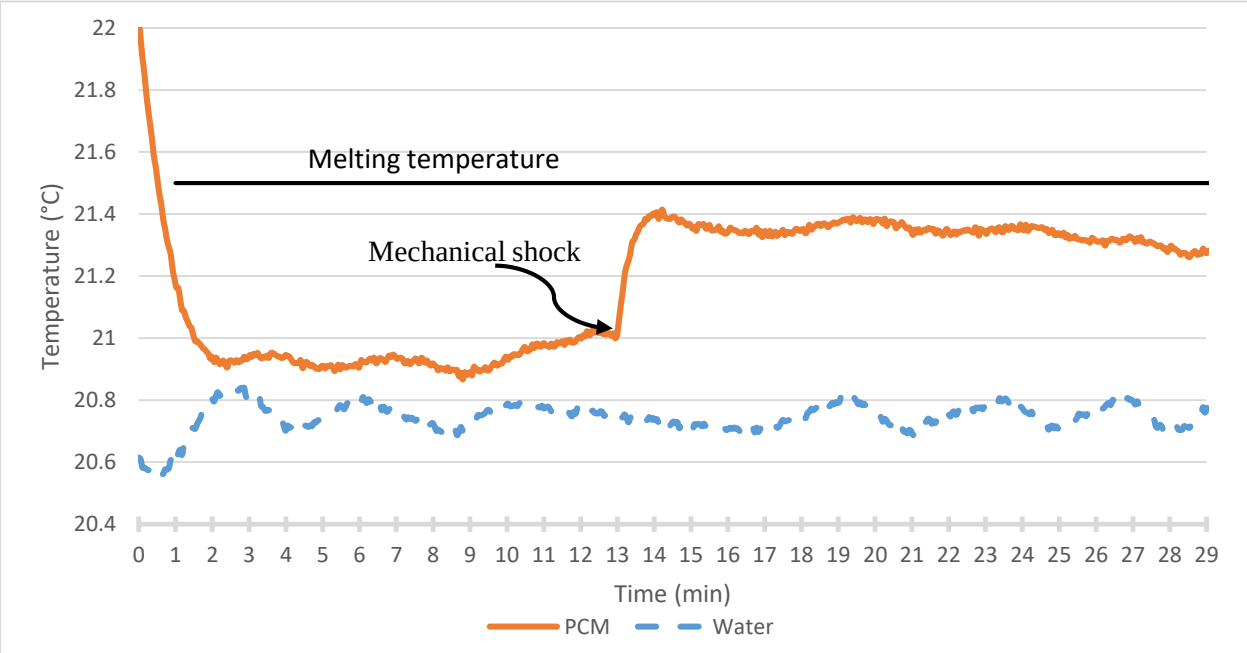

Figure 3.10 Eutectic PCM entering in stable supercooling before applying a mechanical shock

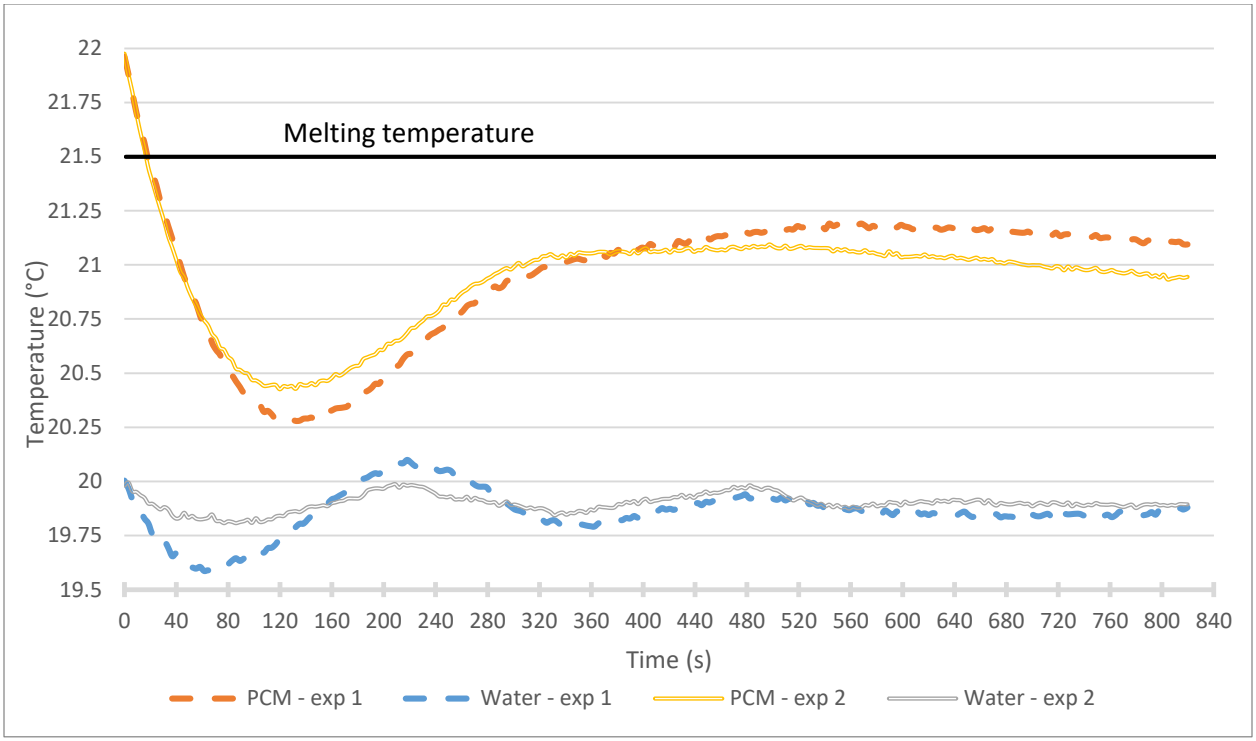

Figure 3.11 Eutectic PCM supercooling behavior by applying two similar coolant average temperatures

3.3.1.3 Sodium acetate trihydrate

The small-scale experiment uses 4.2 g of sodium acetate trihydrate (SAT) crystals. Knowing that the phase change temperature of SAT is between 58 °C and 60 °C as indicated by the manufacturer, the material is heated to 70 °C using a 75 °C hot bath until complete melting. The PCM cooling experiment is repeated using different cooling bath temperatures. In order to calculate the degree of supercooling, 58 °C is considered as the phase change temperature of SAT. In the first trial shown in green in Figure 3.12, the sample is immersed in a precooled bath of average temperature 47.6 °C. The PCM temperature decreases to 58 °C and enters a supercooled state after cooling for 37 seconds. SAT records a supercooling degree of 6.25 °C, then latent heat release raises its temperature from 51.75 °C to 58.5 °C in 10 seconds. In the second trial shown in orange in Figure 3.12, the sample is immersed in a precooled bath that is, on average, 40.8 °C in temperature. The PCM enters in supercooled state for 50 seconds before the initiation of solidification at a 47.4 °C nucleation temperature. The initiation of solidification increases the temperature to reach 58.18 °C in 9 seconds. In this case, the degree of supercooling recorded is 10.6 °C. The third trial shown in blue in Figure 3.12 uses identical coolant temperature as the second trial. However, the PCM stays for only 46 seconds in supercooled state before the initiation of solidification at 48 °C. The temperature increase to 58.26 °C lasts 10 seconds and the recorded degree of supercooling is 10 °C. This slight difference can be due to the unstable nature of supercooling.

Table 3.7 summarizes the results obtained with SAT. Similarly as the observations using the eutectic PCM, as the coolant temperature decreases, the time spent in supercooled state decreases and the supercooling degree increases as shown in Figure 3.12.

Table 3.7 Cooling of SAT using different coolant temperatures

	Coolant temperature (°C)	Nucleation temperature (°C)	Supercooling degree (°C)	Time spent in supercooled state (s)
Trial #1	47.6	51.75	6.25	74
Trial #2	40.8	47.4	10.6	49
Trial #3	40.8	48	10	46

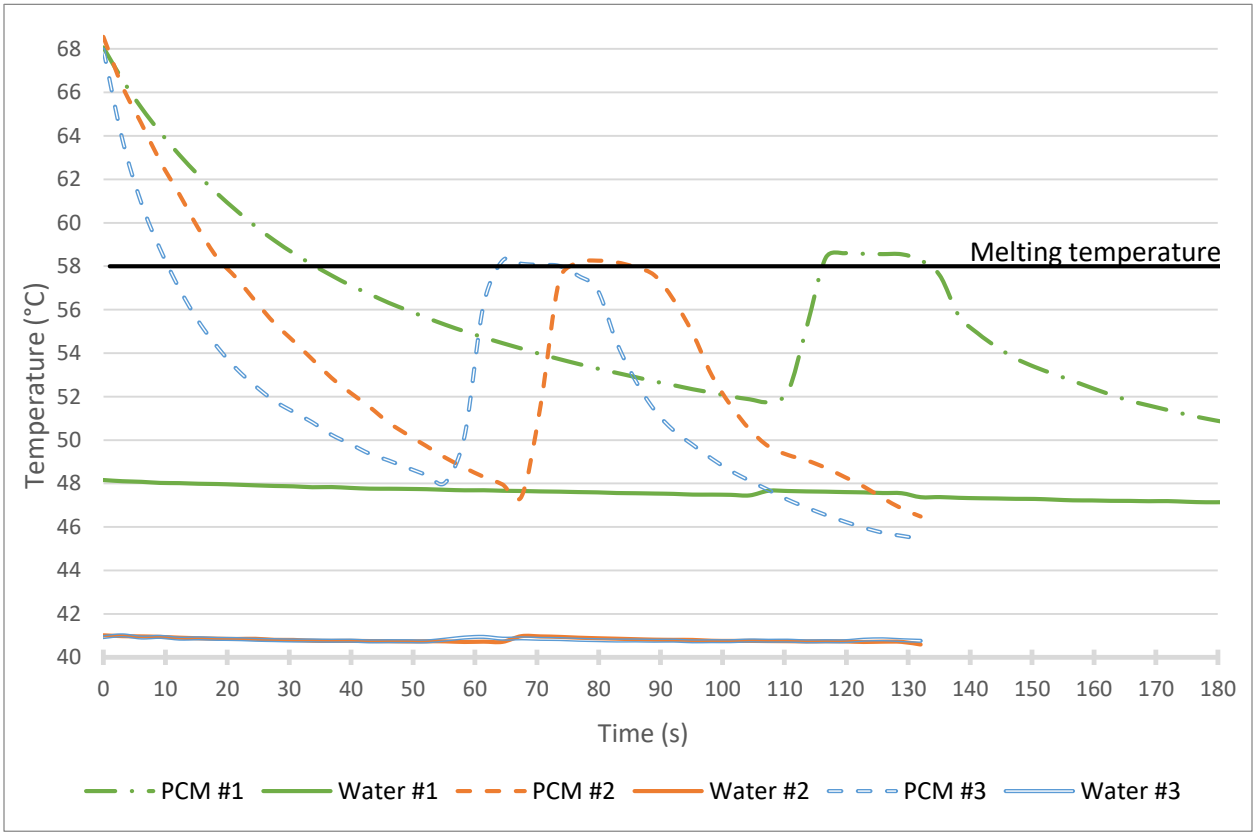

Figure 3.12 SAT temperature variation with time as a function of coolant temperature

3.3.2 Large-scale experiment

The experiments performed in the large-scale experiment are conducted to show the influence of PCM container's volume on the supercooling phenomenon and the effect of natural convection during the heating process. Convection-dominated phase change problems have attracted many investigations over the past 20+ years, and scientists agree on the paramount importance of natural convection in the heat transfer whenever the PCM container's volume allows motion of the liquid PCM. Convection in the liquid PCM actually takes place under the influence of buoyancy forces during the melting process because of variations in density gradients. The effect of natural convection on the melting and solidification processes was examined by Lamberg *et al.* [101] and Souayfane *et al.* [161]. They demonstrated that when the effect of natural convection is neglected in the modeling of the melting, unacceptable numerical results are obtained. When the used PCM melts, the discrepancies between the projected temperature with and

without convection can reach up to 18 °C for container thicknesses more than 1 cm, while they are negligible for thicknesses less than this value [162]. However, accurate predictions are demonstrated during the solidification process, even without taking into account convection [163], [164].

3.3.2.1 Octadecane

The PCM chamber of the large-scale experiment is filled with 900 grams of solid octadecane. Water heated to an average temperature of 36 °C flows in the left chamber to melt the PCM, while water heated to a temperature of 20 °C flows in the right chamber. Results show that the melting front initially has a vertical shape, as seen in Figure 3.13a. The amount of melted PCM grows over time, and the impact of natural convection is more apparent, as the melting front deforms (Figure 3.13b-c). As the melting front area begins to rise, the melting rate increases. As a result, the temperature varies unevenly in the domain. Figure 3.14a shows the PCM transient temperature in a vertical line near the middle of the chamber. The figure demonstrates that even in the non-melted portions of the domain, the higher portion of the PCM is hotter than the lower portion in the vertical plane. Figure 3.14b shows the PCM transient temperature in a horizontal line near the middle of the chamber. As expected, the temperature decreases with decreasing distance from the hot water bath.

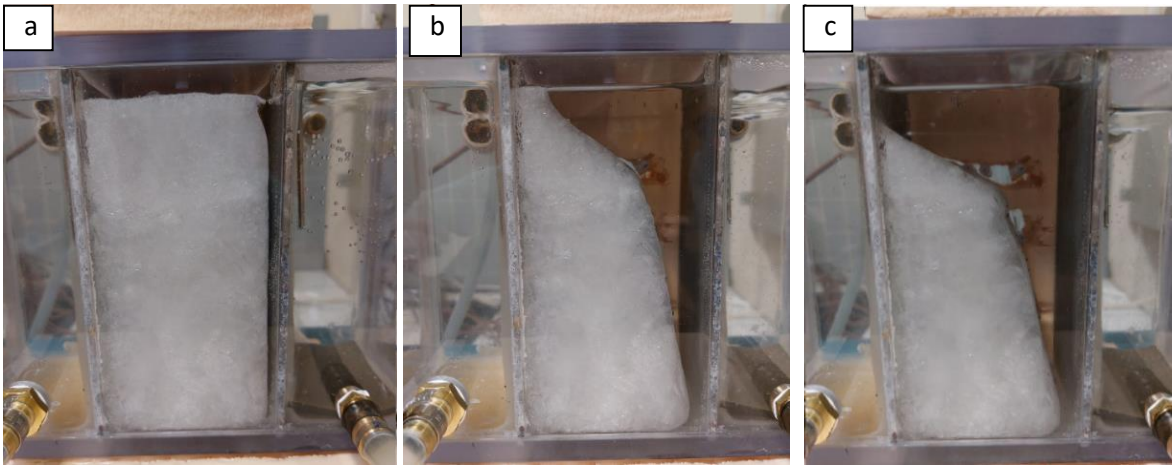

Figure 3.13 Evolution of the solid/liquid interface during melting (a) t=40 min, (b) t=230 min, and (c) t=290 min

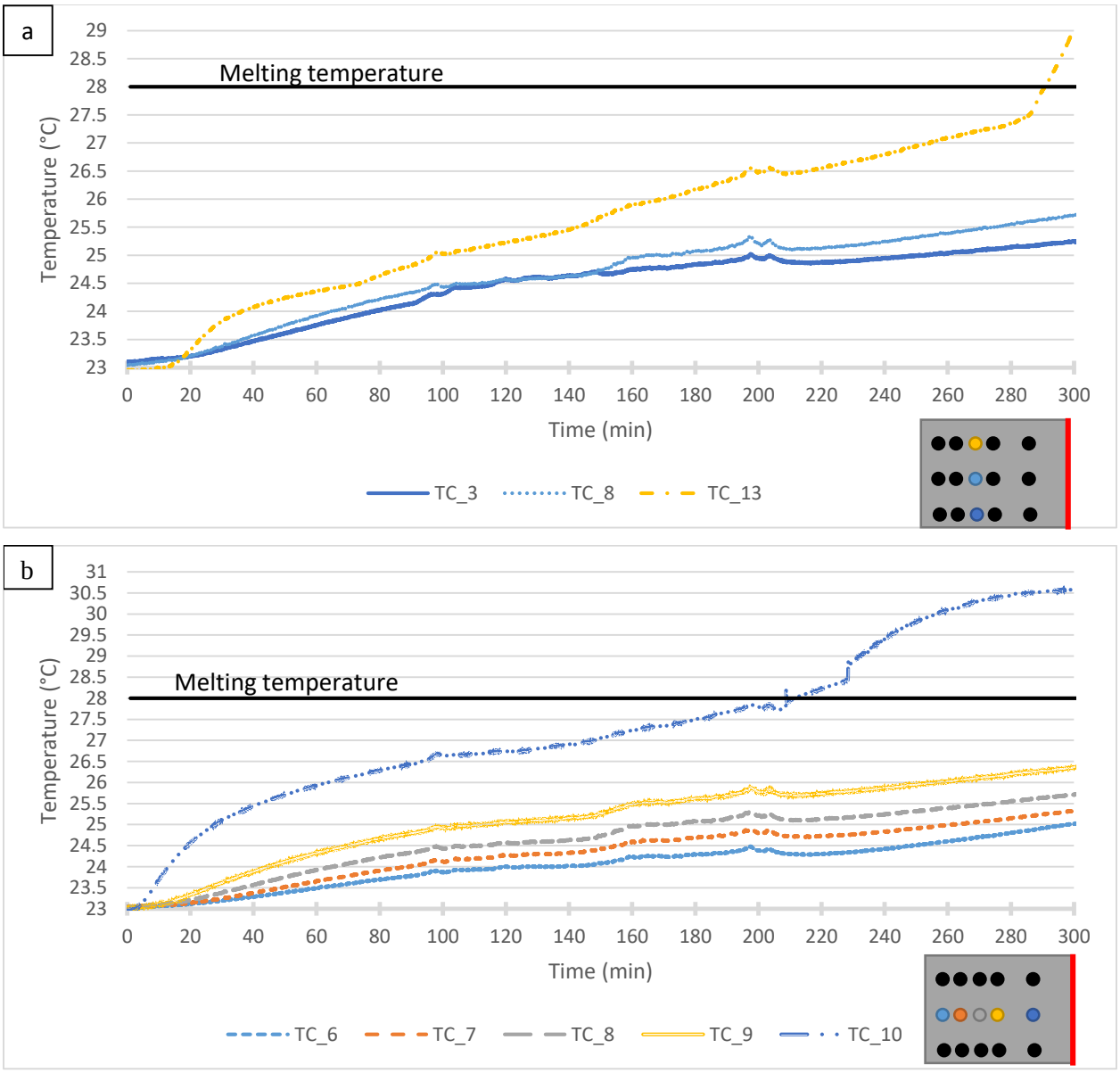

Figure 3.14 Temperature variation of PCM in a) vertical and b) horizontal line during the heating process

To investigate the impact of thermal insulation on the melting process, another experiment is carried out. The front plate is not insulated, whereas the back plate is insulated. The front plate refers to the unheated container side facing the outside ambient environment while the back plate is the opposite side, which holds the PCM thermocouples network. In this case, the front plate's ability to transfer heat to the outside slows the melting process. Figure 3.15 displays the top view of the melting front in both the insulated and not-insulated scenarios. The scenario of an absence of insulation is depicted in Figure 3.15a. More PCM is melted at the back insulated plate than at the front plate. This is because at the back plate, heat is transferred to the solid fraction as opposed to being lost to the environment. Figure 3.15b, however, shows the scenario of a completely insulated container. The melting front is uniform and symmetric.

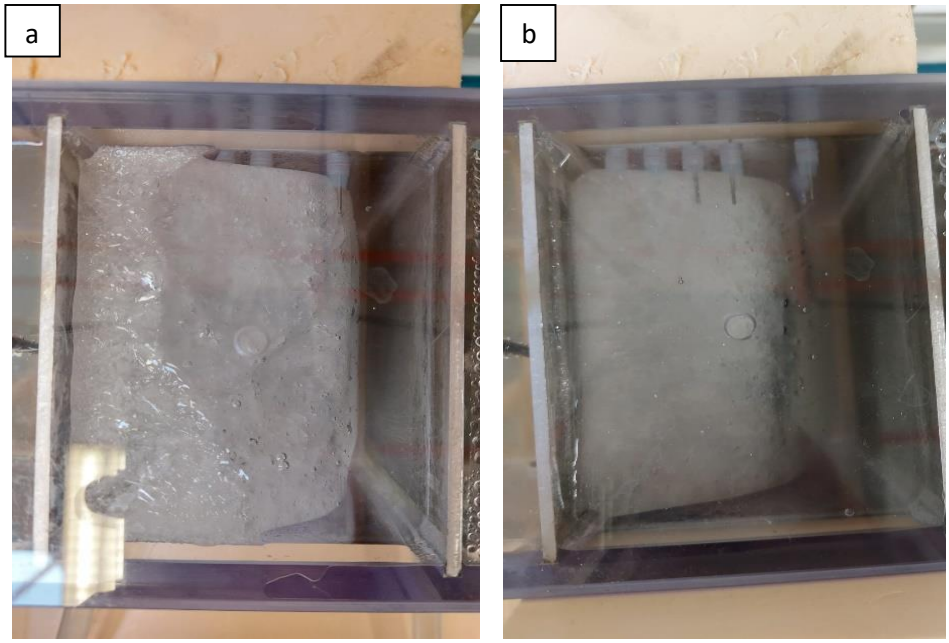

Figure 3.15 Top view showing the effect of insulation on the melting process of octadecane when the front plane is (a) not insulated and (b) insulated

To study the supercooling presence during the cooling process, the right and left chambers are filled with water of average temperature 27.5 °C and 25.5 °C, respectively. No supercooling of the PCM is detected. The PCM gradually solidifies once the solidification initiates from the aluminum surface. As show in Figure 3.16, as the solid fraction rises, the solidification front stays vertical and the PCM's temperature tends to be homogeneous. Study is also done on the impact of natural convection during the cooling process. The variation in temperature as a function of height is presented in Figure 3.16a. There is a slight difference in the liquid phase where the upper part is warmer than the lower part. Later, with a slight lag in time, the temperature in the lower parts reaches the same value, and the PCM solidifies. Natural convection has very little impact on the solidification process. Similar to Figure 3.16b, the thermocouples positioned in the horizontal center direction display the same temperature distribution.

As previously, the impact of insulation on solidification is studied. The experiment is carried out in a room with an ambient temperature lower than the melting point of octadecane. Since the heat exchange via the aluminum plates is greater than that through the front plate, solidification begins there. The propagation of the solidification front, however, is not always vertical and uniform. Figure 3.17 illustrates how the production of a new solidification front from the front plate is caused by the heat loss through it.

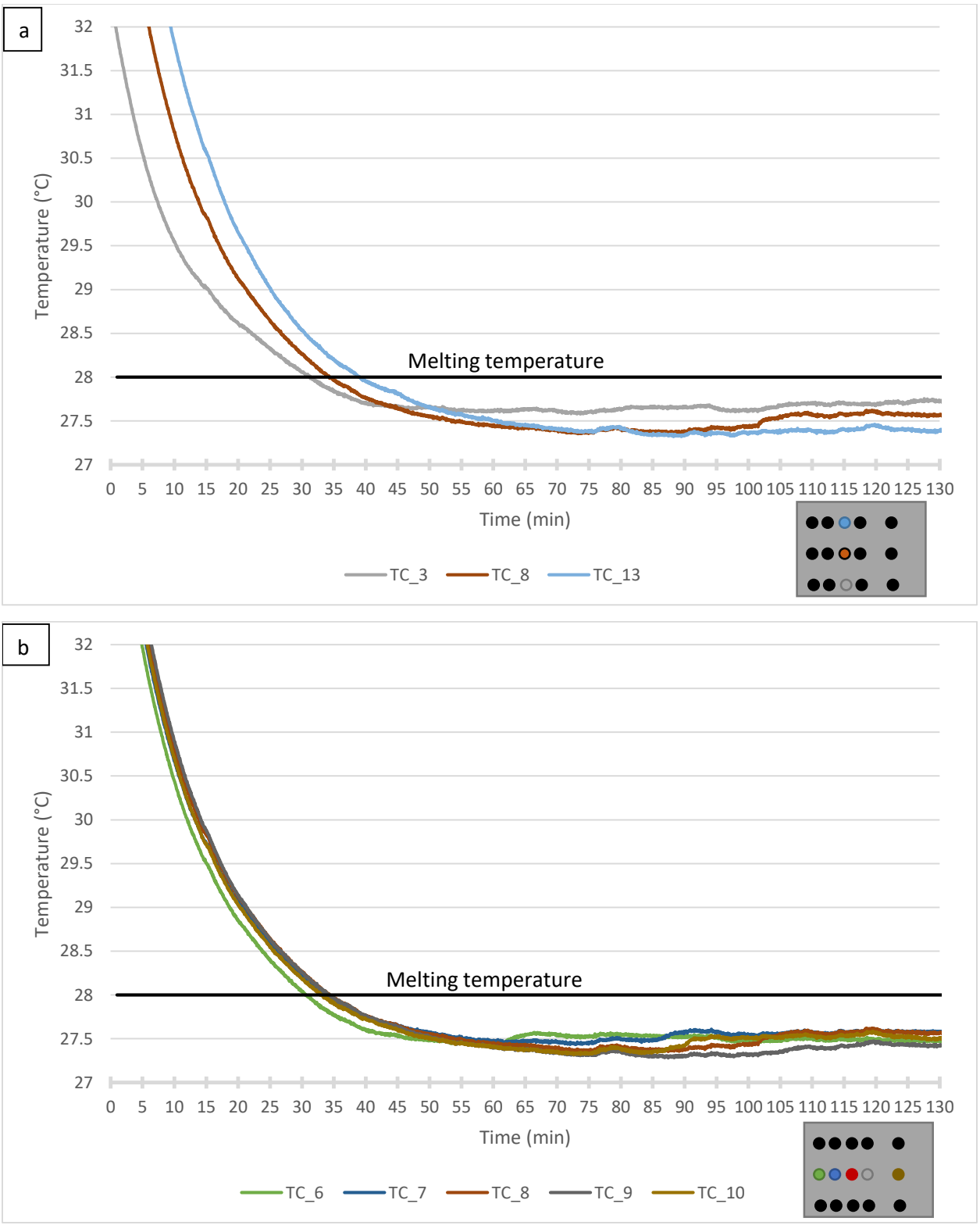

Figure 3.16 Temperature variation of octadecane in a a) vertical and b) horizontal cross-sections during the cooling process

Figure 3.17 Front view showing the solidification initiation due to heat exchange with the exterior

3.3.2.2 Eutectic PCM

The large-scale experiment is set up by filling 960 grams of the eutectic PCM in the PCM chamber of the container. Until the melting process starts, water in the right chamber is kept at an average temperature of 36 °C. Later, to speed up the melting process, the temperature is raised to 50 °C, while the left chamber is filled with still water that is 22 °C. Figure 3.18 depicts the melting front's progression at various times. The experiment begins in a completely solid condition (Figure 3.18a) and as a result of the hot water on the right, the PCM heats up and melts. The influence of natural convection is unclear as the melting front begins vertically. After 45 minutes of heating, this impact begins to manifest itself as depicted in Figure 3.18b. The melting process is accelerated by natural convection, and the melting front is not vertical anymore as seen in Figure 3.18c. The rise in melting rate is evident from the rising melted part as a function of time, where the PCM melts more quickly after 105 minutes (Figure 3.18d).

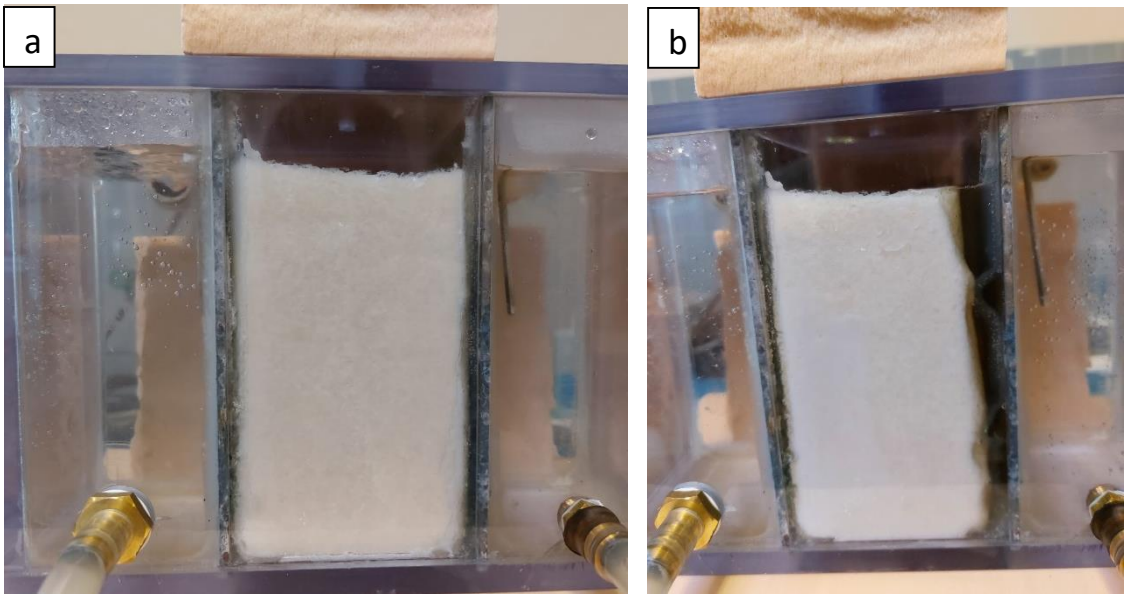

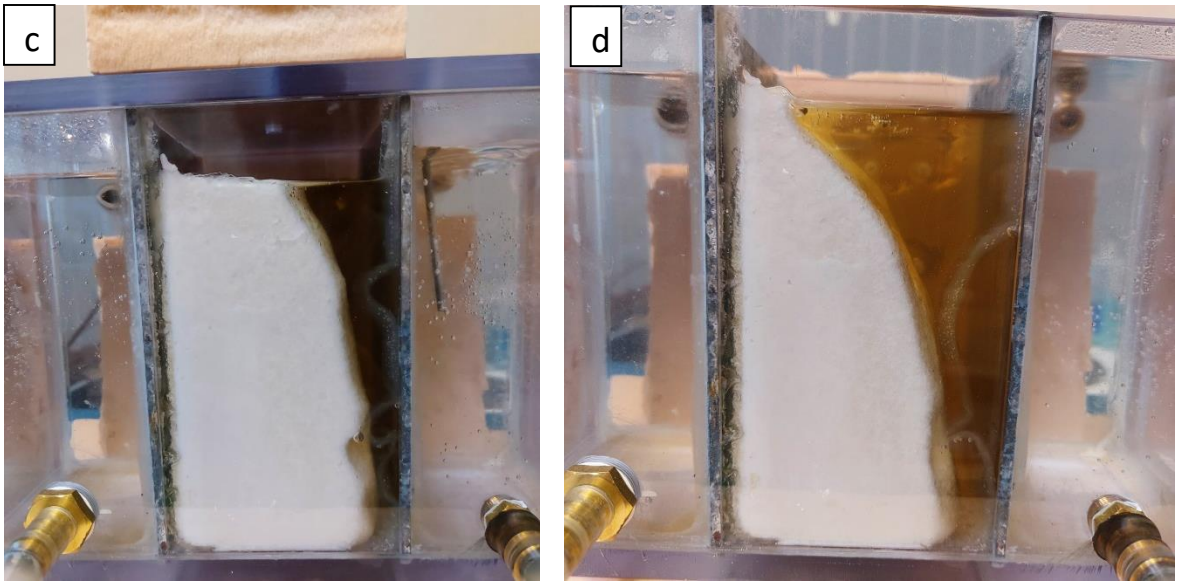

Figure 3.18 Front view showing the evolution of the solid/liquid interface during melting at (a) t=0 min (b) t=45 min (c) t=75 min, and (d) t= 105 min

Plotting the temperature curve for various thermocouples allows showing how natural convection affects the system. A plot of the temperature curve for the three thermocouples close to the hot plate is shown in Figure 3.19. These three thermocouples are arranged vertically from top to bottom and are illustrated in orange, black, and gray color, respectively. The three sites have similar temperatures during the solid state and the beginning of melting. The temperature of the higher thermocouple rises significantly as the melted portion rises until $t = 90$ min, after which it remains constant from $t = 90$ min to $t = 106$ min, despite the fact that the temperature of the water is higher than that of the PCM. This could be explained by the fact that at thermocouple TC_15 location, the heat gain from the aluminum plate is equal to the heat loss to the solid fraction. In other words, the heat gained by the PCM portion close to the boundary is transferred to the PCM portion further away from the boundary. To increase the melting rate and liquid fraction, the temperature of the water shown by the yellow curve is raised to 50 °C after 105 minutes. As the liquid fraction's temperature rises sufficiently, melting begins at the middle thermocouple position shown by the black-colored curve in Figure 3.19.

Similar to this, Figure 3.20 displays the temperature curve for the thermocouples at the same height of 111 mm (TC_13, TC_14, TC_15). The three thermocouples are shown in the orange, black, and gray colors, and are horizontally aligned from the hot plate to the cold plate. As expected, the temperature rises, as the position gets closer to the hot plate. The temperature of TC_10 in Figure 3.19 and that of TC_14 in Figure 3.20 can be compared, nevertheless. This comparison demonstrates that the melting begins and its temperature rises at TC_14 before TC_10 does, knowing that TC_14 is farther than TC_10 from the hot plate but it has a higher position in the vertical plane.

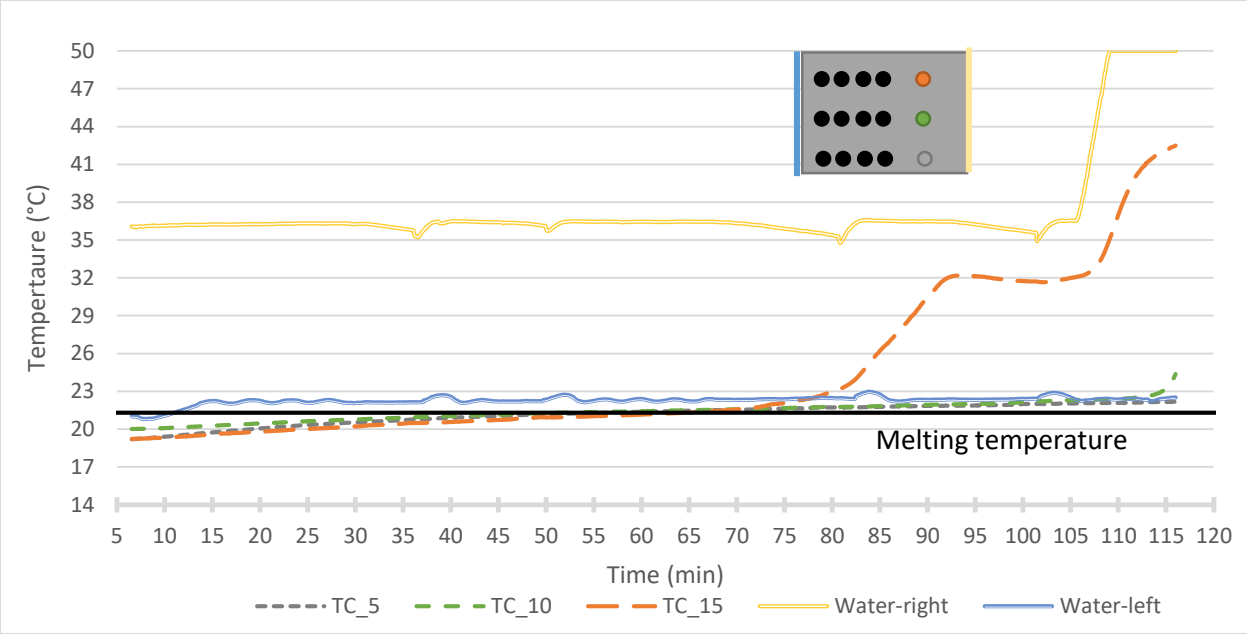

Figure 3.19 Variation of temperature at the bottom (gray), middle (black) and upper (orange) positions near the hot plate

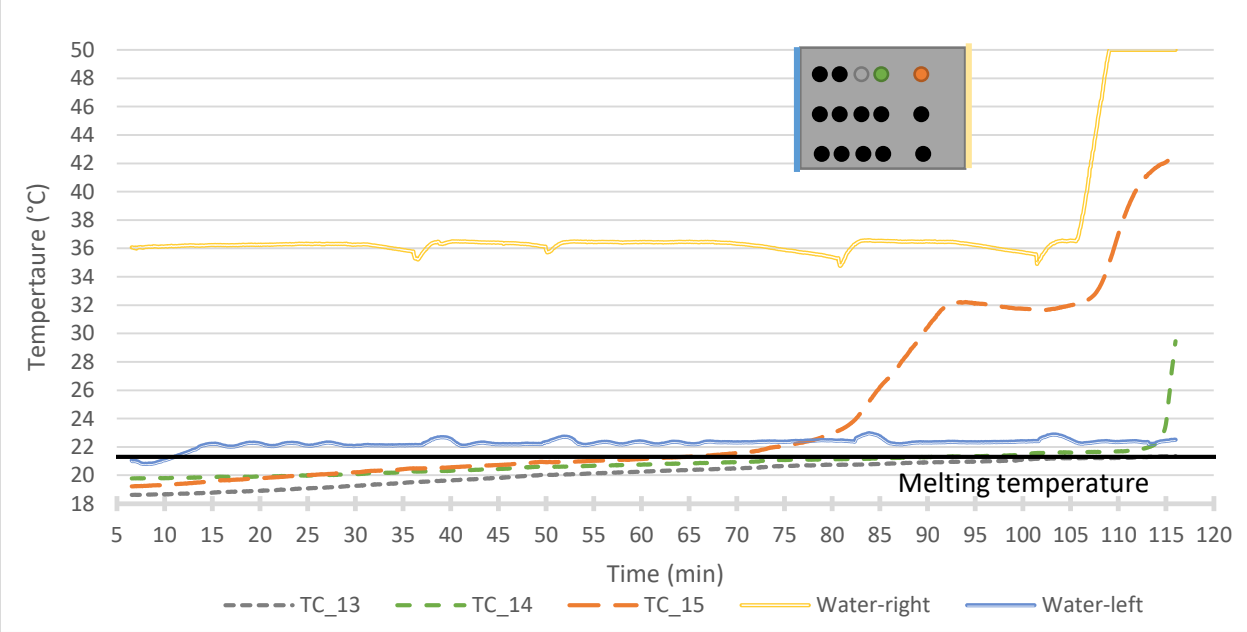

Figure 3.20 Temperature variation in the upper plane increasing distance from the hot plate

During the cooling process, the right and left chambers are filled with water with average temperatures of 25 °C and 15.7 °C respectively. Alike what was observed with octadecane, the eutectic PCM doesn't undergo any supercooling. The solidification initiates from the aluminum surface and expands into the PCM gradually. The temperature change for thermocouples at same height is compared in Figure 3.21. The top, middle, and lower planes are shown in Figure 3.21a, b, and c, respectively. Except the time when the phase change temperature is attained, the three planes exhibit comparable behavior. The plot of temperature variation as a function of vertical location can be seen in Figure 3.22. The temperature

variation in a plane near the cold plate is shown in Figure 3.22a, while that of a plane near the center of the PCM chamber is shown in Figure 3.22b. The liquid at the bottom reaches the phase change temperature before the liquid at the top. The reason for this is that at the start of the cooling process, the melted PCM in the upper sections is warmer than in the lower sections, as a result of natural convection during the previous melting phase. The temperature difference between the thermocouples decreases as solidification progresses. For example, at t =19 min, the vertical temperature difference between each thermocouple is 5 °C. As the temperature approaches the phase change temperature at $t = 100$ min, this difference becomes less than 0.5 °C.

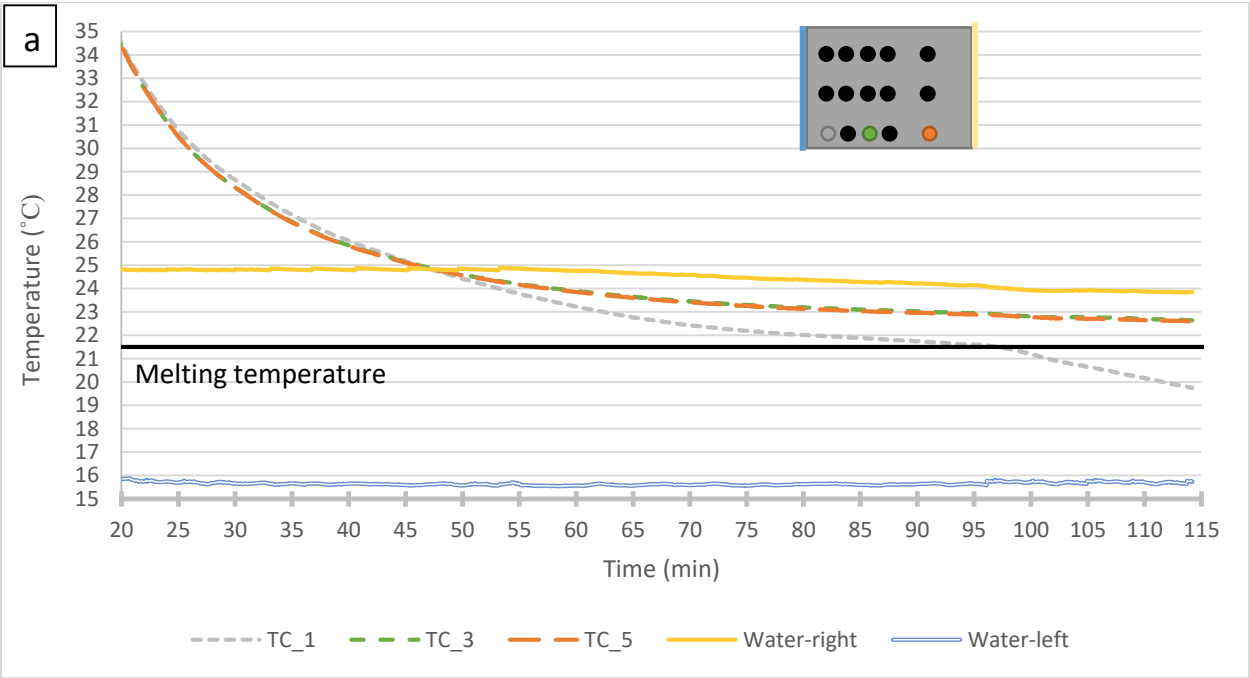

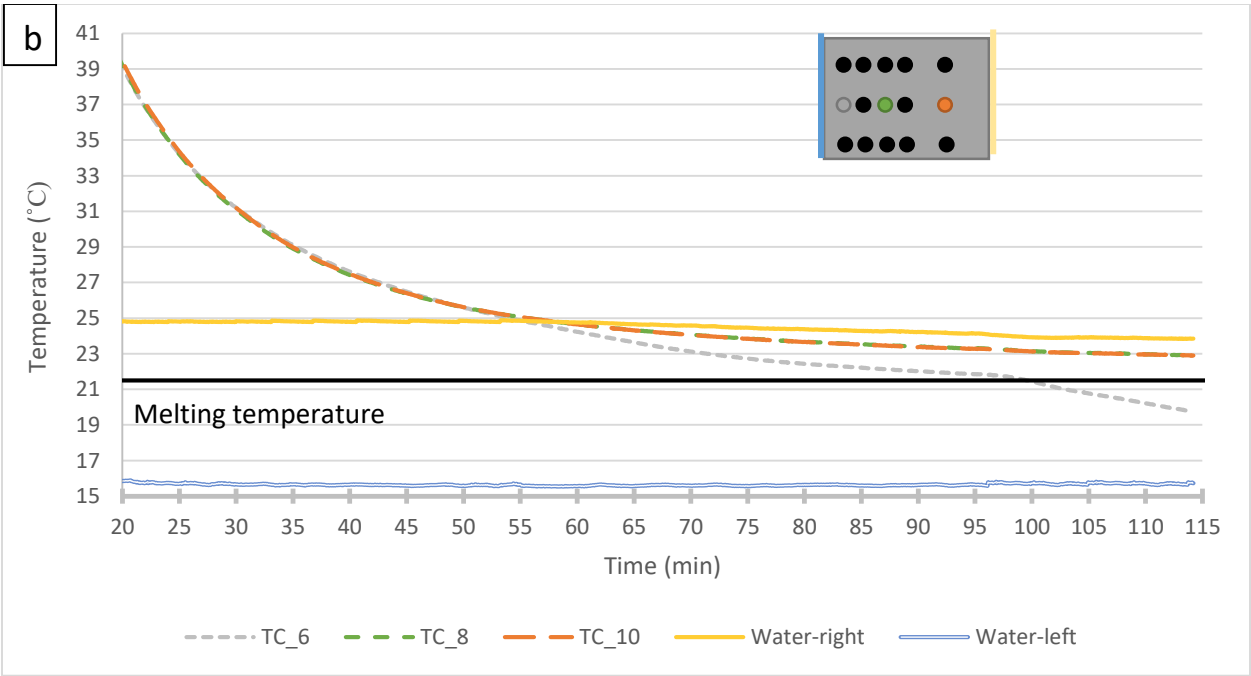

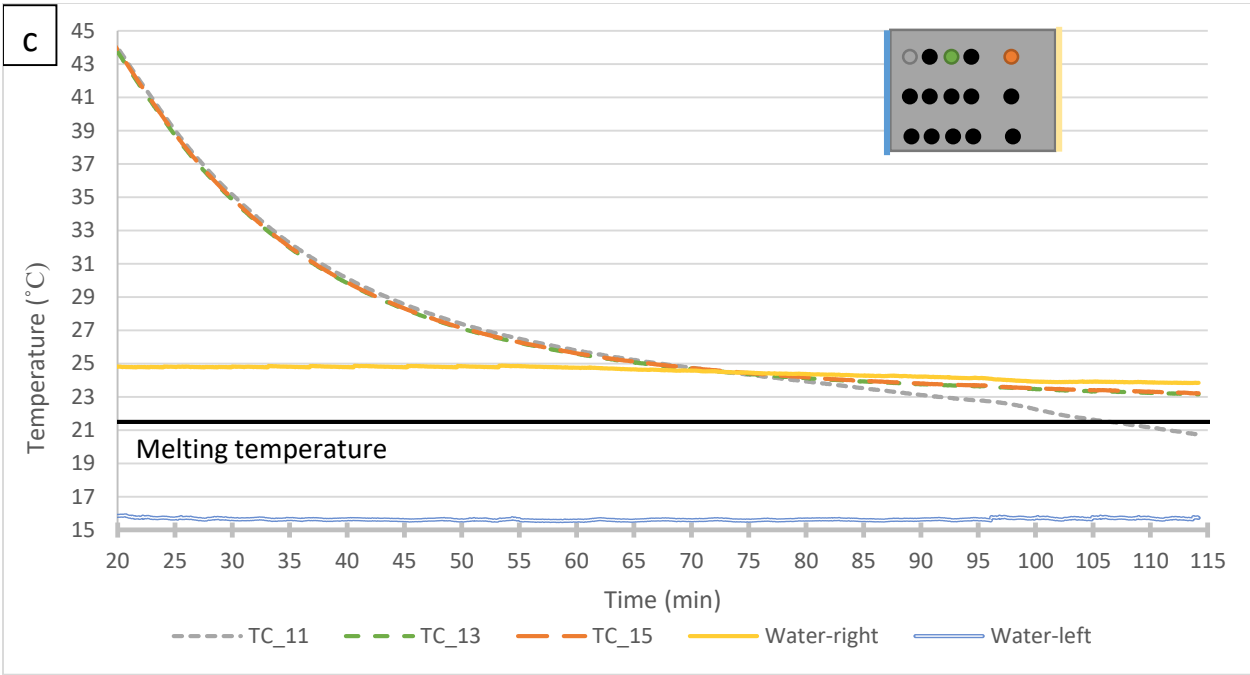

Figure 3.21 Temperature variations at left (gray), middle (green) and right (orange) positions in the a) bottom, b) middle, and c) upper

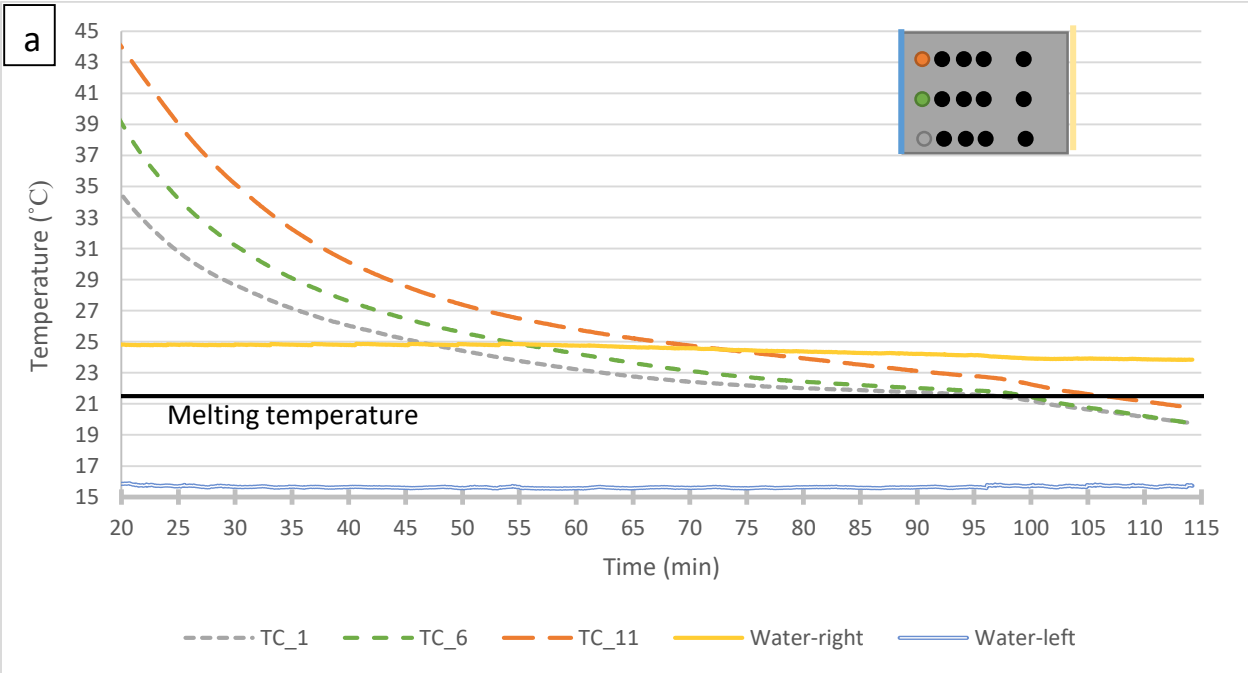

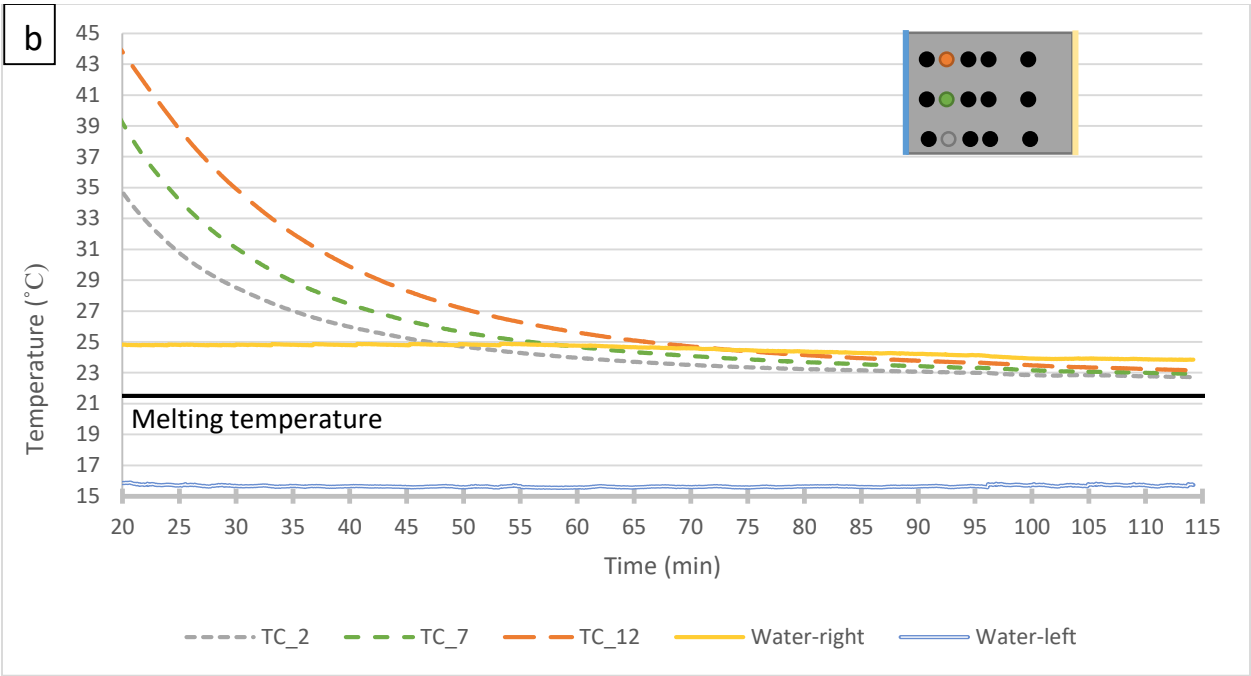

Figure 3.22 Temperature variation at bottom (gray), middle (green) and upper (orange) positions of thermocouples in vertical planes close to the cold plate

Figure 3.23a shows the PCM in a liquid condition just before solidification initiates. As displayed in Figure 3.23b, the solidification begins at the left aluminum plate and spreads out horizontally. The solidification front remains vertical during all the solidification process, demonstrating a limited convection within the chamber. The effect of the thermal insulation is also studied. Its influence is highlighted through the shape of the solid/liquid interface visible when looking at the large-scale experiment from above. Figure 3.24a shows the top view of the solid/liquid interface during the solidification process. The solidification initiates from the left and due to the insulation, the solid-liquid interface is linear with a nearly constant thickness of the solid layer. However, if no insulation is applied to the boundaries, the PCM loses heat to the outside, resulting in the formation of another solidification front starting from these surfaces. A similar behavior is witnessed during melting. Figure 3.24b shows the top view of the melting front when the front plane is not insulated. Melting occurs closer to the front plane and more quickly. This finding does not contradict the result of Figure 3.15. Here, the room's ambient temperature is higher than the PCM's melting point, which allows heat to move from the room to the PCM and rise its temperature.

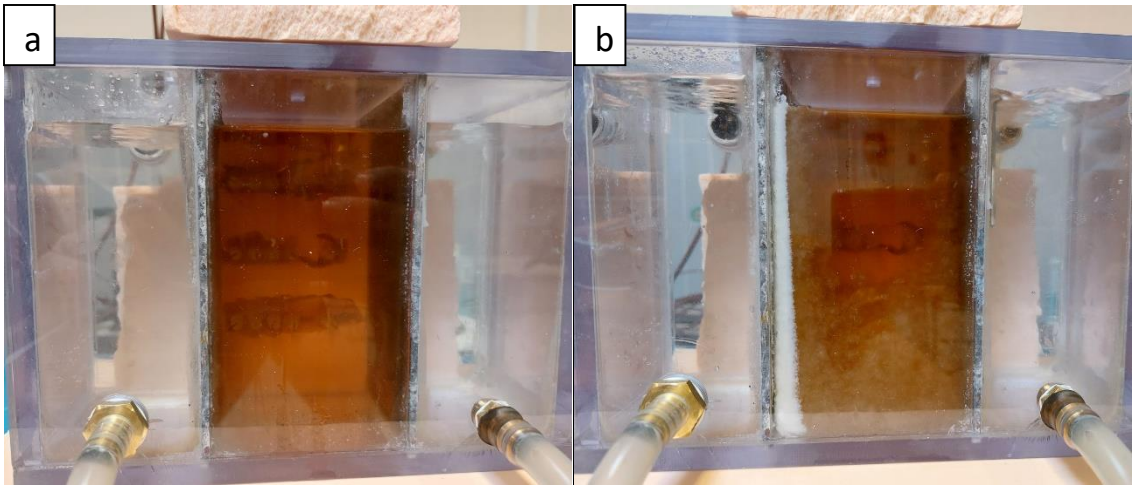

Figure 3.23 Front view showing a) the initiation of solidification and b) the solidification front of eutectic PCM

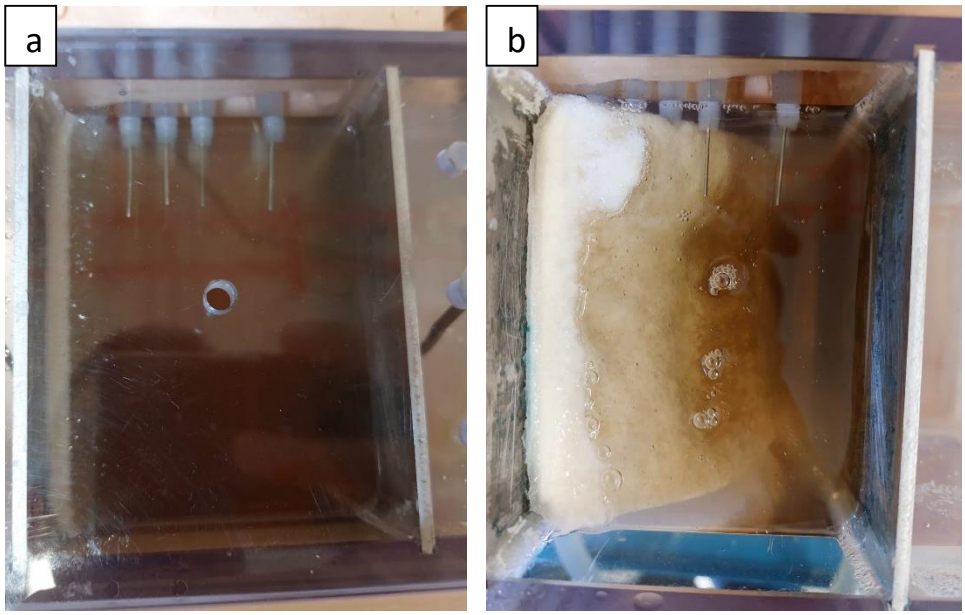

Figure 3.24 Top view of the solid/liquid interfase during a) solidification with thermal insulation and b) melting absence of insulation

3.3.2.3 Sodium acetate trihydrate

The PCM chamber contains 1200 g of solid SAT. To accelerate the heat transfer, a controlled climate chamber is used to melt and cool the PCM. Therefore, the right and left chambers of the PCM container are emptied and contain only air. The climate chamber is a Memmert HPP260, which can control the temperature between -10 ˚C and 70 ˚C with a precision of 0.1 ˚C, and the relative humidity between 10% and 90% with a precision of 0.5 %. The PCM is heated to 62 ˚C until it reaches liquid state, and then cooled by setting the controlled temperature of the chamber to 26 ˚C. Figure 3.25 shows the temperature variation of the air in the chambers on the left and right sides of the PCM. The temperature variation depends on the temperature of the controlled climate chamber and the heat transferred from the PCM chamber via the aluminum plates.

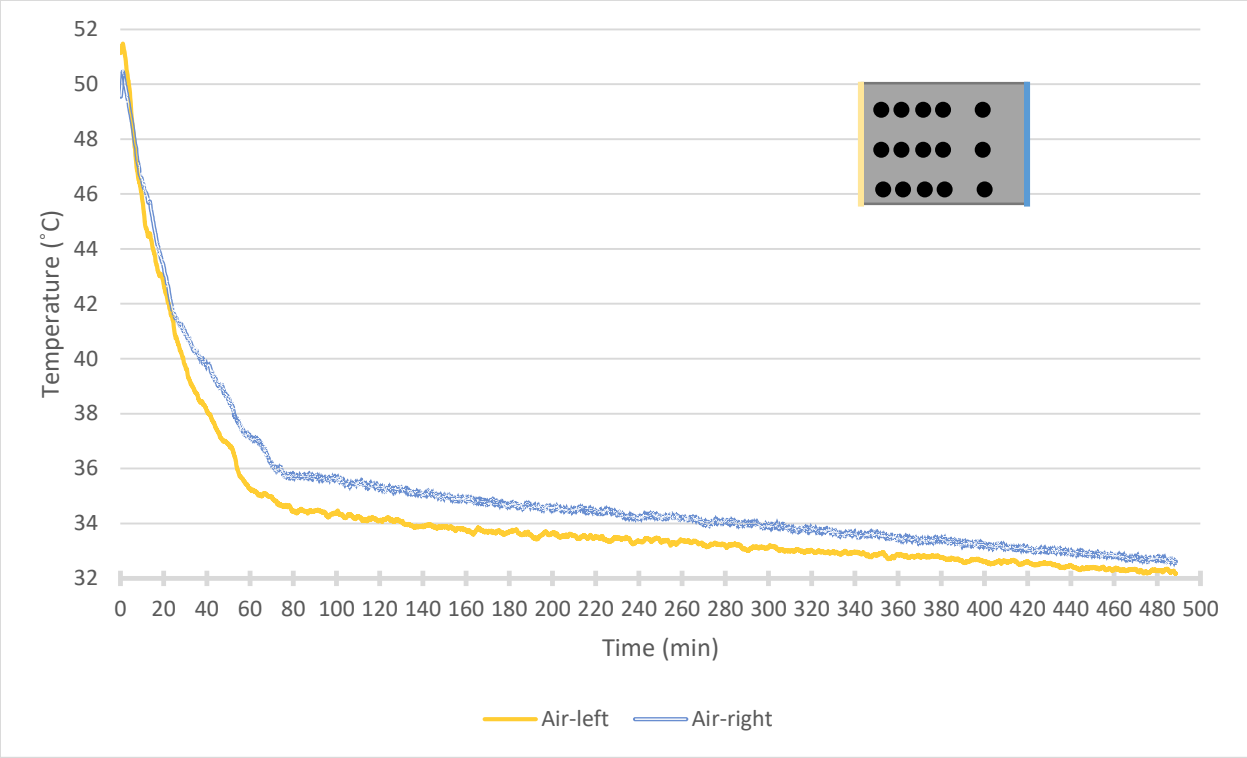

Figure 3.25 Temperature variation of the right and left chambers

Upon cooling, SAT enters a supercooled state and the lowest temperature detected before crystallization is is 53.64 ˚C measured at location TC_6, resulting in a maximum supercooling degree of 4.36 ˚C. The time of nucleation start at each thermocouple location is shown in Table 3.8. It is determined by the instant at which the temperature begins to rise due to latent heat release. The table shows that solidification begins at the top parts of SAT (represented by the thermocouples TC_11 $\rightarrow$ TC_15), spreads to the middle and then to the bottom. Examining the temperature variation of all the thermocouples, it is found that the solidification initiates first from TC_14 at $t = 65.03$ min and $T = 55.83$ ˚C, before spreading in all directions. From the thermocouples located in the middle horizontal cross-section, solidification begins at TC_6 (near the left boundary thermocouple), which has also the lowest temperature among the thermocouples located at the same height. This solidification can be attributed either to reach a temperature too low to maintain the supercooled state, or to the presence of a solid-liquid interface above it at TC_11. Because of the slow spread of the solid-liquid interface, the middle part of the PCM can cool down and reach temperatures lower than the nucleation temperature of the locations where the solidification has been first detected. In other words, the nucleation temperatures detected at each thermocouple in the lower and middle parts of the PCM are lower than that detected at TC_14, as shown in Table 3.9.

Figure 3.26a plots the temperature curves for thermocouples in the upper horizontal cross-section. The temperature fluctuation is caused by the initiation of solidification associated with the sudden release of latent heat. However, thermocouples in the middle and lower horizontal cross-section exhibit a smooth inflection and temperature rise, as shown in Figure 3.26b and Figure 3.26c, respectively. This can be due to the sudden initiation of solidification on top of the PCM container, followed by a slow propagation of the solid liquid interface towards the lower sections. Table 3.8 shows that the propagation takes 10.13

min from TC_11 to TC_6. It is also observed that the PCM near the boundaries loses energy faster than the inner parts, leading to a shorter phase change time. Figure 3.27 shows the temperature variation in a vertical cross-section located close to the middle of the PCM chamber. As expected, because solidification begins in the upper part of the PCM, temperatures there are lower than in the lower parts.

Table 3.8 Time of first SAT solidification at each thermocouple position

	Initiation of solidification (min)				
TC_11 →TC_15	66.72	66.57	66.57	65.03	66.72
TC_6 →TC_10	76.85	79.41	81.71	85.86	83.71
TC_1 →TC_5	81.71	92.61	103.87	111.70	95.12

Table 3.9 SAT nucleation temperature at each thermocouple position

	Nucleation temperature (˚C)				
TC_11 →TC_15	55.48	55.66	55.64	55.83	55.96
TC_6 →TC_10	53.64	54.42	54.08	53.77	54.90
TC_1 →TC_5	53.89	54.07	54.23	53.64	54.76

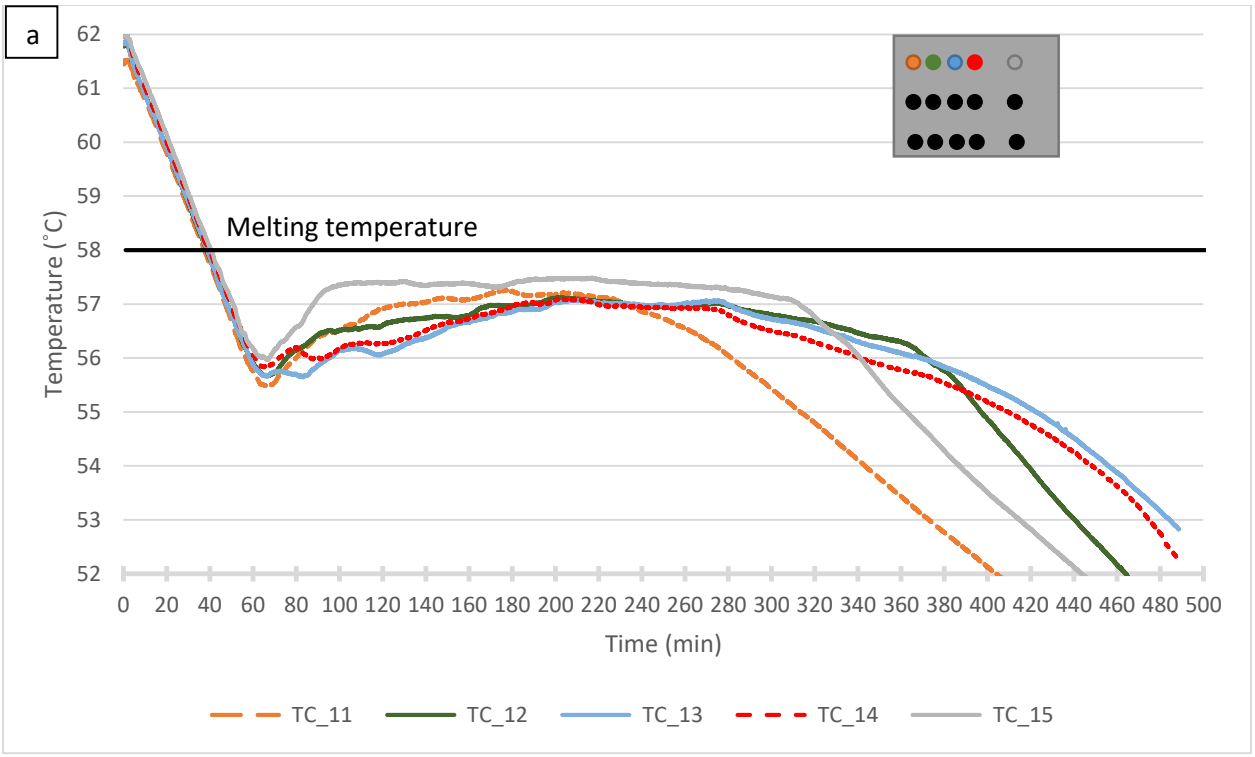
a
Melting temperature
Temperature (°C)
Time (min)
TC_11
TC_12
TC_13
TC_14
TC_15

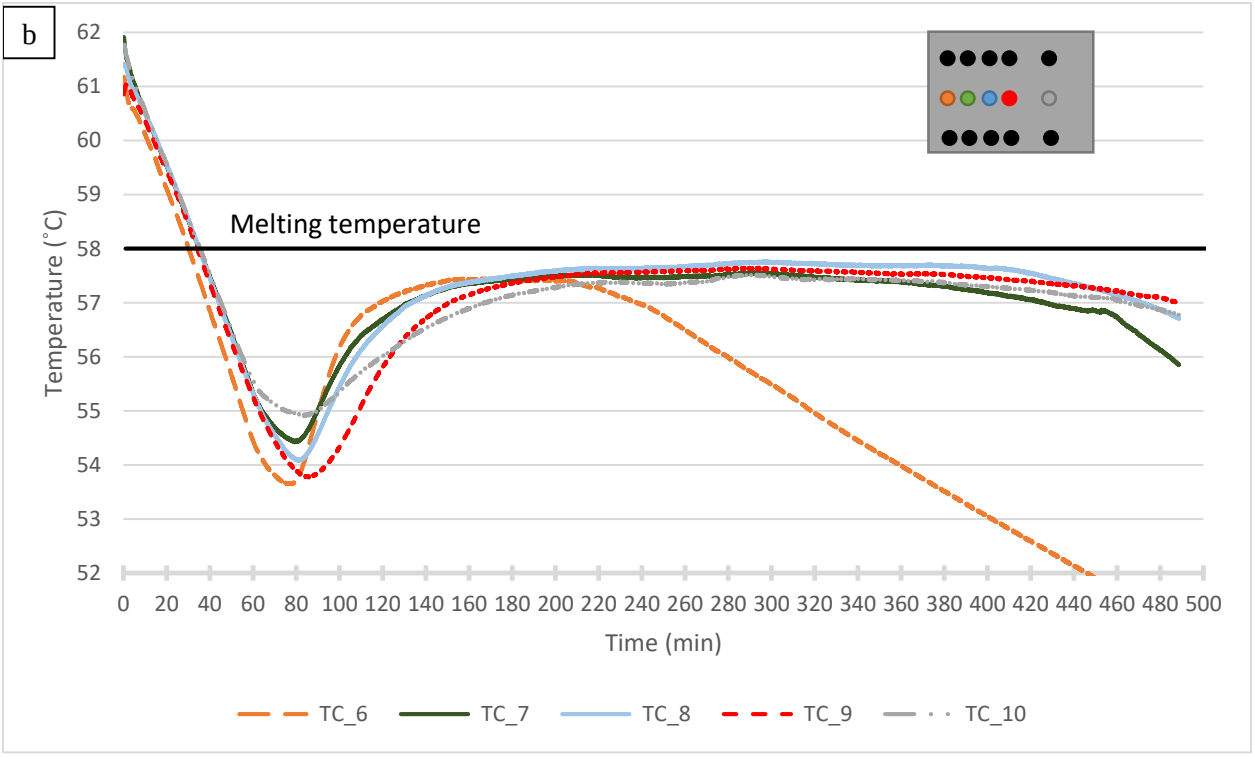
b
Melting temperature
Temperature (°C)
Time (min)
TC_6
TC_7
TC_8
TC_9
TC_10

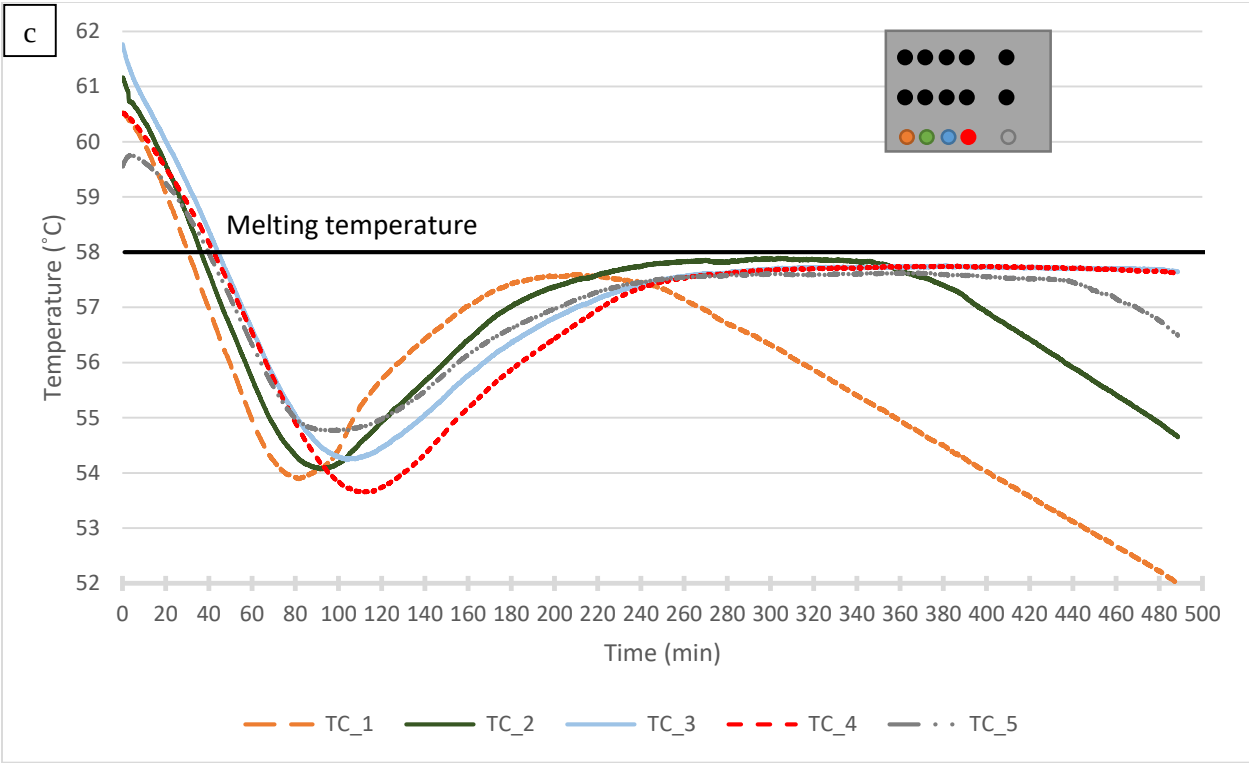

Figure 3.26 SAT temperature variation at the a) upper, b) middle, and c) lower horizontal directions

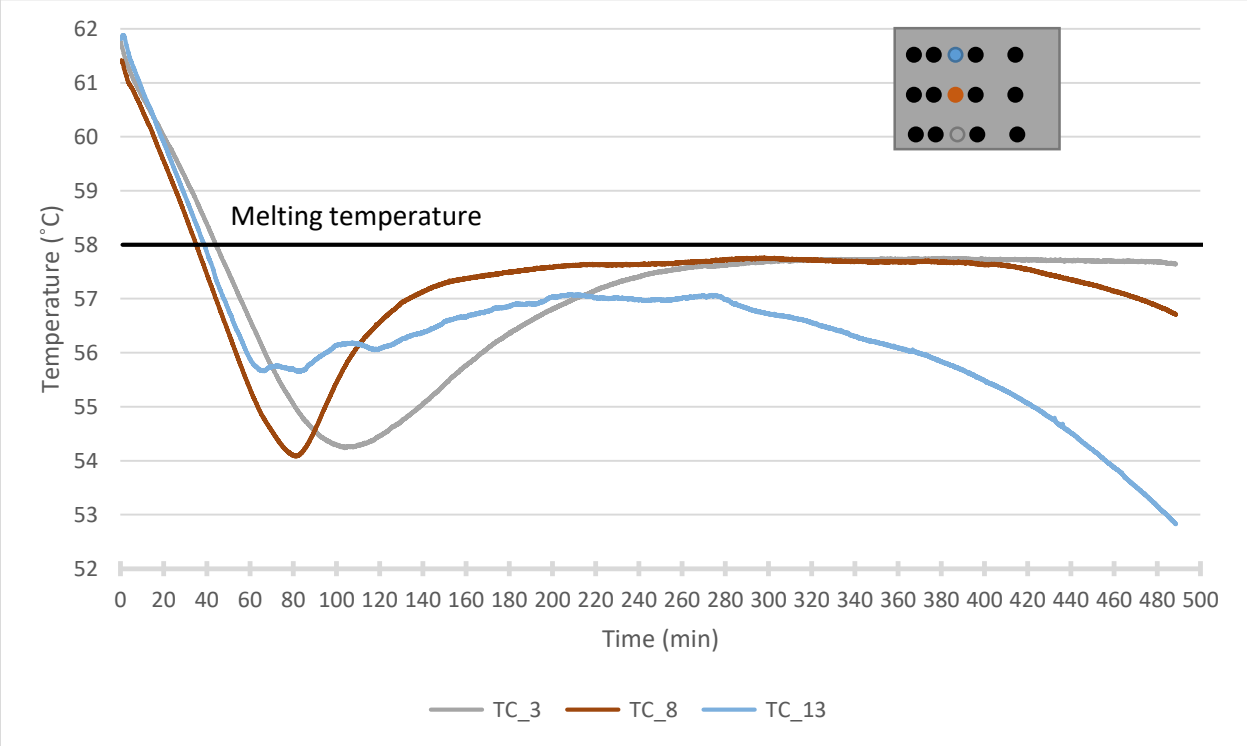

Figure 3.27 SAT temperature variation at the middle vertical direction

3.4 Discussion

Supercoling was observed in all small-scale experiments, whatever the PCM type, but not in all large-scale ones, except for SAT. This can be explained in several ways. First, the PCM volume in small-scale experiments is smaller, which reduces the number of potential nucleation sites. Second, compared to the aluminum plate utilized in the large-scale experiment, the contact surface in the small-scale experiment is smooth. The degree of supercooling reveals to increase as the surface roughness decreases. Third, the uniformity of the surface contact seems to play a role. The small-scale experiment has no sharp edges and is completely uniform and cylindrical. The large-scale experiment, however, is a rectangular polycarbonate box that leads to sharp joints, including two aluminum plates that cause a sharp change in the surface roughness.

The cooling rate is also one of the major factors that affect supercooling. A low cooling temperature causes the PCM to start solidification from its contact with the PCM container's inner surface. This is due to the fast decrease in the surface temperature to a limit where the crystallization initiates spontaneously. The initiation of crystallization causes the PCM temperature to increase due to the release of latent heat. Theoretically, the temperature has to increase to the melting temperature at which the PCM should continue its solidification. However, in the case of low coolant temperatures, the PCM is incapable of reaching the melting temperature, and loses its latent heat during its temperature increase. For that reason, it reaches a temperature inferior to the melting temperature (Figure 3.8). As the coolant temperature decreases, the PCM reaches the nucleation temperature faster, which reduces the time spent in supercooled state, but the PCM also undergoes higher degrees of supercooling. In addition, using small temperature gradients between the coolant and the PCM keeps the PCM in supercooled state for a longer time. This case is obtained using the octadecane and the eutectic PCM (Figure 3.6 and Figure 3.9) where the PCM enters a stable supercooling state and for a longer period, compared to other trials. The PCM stays in liquid state at a temperature lower than the melting temperature and changes states as a function of the cooling temperature. This case shows the disadvantage of supercooling in thermal energy storage systems. Generally, the PCM is cooled using natural sources such as the wind during the night. However, if the temperature difference is not sufficient, the PCM can remain supercooled and cause a system failure the next day due to the prevention of solidification.

The comparison of the three different PCMs reveals that the eutectic PCM undergoes supercooling for a larger range of cooling temperatures; the organic PCM (octadecane) exhibits a small degree of supercooling (0.5 °C), under specific cooling rate conditions and without any mechanical shocks or vibrations; while the inorganic PCM (SAT) undergoes about 10 °C of supercooling. This reveals that the type of PCM (organic, inorganic and eutectic) also affects the behavior of the material. The instability of PCM in supercooled state can be shown in the cases where similar average coolant temperatures are used. Small differences between the trials gives noticeably different results regarding the nucleation temperature and the time spent in supercooled state.

The melting process is greatly impacted by natural convection. A vertical melting front is produced in the computer simulation when natural convection during melting is ignored. However, experimental evidence has shown that as the melted fraction increases, the melting front slopes and the temperature is not equal in the vertical direction. Because of this, neglecting it in numerical models could lead to notable errors in the PCM's state, temperature distribution, and system performance during melting.

However, natural convection has a little impact during the solidification process, since the solidification front stays vertical and the vertical temperature distribution is homogeneous.

Thermal insulation of the PCM container has a considerable impact on both the heating and cooling processes. The performance of the system can be considerably altered by the heat transport into or out of it. An absence of insulation changes the dynamics of melting and solidification by increasing or decreasing the melting and solidification rates, depending on the ambient temperature. It also changes the topology of the phase change as additional melting or solidification fronts are created close to the uninsulated boundaries. In the insulated scenario, the melting or solidification front move perpendicular to the heat transfer surface (aluminum plate in the case of the large-scale experiment).

3.5 Conclusions

This study experimentally studied the effect of the PCM containers' volume, surface roughness, geometry, and PCM type and cooling/heating rate on the supercooling and natural convection phenomena. Three types of PCMs were investigated, an organic PCM, octadecane, of phase change temperature 28 °C, an inorganic PCM, sodium acetate trihydrate (SAT), of phase change temperature 58 °C, and a eutectic PCM of phase change temperature 21.3 °C. It was found that regardless the PCM type, supercooling is facilitated by reduced container's volume, surface rugosity and number sharp corners, and absence of mechanical or electrical shocks. Such characteristics decrease the likelihood of nucleation sites within the material or at its boundaries. It was also found that the chosen cooling rate has a significant effect on the supercooling. Low cooling rates (reduced temperature difference between the PCM and the coolant) facilitate, the PCM entering a stable supercooled state. However, as the cooling rate increases,

- the supercooling degree increases
- the time spent at supercooled state decreases
- the temperature reached, after the latent heat is released, decreases
- solidification initiates from the surface of container

Additionally, it was shown that the impact of natural convection on the solidification process is negligible. Conversely, the melting process is significantly impacted by natural convection. The presence of natural convection causes temperature variations in the vertical direction, the inclination of the melting front, and an increase in melting rate.

Finally, the impact of insulation was investigated. It was demonstrated that poor insulation of the unheated PCM boundaries changed the solidification and melting rates, as additional heat transfer occurred with the ambient. It also modified the topology of the phase change as additional melting or solidification fronts appeared close to the uninsulated surfaces.

The findings of this investigation provide a wide range of experimental data for different PCM characteristics and boundary conditions. The provided experimental details and the obtained results are to be used to validate numerical simulations. One limitation of this study is the presence of the thermocouple network within the PCM. During cooling, that may create new nucleation sites and induce unwanted supercooling. During heating, they may hinder convection transport of the melted PCM. In this regard, the use of developing non-intrusive temperature measurement techniques such as infrared thermometry may provide new insights on the thermal behavior of solid-liquid phase change materials in the presence of supercooling and natural convection.

Chapter 4: Validation of the numerical model and applications

Presentation of the chapter

This chapter is divided into two sections. In its first section, the numerical model detailed in chapter 2 is validated using the experimental results obtained in chapter 3. In the second section, the validated model is used to study the effect of supercooling on two thermal energy storage systems using phase change material, namely a hot water tank and a ventilation system integrated with PCM.

Nomenclature

C_p	Thermal heat capacity (J/kg.K)	T_{app}	Applied temperature (°C)
k	Thermal conductivity (W/m.K)	$RMSE$	Root mean square error (°C)
ρ	Density (kg/m^3)	$PRMSE$	Percentage root mean square error (%)
dT	Phase change temperature interval (°C)	LH	Latent heat of fusion (kJ/kg)
T_m	Melting temperature (°C)	H	Height (cm)
t_s	Time required for crystallization (s)		

4.1 Experimental validation

In chapter 3, supercooling was detected in the small-scale experiments. For that reason, the obtained results are used to validate the numerical module detailed in chapter 2. Figure 4.1 shows the materials of each component of the physical model and the boundary conditions as explained chapter 2 and equations (2.22) and (2.23). The density, thermal conductivity, heat capacity, melting temperature, and latent heat of the PCM are assigned to each simulation. The applied temperature on the boundaries, the nucleation temperature, and the time required to raise the temperature to the melting temperature are assigned based on the experiments chosen.

These values are obtained using the thermocouples included in the experiment, the first of which measures the temperature of the PCM and the second of which measures the temperature of the water. The data presented in this validation study refer to numerical thermocouples, which are responsible for displaying the temperature at the same position as the experiments. To validate this model, the root mean square error $RMSE$ and the percentage root mean square error $PRMSE$ are calculated for each PCM validation process. Using the experimental data as a reference and the numerical data spread around it, the $RMSE$ calculates the spread of numerical results around the experimental ones, and a small value indicates a high concentration and best fit between the two results. According to Veerasamy *et al.* [165], a model having a $RMSE$ with a value greater than 1 is considered inaccurate. Likewise, the $PRMSE$ displays the percentage of this deviation from the true values.

The simulations are done using an Intel Xeon CPU E5-1650 v3 of speed 3.5 GHz, six cores (12 CPUs) and 16 GB RAM.

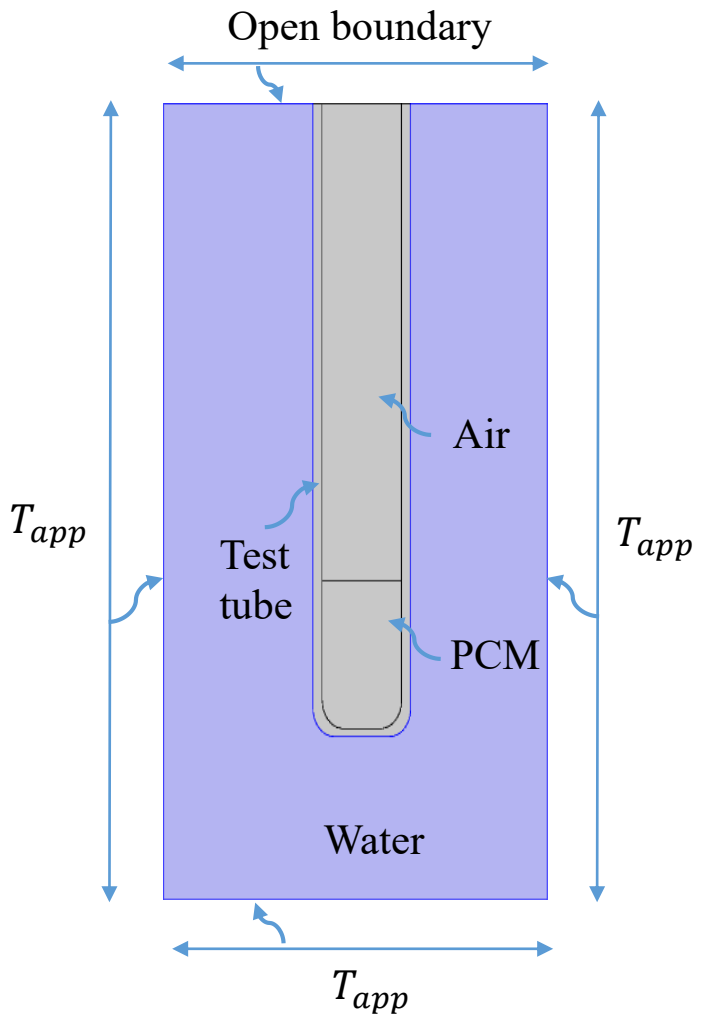

Figure 4.1 Geometry, materials and boundary conditions used in the numerical model

4.1.1 Octadecane

Based on the experimental results obtained in Chapter 3, the following temperature values 27.3 °C, 25.5 °C and 26.36 °C are set for the melting (T_m), nucleation (T_n) and cooling (T_{app}) temperatures, respectively, and the time needed to reach phase change (t_s) is 15 s. The numerical phase change range (dT) chosen is 0.5 °C, where below this value, the model suffers from numerical divergence. The phase transition plays a role in the functions that change the thermophysical property values and the state of the PCM. The transitions become sharper as the phase change range narrows, causing divergence. Several authors have also used similar values such as 2 K [166], 1 K [139], [161] and 0.2 K [167].

First, a mesh independence study is performed by comparing the obtained numerical results from the extremely fine and extra-fine meshes as shown in Figure 4.2. The model shows similar results regardless the mesh size. By calculating the root mean square error and percentage root mean square error for the first 300 seconds of computation for the two meshes, it is found that $RMSE = 0.021$ °C and $PRMSE = 0.075\%$, which shows very good agreement. In the following, the extra-fine mesh is used.

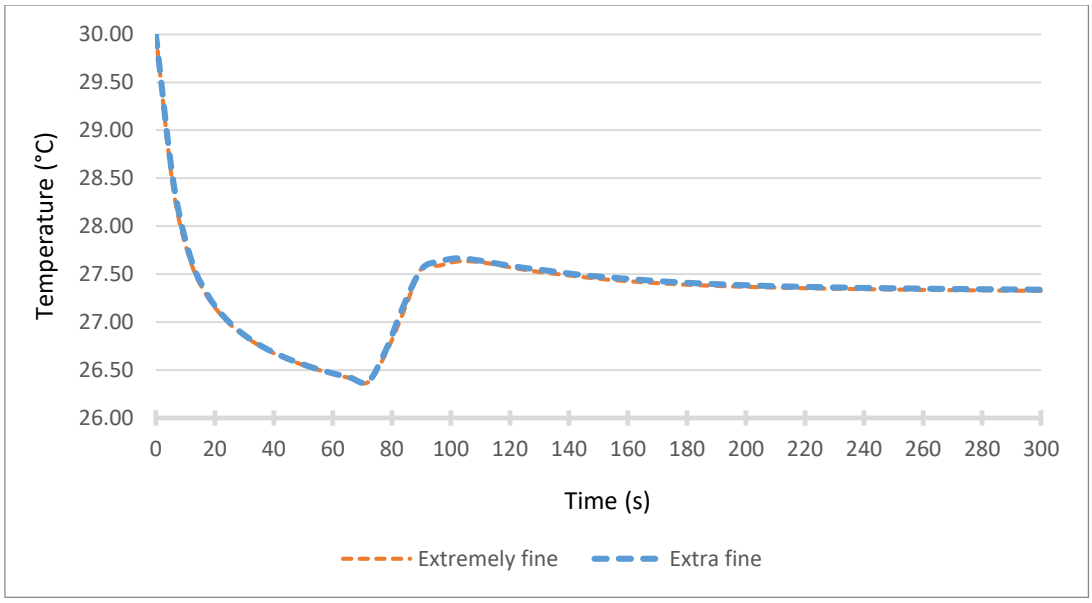

Figure 4.2 Comparison between the results obtained using extremely fine and extra-fine meshes

Figure 4.2 shows that the designed COMSOL model is able to simulate properly the supercooling phenomenon. The PCM remains in the liquid state until reaching 26.37 °C, which is close to the preset temperature of 26.36 °C. At that point, the temperature of the PCM increases until reaching the upper limit from where solidification starts ($T_m + dT/2$). Figure 4.3 compares the results from the numerical model with the experimental results. The model shows similar results and representation of supercooling. By calculating the $RMSE$ and $PRMSE$ between the experimental and numerical results on the extra-fine mesh, it is found that $RMSE = 0.258\ °C$ and $PRMSE = 0.92\%$. The solidification initiates at the same time as the experiment and the time required for temperature increase is almost the same. However, phase change in the numerical model is considered to take place in an interval of temperature (0.5 K). For that reason, the numerical temperature increases to a value higher than the experimental melting temperature.

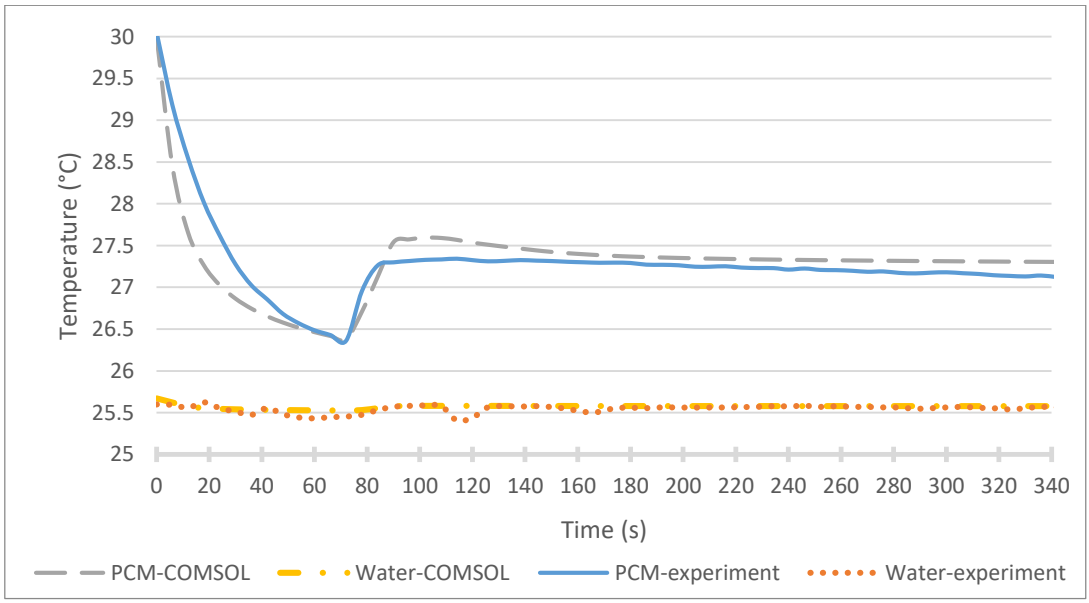

Figure 4.3 Comparison of experimental and numerical results of octadecane undergoing supercooling

4.1.2 Eutectic PCM

Based on the experimental results obtained from trial #1 in Chapter 3, values 21.5 °C, 20.4 °C and 18.1 °C are set for the melting (T_m), nucleation (T_n) and cooling (T_{app}) temperatures, respectively, and the time needed to reach phase change (t_s) is 158 s. The numerical phase change range (dT) chosen is 0.25 °C. The comparison between the experimental and the model's results are shown in Figure 4.4.

Calculating the root mean square error (RMSE) and the percentage root mean square error (PRMSE), it is found that $RMSE = 0.15\ °C$ and $PRMSE = 0.71\ \%$.

However, the model is unable to simulate trial #5 when the cooling rate is very high. Experimentally, the PCM loses its latent heat before reaching the melting temperature and solidifies at a lower temperature. In this case, the model will increase the temperature to $T_m - \frac{dT}{2}$ since the latent heat is theoretically sufficient.

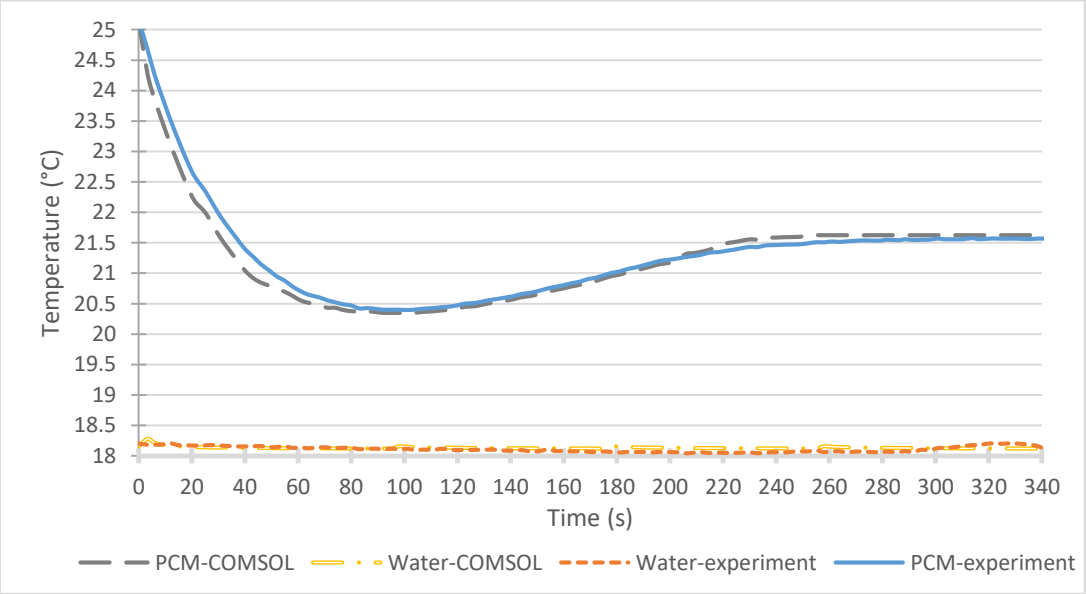

Figure 4.4 Comparison of experimental and numerical results of the eutectic PCM undergoing supercooling

4.1.3 Sodium acetate trihydrate

Based on the experimental results obtained in Chapter 3, values 58 °C, 47.4 °C and 40.8 °C are set for the melting (T_m), nucleation (T_n) and cooling (T_{app}) temperatures, respectively, and the time needed to reach phase change (t_s) is 9 s. The numerical phase change range (dT) chosen is 0.5 °C.

In this simulation, the model provides lower temperatures before solidification. The model accurately simulated the cooling process of the liquid PCM in the two previous PCM validation processes, so the difference in this case can be attributed to a difference between the real thermophysical properties of the PCM and those provided by the supplier. However, the model behaves precisely during the temperature increase phase. The temperature rises in the same way as in the experiment, but to a higher value because the model raises the temperature to ($T_m + dT/2$) as shown in Figure 4.5. Similarly as in section 4.1.2, the solidification of the PCM in the model takes more time than the solidification in the experiment.

By calculating the root mean square error ($RMSE$) and the percentage root mean square error ($PRMSE$), it is found that $RMSE = 2.47°C$ and $PRMSE = 4.63\%$. It should be noted that this error is primarily caused by the part prior to supercooling.

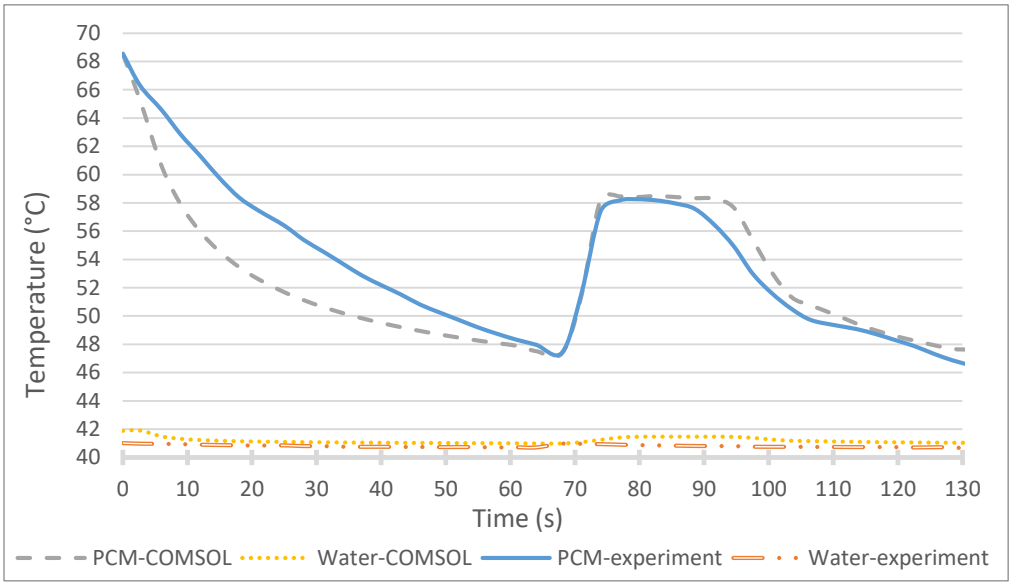

Figure 4.5 Comparison of experimental and numerical results of SAT undergoing supercooling

4.1.4 Discussion

The model performed well, and the supercooling phenomenon was numerically represented using a straightforward method. The onset of solidification and the time required to raise the temperature to the melting temperature are the most important aspects of the model. In cases of rapid temperature increase, the model accurately represents these two. However, the model still requires some improvements. Instead of considering adiabatic temperature rise due to latent heat release, heat transfer should be considered. Because of this omission, the amount of latent heat used to increase temperature to phase change temperature is underestimated, resulting in a longer solidification process represented by the time spent in the interval $[T_m - \frac{dT}{2}, T_m + \frac{dT}{2}]$. This effect is not visible with rapid temperature increases, but with slow temperature increases and high cooling rates, the PCM can lose all of its latent heat without reaching the phase change temperature. The model cannot simulate this scenario. In Chapter 3, for example, the temperature slowly rises (after 89s) during the cooling process of the eutectic PCM using 3.6 °C coolant temperature. The latent heat is theoretically sufficient to raise the temperature from 19.6 °C to 21.5 °C representing a 1.9 °C of supercooling. However, the temperature rises to 20.4 °C rather than 21.5 °C, after which it falls rapidly.

It can be concluded from this validation step that the model performs best when temperatures rise quickly and cooling rates are low. In this case, the temperature exchange to the outside becomes insignificant. However, when high cooling rates are used and the temperature increase is relatively slow, the PCM loses more energy to reach its melting temperature. This model still has some limitations, one of which is its reliance on experimental data. Input data such as the nucleation temperature and the time required to raise the temperature from the nucleation temperature to the melting temperature are critical.

4.2 Hot water tank application

Heating residential spaces and generating hot water are responsible for about 75% of buildings energy consumption [168]. Using clean energy sources such as solar energy is one of the alternatives to cover an important part of this demand. The solar energy is collected using solar panels, transferred most of the time using water in isolated pipes and stored in big isolated tanks. The use of solar energy to heat water decreases the need for electric and gas heaters, and thus decreases the emission of greenhouse gases. A solar water heating system is equipped with a thermally insulated water tank which temperature ranges between 50 ˚C and 60 ˚C [169]. During the day, the water is heated by the sun and stored in the tank. An auxiliary electric resistance situated within the tank is activated when more heat is required. The use of PCM in this system enhances its performance and efficiency. In the following subsections, the different methods used to integrate the PCM are detailed. Then a method is selected to be used to numerically study the effect of supercooling on the system's performance. Supercooling has a direct effect on the system because it prevents solidification, which reduces the amount of energy released to heat the water tank. The previously validated numerical model is used to compare the temperature variation of water with and without supercooling.

4.2.1 Models in the literature

This section presents a set of experimental and numerical models developed by other authors. It aims to select a model with simple geometry in order to use the validated model and demonstrate the effect of supercooling on a solar water heating system.

The literature is rich with various solar-powered thermal energy storage systems. The basic idea is to collect solar energy with a solar panel and store it in a storage tank filled with water or another liquid material. The PCM can be built into the solar panels [170], insulating pipes [171], and storage tank [172].

When integrated into solar panels, the PCM is positioned at the bottom surface of the collector or around the tubes [173], which serves in:

- Preventing energy losses and heat transfer through the network pipes,
- Reducing the initial fixed cost,
- Decreasing the overheating of the panels.

The use of PCM in the storage tank has a number of benefits [174]:

- Control the temperature of the water,
- Increase the thermal capacity of the tank,
- Ability to decrease the volume of the tank,
- Distribute the peak load over off-peak periods.

The benefits listed above improve the system's efficiency and dependability. Several studies have investigated the performance of PCM integrated of solar water tanks. PCM can be introduced in packs at the upper part of the tank as shown in Figure 4.6a. In this experiment, Mazman *et al.* [175] reported that the temperature holding time in a solar water tank with PCM was 6 to 12 hours longer than without PCM. Similarly, Al-Hinti *et al.* [176] filled 38 kg of paraffin wax PCM in aluminum cylindrical containers. Figure 4.6b illustrates the placement of the 38 containers on two levels. The storage tank has a total volume of 107.4 L, of which 58 L is filled with water and the remaining 49.4 L is occupied by the PCM. The tank has an inner diameter of 450 mm, a height of 675 mm, and a rock-wool insulation thickness of 78 mm. They

reported a difference in average water temperature of 13 ˚C to 14 ˚C between systems with and without PCM, as shown in Figure 4.7.

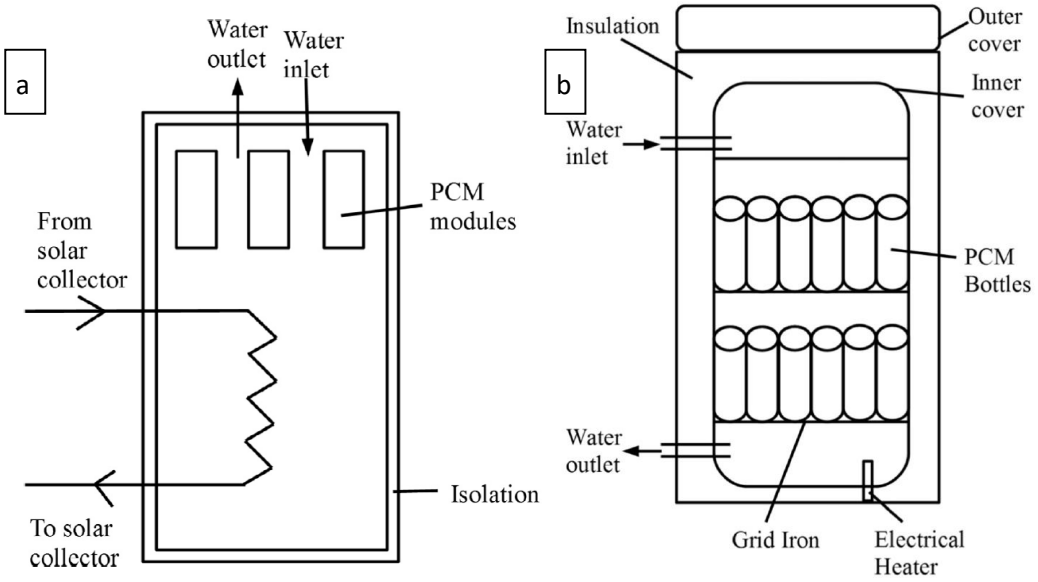

Figure 4.6 Solar heat storage tank integrated by PCM modules a) at the upper part [175]**, b) at two levels** [176]

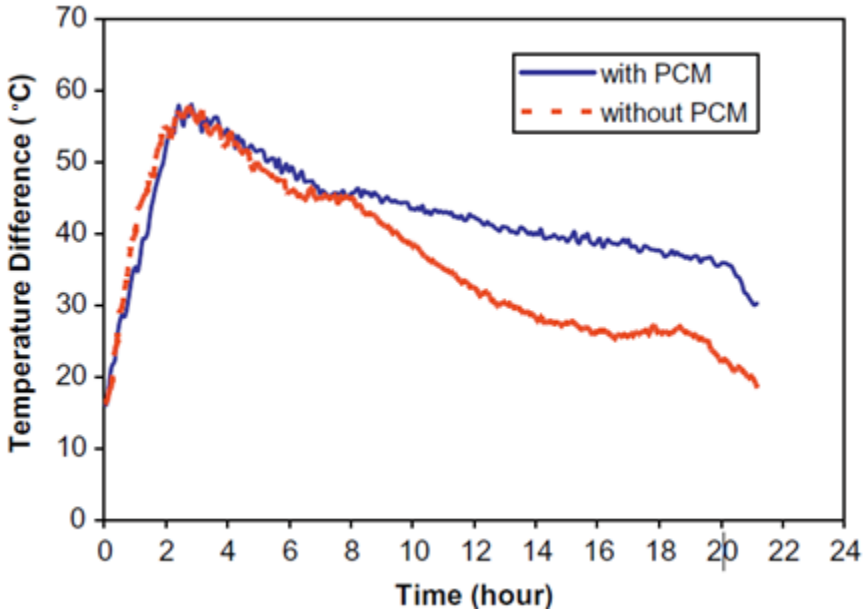

Figure 4.7 Variation of temperature difference between the ambient temperature and water in storage tanks with and without PCM [176]

As shown in Figure 4.8, the PCM can also be used as a jacket to cover the hot water tank. The authors used spherical PCM capsules in a heat exchanger tank in this experiment [177]. The benefits of using the PCM have been reported to be a 25% increase in supply time of 80 ˚C hot water, a 39% increase in storage density, and a 16% increase in exergy.

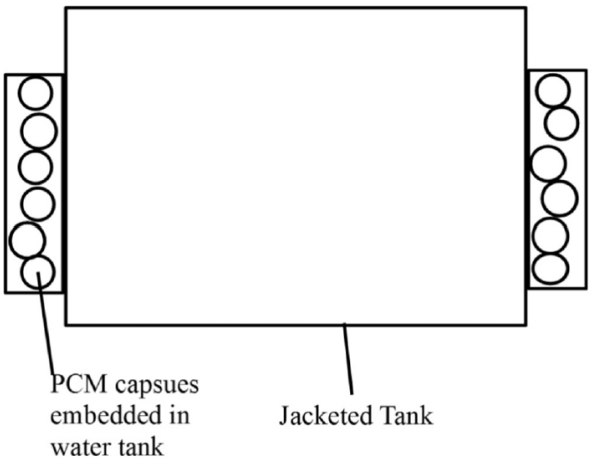

Figure 4.8 Solar water heat storage tank integrated by PCM modules at the periphery of the tank [177]

Cabeza *et al.* [178] built two identical hot water tanks, one of which equipped with PCM. A compound made of sodium acetate trihydrate (SAT) and graphite was placed in two aluminum bottles measuring 31.5 cm in height and 8.8 cm in diameter. A bottle has an estimated volume of 1.5 L, which accounts for about 2% of the total volume of the storage tank, which is 146 L. Figure 4.9 illustrates the experiment layout, including the bottle and tank dimensions. The temperature of the water drops as heat is lost to the outside via the used insulation, which has a U-value of 1.5 $\mathrm{W/m^2K}$.

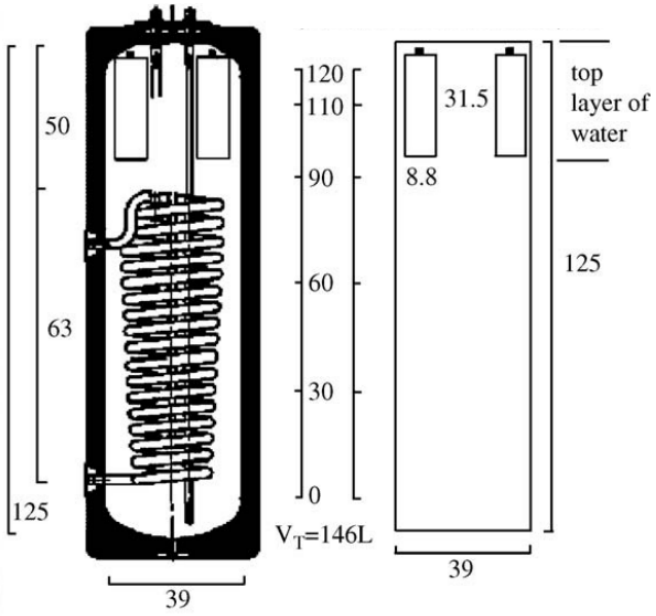

Figure 4.9 Hot water tank equipped by PCM designed by Cabeza *et al.* [178]

Dhaou *et al.* [169] examined two types of hot water tanks with a paraffin wax that is nano-enhanced (Ne-PCM) and having a phase change temperature 52 °C, as shown in Figure 4.10. The type of heat exchanger between the PCM and the flowing water distinguishes the two tanks. The PCM is housed in copper capsules with inner diameters of 4 mm, height of 120 mm, and thicknesses of 1 mm. The circular array inside the tank required the use of 20 capsules. The first tank's heat exchanger is a cylindrical jacket with an inner diameter of 130 mm, height 170 mm, and thickness 6 mm. As shown in Figure 4.10 case 2,

the heat exchanger in the second tank has a spiral shape and is immersed in the tank. The heat exchanger's role in both cases is to heat the PCM and water using solar energy during the off-peak load periods.

Xue [179] used $Ba(OH)_2.8H_2O$ as a PCM in the experimental setup. The heat is extracted from the PCM using a U tube made of copper embedded in the PCM, as shown in Figure 4.11. The diameter and the thickness of the U tube are $8\ \mathrm{mm}$ and $0.8\ \mathrm{mm}$ respectively. The water flowing in the tube is connected to a $90\ \mathrm{L}$ tank.

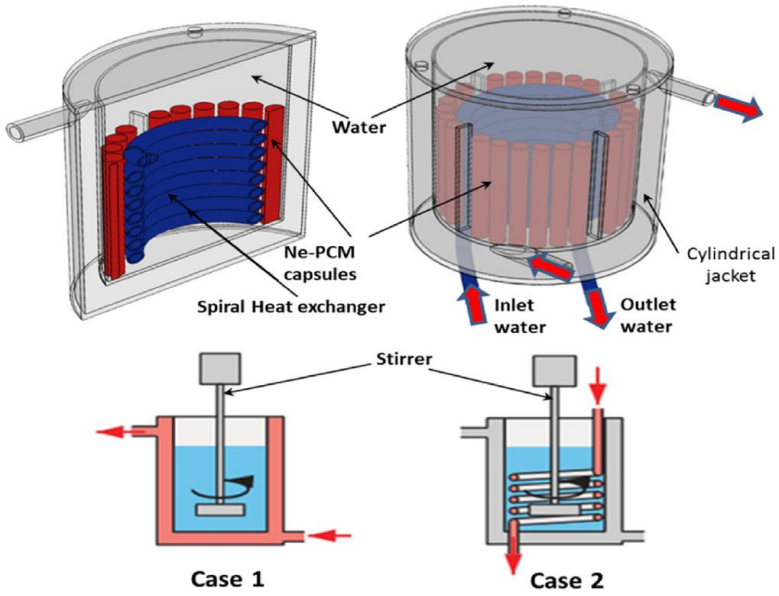

Figure 4.10 Two hot water tank equipped by PCM designed by Dhaou *et al.* [169]

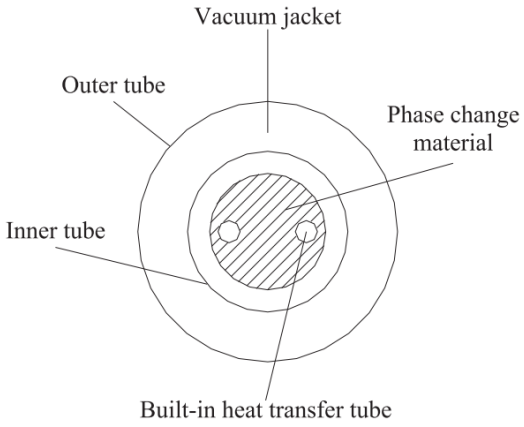

Figure 4.11 Hot water tank equipped by PCM designed by Xue [179]

4.2.2 Present model

To build the present model, the hot water storage tank with PCM in bottle-shaped containers investigated by Cabeza *et al.* [178] was chosen, due to its simple layout. The container measures 39cm in height and 125cm in width. The bottles are commercial aluminum bottles (density 2700 kg/m3) that are assumed rectangular for simplicity. The bottles measure 31.5 cm in height, 8.8 cm in width, and 0.4 mm in thickness. The PCM chosen is sodium acetate trihydrate (SAT), which has the thermophysical properties shown in Table 4.1.

Table 4.1 SAT thermophysical properties [159]

	Solid	Liquid
Cp (J/kg.K)	2900	3100
k (W/m.K)	0.600	0.385
ρ (kg/m³)	1450	1280
T_m = 58 °C	-	-
LH = 264 kJ/kg	-	-

The following scenario occurs in this physical model: the tank is filled with 70 °C hot water until the PCM and aluminum reach this temperature. Then, the hot water is drained and replaced with cold water at 20 °C. A real-life example is a domestic hot water tank heated by a solar panel, where the tank is heated by the solar energy during the day and all of the water is used after sunset, so the tank is refilled with tap cold water. In this case, the PCM is used to reheat the water. Two study cases are simulated: in the first case, the PCM becomes supercooled, whereas in the second, the PCM solidifies without supercooling. The effect of supercooling on the maximum temperature at each thermocouple location in the water is investigated. As a result, the heating part of this application is the most interesting. Therefore, as a boundary condition, the system is considered adiabatic so that no heat is exchanged with the outside. The initial temperature of the water is 20 °C, and the temperature of the bottles and PCM is 70 °C. Figure 4.12 shows the model's geometry, the boundary and initial conditions. A thermocouple is placed in the center of each PCM bottle, and three thermocouples (TC_1, TC_2, and TC_3) are placed 100 cm, 70 cm, and 30 cm above the bottom of the tank, respectively. The thermocouples are shown in red in Figure 4.12.

By taking the bottom of the tank as a reference of height, let H be the height of water with respect to the bottom. The average temperature for the water part at $H > 62.5\ \mathrm{cm}$ and $H > 80\ \mathrm{cm}$ is instantly provided by T_{avg_1} and T_{avg_2}, respectively.

The applied mesh is extra-fine free triangular and the simulated time is 8 hours (480 min).

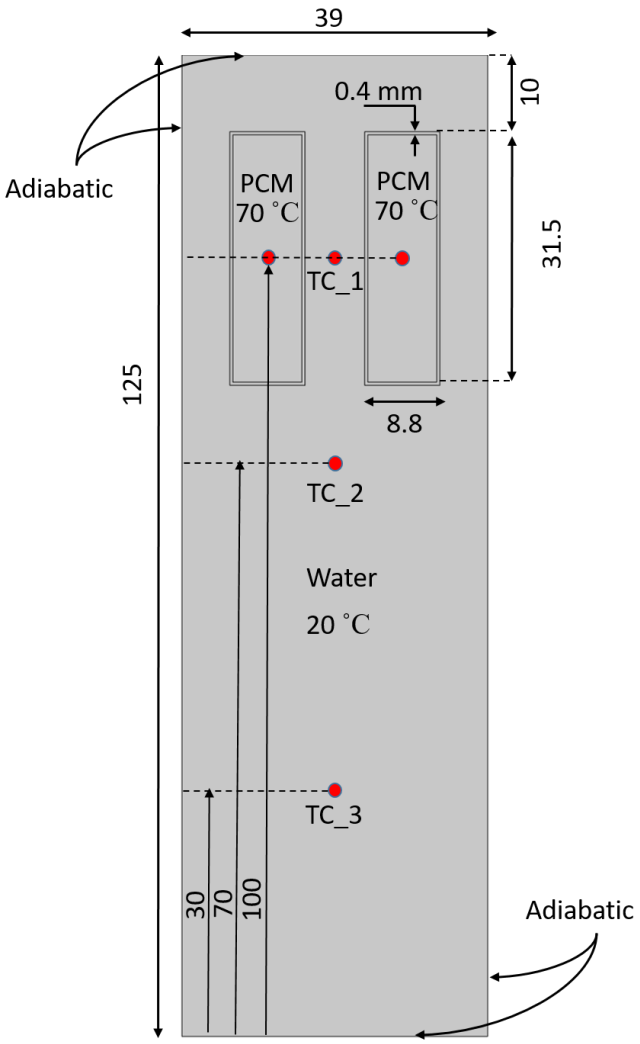

Figure 4.12 Position of thermocouples, geometry, boundary and initial conditions of the hot water tank model

4.2.3 Results

When supercooling is present, the PCM cools down due to the heat transferred to the water. The temperature of the PCM falls below the melting point without changing phase. Because the upper part of the water is heated, there is no natural convection heat transfer in water, and heat is only transferred by conduction. As a result, the water at the bottom remains cold. The maximum temperature reached by water at TC_1 and TC_2 at after $480\ \mathrm{min}$ is 49.26 ^{o}C and 30.32 ^{o}C, respectively. It is worth noting that the maximum temperature of TC_1 is reached at *t* = 130 minutes, after which the temperature drops due to conduction heat transfer to the lower parts.

Without supercooling, the PCM reaches melting temperature and changes phase by releasing its latent heat. The maximum temperature reached by water at TC_1 and TC_2 is 52.23 ^{o}C and 31.70 ^{o}C, respectively. It is worth noting that the maximum temperature of TC_1 is reached at $t = 151\ minutes$, after which the temperature drops due to conduction heat transfer to the lower parts. As a result, in the absence of supercooling, the water at TC_1 is 2.97 ^{o}C hotter than in the presence of supercooling. Figure

4.13 depicts the temperature variation of the PCM and the water over 480 minutes at three different locations. It can be seen that in the presence of supercooled PCM, the water is always colder.

In the absence of supercooling, T_{avg_1} records a temperature of 41.65 °C and 43.02 °C during 300 and 480 minutes, respectively. Similarly, T_{avg_2} records 48.27 °C and 48.78 °C. In the presence of supercooling, however, T_{avg_1} records a temperature of 29.54 °C and 31.93 °C during 300 and 480 minutes, respectively. T_{avg_2} records 45.22 °C and 45.7 °C, respectively. Table 4.2 summarizes these findings. This demonstrates that the PCM significantly heats the upper part of the water. Because water lacks natural convection, heat is transferred slowly to the lower parts via conduction heat transfer. The position of the PCM or the number of PCM cells can be changed depending on the quantity and temperature of hot water required. Supercooling has an important effect, where in the cases with and without supercooling, T_{avg_1} recorded a difference of 12.11 °C and 11.09 °C after 300 and 480 minutes, respectively.

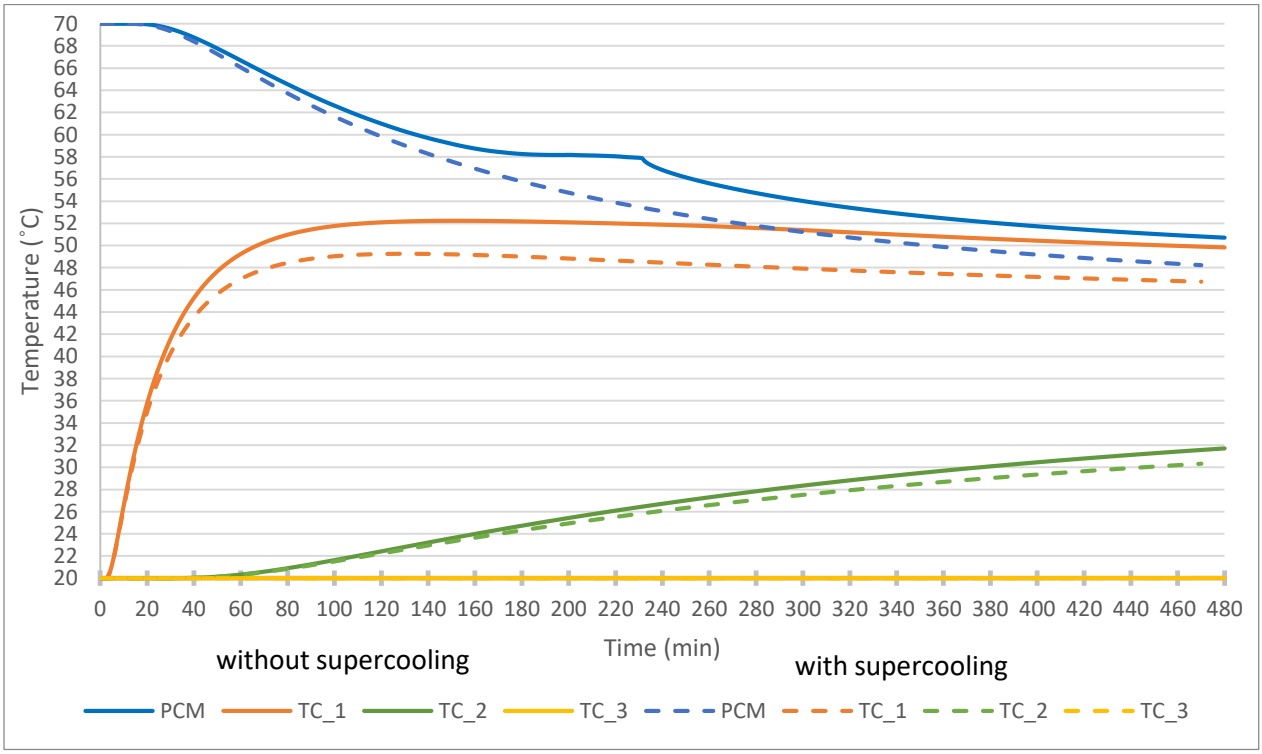

Figure 4.13 Temperature variation of PCM and water at different heights in the case of presence (dashed lines) and absence (solid line) of supercooling

Table 4.2 Temperature of water at different heights and times for the cases with and without supercooling

Thermocouple	Time (min)	Height (cm)	With supercooling	Without supercooling
TC_ 1	480	100	49.26 ^{o}C	52.2 ^{o}C
TC_ 2	480	70	30.32 ^{o}C	31.7 ^{o}C
TC_ 3	480	30	20.01 ^{o}C	20.01 ^{o}C
T_{avg_1}	300	>62.5	29.54 ^{o}C	41.65 ^{o}C
T_{avg_2}	300	>80	45.22 ^{o}C	48.27 ^{o}C
T_{avg_1}	480	>62.5	31.93 ^{o}C	43.02 ^{o}C
T_{avg_2}	480	>80	45.70 ^{o}C	48.78 ^{o}C

4.3 Residential heating

Maintaining a comfortable temperature in a building accounts for the majority of the energy demand [180], which necessitates finding ways to reduce this demand. Latent heat thermal storage systems are one of these solutions in which the PCM can help to conserve energy for later use in cooling and heating processes [181]. The main characteristics that distinguish the PCM are [182]:

- The ability to maintain a constant temperature range during phase change
- The presence of various types of PCM with a wide range of phase change temperatures
- The high value of latent heat

The PCM is used in free cooling and free heating processes, where heat stored during the day is used to heat during the night, and in other systems, where cold is stored during the night and used to cool during the day. The PCM can be installed into a separate system [183], the building's ceiling [184], walls [185], floor [186] or windows [187].

Supercooling can be investigated in both heating and cooling processes. In temperature management (cooling) processes, the PCM absorbs excess heat during the day and release it later in the night. If the PCM is not allowed to solidify at nighttime, it remains liquid and absorbs less energy when heated again during the following day. In building heating processes, the PCM loses its energy to heat the indoor space. Preventing solidification results in less heat being released into the room.

4.3.1 PCM incorporation into the system

According to Iten *et al.* [182], thermal energy storage systems using phase change materials in building applications can be divided into passive and active techniques. Passive technique does not necessitate the use of fans, pumps to increase the heat transfer rate to the PCM. Such techniques include PCM incorporated into building materials. In active techniques, on the other hand, the PCM is integrated in a

system that improves heat release and storage through the use of fans, pumps, and storage tanks. Here, the PCM can be integrated into a building's ceiling, underfloor, and walls.

The following are some examples from the literature that correspond to a passive technique.

Ahmad *et al.* [188] created a small chamber prototype with floor dimensions of 90 x 90 cm, and the PCM was integrated into the chamber walls using PVC panels. Figure 4.14 illustrates the cross section of the wall made of fiber cement, vacuum insulation panel (VIP), PCM, and plywood.

To reduce the demand for heating, Chen *et al.* [189] added a PCM layer to the inner surface of the north wall of an ordinary room, as shown in Figure 4.15. The PCM and cement layers are both the same thickness (20 mm). By using 30 mm thick PCM having $T_m = 23.8\ °C$ and a heating temperature set at 20.8 °C, the rate of energy saving increased by 17%.

Jin *et al.* [190] used protective aluminum foils to encapsulate the PCM. The position of the PCM in the wall was changed to investigate the effect of its location on the system performance. According to their findings, placing the PCM near the interior wall produces the best results.

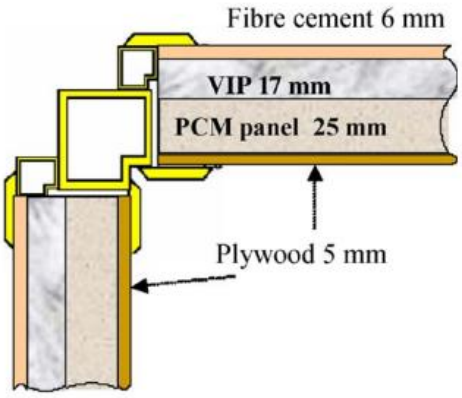

Figure 4.14 PCM integrated in the wallboards [188]

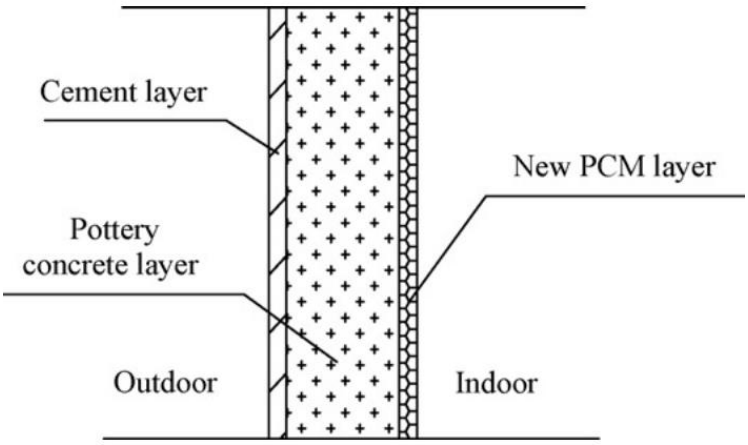

Figure 4.15 PCM integrated to the inner surface of a wall [189]

Liu *et al.* [191] investigated the effect of PCM thickness on the heat exchange in windows. They found that as the thickness increases, the heat transfer decreases non-linearly. The heat exchange became constant once the thickness reached 16 mm.

Su *et al.* [192] designed walls integrating two phase change materials. The encapsulated PCMs had different melting temperatures, with the lower melting temperature placed near the interior surface and the higher melting temperature placed near the exterior. The results show that increasing the thickness of the PCM increases the system's thermal storage capacity, and the PCM can stabilize the temperature for a longer period of time (about 12%) between 21 °C and 28 °C when compared to walls without PCM.

Similarly, Al-Rashed *et al.* [193], Kalbasi [194] and other authors integrated the PCM in the rooms' walls and roof while Sun *et al.* [195] constructed a floor model using two PCM. These systems can be used in the summer and winter to regulate internal temperatures and provide thermal comfort that can be increased by 2.2 times over the case without PCM.

Here are some examples of active techniques used in free cooling and free heating applications.

Butala and Stritih [196] incorporated the PCM into the ventilation system. The PCM was heated by the outside temperature during the day and released heat later at night, as shown in Figure 4.16. The temperature and flow of inlet air are the two most important factors influencing discharge time.

Raj and Velraj [197] proposed the set up shown in Figure 4.17. Using cylindrical disc modules, the PCM is installed in the heat exchanger as shown in Figure 4.18. Dampers 1 and 4 are opened to charge the PCM with cold energy, as a fan pumps the cold wind to cool the PCM located in the heat transfer module. During the day, dampers 2 and 3 are open, allowing hot air from the room to enter the heat exchanger module via natural or forced convection, depending on the required cooling rate. Similarly, the flow, inlet temperature, and spacing between PCM modules are important factors influencing discharging time.

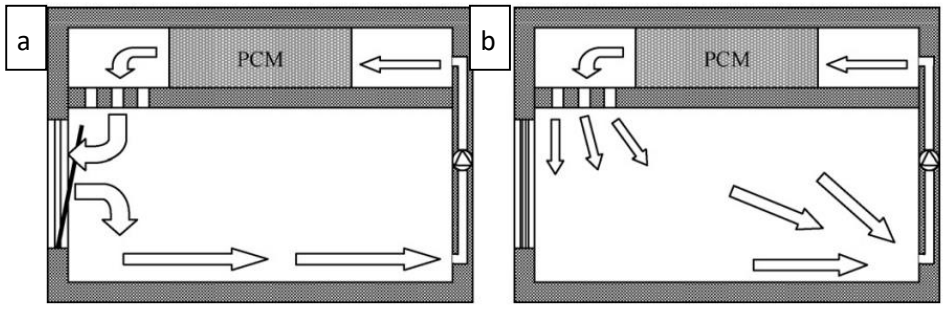

Figure 4.16 a) storage of heat during day and b) free heating using the PCM [196]

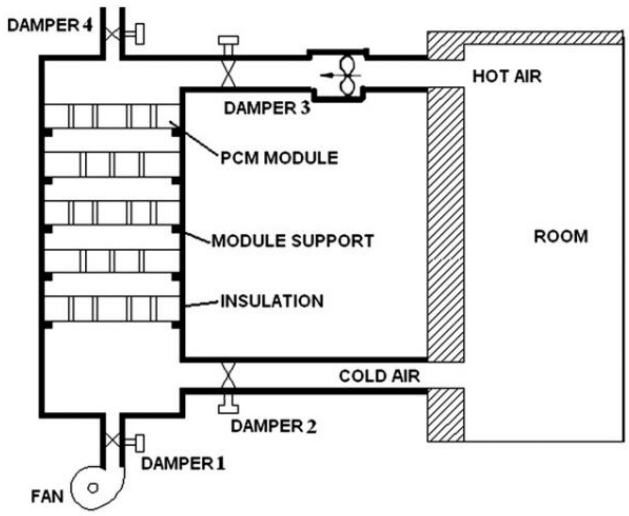

Figure 4.17 Set up of free cooling proposed by Raj and Velraj [197]

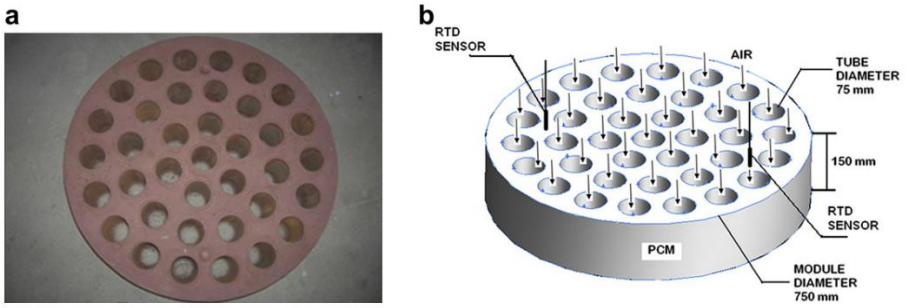

Figure 4.18 a) Photograph and b) isometric view of the PCM module used in the heat exchanger [197]

Lu *et al.* [198] integrated the PCM into the floor, as shown in Figure 4.19, where letters "*a*" to "*d*" represent the layers used for finishing, filling, insulation, and moisture barrier, and *"e"* to "*g"* represent the PCM casing, hot water, and PCM, respectively. Hot water is used to heat the PCM using solar energy, and electricity is used to heat the circulating water when necessary. As a result, the system can save approximately 30% on energy costs compared to system using solely an electric heater. The total cost, however, remains high due to the high cost of materials required to build the system.

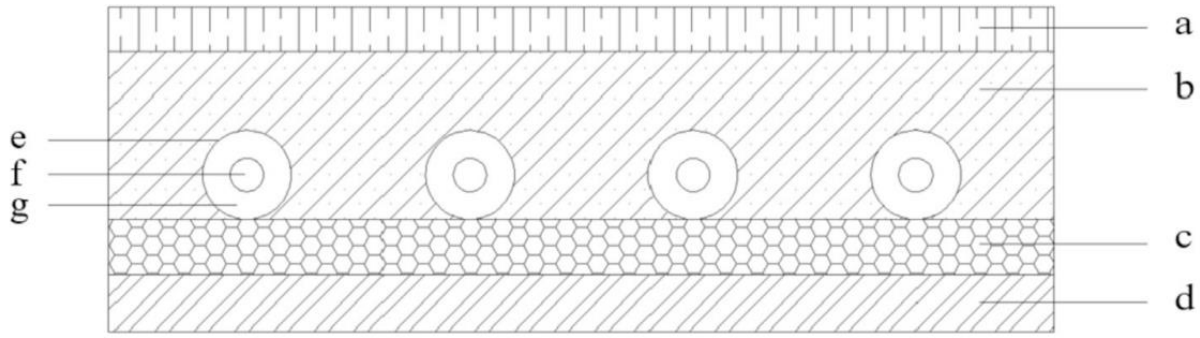

Figure 4.19 Floor heating using PCM [198]

Waqas and Kumar [199] integrated the PCM into a building's ventilation system. The purpose of PCM is to heat the inlet air to the building, which is especially important during the dry, cold summer nights of South Asia. During the day, all hot air passes through the PCM and ventilation system, ensuring that the PCM is charged with heat and arrives at the cold night in a liquid state, as shown in Figure 4.20a. Figure 4.20b shows how the PCM heats a portion of the cold air during the night. As a result, thermal comfort is achieved by lowering the temperature of the hot air during the day and raising the temperature of the cold air during the night. The system performs best in the summer when the PCM has a melting temperature equal to the comfort temperature.

Xiao *et al.* [200] created a numerical model of a residential building room. The PCM is integrated into the room's interior enclosure, as shown in Figure 4.21, and is heated using direct solar energy. During the night, the window is closed, and the PCM heats the room with heat gained during the day. The studied room is 4m long, 5m wide, and 2.8m high, with all the walls being interior except for the southern wall that has the window. Polystyrene, 60mm thick, is used to insulate this wall. Using 20 mm panels, the PCM is integrated into the walls, roof, and floor. The density of the PCM is 900 kg/m^3, the heat capacity is 1.05 kJ/kg.K, the thermal conductivity is 0.2 W/m.K, the latent heat is 35 kJ/kg, and the phase change temperature is 20 ˚C. As a result, the phase change temperature must be chosen based on the amount of radiation available and the temperature of the indoor air. The results show that using PCM on the interior side has little effect on internal room temperature fluctuations, which depend on the heat transfer coefficient between the room and the PCM surface contact.

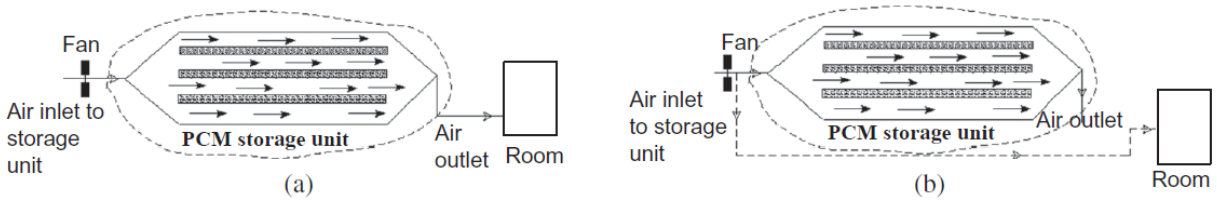

Figure 4.20 Air heating system using PCM a) charging during the day and b) discharging during the night [199]

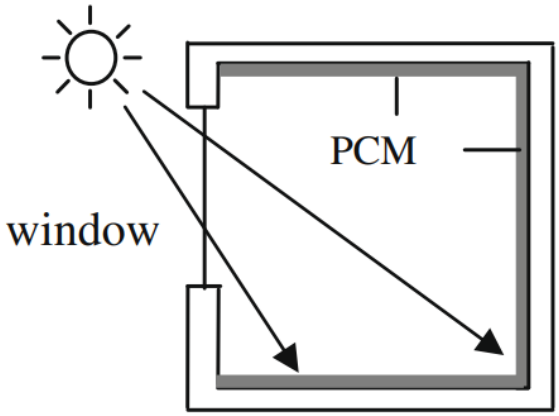

Figure 4.21 PCM integrated in the enclosure of a residential room [200]

4.3.2 Present model

Studying cooling process necessitates a 24-hour system operation monitoring that requires accurate weather data input. A heating process is chosen for this chapter since the study can be done in a shorter period of time. The air heating system presented by Waqas and Kumar [199] is chosen to simulate the effect of supercooling. The system is a ventilation system using latent heat thermal energy storage. The PCM is integrated in the ventilation pipe. The following scenario is used in the present study: the PCM is first heated during the day and the PCM reaches 32 ˚C. Later at night, the ambient temperature drops to 20 ˚C. To simplify the model, the study considers only half of the tube containing PCM, since the model has axisymmetric boundary conditions, as shown in Figure 4.22. The PCM is 2.5 cm thick and 50 cm long. The same dimensions apply to the air cavity above it. The inlet air flow rate is chosen 10 m^3/h, and the chosen PCM is $CaCl_2.6H_2O$, that has the thermophysical properties shown in Table 4.3.

Table 4.3 $CaCl_2.6H_2O$ thermophysical properties used in the residential heating [199]

	Solid	Liquid
Cp (J/kg.K)	1430	2312
k (W/m.K)	1.09	0.54
ρ (kg/m^3)	1710	1500
T_m = 28 °C	-	-
LH = 188.34 kJ/kg	-	-

In the first case study, the PCM becomes supercooled, whereas in the second, the PCM solidifies without supercooling. The effect of supercooling on the temperature of the air at the exit is investigated. As a result, the PCM cooling part of this application is the most interesting. The initial temperature of the air is 20 °C, and the temperature of the PCM is 32 °C. Figure 4.22 shows the model's geometry and the boundary conditions. A thermocouple is placed at the exit of the tube to calculate the temperature of the air after being heated by the PCM. In addition, five thermocouples (TC_1 → TC_5) are placed in the PCM as shown in Figure 4.22.

The applied mesh is extra-fine free triangular and the simulated time is 8 hours (480 min).

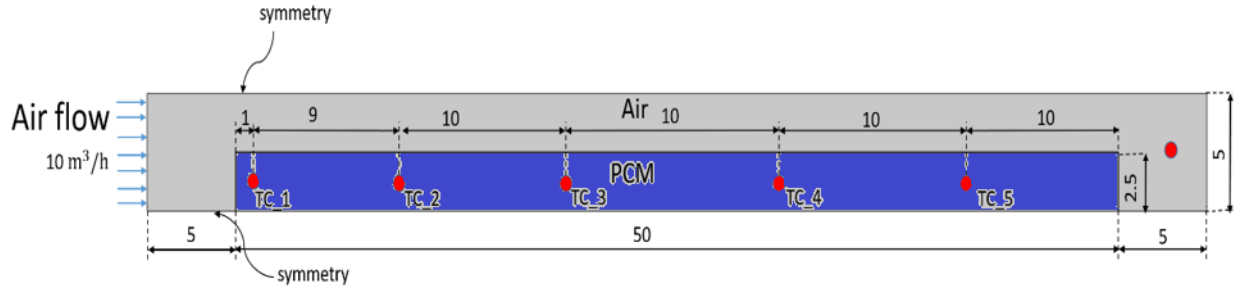

Figure 4.22 Position of thermocouples, geometry and boundary conditions of the pipe model

As shown in Figure 4.23a, the temperature of the PCM decreases due to the incident cold air flow around it. Because of its proximity to the left boundary, the first thermocouple, TC_1, shows a faster temperature decrease than the others. The surface contact with the air is greater in that region, and the air temperature is the lowest. As the air passes through the channel, its temperature rises, resulting in a higher heat flow at first. The first effect of supercooling can be seen in Figure 4.23a, where the supercooled PCM has a lower temperature than the solidified PCM. The temperature gradient between the PCM and the air decreases in this case, resulting in a lower heat flow from the PCM to the air. The effect of supercooling is direct on the temperature of the air at the exit, where the air is heated more in the absence of supercooling, as shown in Figure 4.23b. As expected, the air reaches high temperatures at first while the melted PCM is still hot, and the temperature decreases as the PCM cools. The second effect of supercooling is that the temperature of the air gradually decreases rather than remaining constant over time. The figure demonstrates that the phase change of the material adds more energy to the air, as it maintains a stable temperature of 26.34 ˚C. The difference between the cases with and without supercooling increases from 0.4 ˚C at t = 300 min, to 2.4 ˚C at t = 480 min.

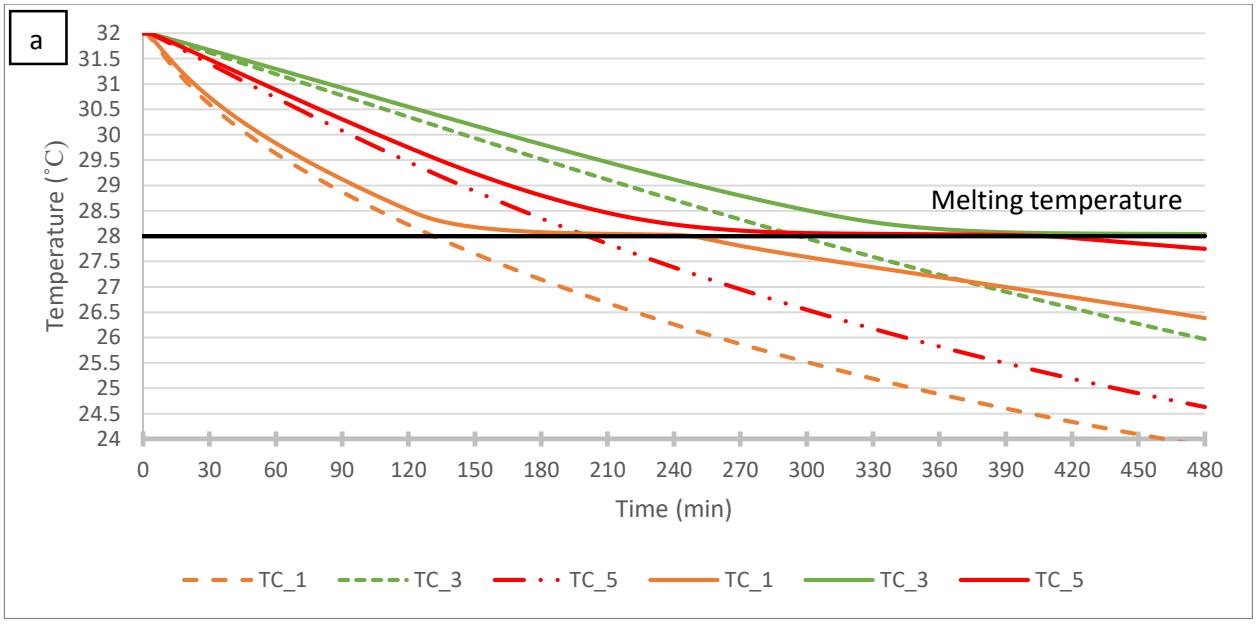

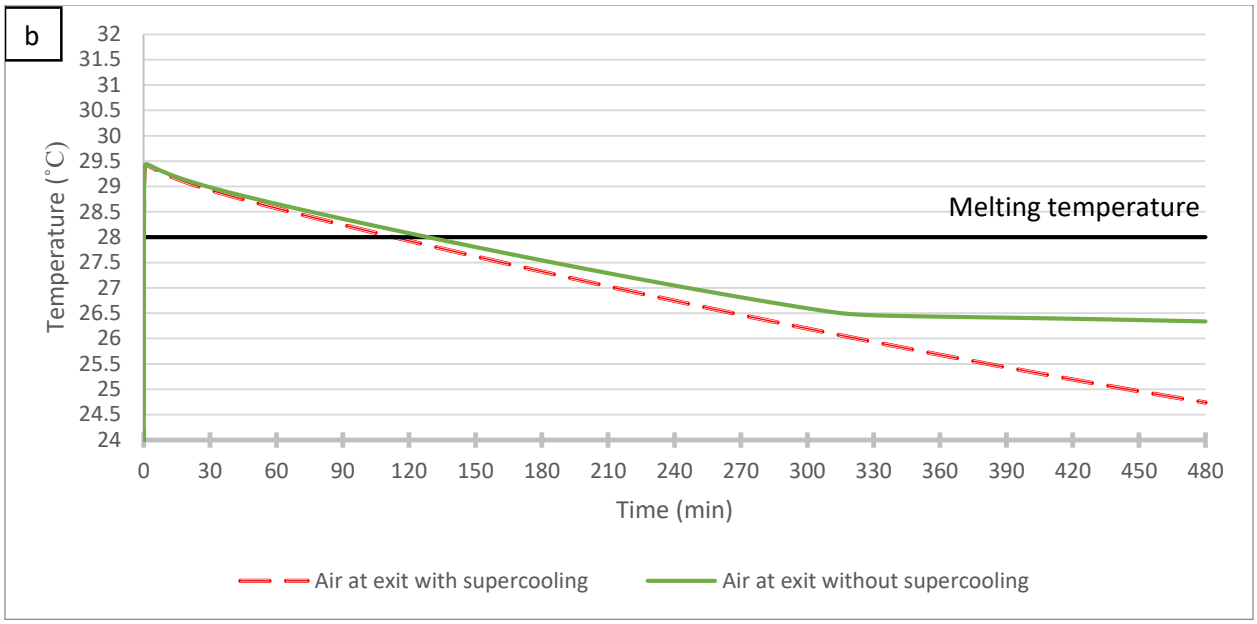

Figure 4.23 Temperature variation of a) PCM and b) air at exit in the case of presence (dashed lines) and absence (solid lines) of supercooling

4.4 Conclusions

Supercooling can be modeled using the proposed COMSOL Multiphysics model. One limitation occurs when the temperature rise caused by latent heat release can no longer be assumed adiabatic. The first is for rapid cooling, in which the PCM loses energy as the temperature rises. As a result, the model calculates the minimum energy required to raise the temperature to the melting point while accounting for heat lost to the outside. In this case, the numerical solidification takes longer than the experiments, because the amount needed to raise the temperature is deducted from the latent heat. The second is during a very slow temperature rise, as demonstrated by the eutectic PCM experiments. In theory, and ignoring heat losses, the latent heat is sufficient to raise the temperature to the melting point. The model, however, does not reach the melting temperature as all of the latent heat is released during the very low temperature rise. Therefore, the model works well for supercooling when the temperature rises quickly but the cooling rate is slow. As future enhancements needed for this model, the heat source function should be improved to include heat losses to the exterior rather than assuming an adiabatic temperature increase.

The use of PCM in thermal energy storage systems has a direct impact on their performance. The PCM is used to raise the temperature of water in a hot tank in the first application studied. The presence of supercooling has a significant effect, as the maximum temperature attained by the water at the end of the simulations was lower in the presence of supercooling. In the second application, the PCM heats the air in a forced ventilation system before it is pumped into the residential rooms. The presence of PCM has a significant effect on the temperature of the air entering, and the presence of supercooling reduces the system performance by lowering the maximum temperature reached by air. This study shows that it is critical to include supercooling this phenomenon in numerical simulations of latent heat energy storage systems using PCMs that may undergo supercooling.

General conclusion and perspectives

The primary goal of this thesis is to build a multidimensional CFD model of supercooling to numerically investigate its effect on the performance of thermal energy storage systems using phase change materials. The latent heat of phase change materials adds a significant amount of heat to the system, significantly increasing the system's efficiency. The presence of supercooling prevents or delays the solidification of the phase change material and the release of latent heat, which has a serious impact on the performance and efficiency of the system.

To achieve the thesis's goal, a literature review on the presence of supercooling and the factors influencing its occurrence is presented. In addition, the existing models found in the literature and the problems encountered during modeling are detailed. This review aids in the development of knowledge on the supercooling phenomenon, including its impact on the material behavior, its effect on the integrated PCM's system, the influencing factors, and aids in the development of a simple, and accurate method for representing this phenomenon in a numerical model. A previously validated numerical model for natural convection is modified to include supercooling during PCM cooling. This model considers the difficulties encountered in modeling the thermal behavior of supercooled PCM and devises a solution for each one. To validate this model, accurate experimental results starting from known model geometry, material properties, and conditions (initial and boundary) are determined. These findings are used to validate the numerical model, which is then used to investigate the performance of two latent heat thermal energy storage systems.

The work completed in each chapter, the obstacles encountered, the results obtained, and the required future work are listed below.

Chapter 1

The first chapter is a review of the literature on the supercooling phenomenon. This chapter begins by defining supercooling and the systems in which it can occur. It has been discovered that supercooling can be a beneficial or harmful phenomenon, depending on the system. Supercooling is beneficial in preservation processes such as for food, medical drugs, and organ transplantation. Furthermore, by preventing solidification, supercooling aids in the survival of animals and plants in cold winter regions. However, in thermal energy storage systems, PCM solidification is critical, and its prevention significantly reduces the systems’ performance. In both cases, the arbitrary presence of supercooling is detrimental, so a review of the main factors that influence this presence is performed. It has been discovered that there are a large number of correlated factors that influence the occurrence and degree of supercoooling. The cooling rate, the volume of the PCM container, mechanical shocks, the purity and the thermal history of the PCM are some of the most important factors. Each factor's effect is investigated independently by presenting the most recent experimental work done in the literature. This review continues with the numerical methods that are commonly used to model a phase change problem. The addition of supercooling to these models complicates the model and presents several challenges. The thermophysical properties of the material are no longer linear and are a function of temperature, where a given temperature lower than the melting temperature can correspond to the solid, supercooled, or temperature increase phases of a PCM. In addition to the method of temperature rise, indicating the temperature at which solidification begins is a challenge. This review discusses various recent models developed by various authors, as well as the criteria used to overcome these difficulties.

Perspectives:

This review demonstrates that supercooling is an important phenomenon, and its instability complicates the system. Its instability is because the presence of supercooling is dependent on several factors. However, these variables are still unconnected. More experiments should be carried out to develop general equations that precisely predict the nucleation temperature based on the crucial factors influencing supercooling. Its omission in numerical models can result in a disparity between real and simulated results.

Chapter 2

Main contributions

The second chapter describes the implemented numerical model. An optimal solution is found to every problem encountered while numerically simulating supercooling. Finally, a consistent model is presented and later validated and used in the following chapters.

The first key issue tackled is the initiation of solidification. The instability of the supercooled liquid and the initiation of solidification at any time present a significant challenge in determining the temperature at which solidification begins. Setting a temperature for solidification initiation at the first node solves the problem. Thus, solidification can occur either by reaching the preset temperature or by being triggered by the solid-liquid interface.

The second key issue is the non-linearity of the problem: the properties of a material can be defined as a function of temperature in a typical phase change problem; however, in the presence of supercooling, a given temperature can correspond to different states of the material. To solve this problem, a new state function $s(s,T)$ is defined. This function subdivides the system into four sections depending on the current state and the temperature of the material. The first is the heating process, the second is the liquid cooling (including supercooled liquid), the third is the temperature rise due to the latent heat release, and the fourth is the solidification and cooling of the solid.

The third key issue deals with the quantity of latent heat: when solidification begins, the PCM uses latent heat to raise its temperature. As a result, the amount of latent heat present during solidification differs from that present during melting. These two processes have already been separated by the state function $s(s,T)$. If the latent heat is sufficient during the cooling process, the temperature rises to the melting point. If not, the PCM releases all of its latent heat and solidifies at a temperature lower than the material's melting point. The value of latent heat during the solidification process is determined by assigning a state variable $nt(s,T)$ that indicates the nucleation temperature at each node. This aids in precisely determining the amount of heat required to raise the temperature to the melting point.

The last major issue concerns the temperature rise due to latent heat release: the PCM's temperature rises as latent heat is released. This section is complex, as it is caused by several factors. The most important of which are the thermophysical properties of the material and the cooling rate. To deal with the complexity, a domain heat source that is a function of the state variable $nt(s,T)$ is defined. Depending on its position and the degree of supercooling, this heat source releases a sufficient amount of heat to raise the temperature at the node.

Limitations and perspectives:

This is the first multidimensional CFD model that attempts to incorporate both supercooling and natural convection. The model is simple and needs several improvements. First, major inputs such as the nucleation temperature and the time required to increase from the nucleation to the melting temperature are not experimentally free. These two factors necessitate a thorough understanding of PCM's chemical behavior to develop general equations for predicting these values. Second, modeling temperature rise as a linear function with an adiabatic reaction is unrealistic. Heat transfer never stops, and the PCM requires more energy to reach the melting temperature and especially at low cooling temperatures.

Chapter 3

Main contributions

The third chapter is the experimental benchmark. This chapter aims to obtain accurate experimental results to use in the validation process of the numerical model. To build the experimental setup efficiently, the most important factors that affect supercooling are taken into consideration. The following factors are considered:

- The volume of the container: Two setups are constructed. The first is a small-scale experiment using a test tube as the PCM container, and the second is a large-scale experiment using a cuboid-shaped container.
- The surface roughness: The test tube has a smooth inner surface with no edges or connections, whereas the cuboid-shaped container has edges connecting the sides, as well as a difference in surface roughness between the aluminum plate used for heat transfer and the polycarbonate sides.
- The cooling rate: a water chiller and a heating circulator are used to study the effect of the cooling rate. These two devices make use of PID controllers to precisely adjust the temperature as needed.
- The type of PCM: The type of PCM, which can be organic, inorganic, or eutectic, influences supercooling. Three PCMs of different types are chosen: octadecane (organic), sodium acetate trihydrate (inorganic salt), and a eutectic PCM.
- Mechanical shocks: Mechanical shocks can cause supercooling to stop and solidification to begin. The experiments are carefully carried out to avoid mechanical shocks. In one of the experiments, the PCM enters a stable supercooling state and is terminated by an applied mechanical shock.
- The container’s thermal insulation: Insulation limits the heat transfer through the aluminum plates and prevents heat loss to the outside. The use of good insulation allows the numerical model to later assume that heat is transferred perpendicular to the aluminum plates and to use adiabatic boundary conditions.

Type T class 1 thermocouples are used to measure temperature at various points. This distribution aids in the investigation of the effects of supercooling and natural convection respectively during the cooling and heating processes.

The results of the experiments show that supercooling occurs in the test tube for all PCM types. However, supercooling proceeds only with the inorganic PCM in the large-scale experiment (sodium acetate trihydrate). The type of PCM, volume of the container, and surface roughness all play a role in

achieving such a result. First, inorganic PCM suffers from supercooling more than other PCM types. How temperature rises due to latent heat release is also material dependent. When solidification begins, the temperature of octadecane increases rapidly, the temperature of eutectic PCM increases slowly, and the temperature of sodium acetate trihydrate increases rapidly in the small-scale experiment and slowly in the large-scale experiment. Second, as the volume of the container decreases, the degree of supercooling increases. Third, as the surface roughness decreases, the supercooling degree increases.

Insulation has a direct effect on the solid-liquid interface during the heating and cooling processes. If no insulation is applied, heat is exchanged with the exterior, and the solid-liquid interface does not have a unique in-depth form (when looking at the PCM container from above), depending on the exterior temperature. If the exterior temperature is higher or lower than the melting temperature of the PCM, heat exchange with the exterior results in a convex or concave melting front of the solid part, respectively.

The cooling rate has a direct effect on the degree of supercooling. It has been demonstrated that, up to a certain point, the degree of supercooling increases as the cooling rate increases. However, as the cooling rate increases, the time spent in the supercooled state decreases. This is because the PCM reaches the nucleation temperature faster. The experiments also demonstrate that by using a low cooling rate, where the temperature of the cooling fluid gradually decreases with a negligible temperature gradient with the PCM, stable supercooling can be achieved. However, if the cooling rate is high during the temperature rise due to latent heat release, the PCM loses its latent heat during this phase and, in some cases, is unable to reach the melting temperature. When considering an adiabatic temperature increase caused by latent heat release, the latent heat is sufficient to raise the temperature to the melting point; however, the PCM does not reach the melting point due to heat loss during this phase.

Natural convection has a significant impact on the melting process during the heating process. The melting front is initially vertical, and as the melted fraction increases, natural convection increases the melting rate, and the solid-liquid interface slopes. The presence of natural convection causes the hot particles of the PCM to rise to the surface, causing the temperature to vary vertically. However, the phenomenon is not observed during the cooling process. The PCM has a nearly identical temperature in the vertical direction, and the solid-liquid interface remains vertical during the solidification process.

Limitations and perspectives:

The obtained results provide an accurate benchmark that different authors can depend on to model the PCM's thermal behavior and validate their numerical models. Future experimental studies should complement the data with the monitoring of the PCM velocity during melting and solidification, using such tools as particle image velocimetry.

Chapter 4

Main contributions

The fourth chapter is divided into two sections: a validation of the implemented model in COMSOL Multiphysics and a numerical study of two thermal energy storage systems. The small-scale experiment is chosen for validation because supercooling occurred in the experiment with all PCMs. The model accurately simulates the supercooling phenomenon for octadecane. A deviation is registered at the temperature reached after latent heat release. This is because, in the experiment, the temperature rises to the melting point, whereas in the numerical model, the phase change is assumed to occur within a temperature range, so the temperature rises to the upper bound of this temperature range.

The model is able to simulate the supercooled process for the eutectic PCM, but differences occur during the solidification process. Experimentally, the slow temperature rise during latent heat release results in energy loss to the PCM's surroundings. In this case, considering an adiabatic temperature rise reduces the estimated amount of energy required to raise the temperature to the melting temperature. The required energy to raise the temperature is deducted from the latent heat. Therefore, the solidification takes longer to complete numerically because the melting temperature was reached with less energy. The model accurately represents the supercooling degree for sodium acetate trihydrate, but the same drawback is observed, which is due in this case to the high cooling rate. The temperature rises quickly, but the high cooling rate causes the PCM to lose some of its energy during the rise.

A hot water tank and a residential heating system integrating PCM are studied. The presence of supercooling has a negative impact on the system's performance in both cases. The phase change adds a significant amount of energy to the system. However, in the presence of supercooling, both the water in the hot water tank and the air in the residential heating system are heated to lower temperatures. Furthermore, during solidification, the air temperature at the outlet remains constant, which is not the case in the presence of supercooling.

Limitations and perspectives:

As a first attempt, the model performs well despite the complexities of supercooling. The model performs more accurately when temperatures rise quickly at the end of the supercooled state and cooling rates are low. The heat loss is very low in this case, and the temperature increase is nearly adiabatic. In the future, the domain heat source should be improved so that the model can estimate the additional heat lost during the temperature rise. Besides, determining the nucleation temperature without referring to experimental results is essential. Finally, the numerical model that takes into account the supercooling phenomenon has provided evidence of its significant impact on the integrated PCM system's efficiency, and highlighted the major importance of implementing supercooling in mathematical models for sizing efficient latent heat thermal energy storage systems.

References

[1] R. Chaturvedi, A. Islam, and K. Sharma, "A review on the applications of PCM in thermal storage of solar energy," *Materials Today: Proceedings*, vol. 43, pp. 293–297, 2021.

[2] C. Yan, W. Shi, X. Li, and S. Wang, "A seasonal cold storage system based on separate type heat pipe for sustainable building cooling," *Renewable Energy*, 2016, doi: 10.1016/j.renene.2015.07.023.

[3] V. Kapsalis and D. Karamanis, "Solar thermal energy storage and heat pumps with phase change materials," *Applied Thermal Engineering*, vol. 99, pp. 1212–1224, 2016.

[4] W. Zhang, R. Mazzarello, and E. Ma, "Phase-change materials in electronics and photonics," *MRS Bulletin*, vol. 44, no. 9, pp. 686–690, 2019.

[5] G. Stonehouse and J. Evans, "The use of supercooling for fresh foods: A review," *Journal of Food Engineering*, vol. 148, pp. 74–79, 2015.

[6] J. F. Nicolalde, M. Cabrera, J. Martínez-Gómez, R. B. Salazar, and E. Reyes, "Selection of a PCM for a Vehicle's Rooftop by Multicriteria Decision Methods and Simulation," *Applied Sciences*, vol. 11, no. 14, p. 6359, 2021.

[7] X. Jin, S. Zhang, M. A. Medina, and X. Zhang, "Experimental study of the cooling process of partially-melted sodium acetate trihydrate," *Energy and buildings*, vol. 76, pp. 654–660, 2014.

[8] H. Mehling and L. F. Cabeza, "Heat and cold storage with PCM," *Heat and mass transfer*, pp. 11–55, 2008.

[9] R. Feigelson, *50 years progress in crystal growth: a reprint collection*. Elsevier, 2004.

[10] H. Garg, S. Mullick, and V. K. Bhargava, *Solar thermal energy storage*. Springer Science & Business Media, 2012.

[11] T. Kang, Y. You, and S. Jun, "Supercooling preservation technology in food and biological samples: A review focused on electric and magnetic field applications," *Food science and biotechnology*, vol. 29, no. 3, pp. 303–321, 2020.

[12] D.-K. Liu, C.-C. Xu, C.-X. Guo, and X.-X. Zhang, "Sub-zero temperature preservation of fruits and vegetables: A review," *Journal of Food Engineering*, vol. 275, p. 109881, 2020.

[13] A. Safari, R. Saidur, F. Sulaiman, Y. Xu, and J. Dong, "A review on supercooling of Phase Change Materials in thermal energy storage systems," *Renewable and Sustainable Energy Reviews*, vol. 70, pp. 905–919, 2017.

[14] N. A. C. Sidik, T. H. Kean, H. K. Chow, A. Rajaandra, S. Rahman, and J. Kaur, "Performance enhancement of cold thermal energy storage system using nanofluid phase change materials: a review," *International Communications in Heat and Mass Transfer*, vol. 94, pp. 85–95, 2018.

[15] B. E. Jebasingh and A. V. Arasu, "A detailed review on heat transfer rate, supercooling, thermal stability and reliability of nanoparticle dispersed organic phase change material for low-temperature applications," *Materials Today Energy*, vol. 16, p. 100408, 2020.

[16] N. Kumar, J. Hirschey, T. J. LaClair, K. R. Gluesenkamp, and S. Graham, "Review of stability and thermal conductivity enhancements for salt hydrates," *Journal of Energy Storage*, vol. 24, p. 100794, 2019.

[17] K. G. Rao, P. Rasoor, G. Anjaneya, J. Nataraj, and M. Srinivas, “A review on methods of preventing super cooling in phase change materials (PCMs),” in *AIP Conference Proceedings*, 2021, vol. 2317, p. 020003.

[18] N. Beaupere, U. Soupremanien, and L. Zalewski, “Nucleation triggering methods in supercooled phase change materials (PCM), a review,” *Thermochimica acta*, 2018.

[19] Y. Zhao, X. Zhang, X. Xu, and S. Zhang, “Research progress in nucleation and supercooling induced by phase change materials,” *Journal of Energy Storage*, vol. 27, p. 101156, 2020.

[20] M. H. Zahir, S. A. Mohamed, R. Saidur, and F. A. Al-Sulaiman, “Supercooling of phase-change materials and the techniques used to mitigate the phenomenon,” *Applied Energy*, vol. 240, pp. 793–817, 2019.

[21] L. Liu, X. Zhang, X. Xu, Y. Zhao, and S. Zhang, “The research progress on phase change hysteresis affecting the thermal characteristics of PCMs: A review,” *Journal of Molecular Liquids*, p. 113760, 2020.

[22] L. Klimeš *et al.*, “Computer modelling and experimental investigation of phase change hysteresis of PCMs: The state-of-the-art review,” *Applied Energy*, vol. 263, p. 114572, 2020.

[23] C. A. Goldman and P. L. Hauta, *Tested Studies for Laboratory Teaching. Proceedings of the Workshop/Conference of the Association for Biology Laboratory Education (ABLE)(7th, Las Vegas, Nevada, June 3-7, 1985; 8th, Ithaca, New York, June 16-20, 1986). Volume 7/8.* ERIC, 1993.

[24] G. C. Packard, M. J. Packard, and L. L. McDaniel, “Seasonal change in the capacity for supercooling by neonatal painted turtles,” *Journal of experimental biology*, vol. 204, no. 9, pp. 1667–1672, 2001.

[25] P. Scholander and J. Maggert, “Supercooling and ice propagation in blood from Arctic fishes,” *Cryobiology*, vol. 8, no. 4, pp. 371–374, 1971.

[26] T. T. Kozlowski and S. G. Pallardy, *Growth control in woody plants*. Elsevier, 1997.

[27] J. Hacker, U. Ladinig, J. Wagner, and G. Neuner, “Inflorescences of alpine cushion plants freeze autonomously and may survive subzero temperatures by supercooling,” *Plant Science*, vol. 180, no. 1, pp. 149–156, 2011.

[28] A. Sicular and F. D. Moore, “The postmortem survival of tissues: the effect of time and temperature on the survival of liver as measured by glucose oxidation rate,” *Journal of Surgical Research*, vol. 1, no. 1, pp. 16–22, 1961.

[29] K. Monzen *et al.*, “The use of a supercooling refrigerator improves the preservation of organ grafts,” *Biochemical and biophysical research communications*, vol. 337, no. 2, pp. 534–539, 2005.

[30] B. Rubinsky, A. Arav, J. Hong, and C. Lee, “Freezing of mammalian livers with glycerol and antifreeze proteins,” *Biochemical and biophysical research communications*, vol. 200, no. 2, pp. 732–741, 1994.

[31] M. Wisniewski, D. M. Glenn, L. Gusta, and M. P. Fuller, “Using infrared thermography to study freezing in plants,” *HortScience*, vol. 43, no. 6, pp. 1648–1651, 2008.

[32] H. C. J. Godfray *et al.*, “Food security: the challenge of feeding 9 billion people,” *science*, vol. 327, no. 5967, pp. 812–818, 2010.

[33] L. Jeremiah and L. Gibson, “The influence of storage temperature and storage time on color stability, retail properties and case-life of retail-ready beef,” *Food Research International*, vol. 34, no. 9, pp. 815–826, 2001.

[34] S. Sampels, “The effects of storage and preservation technologies on the quality of fish products: A review,” *Journal of food processing and preservation*, vol. 39, no. 6, pp. 1206–1215, 2015.

[35] Y. Fukuma, A. Yamane, T. Itoh, Y. Tsukamasa, and M. Ando, “Application of supercooling to long-term storage of fish meat,” *Fisheries science*, vol. 78, no. 2, pp. 451–461, 2012.

[36] Y. You, J.-Y. Her, T. Shafel, T. Kang, and S. Jun, “Supercooling preservation on quality of beef steak,” *Journal of Food Engineering*, vol. 274, p. 109840, 2020.

[37] M. Ando, S. Mizuochi, Y. Tsukamasa, and K.-I. Kawasaki, “Suppression of fish meat softening by strict control of storage temperature,” *Fisheries Science*, vol. 73, no. 3, pp. 705–712, 2007.

[38] A. Duun and T. Rustad, “Quality of superchilled vacuum packed Atlantic salmon (Salmo salar) fillets stored at- 1.4 and- 3.6 C,” *Food Chemistry*, vol. 106, no. 1, pp. 122–131, 2008.

[39] C. James, V. Seignemartin, and S. J. James, “The freezing and supercooling of garlic (Allium sativum L.),” *International Journal of Refrigeration*, vol. 32, no. 2, pp. 253–260, 2009.

[40] C. James, P. Hanser, and S. J. James, “Super-cooling phenomena in fruits, vegetables and seafoods,” in *11th International Congress on Engineering and Food (ICEF 2011), Athens, Greece*, 2011, pp. 22–26.

[41] A. Arshad, H. M. Ali, M. Ali, and S. Manzoor, “Thermal performance of phase change material (PCM) based pin-finned heat sinks for electronics devices: Effect of pin thickness and PCM volume fraction,” *Applied Thermal Engineering*, vol. 112, pp. 143–155, 2017, doi: https://doi.org/10.1016/j.applthermaleng.2016.10.090.

[42] A. H. A. Al-Waeli *et al.*, “Evaluation of the nanofluid and nano-PCM based photovoltaic thermal (PVT) system: An experimental study,” *Energy Conversion and Management*, vol. 151, pp. 693–708, 2017, doi: https://doi.org/10.1016/j.enconman.2017.09.032.

[43] A. Yehya, “Contribution to the experimental and numerical characterization of phase-change materials: consideration of convection, supercooling, and soluble impurities,” PhD Thesis, Artois, 2015.

[44] H. Schranzhofer, P. Puschnig, A. Heinz, and W. Streicher, “Validation of a trnsys simulation model for pcm energy storages and pcm wall construction elements,” in *Ecostock conference*, 2006, pp. 2–7.

[45] J. M. Guzman and S. Braga, “Supercooling water in cylindrical capsules,” *International journal of thermophysics*, vol. 26, no. 6, p. 1781, 2005.

[46] B. Sandnes and J. Rekstad, “Supercooling salt hydrates Stored enthalpy as a function of temperature,” *Solar Energy*, vol. 80, no. 5, pp. 616–625, 2006.

[47] H. Hu, X. Jin, and X. Zhang, “Effect of supercooling on the solidification process of the phase change material,” *Energy procedia*, vol. 105, pp. 4321–4327, 2017.

[48] E. Günther, H. Mehling, and S. Hiebler, “Modeling of subcooling and solidification of phase change materials,” *Modelling and Simulation in Materials Science and Engineering*, vol. 15, no. 8, pp. 879–892, Nov. 2007, doi: 10.1088/0965-0393/15/8/005.

[49] R. Waser, S. Maranda, A. Stamatiou, M. Zaglio, and J. Worlitschek, “Modeling of solidification including supercooling effects in a fin-tube heat exchanger based latent heat storage,” *Solar Energy*, 2018.

[50] T. Adachi, D. Daudah, and G. Tanaka, “Effects of supercooling degree and specimen size on supercooling duration of erythritol,” *Isij International*, vol. 54, no. 12, pp. 2790–2795, 2014.

[51] M. C. Flemings and Y. Shiohara, “Solidification of undercooled metals,” *Materials Science and Engineering*, vol. 65, no. 1, pp. 157–170, 1984.

[52] J.-P. Dumas, “Etude de la rupture de métastabilité et du polymorphisme de corps organiques,” PhD Thesis, 1976.

[53] K. Nakano, Y. Masuda, and H. Daiguji, “Crystallization and melting behavior of erythritol in and around two-dimensional hexagonal mesoporous silica,” *The Journal of Physical Chemistry C*, vol. 119, no. 9, pp. 4769–4777, 2015.

[54] S.-L. Chen and C.-L. Chen, “Effect of nucleation agents on the freezing probability of supercooled water inside capsules,” *Hvac&R Research*, vol. 5, no. 4, pp. 339–351, 1999.

[55] R. A. Taylor, N. Tsafnat, and A. Washer, “Experimental characterisation of sub-cooling in hydrated salt phase change materials,” *Applied Thermal Engineering*, vol. 93, pp. 935–938, 2016.

[56] S.-L. Chen and T.-S. Lee, “A study of supercooling phenomenon and freezing probability of water inside horizontal cylinders,” *International Journal of Heat and Mass Transfer*, vol. 41, no. 4–5, pp. 769–783, 1998.

[57] M. Dannemand and S. Furbo, “Supercooling stability of sodium acetate trihydrate composites in multiple heat storage unitsS,” in *12th IIR Conference on Phase-Change Materials and Slurries for Refrigeration and Air Conditioning*, 2018, pp. 227–231.

[58] M. Alizadeh and D. Ganji, “Multi-objective optimization of an externally finned two-phase closed thermosyphon using response surface methodology,” *Applied Thermal Engineering*, vol. 171, p. 115008, 2020.

[59] K. Kant, P. H. Biwole, I. Shamseddine, G. Tlaiji, F. Pennec, and F. Fardoun, “Recent advances in thermophysical properties enhancement of phase change materials for thermal energy storage,” *Solar Energy Materials and Solar Cells*, vol. 231, p. 111309, 2021.

[60] M. Asgari, M. Javidan, M. Nozari, A. Asgari, and D. Ganji, “Simulation of solidification process of phase change materials in a heat exchanger using branch-shaped fins,” *Case Studies in Thermal Engineering*, vol. 25, p. 100835, 2021.

[61] B. Zhao *et al.*, “Phase transitions and nucleation mechanisms in metals studied by nanocalorimetry: A review,” *Thermochimica acta*, vol. 603, pp. 2–23, 2015.

[62] F. Yin, X. Sun, H. Guan, and Z. Hu, “Effect of thermal history on the liquid structure of a cast nickel-base superalloy M963,” *Journal of Alloys and Compounds*, vol. 364, no. 1–2, pp. 225–228, 2004.

[63] P. Rudolph, H. Koh, N. Schäfer, and T. Fukuda, “The crystal perfection depends on the superheating of the mother phase too--Experimental facts and speculations on the "melt structure" of semiconductor compounds,” *Journal of crystal growth*, vol. 166, no. 1–4, pp. 578–582, 1996.

[64] Q. Mei and J. Li, “Dependence of Liquid Supercooling on Liquid Overheating Levels of Al Small Particles,” *Materials*, vol. 9, no. 1, p. 7, 2016.

[65] J. A. Noël, L. Kreplak, N. N. Getangama, J. R. de Bruyn, and M. A. White, “Supercooling and Nucleation of Fatty Acids: Influence of Thermal History on the Behavior of the Liquid Phase,” *The Journal of Physical Chemistry B*, vol. 122, no. 51, pp. 12386–12395, 2018.

[66] D. Clause, J. Dumas, P. Meijer, and F. Broto, “Phase transformations in emulsions,” *J. Disp. Sci. Tech*, vol. 8, no. 1, 1987.

[67] D. Clausse, *Research Techniques Utilizing Emulsions, Encyclopedia of Emulsion Technology, vol. 2*. Marcel Dekker, New York, 1985.

[68] T. Wada, K. Matsunaga, and Y. Matsuo, "Studies on salt hydrates for latent heat storage. V. Preheating effect on crystallization of sodium acetate trihydrate from aqueous solution with a small amount of sodium pyrophosphate decahydrate," *Bulletin of the Chemical Society of Japan*, vol. 57, no. 2, pp. 557–560, 1984.

[69] T. Wada, F. Kimura, and Y. Matsuo, "Studies on Salt Hydrates for Latent Heat Storage. IV. Crystallization in the Binary System CH3CO2Na–H2O," *Bulletin of the Chemical Society of Japan*, vol. 56, no. 12, pp. 3827–3829, 1983.

[70] T. Wada and Y. Matsuo, "Studies on salt hydrates for latent heat storge. VI. Preheating effect on crystallization of sodium acetate trihydrate from aqueous solution with a small amount of disodium hydrogenphosphate," *Bulletin of the Chemical Society of Japan*, vol. 57, no. 2, pp. 561–563, 1984.

[71] M. Fashandi and S. N. Leung, "Sodium acetate trihydrate-chitin nanowhisker nanocomposites with enhanced phase change performance for thermal energy storage," *Solar Energy Materials and Solar Cells*, vol. 178, pp. 259–265, 2018.

[72] J. B. Johansen, M. Dannemand, W. Kong, J. Fan, J. Dragsted, and S. Furbo, "Thermal conductivity enhancement of sodium acetate trihydrate by adding graphite powder and the effect on stability of supercooling," *Energy Procedia*, vol. 70, pp. 249–256, 2015.

[73] T. Schülli, R. Daudin, G. Renaud, A. Vaysset, O. Geaymond, and A. Pasturel, "Substrate-enhanced supercooling in AuSi eutectic droplets," *Nature*, vol. 464, no. 7292, p. 1174, 2010.

[74] M. Faucheux, G. Muller, M. Havet, and A. LeBail, "Influence of surface roughness on the supercooling degree: Case of selected water/ethanol solutions frozen on aluminium surfaces," *International journal of refrigeration*, vol. 29, no. 7, pp. 1218–1224, 2006.

[75] K. Sakurai, N. Yoshinaga, R. Yagi, N. Tomimatsu, and K. Sano, "Effect of embedding sodium acetate trihydrate on the Ag anode in an electrical nucleation cell of a supercooled latent heat storage material," *Solar Energy*, vol. 173, pp. 1306–1314, 2018.

[76] S. Akio, U. Yoshio, O. Seiji, M. Kazuyuki, and T. Atsushi, "Fundamental research on the supercooling phenomenon on heat transfer surfaces—investigation of an effect of characteristics of surface and cooling rate on a freezing temperature of supercooled water," *International Journal of heat and mass transfer*, vol. 33, no. 8, pp. 1697–1709, 1990.

[77] P. J. Shamberger and M. J. O'Malley, "Heterogeneous nucleation of thermal storage material LiNO3·3H2O from stable lattice-matched nucleation catalysts," *Acta Materialia*, vol. 84, pp. 265–274, 2015, doi: https://doi.org/10.1016/j.actamat.2014.10.051.

[78] M. Telkes, "Nucleation of supersaturated inorganic salt solutions," *Industrial & Engineering Chemistry*, vol. 44, no. 6, pp. 1308–1310, 1952.

[79] D. Turnbull and B. Vonnegut, "Nucleation catalysis.," *Industrial & Engineering Chemistry*, vol. 44, no. 6, pp. 1292–1298, 1952.

[80] G. A. Lane, "Phase change materials for energy storage nucleation to prevent supercooling," *Solar energy materials and solar cells*, vol. 27, no. 2, pp. 135–160, 1992.

[81] P. Hu, D.-J. Lu, X.-Y. Fan, X. Zhou, and Z.-S. Chen, "Phase change performance of sodium acetate trihydrate with AlN nanoparticles and CMC," *Solar Energy Materials and Solar Cells*, vol. 95, no. 9, pp. 2645–2649, 2011, doi: https://doi.org/10.1016/j.solmat.2011.05.025.

[82] X. Li *et al.*, “Preparation and thermal energy storage studies of CH3COONa·3H2O–KCl composites salt system with enhanced phase change performance,” *Applied Thermal Engineering*, vol. 102, pp. 708–715, 2016, doi: https://doi.org/10.1016/j.applthermaleng.2016.04.029.

[83] R. Pilar, L. Svoboda, P. Honcova, and L. Oravova, “Study of magnesium chloride hexahydrate as heat storage material,” *Thermochimica Acta*, vol. 546, pp. 81–86, 2012, doi: https://doi.org/10.1016/j.tca.2012.07.021.

[84] S. Ushak, A. Gutierrez, C. Barreneche, A. I. Fernandez, M. Grágeda, and L. F. Cabeza, “Reduction of the subcooling of bischofite with the use of nucleatings agents,” *Solar Energy Materials and Solar Cells*, vol. 157, pp. 1011–1018, 2016, doi: https://doi.org/10.1016/j.solmat.2016.08.015.

[85] I. M. Sutjahja, S. R. A. U, N. Kurniati, I. D. Pallitine, and D. Kurnia, “The role of chemical additives to the phase change process of CaCl2.6H2O to optimize its performance as latent heat energy storage system,” *Journal of Physics: Conference Series*, vol. 739, p. 012064, Aug. 2016, doi: 10.1088/1742-6596/739/1/012064.

[86] Y. Liu, X. Li, P. Hu, and G. Hu, “Study on the supercooling degree and nucleation behavior of water-based graphene oxide nanofluids PCM,” *International Journal of Refrigeration*, vol. 50, pp. 80–86, 2015.

[87] S.-L. Chen, P.-P. Wang, and T.-S. Lee, “An experimental investigation of nucleation probability of supercooled water inside cylindrical capsules,” *Experimental thermal and fluid science*, vol. 18, no. 4, pp. 299–306, 1998.

[88] B. Yang, J. H. Perepezko, J. W. Schmelzer, Y. Gao, and C. Schick, “Dependence of crystal nucleation on prior liquid overheating by differential fast scanning calorimeter,” *The Journal of chemical physics*, vol. 140, no. 10, p. 104513, 2014.

[89] Z. Zhou, W. Wang, and L. Sun, “Undercooling and metastable phase formation in a Bi95Sb5 melt,” *Applied Physics A*, vol. 71, no. 3, pp. 261–265, 2000.

[90] R. L. Blaine and C. K. Schoff, *Purity determinations by thermal methods*, vol. 838. ASTM International, 1984.

[91] L. Vinet and A. Zhedanov, “A 'missing'family of classical orthogonal polynomials,” *Journal of Physics A: Mathematical and Theoretical*, vol. 44, no. 8, p. 085201, 2011.

[92] D. Turnbull, “Formation of crystal nuclei in liquid metals,” *Journal of Applied Physics*, vol. 21, no. 10, pp. 1022–1028, 1950.

[93] F. Font, S. Mitchell, and T. Myers, “One-dimensional solidification of supercooled melts,” *International Journal of Heat and Mass Transfer*, vol. 62, pp. 411–421, 2013.

[94] B. Ralph, *MF Ashby, DRH Jones, Engineering Materials 2 (An Introduction to Microstructures, Processing and Design), Elsevier, Amsterdam (2006), ISBN 978-0-7506-6381-6 and 0-7506-6331-2, 451 pages, US $49.95,\pounds 24.99, 36.75*. Elsevier, 2006.

[95] V. Alexiades, *Mathematical modeling of melting and freezing processes*. Routledge, 2017.

[96] C. Le Bot and D. Delaunay, “Rapid solidification of indium: modeling subcooling,” *Materials characterization*, vol. 59, no. 5, pp. 519–527, 2008.

[97] A. Y. Uzan, Y. Kozak, Y. Korin, I. Harary, H. Mehling, and G. Ziskind, “A novel multi-dimensional model for solidification process with supercooling,” *International Journal of Heat and Mass Transfer*, vol. 106, pp. 91–102, 2017.

[98] T. Davin, B. Lefez, and A. Guillet, “Supercooling of phase change: A new modeling formulation using apparent specific heat capacity,” *International Journal of Thermal Sciences*, vol. 147, p. 106121, 2020.

[99] S. Liu, Y. Li, and Y. Zhang, “Mathematical solutions and numerical models employed for the investigations of PCMs′ phase transformations,” *Renewable and Sustainable energy reviews*, vol. 33, pp. 659–674, 2014.

[100] P. Tittelein *et al.*, “Simulation of the thermal and energy behaviour of a composite material containing encapsulated-PCM: Influence of the thermodynamical modelling,” *Applied Energy*, vol. 140, pp. 269–274, 2015.

[101] P. Lamberg, R. Lehtiniemi, and A.-M. Henell, “Numerical and experimental investigation of melting and freezing processes in phase change material storage,” *International Journal of Thermal Sciences*, vol. 43, no. 3, pp. 277–287, 2004.

[102] Y. Zhang, K. Du, M. A. Medina, and J. He, “An experimental method for validating transient heat transfermathematical models used for phase change materials (PCMs) calculations,” *Phase Transitions*, vol. 87, no. 6, pp. 541–558, 2014.

[103] Y. Kozak and G. Ziskind, “Novel enthalpy method for modeling of PCM melting accompanied by sinking of the solid phase,” *International Journal of Heat and Mass Transfer*, vol. 112, pp. 568–586, 2017.

[104] S. Hoseinzadeh, R. Ghasemiasl, D. Havaei, and A. Chamkha, “Numerical investigation of rectangular thermal energy storage units with multiple phase change materials,” *Journal of Molecular Liquids*, vol. 271, pp. 655–660, 2018.

[105] M. J. Huang, “The effect of using two PCMs on the thermal regulation performance of BIPV systems,” *Solar Energy Materials and Solar Cells*, vol. 95, no. 3, pp. 957–963, 2011.

[106] A. V. Sá, M. Azenha, H. de Sousa, and A. Samagaio, “Thermal enhancement of plastering mortars with Phase Change Materials: Experimental and numerical approach,” *Energy and Buildings*, vol. 49, pp. 16–27, 2012.

[107] S. Sadasivam, D. Zhang, F. Almeida, and others, “An iterative enthalpy method to overcome the limitations in ESP-r’s PCM solution algorithm,” *Ashrae Transactions*, vol. 117, p. 100, 2011.

[108] F. Almeida, D. Zhang, A. S. Fung, and W. H. Leong, “Comparison of corrective phase change material algorithm with ESP-r simulation,” 2011.

[109] S. Liu, Y. Li, and Y. Zhang, “Mathematical solutions and numerical models employed for the investigations of PCMs? phase transformations,” *Renewable and Sustainable energy reviews*, vol. 33, pp. 659–674, 2014.

[110] Z. Chen, X. Guo, L. Shao, S. Li, and L. Gao, “Sensitivity analysis of the frozen soil nonlinear latent heat and its precise transformation method,” *Geophysical Journal International*, 2021.

[111] D. Heim, “Isothermal storage of solar energy in building construction,” *Renewable energy*, vol. 35, no. 4, pp. 788–796, 2010.

[112] A. Faghri and Y. Zhang, *Transport phenomena in multiphase systems*. Elsevier, 2006.

[113] Y. Fang and M. Medina, “Proposed modifications for models of heat transfer problems involving partially melted phase change processes,” in *Heat-Air-Moisture Transport, 2nd Volume: Measurements and Implications in Buildings*, ASTM International, 2010.

[114] J. Virgone, J. Noël, and R. Reisdorf, “Numerical study of the influence of the thickness and melting point on the effectiveness of phase change materials: application to the renovation of a low inertia school,” 2009.

[115] F. Kuznik, D. David, K. Johannes, and J.-J. Roux, “A review on phase change materials integrated in building walls,” *Renewable and Sustainable Energy Reviews*, vol. 15, no. 1, pp. 379–391, 2011.

[116] L. F. Cabeza, A. Castell, C. de Barreneche, A. De Gracia, and A. Fernández, “Materials used as PCM in thermal energy storage in buildings: A review,” *Renewable and Sustainable Energy Reviews*, vol. 15, no. 3, pp. 1675–1695, 2011.

[117] D. Zhou, C.-Y. Zhao, and Y. Tian, “Review on thermal energy storage with phase change materials (PCMs) in building applications,” *Applied energy*, vol. 92, pp. 593–605, 2012.

[118] A. Pasupathy and R. Velraj, “Mathematical modeling and experimental study on building ceiling system incorporating phase change material (PCM) for energy conservation,” in *ASME International Mechanical Engineering Congress and Exposition*, 2006, vol. 47837, pp. 59–68.

[119] A. Pasupathy, L. Athanasius, R. Velraj, and R. Seeniraj, “Experimental investigation and numerical simulation analysis on the thermal performance of a building roof incorporating phase change material (PCM) for thermal management,” *Applied Thermal Engineering*, vol. 28, no. 5–6, pp. 556–565, 2008.

[120] J. Mazo, M. Delgado, J. M. Marin, and B. Zalba, “Modeling a radiant floor system with Phase Change Material (PCM) integrated into a building simulation tool: Analysis of a case study of a floor heating system coupled to a heat pump,” *Energy and Buildings*, vol. 47, pp. 458–466, 2012.

[121] X. Jin and X. Zhang, “Thermal analysis of a double layer phase change material floor,” *Applied Thermal Engineering*, vol. 31, no. 10, pp. 1576–1581, 2011.

[122] F. Kuznik, J. Virgone, and J. Noel, “Optimization of a phase change material wallboard for building use,” *Applied Thermal Engineering*, vol. 28, no. 11–12, pp. 1291–1298, 2008.

[123] R. Ansuini, R. Larghetti, A. Giretti, and M. Lemma, “Radiant floors integrated with PCM for indoor temperature control,” *Energy and Buildings*, vol. 43, no. 11, pp. 3019–3026, 2011.

[124] P. Damronglerd and Y. Zhang, “Modified temperature-transforming model for convection-controlled melting,” *Journal of thermophysics and heat transfer*, vol. 21, no. 1, pp. 203–208, 2007.

[125] Z. Ma and Y. Zhang, “Solid velocity correction schemes for a temperature transforming model for convection phase change,” *International Journal of Numerical Methods for Heat & Fluid Flow*, 2006.

[126] D. U. Sarwe and V. S. Kulkarni, “Thermal behaviour of annular hyperbolic fin with temperature dependent thermal conductivity by differential transformation method and Pade approximant,” *Physica Scripta*, vol. 96, no. 10, p. 105213, 2021.

[127] S. Wang, A. Faghri, and T. L. Bergman, “A comprehensive numerical model for melting with natural convection,” *International Journal of heat and mass transfer*, vol. 53, no. 9–10, pp. 1986–2000, 2010.

[128] Y. Cao and A. Faghri, “A numerical analysis of phase-change problems including natural convection,” 1990.

[129] A. Joulin, Z. Younsi, L. Zalewski, S. Lassue, D. R. Rousse, and J.-P. Cavrot, “Experimental and numerical investigation of a phase change material: Thermal-energy storage and release,” *Applied Energy*, vol. 88, no. 7, pp. 2454–2462, 2011.

[130] A. Joulin, Z. Younsi, L. Zalewski, D. R. Rousse, and S. Lassue, “A numerical study of the melting of phase change material heated from a vertical wall of a rectangular enclosure,” *International Journal of Computational Fluid Dynamics*, vol. 23, no. 7, pp. 553–566, 2009.

[131] Z. A. Hammou and M. Lacroix, “A new PCM storage system for managing simultaneously solar and electric energy,” *Energy and Buildings*, vol. 38, no. 3, pp. 258–265, 2006.

[132] A. Arnault, F. Mathieu-Potvin, and L. Gosselin, “Internal surfaces including phase change materials for passive optimal shift of solar heat gain,” *International Journal of Thermal Sciences*, vol. 49, no. 11, pp. 2148–2156, 2010.

[133] M. Costa, D. Buddhi, and A. Oliva, “Numerical simulation of a latent heat thermal energy storage system with enhanced heat conduction,” *Energy conversion and management*, vol. 39, no. 3–4, pp. 319–330, 1998.

[134] M. Frémond, R. Gormaz, and J. A. San Martı?n, “A new mathematical model for supercooling,” *Journal of mathematical analysis and applications*, vol. 261, no. 2, pp. 578–603, 2001.

[135] M. Fremond, “Supercooling: a macroscopic predictive theory,” in *Ground freezing 94. Proceedings of the seventh international symposium on ground freezing; Nancy, France; 24-28 October 1994*, 1994, pp. 79–84.

[136] R. Courant, K. Friedrichs, and H. Lewy, “Über die partiellen Differenzengleichungen der mathematischen Physik,” *Mathematische annalen*, vol. 100, no. 1, pp. 32–74, 1928.

[137] J. Bony and S. Citherlet, “Numerical model and experimental validation of heat storage with phase change materials,” *Energy and Buildings*, vol. 39, no. 10, pp. 1065–1072, 2007.

[138] K. Darkwa and P. O'callaghan, “Simulation of phase change drywalls in a passive solar building,” *Applied thermal engineering*, vol. 26, no. 8–9, pp. 853–858, 2006.

[139] P. H. Biwole, D. Groulx, F. Souayfane, and T. Chiu, “Influence of fin size and distribution on solid-liquid phase change in a rectangular enclosure,” *International Journal of Thermal Sciences*, vol. 124, pp. 433–446, 2018.

[140] P. H. Biwole, P. Eclache, and F. Kuznik, “Phase-change materials to improve solar panel’s performance,” *Energy and Buildings*, vol. 62, pp. 59–67, 2013.

[141] A. Brent, V. R. Voller, and K. Reid, “Enthalpy-porosity technique for modeling convection-diffusion phase change: application to the melting of a pure metal,” *Numerical Heat Transfer, Part A Applications*, vol. 13, no. 3, pp. 297–318, 1988.

[142] H. Shokouhmand and B. Kamkari, “Experimental investigation on melting heat transfer characteristics of lauric acid in a rectangular thermal storage unit,” *Experimental Thermal and Fluid Science*, vol. 50, pp. 201–212, 2013.

[143] O. Bertrand *et al.*, “Melting driven by natural convection A comparison exercise: first results,” *International Journal of Thermal Sciences*, vol. 38, no. 1, pp. 5–26, 1999.

[144] I. Shamseddine, F. Pennec, P. Biwole, and F. Fardoun, “Supercooling of phase change materials: A review,” *Renewable and Sustainable Energy Reviews*, vol. 158, p. 112172, 2022.

[145] A. H.-D. Cheng and D. T. Cheng, “Heritage and early history of the boundary element method,” *Engineering analysis with boundary elements*, vol. 29, no. 3, pp. 268–302, 2005.

[146] E. Feulvarch and J.-M. Bergheau, “An implicit fixed-grid method for the finite-element analysis of heat transfer involving phase changes,” *Numerical Heat Transfer, Part B: Fundamentals*, vol. 51, no. 6, pp. 585–610, 2007.

[147] V. R. Voller, C. Swaminathan, and B. G. Thomas, “Fixed grid techniques for phase change problems: a review,” *International journal for numerical methods in engineering*, vol. 30, no. 4, pp. 875–898, 1990.

[148] W. Su, J. Darkwa, and G. Kokogiannakis, “Review of solid–liquid phase change materials and their encapsulation technologies,” *Renewable and Sustainable Energy Reviews*, vol. 48, pp. 373–391, 2015.

[149] R. Sharma, P. Ganesan, V. Tyagi, H. Metselaar, and S. Sandaran, “Developments in organic solid–liquid phase change materials and their applications in thermal energy storage,” *Energy Conversion and Management*, vol. 95, pp. 193–228, 2015.

[150] V. Tyagi *et al.*, “A comprehensive review on phase change materials for heat storage applications: Development, characterization, thermal and chemical stability,” *Solar Energy Materials and Solar Cells*, vol. 234, p. 111392, 2022.

[151] K. Kant, P. Biwole, I. Shamseddine, G. Tlaiji, and F. Pennec, “Advances in solar greenhouse systems for cultivation of agricultural products,” in *Solar Energy Advancements in Agriculture and Food Production Systems*, Elsevier, 2022, pp. 77–111.

[152] H. Huang, J. Fan, J. Lin, Q. Zhao, Y. Zhang, and Y. Xiao, “Numerical phase change model considering crystal growth under supercooling,” *Applied Thermal Engineering*, vol. 200, p. 117685, 2022.

[153] B. Zhao and R. Wang, “A novel 3-D model of an industrial-scale tube-fin latent heat storage using salt hydrates with supercooling: A model validation,” *Energy*, vol. 213, p. 118852, 2020.

[154] C. Barreneche, H. Navarro, S. Serrano, L. F. Cabeza, and A. I. Fernández, “New database on phase change materials for thermal energy storage in buildings to help PCM selection,” *Energy Procedia*, vol. 57, pp. 2408–2415, 2014.

[155] “ANSI/ASHRAE Addendum a to ANSI/ASHRAE Standard 55-2020,” p. 9.

[156] S. Yu, X. Wang, and D. Wu, “Microencapsulation of n-octadecane phase change material with calcium carbonate shell for enhancement of thermal conductivity and serving durability: synthesis, microstructure, and performance evaluation,” *Applied energy*, vol. 114, pp. 632–643, 2014.

[157] A. Yehya, H. Naji, and L. Zalewski, “Experimental and numerical characterization of an impure phase change material using a thermal lattice Boltzmann method,” *Applied Thermal Engineering*, vol. 154, pp. 738–750, 2019.

[158] F. Souayfane, P. H. Biwole, F. Fardoun, and P. Achard, “Energy performance and economic analysis of a TIM-PCM wall under different climates,” *Energy*, vol. 169, pp. 1274–1291, 2019, doi: https://doi.org/10.1016/j.energy.2018.12.116.

[159] G. Wang *et al.*, “Review on sodium acetate trihydrate in flexible thermal energy storages: Properties, challenges and applications,” *Journal of Energy Storage*, vol. 40, p. 102780, 2021.

[160] Y. Wang, K. Yu, H. Peng, and X. Ling, “Preparation and thermal properties of sodium acetate trihydrate as a novel phase change material for energy storage,” *Energy*, vol. 167, pp. 269–274, 2019.

[161] F. Souayfane, P. H. Biwole, and F. Fardoun, “Melting of a phase change material in presence of natural convection and radiation: A simplified model,” *Applied Thermal Engineering*, vol. 130, pp. 660–671, 2018, doi: https://doi.org/10.1016/j.applthermaleng.2017.11.026.

[162] X. Faure, “Enveloppe hybride pour bâtiment à haute performance énergétique,” PhD Thesis, Université Joseph-Fourier-Grenoble I, 2007.

[163] M. Kirincic, A. Trp, and K. Lenic, “Influence of natural convection during melting and solidification of paraffin in a longitudinally finned shell-and-tube latent thermal energy storage on the applicability of developed numerical models,” *Renewable Energy*, vol. 179, pp. 1329–1344, 2021.

[164] M. Farid and A. K. Mohamed, “Effect of Natural Convection on the Process of Melting and Solidification of Paraffin Wax,” in *Thermal Energy Storage with Phase Change Materials*, CRC Press, 2021, pp. 83–103.

[165] R. Veerasamy, H. Rajak, A. Jain, S. Sivadasan, C. P. Varghese, and R. K. Agrawal, “Validation of QSAR models-strategies and importance,” *Int. J. Drug Des. Discov*, vol. 3, pp. 511–519, 2011.

[166] S. Khanna, K. Reddy, and T. K. Mallick, “Optimization of finned solar photovoltaic phase change material (finned pv pcm) system,” *International Journal of Thermal Sciences*, vol. 130, pp. 313–322, 2018.

[167] L. Kasper, D. Pernsteiner, M. Koller, A. Schirrer, S. Jakubek, and R. Hofmann, “Numerical studies on the influence of natural convection under inclination on optimal aluminium proportions and fin spacings in a rectangular aluminium finned latent-heat thermal energy storage,” *Applied Thermal Engineering*, vol. 190, p. 116448, 2021.

[168] A. Shukla, D. Buddhi, and R. Sawhney, “Solar water heaters with phase change material thermal energy storage medium: A review,” *Renewable and Sustainable Energy Reviews*, vol. 13, no. 8, pp. 2119–2125, 2009.

[169] M. H. Dhaou, S. Mellouli, F. Alresheedi, and Y. El-Ghoul, “Experimental assessment of a solar water tank integrated with nano-enhanced PCM and a stirrer,” *Alexandria Engineering Journal*, vol. 61, no. 10, pp. 8113–8122, 2022.

[170] H. H. Al-Kayiem and S. C. Lin, “Performance evaluation of a solar water heater integrated with a PCM nanocomposite TES at various inclinations,” *Solar Energy*, vol. 109, pp. 82–92, 2014.

[171] E. M. Alawadhi, “Thermal analysis of a pipe insulation with a phase change material: Material selection and sizing,” *Heat transfer engineering*, vol. 29, no. 7, pp. 624–631, 2008.

[172] M. H. Abokersh, M. Osman, O. El-Baz, M. El-Morsi, and O. Sharaf, “Review of the phase change material (PCM) usage for solar domestic water heating systems (SDWHS),” *International journal of energy research*, vol. 42, no. 2, pp. 329–357, 2018.

[173] M. A. Sharif *et al.*, “Review of the application of phase change material for heating and domestic hot water systems,” *Renewable and Sustainable Energy Reviews*, vol. 42, pp. 557–568, 2015.

[174] R. Elarem *et al.*, “A comprehensive review of heat transfer intensification methods for latent heat storage units,” *Energy Storage*, vol. 3, no. 1, p. e127, 2021.

[175] M. Mazman, L. F. Cabeza, H. Mehling, M. Nogues, H. Evliya, and H. Ö. Paksoy, “Utilization of phase change materials in solar domestic hot water systems,” *Renewable energy*, vol. 34, no. 6, pp. 1639–1643, 2009.

[176] I. Al-Hinti, A. Al-Ghandoor, A. Maaly, I. A. Naqeera, Z. Al-Khateeb, and O. Al-Sheikh, “Experimental investigation on the use of water-phase change material storage in conventional solar water heating systems,” *Energy Conversion and Management*, vol. 51, no. 8, pp. 1735–1740, 2010.

[177] M. A. Fazilati and A. A. Alemrajabi, “Phase change material for enhancing solar water heater, an experimental approach,” *Energy conversion and management*, vol. 71, pp. 138–145, 2013.

[178] L. F. Cabeza, M. Ibanez, C. Sole, J. Roca, and M. Nogues, "Experimentation with a water tank including a PCM module," *Solar Energy Materials and Solar Cells*, vol. 90, no. 9, pp. 1273–1282, 2006.

[179] H. S. Xue, "Experimental investigation of a domestic solar water heater with solar collector coupled phase-change energy storage," *Renewable Energy*, vol. 86, pp. 257–261, 2016.

[180] L. Pérez-Lombard, J. Ortiz, and C. Pout, "A review on buildings energy consumption information," *Energy and buildings*, vol. 40, no. 3, pp. 394–398, 2008.

[181] B. M. Diaconu, "Thermal energy savings in buildings with PCM-enhanced envelope: Influence of occupancy pattern and ventilation," *Energy and Buildings*, vol. 43, no. 1, pp. 101–107, 2011.

[182] M. Iten, S. Liu, and A. Shukla, "A review on the air-PCM-TES application for free cooling and heating in the buildings," *Renewable and Sustainable Energy Reviews*, vol. 61, pp. 175–186, 2016.

[183] E. Osterman, V. Butala, and U. Stritih, "PCM thermal storage system for 'free'heating and cooling of buildings," *Energy and buildings*, vol. 106, pp. 125–133, 2015.

[184] H. Weinläder, F. Klinker, and M. Yasin, "PCM cooling ceilings in the Energy Efficiency Center—passive cooling potential of two different system designs," *Energy and Buildings*, vol. 119, pp. 93–100, 2016.

[185] R. A. Kishore, M. V. Bianchi, C. Booten, J. Vidal, and R. Jackson, "Optimizing PCM-integrated walls for potential energy savings in US Buildings," *Energy and Buildings*, vol. 226, p. 110355, 2020.

[186] S. Valizadeh, M. Ehsani, and M. Torabi Angji, "Development and thermal performance of wood-HPDE-PCM nanocapsule floor for passive cooling in building," *Energy Sources, Part A: Recovery, Utilization, and Environmental Effects*, vol. 41, no. 17, pp. 2114–2127, 2019.

[187] D. Li, Y. Wu, C. Liu, G. Zhang, and M. Arıcı, "Energy investigation of glazed windows containing Nano-PCM in different seasons," *Energy conversion and management*, vol. 172, pp. 119–128, 2018.

[188] M. Ahmad, A. Bontemps, H. Sallée, and D. Quenard, "Thermal testing and numerical simulation of a prototype cell using light wallboards coupling vacuum isolation panels and phase change material," *Energy and buildings*, vol. 38, no. 6, pp. 673–681, 2006.

[189] C. Chen, H. Guo, Y. Liu, H. Yue, and C. Wang, "A new kind of phase change material (PCM) for energy-storing wallboard," *Energy and Buildings*, vol. 40, no. 5, pp. 882–890, 2008.

[190] X. Jin, M. A. Medina, and X. Zhang, "On the importance of the location of PCMs in building walls for enhanced thermal performance," *Applied energy*, vol. 106, pp. 72–78, 2013.

[191] C. Liu, Y. Wu, Y. Zhu, D. Li, and L. Ma, "Experimental investigation of optical and thermal performance of a PCM-glazed unit for building applications," *Energy and Buildings*, vol. 158, pp. 794–800, 2018.

[192] W. Su, J. Darkwa, and G. Kokogiannakis, "Numerical thermal evaluation of laminated binary microencapsulated phase change material drywall systems," in *Building Simulation*, 2020, vol. 13, no. 1, pp. 89–98.

[193] A. A. Al-Rashed, A. A. Alnaqi, and J. Alsarraf, "Energy-saving of building envelope using passive PCM technique: A case study of Kuwait City climate conditions," *Sustainable Energy Technologies and Assessments*, vol. 46, p. 101254, 2021.

[194] R. Kalbasi, “Usefulness of PCM in building applications focusing on envelope heat exchange–energy saving considering two scenarios,” *Sustainable Energy Technologies and Assessments*, vol. 50, p. 101848, 2022.

[195] W. Sun, Y. Zhang, Z. Ling, X. Fang, and Z. Zhang, “Experimental investigation on the thermal performance of double-layer PCM radiant floor system containing two types of inorganic composite PCMs,” *Energy and Buildings*, vol. 211, p. 109806, 2020.

[196] V. Butala and U. Stritih, “Experimental investigation of PCM cold storage,” *Energy and Buildings*, vol. 41, no. 3, pp. 354–359, 2009.

[197] V. A. A. Raj and R. Velraj, “Heat transfer and pressure drop studies on a PCM-heat exchanger module for free cooling applications,” *International Journal of Thermal Sciences*, vol. 50, no. 8, pp. 1573–1582, 2011.

[198] S. Lu, J. Gao, H. Tong, S. Yin, X. Tang, and X. Jiang, “Model establishment and operation optimization of the casing PCM radiant floor heating system,” *Energy*, vol. 193, p. 116814, 2020.

[199] A. Waqas and S. Kumar, “Utilization of latent heat storage unit for comfort ventilation of buildings in hot and dry climates,” *International Journal of Green Energy*, vol. 8, no. 1, pp. 1–24, 2011.

[200] W. Xiao, X. Wang, and Y. Zhang, “Analytical optimization of interior PCM for energy storage in a lightweight passive solar room,” *Applied Energy*, vol. 86, no. 10, pp. 2013–2018, 2009.

Annex 1: Publications

During this PhD work, the PhD candidate wrote the following articles, which were co-written by the thesis supervisors Pascal Biwole, Farouk Fardoun, and Fabienne Pennec.

Journal papers

- **I Shamseddine**, F Pennec, P Biwole, F Fardoun, Supercooling of phase change materials: A review; ***Renewable and Sustainable Energy Reviews, 2022***. (Impact factor = 16.8) https://doi.org/10.1016/j.rser.2022.112172
- **I Shamseddine**, P Biwole, F Fardoun, F Pennec, Numerical and experimental investigation of supercooling and natural convection in octadecane phase change material. ***Energy Reports, 2022.*** (Impact factor = 6.87) https://doi.org/10.1016/j.egyr.2022.06.089
- **I Shamseddine**, P Biwole, F Pennec, F Fardoun, Experimental benchmark on solid-liquid phase change in the presence of supercooling and natural convection. Submitted to the ***International Journal of Thermal Sciences, 2022.*** (Impact factor = 3.744)

Conference papers:

- **I Shamseddine**, P Biwole, F Fardoun, F Pennec, Modélisation de la surfusion des MCP: enjeux et verrous scientifiques. ***Congrès National de la Recherche des IUT (CNRIUT), Lyon, 3-4 June 2021*** – Poster and online participation
- **I Shamseddine**, P Biwole, F Fardoun, F Pennec, Numerical and experimental investigation of supercooling and natural convection in octadecane phase change material. ***International Conference on Technologies and Materials for Renewable Energy, Energy and Sustainability (TMREES22Fr), Metz-Grand Est, 9-11 May 2022***– PowerPoint presentation and paper participation
- **I Shamseddine**, P Biwole, F Fardoun, F Pennec, Numerical and experimental investigation of supercooling and natural convection in octadecane phase change material. ***Colloque recherche de l'IUT Clermont Auvergne, Montluçon, 5-6 July 2022 –*** *PowerPoint p*resentation

Awards:

"Best Paper Award" awarded from the European Academy for Sustainable Development to the conference article:

I Shamseddine, P Biwole, F Fardoun, F Pennec, Numerical and experimental investigation of supercooling and natural convection in octadecane phase change material. ***International Conference on Technologies and Materials for Renewable Energy, Energy and Sustainability (TMREES22Fr), Metz-Grand Est, 9-11 May 2022***

Résumé substantiel en français

Introduction

L'objectif principal de cette thèse est d'étudier numériquement l'effet de la surfusion sur les performances d'un système de stockage d'énergie thermique utilisant des matériaux à changement de phase (MCP). La chaleur latente des MCP apporte une quantité importante de chaleur au système, augmentant considérablement l'efficacité du système. La présence de surfusion empêche ou retarde la solidification du MCP et le dégagement de chaleur latente, ce qui a un impact néfaste sur les performances et l'efficacité du système.

Pour atteindre l'objectif de la thèse, une revue de la littérature sur la présence de surfusion et les facteurs influençant son apparition est présentée. De plus, les modèles existants trouvés dans la littérature et les problèmes rencontrés lors de la modélisation sont détaillés. Cette revue contribue au développement des connaissances sur le phénomène de surfusion, y compris son impact sur le comportement du matériau, son effet sur les systèmes intégrant des MCP ou encore les facteurs d'influence et aide au développement d'une méthode simple, directe et précise de prise en compte de ce phénomène dans un modèle numérique. Un modèle numérique précédemment validé pour décrire la convection naturelle a été modifié pour inclure la surfusion pendant le refroidissement. Ce modèle tient compte des difficultés rencontrées dans la modélisation du comportement thermique des MCP surfondus et élabore une solution pour chacune d'entre elles. Pour valider ce modèle, des résultats expérimentaux impliquant un protocole rigoureux sont nécessaires. Ces résultats, obtenus avec une géométrie de dispositif, des propriétés de matériaux et des conditions (initiales et limites) clairement spécifiées, sont utilisés pour valider le modèle implémenté sous COMSOL Multiphysics. Ce dernier est ensuite employé pour étudier les performances de deux systèmes de stockage d'énergie thermique à chaleur latente.

Les travaux réalisés dans chaque chapitre, les obstacles rencontrés, les résultats obtenus et les travaux futurs requis sont énumérés ci-dessous.

Chapitre 1

Le premier chapitre est une revue de la littérature sur le phénomène de surfusion. Ce chapitre commence par décrire la surfusion et les systèmes dans lesquels elle peut se produire. Les recherches montrent que la surfusion peut être un phénomène bénéfique ou néfaste, selon le système concerné. La surfusion est, par exemple, bénéfique dans les processus de conservation des aliments, des médicaments ou pour la transplantation d'organes. L’absence de solidification en raison de la surfusion nécessite moins d’énergie pour atteindre la température souhaitée et d’autre part permet de conserver à des températures plus basses sans dégrader les éléments à conserver. De plus, en empêchant la solidification, la surfusion aide à la survie des animaux et des plantes dans les régions hivernales particulièrement froides en protégeant leurs organes du changement de phase. Cependant, dans les systèmes de stockage d'énergie thermique, la solidification du MCP est critique et si elle n’a pas lieu ou est retardée, cela réduit considérablement les performances du système. Les technologies de tels systèmes reposent sur le changement de phase du MCP qui va apporter une quantité raisonnable d'énergie grâce à sa chaleur latente. Dans les deux cas, la présence arbitraire de surfusion est préjudiciable, aussi une revue des principaux facteurs qui influencent cette présence est-elle effectuée. Les recherches actuelles montrent qu’un grand nombre de facteurs corrélés existe. L'effet de chaque facteur est étudié indépendamment en présentant les travaux expérimentaux les plus récents réalisés dans la littérature. On constate que le degré de surfusion augmente avec l'augmentation de la vitesse de refroidissement et la pureté du MCP,

cependant, il diminue avec l'augmentation du volume du récipient et de la rugosité de la surface de contact. Le MCP surfondu est instable et tout choc mécanique, vibration ou tension appliquée peut initier sa nucléation.

Cet état de l'art se poursuit avec les méthodes numériques couramment utilisées pour modéliser un changement de phase. L'ajout de la surfusion à ces modèles présente plusieurs défis. Les propriétés thermophysiques du matériau ne sont notamment plus linéaires et sont fonction de la température. Une température donnée inférieure à la température de fusion peut correspondre aux phases solide, surfondue ou de montée en température du MCP. De plus, la température à laquelle la solidification du MCP commence est difficile à définir dans le modèle pour se rapprocher au mieux du comportement thermique du MCP en présence de surfusion. Cette revue examine ainsi de modèles récents développés par divers auteurs, ainsi que les critères utilisés pour surmonter ces difficultés.

Perspectives :

Cette revue démontre que la surfusion est un phénomène important, et son instabilité peut être nuisible au système comportant des MCP. Son instabilité est due au fait que la présence de surfusion dépend de plusieurs facteurs. Cependant, ces variables ne sont toujours pas bien connues et les corrélations entre elles pas bien définies. D'autres expériences devraient être menées pour développer des équations générales qui déterminent avec précision la température de nucléation en fonction des facteurs mis en avant influençant la surfusion. Son omission dans les modèles numériques peut entraîner une grande disparité entre les résultats réels et simulés.

Chapitre 2

Le deuxième chapitre décrit le modèle numérique implémenté. Une solution optimale est trouvée à chaque problème rencontré lors de la simulation numérique de la surfusion. Enfin, un modèle cohérent est présenté et sera validé et testé dans les chapitres suivants.

Modèle existant sans surfusion

Le modèle construit dans cette étude est une modification d'un modèle déjà existant de Biwole et al. [1], [2], qui est lui aussi une modification du modèle enthalpie-porosité de Brent et al. [3]. Le modèle suppose que le changement de phase se produit sur un intervalle de température $[T_m - dT/2,\ T_m + dT/2]$ plutôt qu'à une température constante. La fraction liquide est calculée à l'aide de la fonction $B(T)$ donnée par l'équation (1). $B(T)$ vaut 0 pour les températures inférieures à $T_m - dT/2$ et 1 pour les températures supérieures à $T_m + dT/2$, et varie linéairement entre ces deux valeurs comme le montre la Figure 1. La densité et la conductivité thermique sont modifiées en fonction de la température en utilisant la fonction par morceaux $B(T)$ comme indiqué dans les équations (2) et (3).

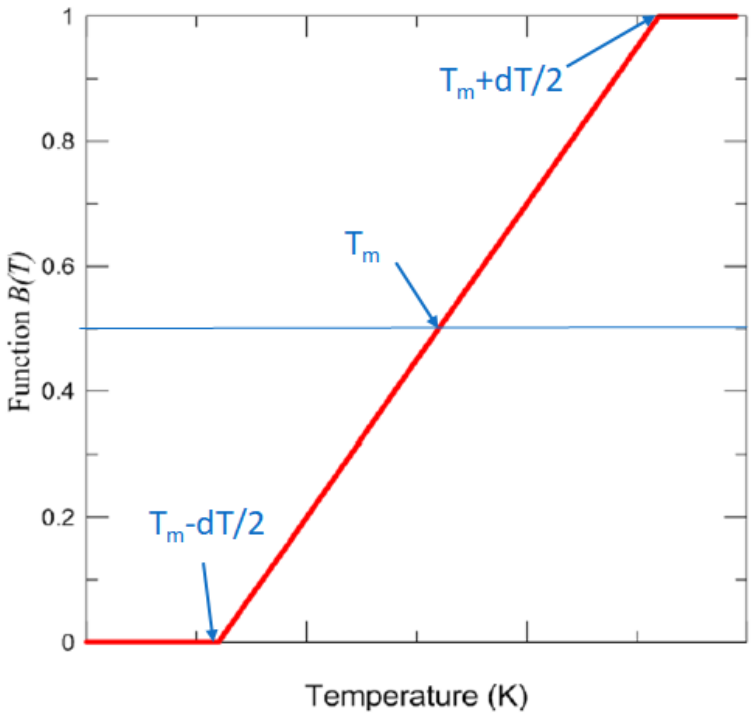

Figure 1 Variation de $B(T)$ en fonction de la température

Pour inclure la chaleur latente lors du changement de phase, la valeur de la capacité calorifique spécifique est modifiée dans l'intervalle $[T_m - dT/2, T_m + dT/2]$ en appliquant une fonction gaussienne notée $D(T)$ dont l'expression est donnée par l'équation (5). $D(T)$ est multiplié par la chaleur latente du MCP et ajouté à la capacité thermique comme indiqué dans l'équation (5).

$$B(T) = \begin{cases} 0, & T \le Tm - dT/2 \\ \dfrac{T - Tm + dT/2}{dT}, & Tm - \dfrac{dT}{2} < T < Tm + \dfrac{dT}{2} \\ 1, & T \ge Tm + \dfrac{dT}{2} \end{cases} \quad (1)$$

$$k(T) = k_s + (k_l - k_s)B(T) \quad (2)$$

$$\rho(T) = \rho_s + (\rho_l - \rho_s)B(T) \quad (3)$$

$$D(T) = e^{\frac{(T-Tm)^2}{dT^2/4}} \Big/ \sqrt{\pi dT^2/4} \quad (4)$$

$$C_P(T) = C_{P_s} + \left(C_{P_l} - C_{P_s}\right)B(T) + L_F D(T) \quad (5)$$

Le matériau est figé dans la phase solide. Pour représenter la phase solide, la viscosité du MCP croit à l'aide d'une fonction $A(T)$ et désigne comme suit :

$$A(T) = \frac{C_1(1 - B(T))^2}{B(T)^3 + C_2} \quad (6)$$

où C_1 et C_2 sont des constantes. C_1 a une valeur très élevée qui dépend du matériau, comme expliqué dans [1], tandis que C_2 a une valeur très faible et empêche la division par zéro lorsque le MCP est à l'état solide. A l'état solide $B(T) = 0$ et $A(T) = C_1/C_2$ ce qui correspond à une valeur très grande, alors qu'à l'état liquide $B(T) = 1$ et $A(T) = 0$. La fonction de viscosité s'écrit alors :

$$\mu(T) = \mu_l(1 + A(T)) \tag{7}$$

Dans l'équation de conservation de la quantité de mouvement, une force volumique $\overrightarrow{F_a}$ est également ajoutée pour dominer toutes les autres forces dans la phase solide. Lorsque cette force surmonte toutes les autres forces, la vitesse du MCP ($\vec{u}$ converge vers zéro, ce qui correspond à l'état solide :

$$\overrightarrow{F_a} = -A(T).\vec{u} \tag{8}$$

La convection naturelle est incluse en utilisant une force volumique donnée par :

$$\overrightarrow{F_b} = -\rho_l\beta(T - T_m))\vec{g} \tag{9}$$

où β est le coefficient de dilatation thermique

Le modèle a déjà été validé pour la convection naturelle lors de la fusion dans [1], [2]. Dans ces articles, la fusion du matériau RT25 et d'acide laurique dans des enceintes rectangulaires a été simulée et comparée à une expérience en laboratoire et au travail expérimental de Shokouhmand et Kamkari [4].

Modifications et ajouts pour tenir compte de la surfusion

Dans la présente étude, le modèle est modifié pour inclure la surfusion lors du refroidissement. Pour résoudre le problème des propriétés thermophysiques qui ne peuvent plus être représentées comme une fonction bijective de la température, une nouvelle fonction d'état par morceaux $s(s, T)$ est développée pour représenter précisément l'état du matériau. Cette fonction varie selon l'état et la température du matériau comme suit :

$$s(s,T) = \begin{cases} 1. & \text{Processus de chauffage} \\ 2. & \text{États liquides et surfondus} \\ 3. & \text{Hausse de température} \\ 4. & \text{Processus de solidification et refroidissement du solide} \end{cases} \tag{10}$$

La température de nucléation T_n est la température à laquelle la solidification s'initie. En d'autres termes, il s'agit de la température la plus basse qu'un MCP atteint à l'état liquide. La température de nucléation diffère d'un nœud de la grille de calcul à l'autre. Pour cette raison, il est calculé séparément pour chaque nœud et noté nt. La stratégie suivante est utilisée pour modéliser la surfusion :

- Premièrement, le MCP à l'état liquide reste liquide jusqu'à ce que la solidification soit déclenchée, soit par la solidification du nœud adjacent, soit si un nœud atteint une température de nucléation prédéfinie T_n.

- Deuxièmement, lorsque la solidification commence, le MCP utilise une partie de la chaleur latente pour augmenter sa température jusqu'à la limite de température supérieure de la plage de fusion $T_m + dT/2$. L'énergie nécessaire peut être calculée égale à $C_{P_l}(T_m - nt)$, comme détaillé dans [5]. Par conséquent, le modèle augmente sa température à l'aide de la source de chaleur $Q(W/m^3)$ exprimée selon l'équation (11) :

$$Q = \rho_l C_{P_l}(T_m - nt)/t_s \tag{11}$$

où t_s est le temps nécessaire pour élever la température de nt à $(T_m + dT/2)$ et est défini sur la base d'observations expérimentales

- Troisièmement, lorsque la température du MCP atteint $(T_m + dT/2)$, celui-ci poursuit sa solidification de manière habituelle dans un intervalle dT. Par la suite, la valeur de la chaleur latente est réduite de $C_{P_l}(T_m - nt)$, qui est l'énergie consommée nécessaire pour augmenter la température de nt à T_m.

Cependant, si la chaleur latente est insuffisante, c'est-à-dire $C_{P_l}(T_m - nt) > L_F$, la température du nœud monte à une valeur inférieure à la température de fusion. Sachant que toute la chaleur latente sera dégagée, l'équation (12) est utilisée et la température atteinte T est calculée à l'aide de l'équation (13):

$$L_F = C_{P_l}(T - nt) \tag{12}$$

$$T = \frac{L_F}{C_{pl}} + nt \tag{13}$$

Si la chaleur latente est insuffisante, la température monte à la valeur précédemment indiquée et le MCP change sa phase directement en phase solide.

Dans les équations suivantes, $s(s,T)$ sera écrit "s" pour plus de simplicité. Après avoir défini la signification de chaque valeur de la fonction s et les cas possibles, la fonction d'état peut s'écrire comme suit :

$$s(s,T) = \begin{cases} 1, & s = 4 \; et \; T_{app} > T_m \\ 2, & s = 1 \; et \; T > T_m \; et \; T_{app} < T_m \\ 3, & s = 2 \; et \; T_{app} < T_m \; et \; (T = T_n \; or \; \dfrac{\partial T}{\partial t} > 0) \\ 4, & \begin{matrix} s = 3 \; et \; Q \le L_F \; et \; T \ge T_m + dT/2 \\ \text{ou} \\ s = 3 \; et \; Q > L_F \; et \; T \ge L_F/C_{pl} + nt \end{matrix} \end{cases} \tag{14}$$

La température de nucléation nt et la source de chaleur peuvent maintenant être définies comme :

$$nt(s,T) = \begin{cases} T_m, & s = 1 \\ \min(T_m, T), & s = 2 \\ nt, & s \geq 3 \end{cases} \quad (15)$$

$$Q(s,T) = \begin{cases} \rho_l C_{P_l}(T_m - nt)/t_s, & s = 3 \\ 0, & autre \end{cases} \quad (16)$$

La chaleur latente modifiée L_H dépend de l'état du matériau et est définie comme suit :

$$L_H(s,T) = \begin{cases} L_F, & s \leq 3 \\ 0, & s = 4 \; et \; \rho_l C_{P_l}(T_m - nt) > L_F \\ L_F - C_{P_l}(T_m - nt), & autre \end{cases} \quad (17)$$

En état surfondu et lors de la montée en température, le matériau est à l'état liquide, donc les propriétés thermophysiques du MCP correspondent aux propriétés liquides. La densité modifiée, la conductivité thermique, la capacité calorifique et la viscosité sont alors représentées par les équations (18), (19), (20) et (21) respectivement.

$$\rho(s,T) = \begin{cases} \rho_s + (\rho_l - \rho_s)B(T), & s = 1 \; ou \; s = 4 \\ \rho_l, & s = 2 \; ou \; s = 3 \end{cases} \quad (18)$$

$$k(s,T) = \begin{cases} k_s + (k_l - k_s)B(T), & s = 1 \; ou \; s = 4 \\ k_l, & s = 2 \; ou \; s = 3 \end{cases} \quad (19)$$

$$C_p(s,T) = \begin{cases} C_{ps} + \left(C_{pl} - C_{ps}\right)B(T) + LH * D(T), & s = 1 \; ou \; s = 4 \\ C_{pl}, & s = 2 \; ou \; s = 3 \end{cases} \quad (20)$$

$$\mu(s,T) = \begin{cases} \mu_l(1 + A(T), & s = 1 \; ou \; s = 4 \\ \mu_l, & s = 2 \; ou \; s = 3 \end{cases} \quad (21)$$

Modèle physique

Le modèle est une représentation 2D d'un tube à essai partiellement rempli de MCP et immergé dans un bain d'eau. Le tube mesure 1,5 mm d'épaisseur, 13 mm de diamètre interne et 7,5 mm de hauteur. La Figure 2 montre les matériaux employés dans le modèle et les conditions aux limites. La condition aux limites supérieure est ouverte, tandis que les autres frontières ont des conditions de Dirichlet avec une température fixe notée T_{app}, représentant la température du bain d'eau. La condition aux limites de Dirichlet (ou de premier type) est une conditions aux limites utilisées dans la résolution des équations différentielles en mathématiques [6]. Elle spécifie, dans l'équation différentielle, les valeurs qu'une solution doit prendre sur le bord du domaine. Lorsqu'une condition de Dirichlet est donnée, il n'est pas nécessaire de résoudre la variable dépendante car elle est prédéterminée. En conséquence, le problème peut être résolu sans utiliser d'équations pour ces degrés de liberté. La condition aux limites ouverte implique un flux conducteur nul sur la frontière pour un écoulement de fluide sortant selon l'équation (22) :

$$-n.q = 0, \qquad n.u \geq 0 \tag{22}$$

où n et q sont respectivement le vecteur normal pointant hors du domaine et le flux de chaleur conducteur.

Il prend automatiquement en considération le flux de chaleur causé par le débit à travers une condition de Danckwerts sur l'enthalpie pour un flux entrant de champ de vitesse u à travers la frontière donnée par l'équation (23) :

$$-n.q = \rho \Delta H u.n, \qquad n.u < 0 \tag{23}$$

où ΔH est l'enthalpie sensible

Le MCP, le tube et l'air au-dessus du MCP ont la même température initiale tandis que la température initiale de l'eau est T_{app}. Si la température initiale du MCP est supérieure à la température de changement de phase, il est supposé être à l'état liquide ; sinon, il est supposé à l'état solide.

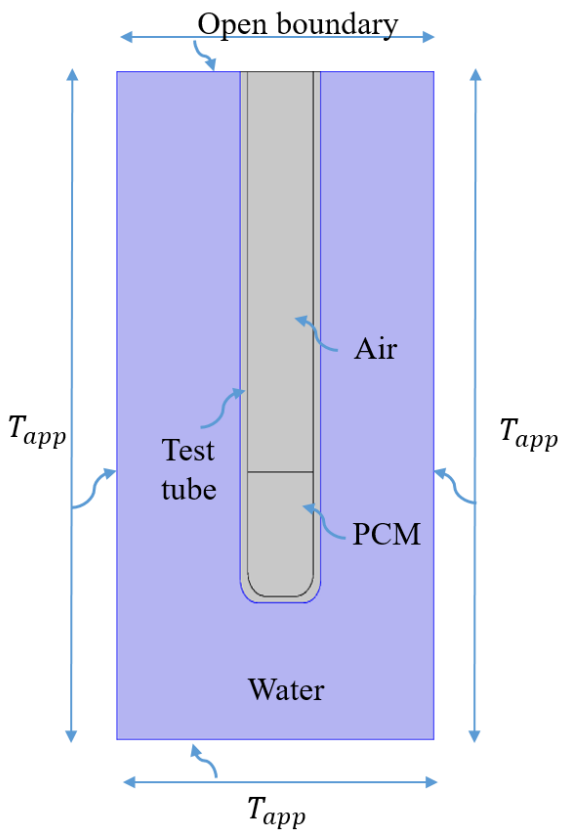

Figure 2 Géométrie, matériaux et conditions aux limites utilisés dans le modèle numérique

Schéma numérique

L'approche par éléments finis est fréquemment utilisée pour la simulation numérique des opérations de traitement thermique, de coulée ou de soudage. En raison des effets de la chaleur latente, la simulation des changements de phase nécessite la simulation de problèmes extrêmement non linéaires. Le défi numérique de l'analyse par éléments finis des systèmes de transfert de chaleur incorporant des changements de phase a reçu beaucoup d'attention ces derniers temps [7]. La technique à grille fixe s'appuie sur le profil de température pour déterminer la position de l'interface de changement de phase. Par conséquent, l'interface peut avoir un front continu, lisse ou non. Ces trois différentes approches de grille fixe peuvent être divisées en trois groupes et sont décrites en profondeur par Voller et al. [8]:

- Les méthodes fictives de flux de chaleur
- La technique de la capacité calorifique effective
- Les méthodes d'enthalpie totale

Le modèle mathématique décrit ci-dessus est implémenté dans un maillage construit à l'aide d'éléments triangulaires libres linéaires ((Figure 3). La taille de maille est définie en assurant un nombre de Péclet massique de maille inférieur à deux comme indiqué dans l'équation (24), pour aider à la convergence numérique. Les simulations s'exécutent d'abord avec un maillage extra-fin comportant 9818 éléments (Figure 3a), puis un deuxième lot de simulations est exécuté avec un maillage extrêmement raffiné composé de 21262 éléments (Figure 3b).

.

$$Pe = \frac{u\Delta x}{\mu/\rho} < 2 \quad (24)$$

où Δx est la longueur maximale des mailles

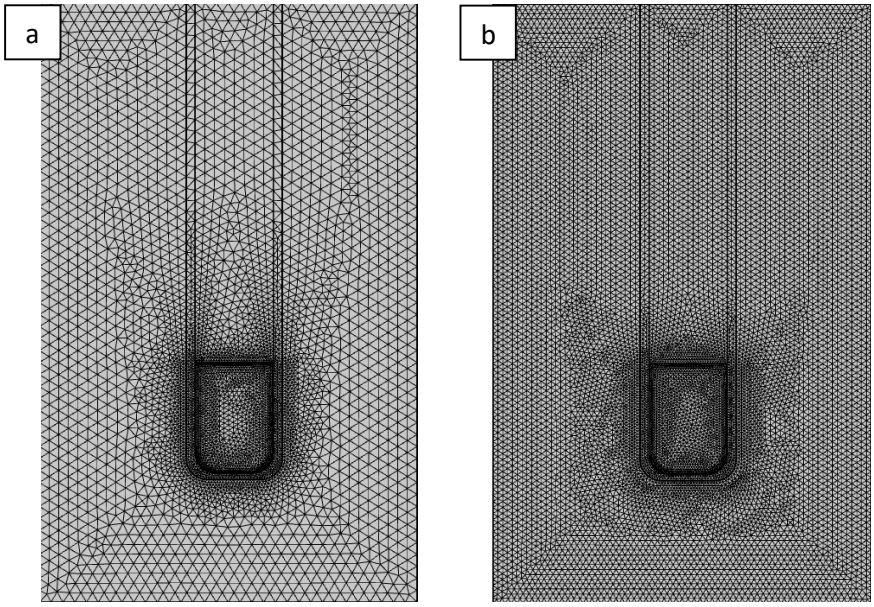

Figure 3 Maillages utilisés dans le modèle numérique COMSOL Multiphysics : a) extra fin et b) extrêmement fin

Perspectives

Il s'agit du premier modèle numérique qui intègre à la fois la surfusion et la convection naturelle. Le modèle est simple et nécessite encore des améliorations. Premièrement, les principaux paramètres d'entrée telles que la température de nucléation et le temps nécessaire pour passer de la nucléation à la température de fusion ne sont pas des données expérimentales aléatoires. Ces deux paramètres nécessitent une compréhension approfondie du comportement chimique du MCP pour développer des équations générales permettant de prédire ces valeurs. Deuxièmement, modéliser l'élévation de température comme une fonction linéaire avec une réaction adiabatique n'est pas réaliste.

Chapitre 3

Le troisième chapitre est consacré à une étude expérimentale. Ce chapitre vise à obtenir des résultats expérimentaux précis qui vont permettre la validation du modèle numérique. Pour construire efficacement la configuration expérimentale, les facteurs les plus importants qui affectent la surfusion sont pris en considération.

Analyse de l'influence du type de MCP, volume et rugosité de surface du contenant

Le type de MCP, qui peut être organique, inorganique ou eutectique, influence la surfusion. Trois MCP de types différents sont choisis : l'octadécane (organique, $T_m = 28\,°C$), l'acétate de sodium trihydraté (sel inorganique, $T_m = 58\,°C$), et un MCP eutectique ($T_m = 21.3\,°C$). Deux configurations sont construites. La première est une expérience à petite échelle utilisant un tube à essai comme contenant du MCP, et la seconde est une expérience à grande échelle utilisant un réservoir rectangulaire comme

contenant du MCP. Les résultats des expériences ont montré qu'une surfusion se produisait dans le tube à essai pour tous les types de MCP. Cependant, la surfusion n'a eu lieu qu'avec le MCP inorganique dans l'expérience à grande échelle (acétate de sodium trihydraté). Le type de MCP, le volume du récipient et la rugosité de la surface jouent tous un rôle dans l'obtention d'un tel résultat. Premièrement, le MCP inorganique est plus sujet à la surfusion que les autres types. La façon dont la température augmente en raison du dégagement de chaleur latente dépend également du matériau. Lorsque la solidification a commencé, la température de l'octadécane a augmenté rapidement, la température du MCP eutectique a augmenté lentement et la température de l'acétate de sodium trihydraté a augmenté rapidement dans l'expérience à petite échelle et lentement dans l'expérience à grande échelle. Deuxièmement, à mesure que le volume du récipient diminue, le degré de surfusion augmente. Troisièmement, à mesure que la rugosité de la surface diminue, le degré de surfusion augmente. Le tube à essai a une surface intérieure lisse sans bords ni arêtes vives, tandis que le récipient rectangulaire comporte des arêtes vives et la rugosité de surface diffère d'un bord à l'autre puisque des plaques d'aluminium sont utilisées pour le transfert de chaleur et du polycarbonate pour ses propriétés transparente et isolante.

Analyse de l'influence des chocs mécaniques

Les chocs mécaniques peuvent provoquer l'arrêt de la surfusion et le début de la solidification. Les expériences sont menées avec soin pour éviter les chocs mécaniques. Par contre, dans l'une des expériences, l'état de surfusion stable du MCP a été volontairement interrompu par un choc mécanique, comme illustré à la Figure 4.

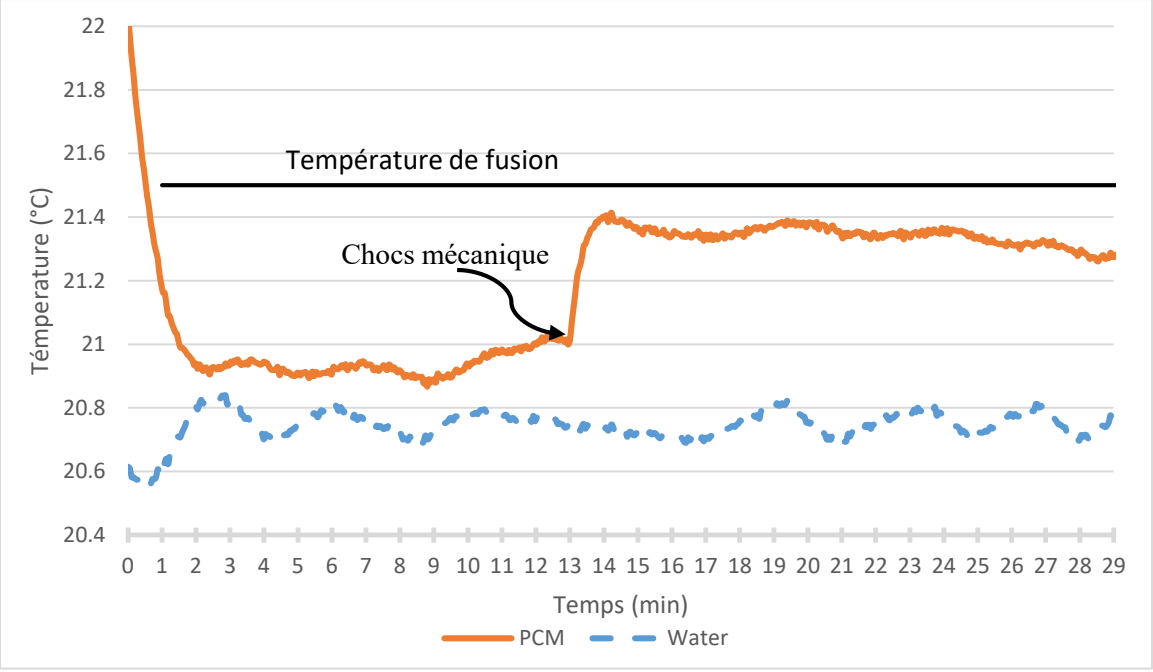

Figure 4 MCP eutectique entrant en surfusion stable avant d'appliquer un choc mécanique

Analyse de l'influence de l'isolation thermique

L'isolation limite le transfert de chaleur à travers les plaques d'aluminium et évite les pertes de chaleur vers l'extérieur. Le modèle numérique supposant que le transfert de chaleur est unidirectionnel (perpendiculaire aux plaques d'aluminium) et appliquant des conditions aux limites thermiquement

isolées, l'étude de l'impact de l'isolation thermique sur le processus de fusion a été menée expérimentalement. Dans ce cadre, l'expérience suivant a été réalisée : la plaque avant du réservoir n'est pas isolée, tandis que la plaque arrière est isolée. La face avant fait référence au côté non chauffé du réservoir en contact avec l'environnement ambiant extérieur tandis que la face arrière est le côté opposé, qui contient le réseau de thermocouples du MCP. Dans ce cas, le transfert de chaleur vers l'extérieur au niveau de la face avant ralentit le processus de fusion. La (Figure 5) montre la vue de dessus du front de fusion dans les scénarios isolé et non isolé. Le scénario sans isolation est représenté sur la Figure 5a. observé davantage de MCP fondu sur la plaque isolée arrière que sur la plaque avant. En effet, au niveau de la face arrière, la chaleur est transférée à la fraction solide au lieu d'être perdue dans l'environnement. La Figure 5b, à l'inverse, montre le scénario d'un réservoir complètement isolé. Le front de fusion est alors uniforme et symétrique.

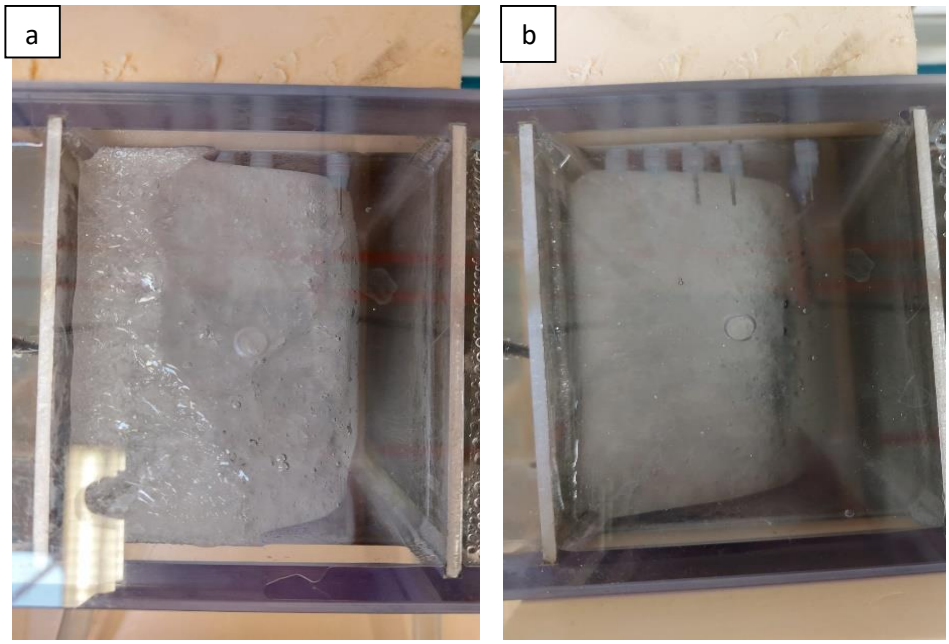

Figure 5 Vue de dessus montrant l'effet de l'isolation sur le processus de fusion de l'octadécane lorsque la face avant est (a) non isolée et (b) isolée

L'impact de l'isolation sur la solidification est également étudié. L'expérience est réalisée dans une pièce à température ambiante inférieure à la température de fusion de l'octadécane. L'échange thermique via les plaques d'aluminium étant supérieur à celui via la plaque avant, la solidification commence sur la face avant. La propagation du front de solidification n'est cependant pas toujours verticale et uniforme. La Figure 6 illustre comment la survenue d'un nouveau front de solidification à partir de la face avant est provoquée par la perte de chaleur à travers celle-ci.

Figure 6 Vue de face montrant l'initiation de la solidification due à l'échange de chaleur avec l'extérieur

Analyse de l’influence du taux de refroidissement

La vitesse de refroidissement a un effet direct sur le degré de surfusion. Il a été démontré que, jusqu'à un certain point, le degré de surfusion augmente à mesure que la vitesse de refroidissement augmente. Cependant, à mesure que la vitesse de refroidissement augmente, le temps passé à l'état surfondu diminue, comme indiqué dans le Tableau 1. En effet, le MCP atteint la température de nucléation plus rapidement.

Tableau 1 Refroidissement du SAT en utilisant différentes températures de liquide de refroidissement

	Température du liquide de refroidissement (°C)	Température de nucléation (°C)	Degré de surfusion (°C)	Temps passé en état de surfusion (s)
Essai #1	47.6	51.75	6.25	74
Essai #2	40.8	47.4	10.6	49
Essai #3	40.8	48	10	46

Les expériences ont également démontré qu'en utilisant une faible vitesse de refroidissement, où la température du fluide de refroidissement diminue progressivement avec un gradient de température négligeable, une surfusion stable peut être obtenue, comme le montre la Figure 7.

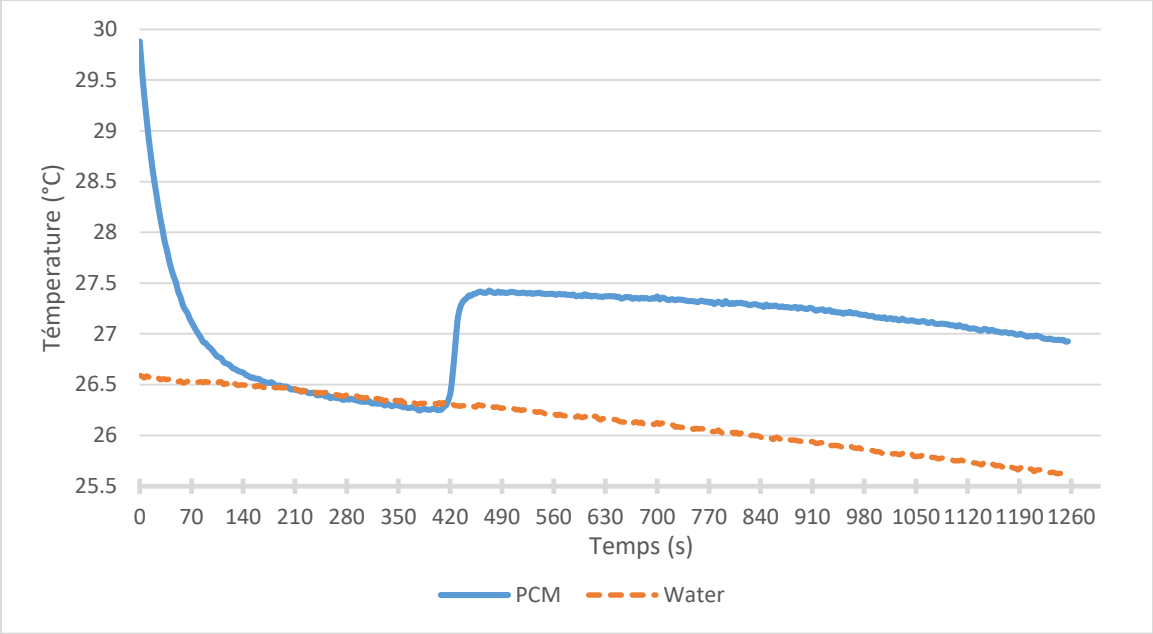

Figure 7 Octadécane entrant en surfusion stable avec une température de bain de refroidissement relativement élevée

Cependant, si la vitesse de refroidissement est élevée pendant la montée en température du MCP, le MCP perd sa chaleur latente pendant cette phase et, dans certains cas, est incapable d'atteindre la température de fusion. Ce phénomène est observé même lorsque la chaleur latente est suffisante si l'augmentation de température est considérée comme adiabatique comme le montre la Figure 8.

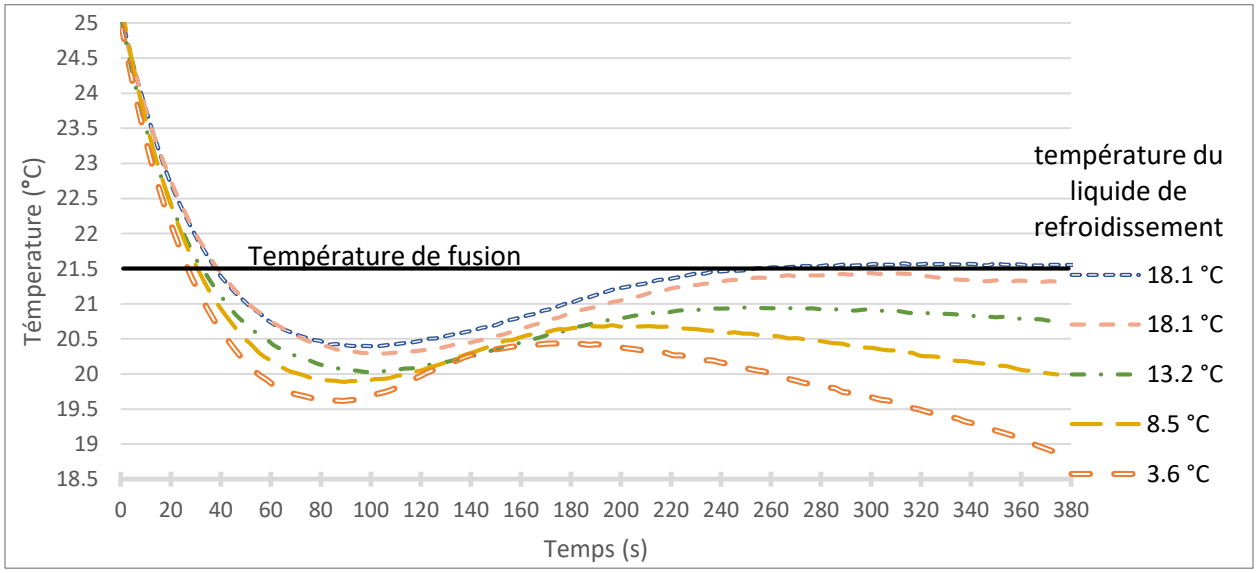

Figure 8 Température transitoire eutectique du MCP sous différentes températures de liquide de refroidissement

Analyse de l'influence de la convection naturelle

La convection naturelle a un impact significatif sur le processus de fusion au cours du chauffage. Le front de fusion est initialement vertical, et au fur et à mesure que la fraction liquide augmente, la convection

naturelle augmente la vitesse de fusion, et l'interface solide-liquide suit un pan incliné. La présence de la convection naturelle fait monter les particules chaudes du MCP vers la surface, ce qui entraîne une variation verticale de la température, comme le montre la Figure 9.

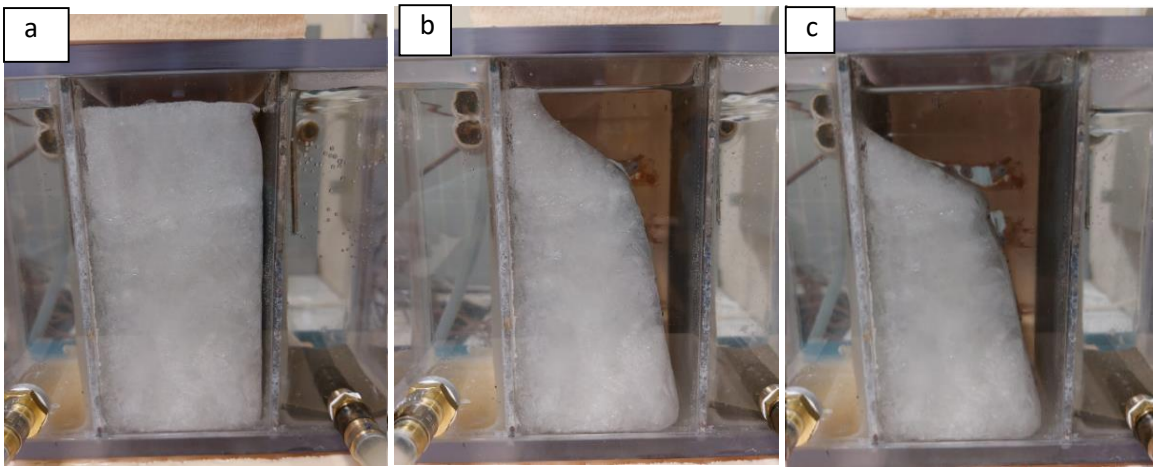

Figure 9 Evolution de l'interface solide/liquide lors de la fusion (a) t=40 min, (b) t=230 min, et (c) t=290 min

Cependant, le phénomène n'est pas observé pendant le processus de refroidissement. Le MCP a une température presque identique dans le sens vertical et l'interface solide-liquide reste verticale pendant le processus de solidification.

Perspectives

Les résultats obtenus fournissent des données expérimentales de référence précises sur laquelle différents auteurs peuvent s'appuyer pour modéliser au plus près le comportement thermique du MCP et valider leurs modèles numériques.

Chapitre 4

Le quatrième chapitre explore le modèle numérique et est divisé en deux sections : une validation du modèle implémenté dans COMSOL Multiphysics et une étude numérique de deux systèmes de stockage d'énergie thermique.

Validation expérimentale

L'expérience à petite échelle a été choisie pour la validation du modèle car une surfusion a été observée avec tous les MCP. Le modèle simule avec précision le phénomène de surfusion de l'octadécane. Un écart est cependant enregistré pour la température maximale atteinte après le dégagement de chaleur latente. En effet, dans l'expérience, la température monte jusqu'au point de fusion, alors que dans le modèle numérique, le changement de phase est supposé se produire dans une plage de température, si bien que la température monte jusqu'à la limite supérieure de cette plage, comme le montre la Figure 10.

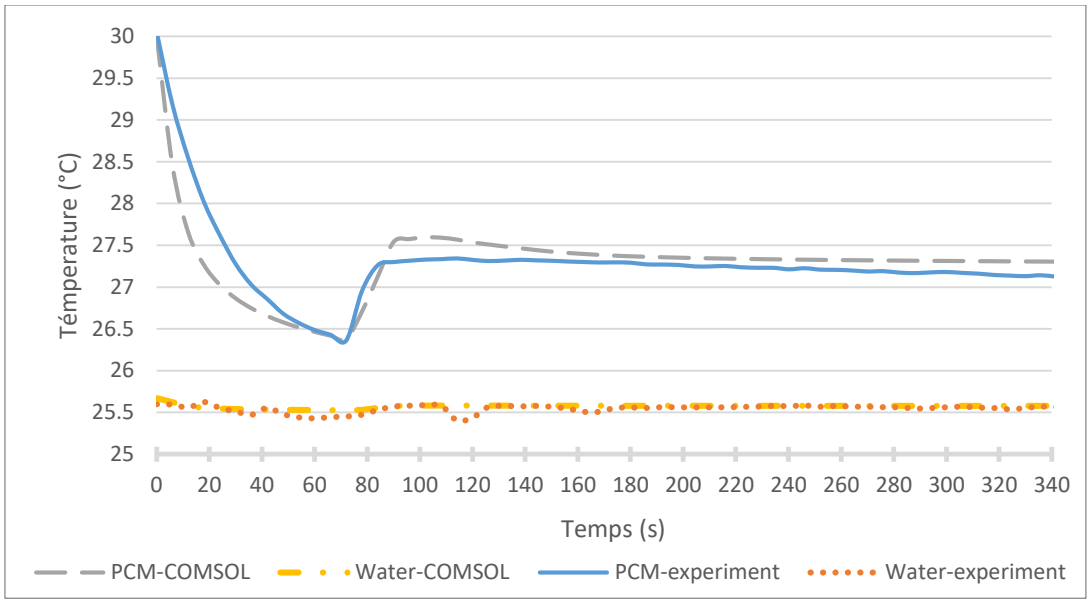

Figure 10 Comparaison des résultats expérimentaux et numériques de l'octadécane en surfusion

Le modèle a été capable de simuler le processus de surfusion du MCP eutectique, mais une déviation est enregistrée pendant le processus de solidification. La lente augmentation de température pendant le dégagement de chaleur latente a entraîné une perte d'énergie dans l'environnement du MCP. Dans ce cas, considérer une élévation de température adiabatique réduit la quantité estimée d'énergie nécessaire pour élever la température à la température de fusion. La solidification prend plus de temps à se terminer numériquement car la température de fusion a été atteinte avec moins d'énergie. Le modèle représente avec précision le degré de surfusion pour l'acétate de sodium trihydraté, mais le même inconvénient a été observé, dû dans ce cas à une vitesse de refroidissement élevée, comme le montre la Figure 11. La température a augmenté rapidement, mais la vitesse de refroidissement élevée est responsable de la perte d'une partie de l'énergie du MCP lors de la montée.

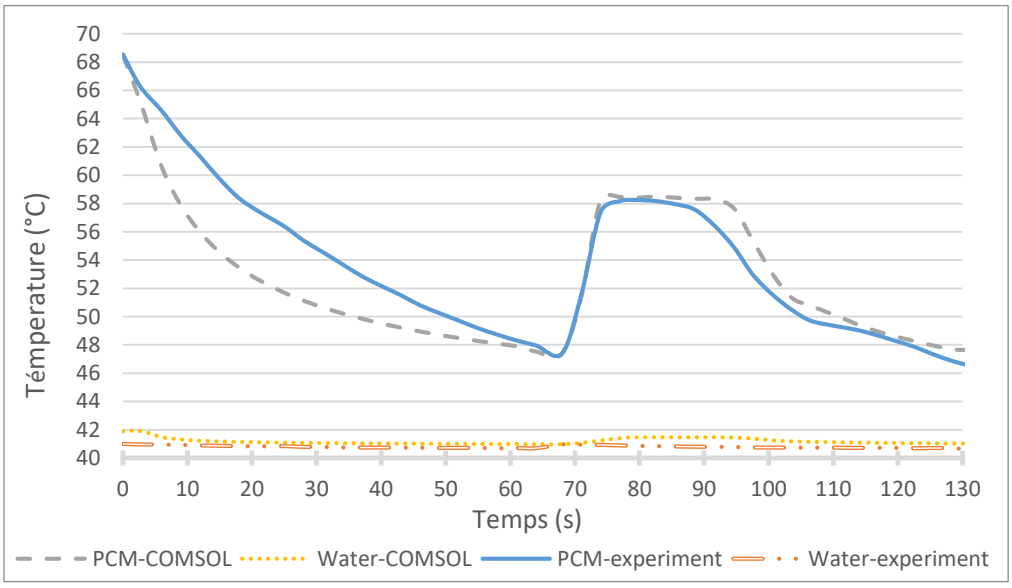

Figure 11 Comparaison des résultats expérimentaux et numériques de SAT subissant une surfusion

Impact de la surfusion sur un système de stockage d'eau chaude

Le modèle développé et validé est à présent utilisé pour démontrer l'effet de la surfusion sur un ballon d'eau chaude contenant des MCP dans des conteneurs en forme de bouteille. Ce dispositif a été étudié par Cabeza et al [9] . Le conteneur mesure 39cm de hauteur et 125cm de largeur. Les bouteilles sont des bouteilles commerciales en aluminium (densité 2700 kg/m3) supposées rectangulaires pour simplifier le modèle numérique. Les bouteilles mesurent 31,5 cm de hauteur, 8,8 cm de largeur et 0,4 mm d'épaisseur. Le MCP choisi est l'acétate de sodium trihydraté (SAT), qui possède les propriétés thermophysiques présentées dans le Tableau 2.

Tableau 2 Propriétés thermophysiques du SAT [10]

	Solide	**Liquide**
Cp (J/kg.K)	2900	3100
k (W/m.K)	0.600	0.385
ρ (kg/m³)	1450	1280
T_m = 58 °C	-	-
LH = 264 kJ/kg	-	-

Le scénario suivant se produit dans le modèle physique : le réservoir est rempli d'eau chaude à 70 °C jusqu'à ce que le MCP et l'aluminium atteignent cette température. Ensuite, l'eau chaude est vidangée et remplacée par de l'eau froide à 20 °C. Un exemple concret est un réservoir d'eau chaude domestique relié à un panneau solaire, où le réservoir est chauffé par l'énergie solaire pendant la journée et toute l'eau est utilisée après le coucher du soleil, de sorte que le réservoir est rempli par la suite d'eau froide du robinet. Dans ce cas, le MCP est utilisé pour réchauffer l'eau. Deux cas d'étude sont simulés : dans le premier cas, le MCP rentre en surfusion, alors que dans le second, le MCP se solidifie sans surfusion. L'effet de la surfusion sur la température maximale atteinte par l'eau à différents points du réservoir est étudié. Le système est considéré comme adiabatique, de sorte qu'aucun échange de chaleur avec l'extérieur ne peut avoir lieu. La température initiale de l'eau est de 20 °C et la température des bouteilles et du MCP est de 70 °C. La Figure 12 montre la géométrie du modèle, les conditions aux limites et initiales. Un thermocouple est placé au centre de chaque bouteille MCP et trois thermocouples (TC_1, TC_2 et TC_3) sont placés respectivement à 100 cm, 70 cm et 30 cm du fond du réservoir. Les thermocouples sont représentés en rouge sur la Figure 12.

En prenant le fond du réservoir comme référence de hauteur H la température moyenne de l'eau pour $H > 62{,}5\ cm$ et $H > 80$ cm est instantanément fournie par T_{avg_1} et T_{avg_2}, respectivement.

Le maillage appliqué est maillage extra-fin avec des mailles triangulaires et le temps simulé est de 8 heures (480 min).

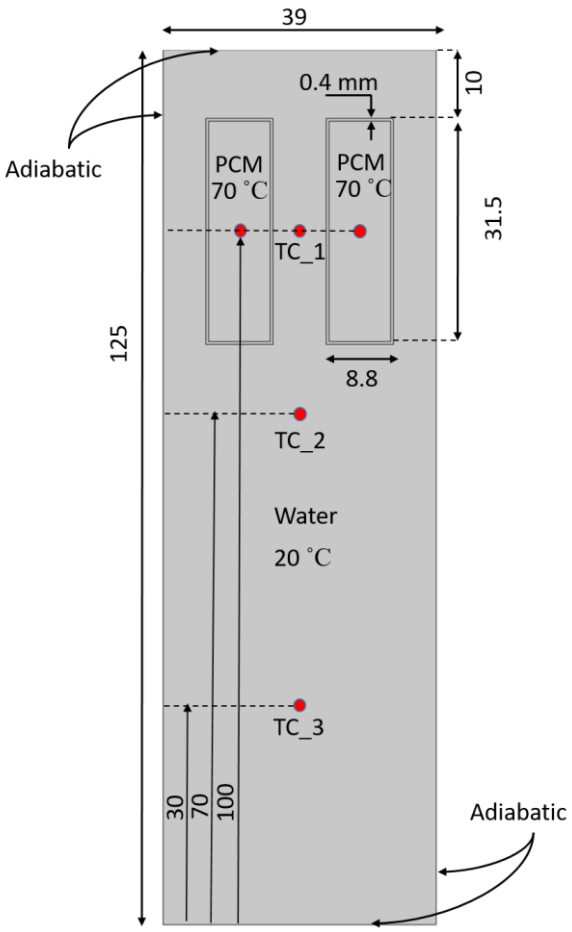

Figure 12 Position des thermocouples, géométrie, conditions aux limites et initiales du modèle de ballon d'eau chaude

En cas de surfusion, le MCP se refroidit en raison des pertes de chaleur dans l'eau. La température du MCP tombe alors en dessous du point de fusion sans changer de phase. Étant donné que la partie supérieure de l'eau est chauffée, il n'y a pas de transfert de chaleur par convection naturelle dans l'eau et la chaleur n'est transférée que par conduction. De ce fait, l'eau du fond reste froide. La température maximale atteinte par l'eau à TC_1 et TC_2 après 480 min est de 49,26 °C et 30,32 °C, respectivement. Il convient de noter que la température maximale de TC_1 est atteinte à $t = 130\ minutes$, après quoi la température chute en raison du transfert de chaleur par conduction vers les parties inférieures. Sans surfusion, le MCP atteint sa température de fusion et change de phase en libérant sa chaleur latente. La température maximale atteinte par l'eau à TC_1 et TC_2 est respectivement de 52,23 °C et 31,70 °C au bout de 480 min. Il convient de noter que la température maximale de TC_1 est atteinte à $t = 151\ minutes$, après quoi la température chute en raison du transfert de chaleur par conduction vers les parties inférieures. En conséquence, en l'absence de surfusion, l'eau à TC_1 est 2,97 °C plus chaude qu'en présence de surfusion. La Figure 13 illustre la variation de température du MCP et de l'eau sur 480 minutes à trois endroits différents. On constate qu'en présence de MCP surfondu, l'eau est toujours plus froide. En l'absence de surfusion, T_{avg_1} enregistre une température de 41,65 °C et 43,02 °C au bout de 300 et 480 minutes, respectivement. De même, T_{avg_2} enregistre 48,27 °C et 48,78 °C. En présence de surfusion, cependant, T_{avg_1} enregistre une température de 29,54 °C et 31,93 °C au bout de 300 et 480 minutes,

respectivement. T_{avg_2} enregistre respectivement 45,22 °C et 45,7 °C. Le Tableau 3 résume ces résultats. Cela démontre que le MCP chauffe considérablement la partie supérieure de l'eau. Parce que l'eau manque de convection naturelle, la chaleur est transférée lentement vers les parties inférieures via un transfert de chaleur par conduction. La surfusion a un effet important, où dans les cas avec et sans surfusion, T_{avg_1} a enregistré une différence de 12,11 °C et 11,09 °C après 300 et 480 minutes, respectivement.

La position du MCP ou le nombre de cellules MCP peut être modifié en fonction de la quantité et de la température d'eau chaude requise.

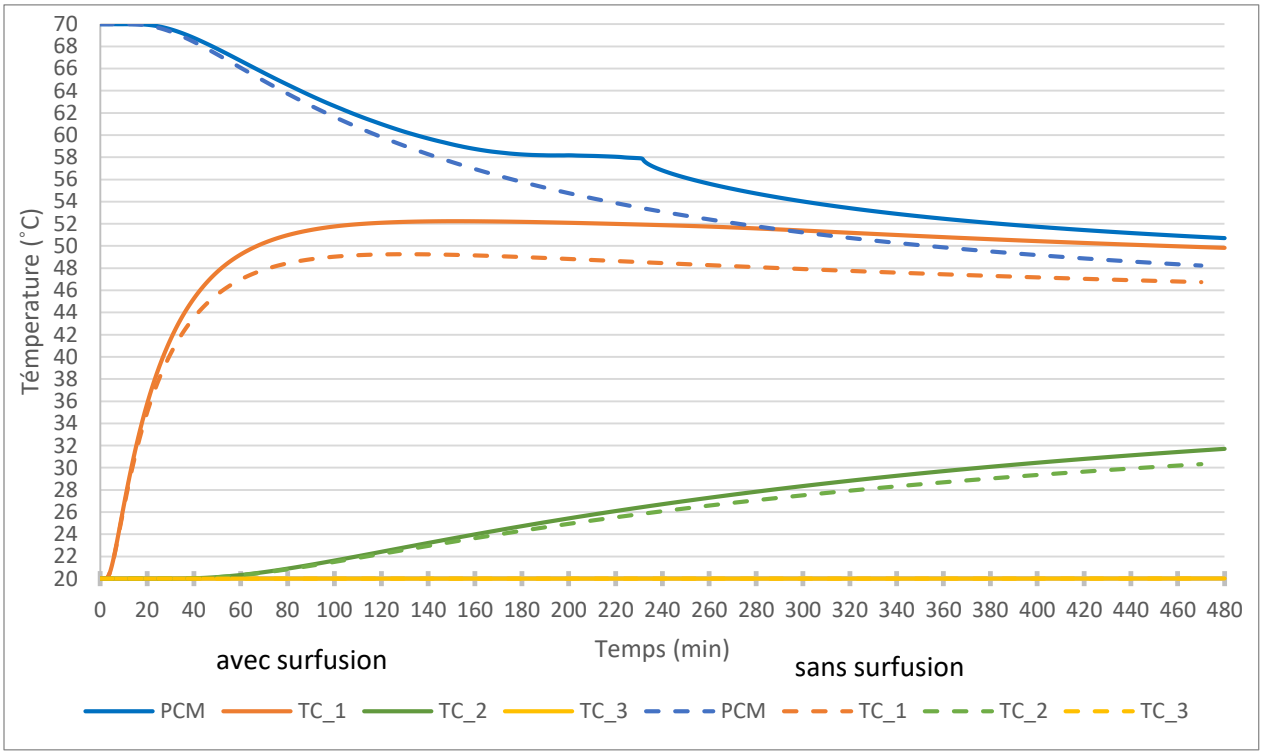

Figure 13 Variation de température du MCP et de l'eau à différentes hauteurs en cas de présence (lignes pointillées) et d'absence (ligne continue) de surfusion

Tableau 3 Température de l'eau à différentes hauteurs et instants pour les cas avec et sans surfusion

Thermocouple	Temps (min)	Hauteur (cm)	Avec surfusion	Sans surfusion
TC_ 1	480	100	49.26 °C	52.2 °C
TC_ 2	480	70	30.32 °C	31.7 °C
TC_ 3	480	30	20.01 °C	20.01 °C
T_{avg_1}	300	>62.5	29.54 °C	41.65 °C
T_{avg_2}	300	>80	45.22 °C	48.27 °C
T_{avg_1}	480	>62.5	31.93 °C	43.02 °C
T_{avg_2}	480	>80	45.70 °C	48.78 °C

Impact de la surfusion sur un système chauffage résidentiel

Le système de chauffage de l'air présenté par Waqas and Kumar [11] est à présent choisi pour simuler l'effet de la surfusion. Le système est un système de ventilation utilisant le stockage d'énergie thermique par chaleur latente. Le MCP est intégré dans le tuyau de ventilation. Le scénario suivant est utilisé dans la présente étude : le MCP est d'abord chauffé pendant la journée et sa température atteint 32 °C. Plus tard dans la nuit, la température ambiante chute à 20 ˚C. Pour simplifier le modèle, l'étude ne considère que la moitié du tube contenant le MCP, puisque le modèle a des conditions aux limites axisymétriques, comme le montre la Figure 14. Le MCP a une épaisseur de 2,5 cm et une longueur de 50 cm. Les mêmes dimensions s'appliquent à la cavité d'air au-dessus. Le débit d'air d'entrée est choisi égal à 10 m^3/h, et le MCP choisi est du $CaCl_2.6H_2O$, qui a les propriétés thermophysiques indiquées dans le Tableau 4.

Tableau 4 Propriétés thermophysiques du $CaCl_2.6H_2O$ utilisé dans le chauffage résidentiel [11]

	Solide	**Liquide**
Cp (J/kg.K)	1430	2312
k (W/m.K)	1.09	0.54
ρ (kg/m³)	1710	1500
T_m = 28 °C	-	-
LH = 188.34 kJ/kg	-	-

Dans la première étude de cas, le MCP rentre en surfusion, alors que dans la seconde, le MCP se solidifie sans surfusion. L'effet de la surfusion sur la température de l'air à la sortie est étudié. De ce fait, la partie refroidissement du MCP de cette application est la plus intéressante. La température initiale de l'air est

de 20 °C et la température du MCP est de 32 °C. La Figure 14 montre la géométrie du modèle et les conditions aux limites. Un thermocouple est placé à la sortie du tube pour calculer la température de l'air après avoir été réchauffé par le MCP. De plus, cinq thermocouples (TC_1 → TC_5) sont placés dans le MCP comme illustré à la Figure 14.

Le maillage appliqué est un maillage extra-fin avec des mailles triangulaires et le temps simulé est de 8 heures (480 min).

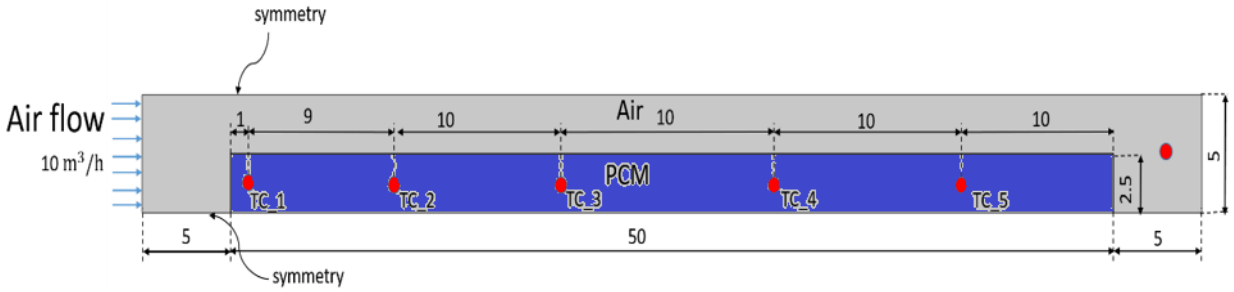

Figure 14 Position des thermocouples, géométrie et conditions aux limites du modèle de conduite

Comme le montre la Figure 15a, la température du MCP diminue en raison du flux d'air froid incident qui l'entoure. En raison de sa position, le premier thermocouple, TC_1, enregistre une baisse de température plus rapide que les autres. La surface de contact avec l'air est plus importante dans cette région et la température de l'air plus faible. Au fur et à mesure que l'air traverse le canal, sa température augmente, entraînant dans un premier temps un flux de chaleur plus élevé. Le premier effet de la surfusion est visible sur la Figure 15a, où le MCP surfondu a une température inférieure à celle du MCP solidifié. Le gradient de température entre le MCP et l'air diminue dans ce cas, ce qui entraîne un flux de chaleur plus faible du MCP vers l'air. L'effet de la surfusion est direct sur la température de l'air à la sortie, où l'air atteint une température plus élevée en l'absence de surfusion, comme le montre la Figure 15b. Comme prévu, l'air enregistre d'abord des températures élevées alors que le MCP fondu est encore chaud, puis la température diminue à mesure que le MCP se refroidit. Le deuxième effet de la surfusion est que la température de l'air diminue progressivement au lieu de rester constante dans le temps. La figure montre que le changement de phase du matériau ajoute plus d'énergie à l'air, car il maintient une température stable de 26,34 ˚C. La différence entre les cas avec et sans surfusion augmente de 0,4 ˚C à t = 300 min, à 2,4 ˚C à t = 480 min.

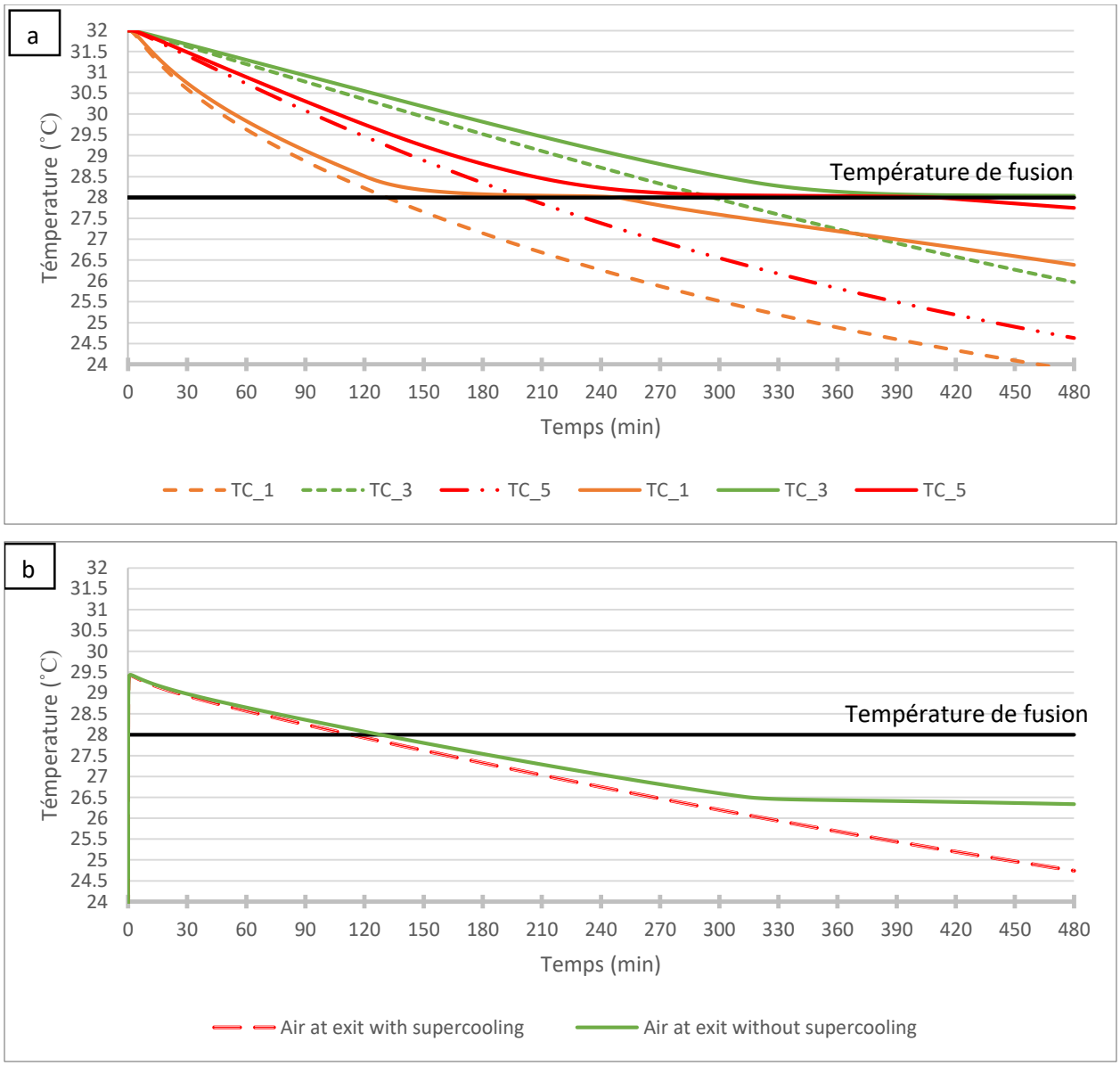

Figure 15 Variation de température a) du MCP et b) de l'air en sortie en cas de présence (lignes pointillées) et d'absence (lignes pleines) de surfusion

Conclusion

La surfusion peut être modélisée à l'aide du modèle COMSOL Multiphysics proposé. Une limitation survient lorsque l'élévation de température causée par le dégagement de chaleur latente ne peut plus être considérée adiabatique. C'est le cas lors d'un refroidissement rapide, où le MCP perd de l'énergie à mesure que la température augmente. En conséquence, le modèle calcule l'énergie minimale nécessaire pour élever la température au point de fusion tout en tenant compte de la chaleur perdue vers l'extérieur. Dans ce cas, la solidification numérique prend plus de temps que les expériences, car la quantité nécessaire pour élever la température est déduite de la chaleur latente. Un deuxième cas se produit lors d'une montée en température très lente, comme le démontrent les expériences sur le MCP eutectique. En théorie, et en faisant abstraction des pertes de chaleur, la chaleur latente est suffisante pour élever la température jusqu'au point de fusion. Le modèle, cependant, n'atteint pas la température de fusion car

toute la chaleur latente est libérée lors de la très faible montée en température. Par conséquent, le modèle fonctionne bien pour la surfusion lorsque la température augmente rapidement mais que la vitesse de refroidissement est lente. Pour améliorer ce modèle, la fonction source de chaleur devrait être modifiée pour inclure les pertes de chaleur vers l'extérieur plutôt que de supposer une augmentation adiabatique de la température.

L'utilisation de MCP dans les systèmes de stockage d'énergie thermique a un impact direct sur leurs performances. Dans la première application étudiée, le MCP est utilisé pour augmenter la température de l'eau dans un réservoir d'eau chaude. La présence de surfusion a un effet significatif, car la température maximale atteinte par l'eau à la fin des simulations était plus faible en présence de surfusion. Dans la deuxième application, le MCP chauffe l'air dans un système de ventilation forcée avant qu'il ne soit pompé dans les pièces résidentielles. La présence de MCP a un effet significatif sur la température de l'air entrant, et la présence de surfusion réduit les performances du système en abaissant la température maximale atteinte par l'air. Cette étude montre qu'il est essentiel d'inclure la surfusion de ce phénomène dans les simulations numériques de systèmes de stockage d'énergie à chaleur latente utilisant des MCP pouvant subir une surfusion.

Remerciements

Ce travail de recherche a été financé par le Conseil départemental de l'Allier. Il s'agit d'un projet de recherche international entre l'Université Clermont Auvergne (UCA), France et l'Université Libanaise (LU), Liban, sous la direction du professeur Pascal Henry Biwole (UCA), du professeur Farouk Fardoun (LU) et du maître de conférences Fabienne Pennec (UCA).

Références

[1] P. H. Biwole, D. Groulx, F. Souayfane, and T. Chiu, “Influence of fin size and distribution on solid-liquid phase change in a rectangular enclosure,” *International Journal of Thermal Sciences*, vol. 124, pp. 433–446, 2018.

[2] P. H. Biwole, P. Eclache, and F. Kuznik, “Phase-change materials to improve solar panel’s performance,” *Energy and Buildings*, vol. 62, pp. 59–67, 2013.

[3] A. Brent, V. R. Voller, and K. Reid, “Enthalpy-porosity technique for modeling convection-diffusion phase change: application to the melting of a pure metal,” *Numerical Heat Transfer, Part A Applications*, vol. 13, no. 3, pp. 297–318, 1988.

[4] H. Shokouhmand and B. Kamkari, “Experimental investigation on melting heat transfer characteristics of lauric acid in a rectangular thermal storage unit,” *Experimental Thermal and Fluid Science*, vol. 50, pp. 201–212, 2013.

[5] I. Shamseddine, F. Pennec, P. Biwole, and F. Fardoun, “Supercooling of phase change materials: A review,” *Renewable and Sustainable Energy Reviews*, vol. 158, p. 112172, 2022.

[6] A. H.-D. Cheng and D. T. Cheng, “Heritage and early history of the boundary element method,” *Engineering analysis with boundary elements*, vol. 29, no. 3, pp. 268–302, 2005.

[7] E. Feulvarch and J.-M. Bergheau, “An implicit fixed-grid method for the finite-element analysis of heat transfer involving phase changes,” *Numerical Heat Transfer, Part B: Fundamentals*, vol. 51, no. 6, pp. 585–610, 2007.

[8] V. R. Voller, C. Swaminathan, and B. G. Thomas, “Fixed grid techniques for phase change problems: a review,” *International journal for numerical methods in engineering*, vol. 30, no. 4, pp. 875–898, 1990.

[9] L. F. Cabeza, M. Ibanez, C. Sole, J. Roca, and M. Nogues, “Experimentation with a water tank including a PCM module,” *Solar Energy Materials and Solar Cells*, vol. 90, no. 9, pp. 1273–1282, 2006.

[10] G. Wang *et al.*, “Review on sodium acetate trihydrate in flexible thermal energy storages: Properties, challenges and applications,” *Journal of Energy Storage*, vol. 40, p. 102780, 2021.

[11] A. Waqas and S. Kumar, “Utilization of latent heat storage unit for comfort ventilation of buildings in hot and dry climates,” *International Journal of Green Energy*, vol. 8, no. 1, pp. 1–24, 2011.